

Newcastle
University

Institute of Genetic Medicine

**Improving our understanding of autosomal
dominant Retinitis Pigmentosa using *PRPF31*
patient-specific induced pluripotent stem cells
(iPSCs)**

Adriana Goes Barbosa Buskin

A thesis submitted to Newcastle University for the
degree of Doctor of Philosophy (PhD)

August 2019

Abstract

Retinitis pigmentosa (RP) is a genetic condition in which degeneration of photoreceptors, especially rods, gradually leads to visual loss. Patients with RP present symptoms such as dark adaptation or "night blindness," followed by "tunnel vision" and loss of central vision later on in the disease. *PRPF31*, a widely expressed splicing factor gene causative of RP, encodes a component of the U4/U6.U5 small tri-nuclear ribonucleic protein (tri-snRNP) complex, which is a constituent of the pre-mRNA processing spliceosome. Mechanisms correlating mutations in splicing factors and retina-specific cell death are still poorly understood. To address this, induced pluripotent stem cells (iPSCs), which can differentiate into any cell types of the three germ layers and are capable of self-renewal, were used to generate patient-specific retinal pigment epithelium (RPE) models to investigate the pathogenesis of the *PRPF31* form of RP.

PRPF31-RPE patient-derived cells presented defects that impaired normal RPE structure and function, including disrupted apical-basal polarity, reduced trans-epithelial resistance and phagocytic capacity.

Transcriptome profiles from *PRPF31*-RPE and other cell types revealed that disrupted alternative splicing was more pronounced in the RPE splicing programme. Mis-splicing of genes encoding pre-mRNA splicing proteins was limited to patient-specific RPE and retinal cells. Mis-splicing of genes implicated in ciliogenesis and cellular adhesion was associated with decreased cilia length and incidence, which in turn may have contributed with the severe RPE defects described above.

In situ gene correction of a *PRPF31* mutation rescued protein expression and key cellular phenotypes in RPE, providing proof-of-concept for future therapeutic strategies.

In summary, the results generated by this study highlighted the applicability and importance of patient-specific iPSCs in disease modeling, unraveling more of the underlying molecular and cellular mechanisms responsible for causing RP.

Acknowledgments

I would like to thank my supervisors – Prof. Majlinda Lako, Dr. Joseph Collin, Dr. David Steel and Prof. Lyle Armstrong and for all their guidance, advice and pertinent suggestions. This PhD work would not be possible without them.

I am profoundly grateful to all the university technical staff for their help and support over the years. Special thanks to Dr. Lisa Hodgson, Dr. Alex Laude, Dr. Andy Filby, Dr. Kathryn White, Paul Sydney and Debra Jones.

My sincere thanks to all my colleagues – Dr. Lili Zhu, Dr. Carla Mellough, Dr. Irina Neganova, Dr. Dean Hallam, Dr. Birthe Hilgen, Dr. Valeria Chichagova, Katja Gassner, Dr. Georgios Anyfantis and the stem cell group, for all the help during all this time.

I would also like to thank some collaborators for their very import work and contribution to this project. My sincere thanks to Dr. Basudha Basu, Dr. Sina Mozaffari-Jovin, Dr. David Dolan, Dr. Alastair Droop, Katarzyna Bialas, Dr. Git Chung, Dr. Gabrielle Wheway, Dr. Martin McKibbin, Prof. Chris F. Inglehearn, Prof. David J. Elliott, Prof. Robin R. Ali, , Prof. Reinhard Lührmann, Dr. Sushma-Nagaraja Grellscheid and Prof. Colin A. Johnson.

My deepest thanks and gratitude to my family, friends and my husband, who always believed in me and kept me going – thank you!

Table of Contents

Chapter 1 - Introduction.....	1
1.1. Retinitis Pigmentosa (RP)	1
1.1.1. Definition of RP.....	1
1.1.2. Classification of RP	2
1.1.3. Inheritance modes	2
1.1.4. Epidemiology of RP	5
1.1.5. Clinical presentation of RP	6
1.1.6. Pathophysiology of RP	9
1.1.7. PRPF31 gene organisation and protein structure.....	11
1.1.8. Role of PRPF31 protein.....	12
1.1.9. Impact of PRPF31 mutations in the Retina.....	14
1.1.10. Diagnosis and Management of RP	16
1.2. Pluripotent Stem Cells.....	20
1.2.1. Origin of Pluripotent Stem Cells.....	21
1.2.2. Characteristics of Pluripotent Stem Cells	22
1.2.3. Induced Pluripotent Stem Cells	23
1.2.4. Generation of iPSCs.....	25
1.2.5. Advantages of using iPSC technology.....	28
1.2.6. Challenges in iPSC technology	29
1.2.7. The use of iPSCs in disease modeling	32
1.3. Retinal Pigment Epithelium	35

1.3.1.	The role of primary cilia in RPE	37
1.3.2.	RPE development in vivo.....	40
1.3.3.	Differentiation of human iPSCs into RPE cells	41
1.3.4.	Attempts to explore disease pathogenesis in PRPF31-RP ..	42
1.4.	Aims	45
Chapter 2 - Methods		46
2.1.	Human Subjects	46
2.2.	iPSC Generation.....	46
2.3.	iPSC Culture.....	46
2.4.	Mutation validation.....	47
2.5.	RNA isolation and reverse transcription	47
2.6.	Polymerase chain reaction (PCR)	48
2.7.	Quantitative real time polymerase chain reaction (qRT-PCR)	48
2.8.	Detection of pluripotency markers by immunocytochemistry	49
2.9.	Detection of pluripotency markers by flow cytometry analysis.....	49
2.10.	<i>In vitro</i> and <i>in vivo</i> three germ layers differentiation assay.....	50
2.11.	Genomic DNA Extraction	50
2.12.	SNP array.....	51
2.13.	iPSC Differentiation to Retinal Pigment Epithelium (RPE)	51
2.14.	Counting of pigmented areas and measurement of pigment intensity	51
2.15.	Measurement of Trans-Epithelial Resistance (TER)	52
2.16.	Transmission Electron Microscopy (TEM).....	52
2.17.	Serial Block Face SEM (SBFSEM)	53

2.18.	Phagocytosis Assay	53
2.19.	RPE Cytokine Secretion Studies.....	54
2.20.	RPE Characterisation by Immunocytochemistry	54
2.21.	Inhibition of nonsense-mediated mRNA decay (NMD).....	55
2.22.	Western blot analysis.....	55
2.23.	E1A alternative splicing assays.....	56
2.24.	RNA Sequencing	56
2.25.	Cilia Length and Frequency Measurements in RPE Cells.....	57
2.26.	CRISPR/Cas9 Correction of PRPF31 Mutation in the RP11VS ..	57
2.27.	Quantification and Statistical Analysis.....	58
Chapter 3 - Generation and characterisation of iPSCs		62
3.1.	Introduction	62
3.2.	Aims	64
3.3.	Control and patient's samples	65
3.4.	Confirmatory mutation screening analysis.....	67
3.5.	Generation of control and PRPF31 patient-specific iPSC	71
3.6.	Detection of Sendai virus genome and reprogramming transgenes	74
3.7.	<i>In vitro</i> assessment of pluripotency	75
3.8.	Three Germ Layers and Teratoma Assays	78
3.9.	Cytogenetic Analysis	81
3.10.	Discussion.....	83
Chapter 4 - Differentiation and Characterisation of Retinal Pigment Epithelium (RPE) Cells		87
4.1.	Introduction	87

4.2.	Aims	88
4.3.	Retinal Pigment Epithelium Differentiation	89
4.4.	Measurement of trans-epithelial resistance	95
4.5.	Transmission Electron Microscopy	96
4.6.	Phagocytosis Assay	98
4.7.	RPE Polarity studies.....	99
4.7.1.	PEDF and VEGF protein levels	100
4.7.2.	Detection of polarity markers by immunocytochemistry	100
4.8.	Discussion	101
Chapter 5 - Molecular Pathogenesis of Splicing Factor <i>PRPF31</i>		106
5.1.	Introduction.....	106
5.2.	Description and effects of <i>PRPF31</i> mutation c.1115_1125 del11108	
5.3.	Modulators of <i>PRPF31</i> expression & Penetrance	111
5.4.	<i>PRPF31</i> expression by Immunocytochemistry	113
5.5.	Splicing & RNA-Seq analysis	114
5.6.	Cilia length and incidence.....	118
5.7.	Crispr-Cas9 correction of <i>PRPF31</i> mutation	120
5.8.	Discussion	122
Chapter 6 - Discussion and Conclusions		127
Chapter 7 - Appendices		133
7.1.	Appendix 1	133
7.2.	Appendix 2	134
Chapter 8 - References.....		136

List of Figures

Figure 1.1. Overview of a healthy and an affected retina by RP. A: Schematic representation of a cross-section of the human eye. B: Schematic representation of a healthy laminated retina. Choroidal capillaries (CC); Bruch's membrane (BrM); Retinal pigment epithelium (RPE); Outer nuclear layer (ONL), containing rod cells (RC) and cone cells (CC); Outer plexiform layer (OPL); Inner nuclear layer (INL), containing horizontal cells (HC), müller cells (MC), bipolar cells (BC) and amacrine cells (AC); Inner plexiform layer (IPL) and Ganglion cell layer (GCL), containing ganglion cells (GC). C: Schematic representation of an affected retina by RP. Adapted from Singh (2018).....	1
Figure 1.2. Images of a normal visual field (left panel) and tunnel vision (right panel). The blackness surrounding the central image indicates loss of peripheral vision.	7
Figure 1.3. Photographs of a normal (left) and RP retina (right). Typical features of RP, such as waxy optic disc pallor, retinal vascular narrowing and 'bone spicule' intra-retinal pigmented deposits, are clearly observed in the RP retina. Reproduced from Farrar <i>et al.</i> (2002).	8
Figure 1.4. Histological appearance of healthy human retina (left) and retina of a patient with retinitis pigmentosa (right). The space between the retinal pigment epithelium and the outer nuclear layer in the diseased retina is a processing artefact. Reproduced from Hartong <i>et al.</i> (2006).....	10
Figure 1.5. Location and structure of <i>PRPF31</i> gene. This gene is located in the long arm of chromosome 19 and encompasses 14 exons. Exon-intron arrangements and untranslated regions are shown. Adapted from Rose <i>et al.</i> (2017) and NCBI.....	11
Figure 1.6. Representation of PRPF31 protein. Alpha helical NOP domain (blue), 15.5K/SNU13 (red) and U4/U5 (yellow/green backbone). Adapted from Liu <i>et al.</i> (2007).	12
Figure 1.7. Spliceosome assembly and function. PRPF31 (grey box) interacts with U4 and is required during U4/U6.U5 tri-snRNP assembly and maintenance in spliceosomes. Reproduced from Rose <i>et al.</i> (2017).....	14
Figure 1.8. <i>CNOT3</i> combinations in patients carrying <i>PRPF31</i> mutations. L represents a low-expressing <i>CNOT3</i> allele, leading to high levels of <i>PRPF31</i> ; H represents a high-expressing <i>CNOT3</i> allele, and due to its repressive nature, leads to lower levels of <i>PRPF31</i> ; and P represents <i>PRPF31</i> . The only symptomatic individual "D" inherits the two copies of high-expressing <i>CNOT3</i> , masking <i>PRPF31</i> expression. Adapted from Rose <i>et al.</i> (2014).....	16
Figure 1.9. Potential of pluripotent embryonic stem cells. The pluripotency is determined by the ability of the cells to differentiate into any cell types belonging to all three germ layers. Reproduced from Meregalli (2011).....	21
Figure 1.10. Differentiation of iPSCs. Induced pluripotent stem cells are generated by reprogramming adult somatic cells. Reproduced from Amabile and Meissner (2009).	24
Figure 1.11. Schematic representation of the human eye, retina and location of the RPE. Reproduced from https://www.closerlookatstemcells.org/stem-cells-medicine/macular-degeneration/	35
Figure 1.12. Schematic representation of the RPE cells and its support functions. Reproduced from Lehmann <i>et al.</i> (2014).	37
Figure 1.13. Schematic representation of primary cilium. The cilium is made of a basal body and microtubular backbone, the axoneme, arranged in a typical '9+0' architecture with nine outer microtubules doublets. The motile cilium has a '9+2' architecture with a central pair of microtubules. Ciliary proteins, synthesized in the cell body, are transported to the tip of the axoneme by the intraflagellar transport (IFT), comprised of polypeptide	

complexes (IFT particles) that move along the length of the ciliary axoneme. Reproduced from <https://ciliopathyalliance.org/cilia>.39

Figure 1.14. Stages of eye development and RPE specification. A: during early stages of eye development, the neuroepithelium invaginates together with the surface ectoderm forming the optic vesicle. B: The inner layer of the optic cup gives rise to neural retina and the outer layer gives rise to the RPE. C: The lens, neural retina and RPE. Reproduced from Ali and Sowden (2011).41

Figure 3.1. Sources of genetic variation throughout the process of iPSC generation and differentiation. Transduction of iPSCs with reprogramming transgenes (RTs) can lead to mutagenesis by integration of transgenes to the host's genomes. Incomplete reprogramming can result in genetic variation due to failure of the removal of somatic epigenetic marks in the reprogrammed cells. CNVs: copy number variants, SNVs: single nucleotide variants.63

Figure 3.2. Family pedigrees of RP-PRPF31 patients and their respective mutations. A: Paternal aunt and two siblings harbouring mutation c.1115_1125del11. B: Mother and two siblings harbouring mutation c.522_527+10del. C: Single patient harbouring mutation c.201delT. Question marks represent unknown genotypes/phenotypes.65

Figure 3.3. Sequences of *PRPF31* exon 11 from WT1 control iPSC (upper), RP11VS iPSC (middle) and RP11VS fibroblast (lower). As the mutation is heterozygous, the middle and lower images show both the mutated and normal sequences superimposed after the deletion. The spaces inside the red box were created to facilitate the view of the deletion and the alignment of the control and PRPF31-RP sequences. The other two patients of the same family showed the same deletion.68

Figure 3.4. Predicted effects of the *PRPF31* c.1115_1125del mutation on its own transcripts. The mutation, represented by the vertical dotted bar, result in either a long mRNA transcript containing the deletion in exon 11 and a PTC just before the termination codon in exon 14, or a short mRNA transcript formed by the skipping of exon 11 during splicing and a PTC in exon 12.68

Figure 3.5. Sequences of *PRPF31* exon 6 from WT1 control iPSC (upper), RP11S2 iPSC (middle) and RP11S2 fibroblast (lower). As the mutation is heterozygous, the middle and lower images show both the mutated and normal sequences superimposed after the deletion. The spaces inside the red box were created to facilitate the view of the deletion and the alignment of the control and PRPF31-RP sequences. The other two patients of the same family showed the same deletion.69

Figure 3.6. Predicted effects of the *PRPF31* c.522_527+10del mutation on its own transcripts. The mutation, represented by the vertical dotted bar, result in either a mRNA transcript containing the deletion in exon 6, including intron 6, or a short mRNA transcript formed by the skipping of exon 6 entirely.70

Figure 3.7. Sequences of *PRPF31* exon 3 from control iPSC (upper), RP11S4 iPSC (middle) and RP11S4 fibroblast (lower). As the mutation is heterozygous, the middle and lower images show both the mutated and normal sequences superimposed after the deletion. The single space inside the red box was created to facilitate the view of the deletion and the alignment of the control and patient sequences.70

Figure 3.8. Overview of the reprogramming process. A: Reprogramming timeline for generation of iPSCs. B: Microscope images showing changes from patient-specific RP11S2-PRPF31 fibroblasts to induced pluripotent stem cells. Day 1: Fibroblasts of passage 5. Day 7: Cells changing morphology. Day 15: Observation of the first colonies. Day 23: Colonies showing typical iPSC morphology, ready to be picked and transferred to matrigel. Day 30: Colonies on matrigel passage 1 show typical morphology of iPSCs.72

Figure 3.9. Detection of residual expression of Sendai (SeV) genome and reprogramming transgenes in controls and PRPF31-iPSC lines by RT-PCR. At passage 15, controls and

PRPF31-iPSC lines did not express Sendai and reprogramming vectors KOS (KLF4, OCT3/4, SOX2) KLF4 and C-MYC. Positive controls consisted of RNA that was extracted from fibroblasts at day-7 post transduction. Nuclease-free water was used as negative control to confirm absence of contamination in the PCR reagents or primer-dimer formation.....74

Figure 3.10. Detection of pluripotency-associated markers by immunocytochemistry. Brightfield and Immunocytochemistry images showing expression of OCT4 (green) and SSEA-4 (red) in control and PRPF31-iPSC lines. Nuclei were stained with DAPI. Negative control of SSEA-4 antibody was not performed because it is conjugated.....76

Figure 3.11. Quantification of pluripotency-associated markers by flow cytometry. Representative images showing double-positive cell population of NANOG and TRA-1-60 in controls and PRPF31-iPSC lines.77

Figure 3.12. Three germ-layer assay by immunocytochemistry. Differentiated cells from controls and PRPF31-mutated lines showing positive staining for two markers of each germ layer. Endoderm: AFP (green) and FOXA2 (red). Mesoderm: SMA (red) and HAND1 (green). Ectoderm: PAX6 (red) and TUJ1 (green).79

Figure 3.13. Teratoma formation assay in SCID mice. A: Representative images of tumours generated from control and PRPF31-iPSC lines. B: Structures found in the tumours of endodermal, mesodermal and ectodermal origin.80

Figure 3.14. Confirmation of genetic Identity of parental fibroblasts and iPSCs by SNP microarray. SNP patterns revealed correlation of the genetic identity profile from parental fibroblasts and iPSCs, confirming the authenticity of the lines used in this study.82

Figure 4.1. Differentiation capacities of clones 1, 2 and 3 of control WT1-iPSC. The mean of the number of pigmented foci and intensity of pigmentation per cm² of each clone is not significantly different from one another, except for intensity of pigmentation between clones 1 and 2. Data shown as mean \pm SEM, n = 3.89

Figure 4.2. Representative images of RPE differentiation with only base medium, derived from controls and PRPF31-iPSCs. The images were scanned from 6-well plates. A: H9-hESC. B: WT1-iPSC. C: RP11S1-iPSC. D: RP11M-iPSC. E: RP11VS-iPSC. Examples are representative of at least three independent experiments.91

Figure 4.3. RPE differentiation efficiency. A: Formation of pigmented foci per cm² in controls H9-hESC and WT1-iPSC (Mean of all clones) and PRPF31-iPSCs (RP11S1, RP11M and RP11VS). The differences between the mean of all time points of H9 vs RP11M and RP11VS and between WT1 vs RP11S1 were significant. RP11S1 is also significantly different from RP11M and RP11VS. B: Intensity of pigmentation per cm² in controls H9-hESC and WT1-iPSC (Mean of all clones) and PRPF31-iPSCs (RP11S1, RP11M and RP11VS). The differences between H9 vs RP11S1, WT1 vs RP11S1, and between RP11S1 vs RP11M and RP11VS were significant. Data shown as mean \pm SEM, n = 3.92

Figure 4.4. Representation of directed stem cells differentiation to RPE cells. A: Inhibition of transforming growth factor beta (TGF- β) and bone morphogenic protein (BMP) pathways suppresses differentiation towards mesodermal and endodermal lineages, leading the cells to an ectodermal fate. B: Cells were directed to become retinal precursors. C: Wnt pathway was stimulated to further direct the cells to RPE.....93

Figure 4.5. Timing of factor addition directing pluripotent cells toward RPE fate. From days 0-5, SB431542 (TGF- β inhibitor) and Noggin (BMP inhibitor) were added to the differentiation media followed by the addition of Noggin from days 6-9. Activin A was added to the differentiation media from days 10-15. CHIR99021 (Wnt agonist) was added to the media from days 16-21. After day 21 the cultures were fed with only base medium containing B27 and pigmented patches were picked and expanded to form RPE monolayers until they were used for analysis around week 21 (~6months) and further on, around week 43 (~11 months).93

Figure 4.6. Comparison of RPE differentiation protocols with and without small molecules using RP11M at week 16 (~04 months). A: Pigmented patches at week 15 (~04 months) of differentiation with only basal medium and basal medium supplemented with small molecules. B: A significant difference was seen between the two protocols ($P < 0.05$). Data shown as mean \pm SEM, $n = 3$94

Figure 4.7. Trans-epithelial resistance of controls and PRPF31-RPE cells. A: TER values show that there is a significant difference between the mean of controls (WTs) and PRPF31-mutant lines. Data shown as mean \pm SEM, $n = 3$. B: All PRPF31-RPE cells formed a cobblestone monolayer, with polygonal cells, typical of RPE morphology.....95

Figure 4.8. Abnormal ultrastructural features of RPE PRPF31-mutant cells. TEM of PRPF31-RPE cells at 21 and 43 weeks shows shorter and fewer microvilli in PRPF31-RPE cells (average length of $3.1 \mu\text{m} \pm 0.49 \text{ SEM}$ in WT3 and $1.4 \mu\text{m} \pm 0.33 \text{ SEM}$ in RP11S1) and large basal deposits that were not observed in controls. Representative images of at least three independent experiments.97

Figure 4.9. Photoreceptor outer segments phagocytosis assay of iPSC-derived RPE cells by flow cytometry. A: FITC-labelled POSs. B: The results of the phagocytosis assay demonstrated that iPSC-derived RPE were able to phagocytose but PRPF31-severe patients showed deficiency in the ability of ingesting more POSs per cell, as determined by median fluorescence intensity values. All cells were age-matched with regards to the length of differentiation time (~6 months). Data shown as mean \pm SEM, $n = 3$. C: Example of the results with cells fed with FITC-labelled POSs and non-labelled POSs. .99

Figure 4.10. ELISA assays for apical and basal secretion of PEDF and VEGF, respectively, in controls and PRPF31-RPE cells. Data of three independent experiments obtained from RPE at week 21 of differentiation. Data shown as mean \pm SEM, $n = 3$ 100

Figure 4.11. Detection of polarity markers by immunocytochemistry. A: Immunostaining for basolateral markers BEST1 and apical Na^+/K^+ -ATPase. B: Correct basolateral distribution of collagen IV (C-IV) and apical MERTK was seen in unaffected control (WT3) but not in RP11 RPE cells. Representative images from three independent experiments. 101

Figure 5.1. Schematic representation of the tri-snRNP component of the spliceosome and proteins associated with adRP. Elements of the U5 snRNP are presented in different shades of red, and those belonging to the U4/U6 snRNP are in shades of blue. Adapted from Tanackovic *et al.* (2011). 107

Figure 5.2. *PRPF31* expression in patient-specific cells. A: Short mutant (SM) isoform of 130 bp is only present upon inhibition of NMD with puromycin (indicated by +). B: Quantification of *PRPF31* mRNA in patient cells relative to GAPDH. Data are representative of at least three independent repeats. RO: retinal organoids. 109

Figure 5.3. Sequences of *PRPF31*-exon 11 cDNA in WT3-RPE and RP11VS-RPE samples. WT allele: absence of the mutation, 203 bp; LM allele: 192 bp; SM allele: 130 bp..... 110

Figure 5.4. *PRPF31*-exon 11 amino acid sequences in WT3-RPE and RP11VS-RPE samples. WT isoform: presence of exon 11; LM isoform: a frame shift after amino acid 371 creates a long mutant (LM) transcript; SM isoform: skipping of exon 11 leads to a truncated NMD-sensitive short mutant (SM) transcript. Met: open reading frame AUG; Stop codon: UAA. 110

Figure 5.5. Expression of *PRPF31* and *CNOT3* in primary fibroblasts, iPSCs, iPSC-derived RPE and retinal organoids from WT3 control and patient RP11VS by RNA sequencing. In patient's cells, the combined total *CNOT3* expression of biological triplicates was higher than in controls, whilst *PRPF31* was lower in patient's cells. Data from three independent replicates. Graph courtesy of Mr David Dolan. 112

Figure 5.6. Colocalisation of PRPF31 with spliceosomal component (Y12) in iPSC-derived RPE. These are representative examples of at least three independent experiments.	113
Figure 5.7. PRPF31 expression in patient-specific cells and effects on pre-mRNA splicing. A: Wild-type PRPF31 is significantly reduced in patient RPE cells. The LM form and reduced SART1 is observed only in the patient RPE cells. B: The bar graph shows wild-type PRPF31 levels in patient cells normalized to SF3b15. C: Schematic representation of alternative splice variants of E1A minigene reporter. D: Patient RPE cells showed a notable defect in the alternative splicing of E1A minigene reporter, with reduction of the 9S and 10S isoforms and accumulation of pre-mRNA.	115
Figure 5.8. Differential alternative splicing analysis from RNA sequencing data of fibroblasts, iPSC, retinal organoids and RPE. A: Schematic representation of alternative splicing events, adapted from Park <i>et al.</i> (2013). B: rMATS analysis showing that PRPF31-RPE have the highest percentage of transcripts containing retained introns (RI) and alternative 3' splice sites (A3SS). C: Gene Ontology enrichment analysis showing biological and cellular processes affected by alternative splicing, in all four cell types. .	117
Figure 5.9. PRPF31-RPE cells have defects in cilia formation and structure. A: Immunostaining of RPE cells with cilia markers ARL13B (green) and Pericentrin (red). Representative images from n = 3 independent experiments. B: Quantification of cilia length and incidence showing the decrease of both parameters in PRPF31-mutant patients; C, D: TEM and 3D SBFSEM images showing shorter cilia in PRPF31-RPE cells with bulbous tip.	119
Figure 5.10. Correction of <i>PRPF31</i> mutation results in reversal of cellular and functional phenotypes in PRPF31-RPE. A: Quantitative RT-PCR analysis confirming the increased expression of PRPF31 in CRISPR/Cas9 corrected clone. B: Presence of the correction site in Cas9-RP11VS-iPSC sequence. C: Quantification of <i>PRPF31</i> expression in corrected cell line. D,E: Quantification of cilia length and incidence in controls, PRPF31-RPE and Cas9-RP11VS-RPE. F: TEM images of Cas9-RP11VS-RPE showing morphologically normal cilia, compared to uncorrected PRPF31-RPE. G: Rescued phagocytic capacity in Cas9-RP11VS-RPE. H,I,J: Restoration of apical-basal polarity in Cas9-RP11VS-RPE.	121
Figure 7.1. Sequencing of a MSR1 region adjacent to <i>PRPF31</i> core promoter in control WT3 iPSC. All cell lines showed the same sequence. Work performed by Ms Kasia Bialas.	133
Figure 7.2. Distribution of RPE cells derived from iPSC control WT3 (AD4), RPE-iPSC patient RP11S1 (F116), early RPE-iPSC and control iPSC WT3 (AD4).	134

List of Tables

Table 1.1. List of the 89 RP-associated genes (RetNet), their inheritance mode and the overlap between some genes and inheritance modes. Seven genes (in bold) are associated with either adRP or arRP.	5
Table 1.2. Comparison of published methods for the reprogramming of human somatic cells into iPSCs. Adapted from Rao and Malik (2012).	27
Table 3.1. Age matched controls and PRPF31-mutant patients used in this study. All patients, shown in column 'Sample No.', are named as RP11 followed by A (asymptomatic), M (moderate), S (severe) and VS (very severe) and two unaffected controls are referred to as WT1 and WT3.	66
Table 3.2. Reprogramming efficiencies of control and PRPF31 lines. The number of clones generated is an estimate of the total number of clones that were originated from the transduced cells plated on MEF feeder plates (230.000 cells per plate) over a period of 30 days. The reprogramming efficiency for each cell line was calculated using the number of clones generated and the original number of fibroblasts that were transduced with Sendai containing reprogramming transgenes.	73
Table 3.3. Summary of cytogenetic analysis of controls and PRPF31-mutated cells lines by SNP array. No abnormalities were detected in the controls and PRPF31-iPSC lines.	81

Abbreviations

A3SS	Alternative 3' splice sites
ADRP	Autosomal dominant RP
AFP	Alpha-fetoprotein
AMD	Age-related macular degeneration
AP	Alkaline phosphatase
ARRP	Autosomal recessive RP
ASOS	Antisense oligonucleotides
BEST-1	Bestrophin-1
BFGF	Fibroblast growth factor
BMP	Bone morphogenic protein
C-IV	Collagen IV
CMD	Cellular memory disc
CNOT3	CCR4-NOT transcription complex
CNVs	Copy number variants
DEAH	Asp-Glu-Ala-His
DHA	Docosahexaenoic acid
EBS	Embryoid bodies
EC	Embryonal carcinoma
ELISA	Enzyme-linked immunosorbent assay
ESCs	Embryonic stem cells
FOXA2	Forkhead box protein A2
GO	Gene Ontology
HAND1	Heart- and neural crest derivatives-expressed protein 1
HEK293	Human embryonic kidney 293 cells
ICC	Immunocytochemistry
ICM	Inner cell mass
IFT	Intraflagellar transport
iPSCs	Induced pluripotent stem cells
LCA	Leber congenital amaurosis

LIF	Leukemia inhibitory factor
LM	Long mutant
MERTK	Mer tyrosine kinase
MET	Mesenchymal-epithelial transition
MFI	Median fluorescence intensity
MIRNAs	MicroRNAs
MITF	Melanocyte Inducing Transcription Factor
MSR1	Minisatelite repeat element 1
NGS	Next generation sequencing
NIC	Nicotinamide
NMD	Nonsense-mediated mRNA decay
ONL	Outer nuclear layer
PAX6	Paired box-6
PBS	Phosphate Buffer Saline
PEDF	Pigment epithelium-derived factor
POS	Photoreceptors outer segments
PRPF31	Pre-mRNA splicing factor 31
PRPFS	Pre-mRNA processing factors
PRPH2	Peripherin 2
PSC	Pluripotent stem cells
PTC	Premature termination codon
QRT-PCR	Quantitative real time polymerase chain reaction
RHO	Rhodopsin
RI	Retained introns
RMATS	Replicate Multivariate Analysis of Transcript Splicing
RNP	Ribonucleoprotein
RP	Retinitis pigmentosa
RPE	Retinal pigment epithelium
RT-PCR	Reverse transcription polymerase chain reaction
RTS	Reprogramming transgenes
SBFSEM	Serial Block Face SEM

SCID	Severe combined immunodeficient
SEM	Standard error of mean
SFEB	Serum-free floating culture of embryoid body-like aggregates
SHH	Sonic Hedgehog
SHRNA	Short-hairpin RNA
SM	Short mutant
SMA	Smooth muscle actin
SNPs	Single nuclear polymorphisms
SNVs	Single nucleotide variants
SSEA	Stage specific embryonic antigens
SSODN	Single-stranded oligodeoxynucleotide
TEM	Transmission Electron Microscopy
TER	Transepithelial resistance
TGF- β	Transforming growth factor β
TGF- β	Transforming growth factor β
TRA-1-60	Tumor-rejection antigen 1-60
TRI-SNRNP	Tri-small nuclear ribonucleic protein
TUJ1	β III tubulin
VEGF	Vascular endothelial growth factor
VPA	Valproic acid
WT	Wild type
XLRP	X-Linked RP

Chapter 1 - Introduction

1.1. Retinitis Pigmentosa (RP)

1.1.1. Definition of RP

Retinitis pigmentosa (RP) is the clinically descriptive name given to a diverse group of hereditary retinal diseases in which gene mutations, typically affecting primarily the rod photoreceptors, gradually leads to visual loss (Figure 1.1). Patients with RP classically present symptoms such as dark adaptation or “night blindness”, followed by “tunnel vision”, which can lead to loss of central vision later on in the disease caused by secondary degeneration of cones. The name ‘retinitis pigmentosa’ refers to pigment deposits present in the retina of RP patients. (Pagon, 1988; Openshaw, 2008; Verbakel et al., 2018).

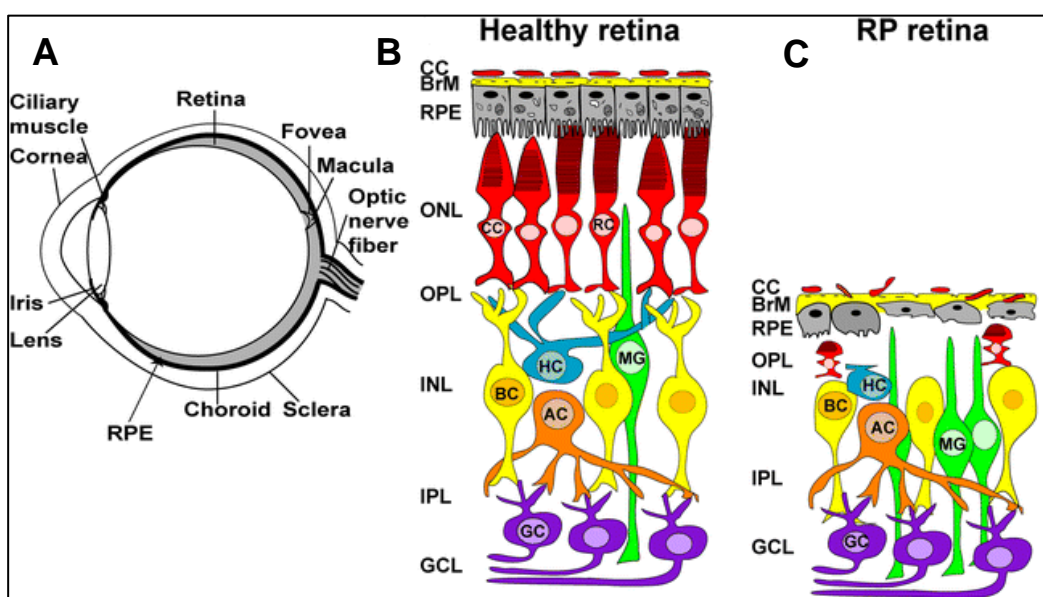


Figure 1.1. Overview of a healthy and an affected retina by RP. A: Schematic representation of a cross-section of the human eye. B: Schematic representation of a healthy laminated retina. Choroidal capillaries (CC); Bruch's membrane (BrM); Retinal pigment epithelium (RPE); Outer nuclear layer (ONL), containing rod cells (RC) and cone cells (CC); Outer plexiform layer (OPL); Inner nuclear layer (INL), containing horizontal cells (HC), müller cells (MC), bipolar cells (BC) and amacrine cells (AC); Inner plexiform layer (IPL) and Ganglion cell layer (GCL), containing ganglion cells (GC). C: Schematic representation of an affected retina by RP. Adapted from Singh (2018).

1.1.2. Classification of RP

Retinitis pigmentosa can be classified as non-syndromic, syndromic or systemic. It is non-syndromic or "simple" when it does not affect other organs or tissues; syndromic, when it affects other neurosensory systems such as hearing; or systemic, when it affects multiple organs (Pagon, 1988; Fahim *et al.*, 2017).

In the majority of cases, RP is an isolated disorder (simple or non-syndromic); only the sight is affected. However, 20-30% of RP syndromes can happen when RP is combined with extra-ocular abnormalities. One example of this is Usher syndrome, in which individuals develop hearing and sight loss. Others include Refsum, Alström, Joubert syndrome (JBTS), and Laurence-Moon-Bardet- Biedl (LMBB) syndromes (Ferrari *et al.*, 2011; Verbakel *et al.*, 2018).

This project focuses on a non-syndromic form of RP. The inheritance modes of non-syndromic RP include autosomal dominant, autosomal recessive, or X-linked. Rare digenic forms also occur (Kajiwara *et al.*, 1994).

1.1.3. Inheritance modes

Autosomal Dominant RP

Autosomal dominant inheritance mode accounts for approximately 15-25% of all RP cases, occurring when a mutation affects one gene of a pair of autosomes and only one copy of a gene is sufficient to cause RP (RetNet; Fahim *et al.*, 2017; Bhatia *et al.*, 2018). Men and women are equally affected, and the mutated gene is passed on from an affected parent to a son or a daughter. The chance of a child being affected is 50:50 in each pregnancy (Fahim *et al.*, 2017).

Autosomal dominant RP (adRP) can be very variable between and within the same families. Some family members can be affected mildly and others more severely, despite of their ages. Occasionally the effects of the adRP gene seem to 'skip a generation' due to the variability in the severity of RP in different individuals or generations (Fahim *et al.*, 1993; Haim, 2002; Fahim *et al.*, 2017).

To date, about 30% of all RP mapped genes account for adRP, including *ADIPOR1*, *ARL3*, *BEST1*, *CA4*, *CRX*, *FSCN2*, *GUCA1B*, *HK1*, *IMPDH1*, *IMPG1*, *KLHL7*, *NR2E3*, *NRL*, *PRPF3*, *PRPF4*, *PRPF6*, *PRPF8*, *PRPF31*, *PRPH2*, *RDH12*, *RHO*, *ROM1*, *RP*, *RP9*, *RPE65*, *SAG*, *SEMA4*, *SNRNP200*, *SPP2*, and *TOPORS* (RetNet).

The most common cause of adRP are mutations in the rhodopsin (*RHO*) gene, the first identified gene involved in adRP (Dryja *et al.*, 1990), accounting for approximately 30-40% of all autosomal dominant mutations, followed by peripherin (*PRPH2*) gene (5-10%) and the pre-mRNA splicing factor (*PRPF31*) gene (2.5-5%). These genes together are responsible for 40-50% of all adRP cases (RetNet; Fahim *et al.*, 2017).

Autosomal Recessive RP

Autosomal recessive RP (arRP) accounts for approximately 5-20% of all RP cases and, like adRP, it affects men and women in the same way, as the mutated genes are harboured on the autosomal chromosomes. Both copies of the relevant gene are defective in arRP. An affected individual inherits one faulty gene from each parent, called 'carriers' when they also have one normal copy of the gene. Each child of carrier parents has a 50% chance of being an asymptomatic carrier, a 25% chance of being affected and a 25% chance of being unaffected and not carry the faulty gene (RetNet; Fahim *et al.*, 2017).

To date, over 60 genes have been associated with arRP. The most common arRP-associated gene is *USH2A*. Mutations in *USH2A* are responsible for 10 to 15% of all cases of autosomal recessive retinitis pigmentosa (RetNet; Fahim *et al.*, 2017).

X-Linked RP

X-Linked RP (xLRP) inheritance mode accounts for approximately 5-15% of all RP cases (Fahim *et al.*, 2017). Retinal diseases in females with xLRP are less severe than that noticed in males because heterozygous xLRP females may be unaffected or express minimal retinal degeneration (Souied *et al.*, 1997; Grover *et al.*, 2000). In contrast, males and females are equally affected in adRP. Some families, in which females are affected with xLRP, can be mistaken for families with adRP (Daiger *et al.*,

2008). Three genes have been associated with xLRP: *OFD1*, *RP2* and *RPGR*. *RPGR* accounts for 15% of male xLRP cases (RetNet).

Although different types of retinitis pigmentosa are well documented, it is still difficult to classify RP into specific groups, as RP is a complex class of diseases in which mutations in many different genes can cause the same RP phenotype. In addition to that, many different disease-associated mutations can occur in the same gene due to high allelic heterogeneity, and some mutations in the same gene can cause different phenotypes. For instance, mutations in the rhodopsin (*RHO*) gene can cause autosomal dominant RP or autosomal recessive RP (Table 1.1). Mutations in the peripherin (*PRPH2*) gene can cause autosomal dominant macular degeneration, autosomal dominant RP, or, with a mutation in *ROM1*, it can cause digenic RP. Digenic inheritance mode occurs when mutations inherited in two different genes are required to cause the disease (Daiger *et al.*, 2007; Schaffer, 2013; Fahim *et al.*, 2017).

Because of the reasons described above, around 40% of RP cases haven't been classified or are treated as simplex, referring to a single occurrence of a disorder in a family (Fahim *et al.*, 2017).

autosomal dominant Retinitis Pigmentosa (adRP)	autosomal recessive Retinitis Pigmentosa (arRP)		X-linked Retinitis Pigmentosa (xLRP)
30 genes	63 genes		3 genes
<i>ADIPOR1</i>	<i>ABCA4</i>	<i>MAK</i>	<i>OFD1</i>
<i>ARL3</i>	<i>AGBL5</i>	<i>MERTK</i>	<i>RP2</i>
<i>BEST1</i>	<i>AHR</i>	<i>MVK</i>	<i>RPGR</i>
<i>CA4</i>	<i>ARHGEF18</i>	<i>NEK2</i>	
<i>CRX</i>	<i>ARL6</i>	<i>NEUROD1</i>	
<i>FSCN2</i>	<i>ARL2BP</i>	<i>NR2E3</i>	
<i>GUCA1B</i>	<i>BBS1</i>	<i>NRL</i>	
<i>HK1</i>	<i>BBS2</i>	<i>PDE6A</i>	
<i>IMPDH1</i>	<i>BEST1</i>	<i>PDE6B</i>	
<i>IMPG1</i>	<i>C2orf71</i>	<i>PDE6G</i>	
<i>KLHL7</i>	<i>C8orf37</i>	<i>POMGNT1</i>	
<i>NR2E3</i>	<i>CERKL</i>	<i>PRCD</i>	
<i>NRL</i>	<i>CLCC1</i>	<i>PROM1</i>	
<i>PRPF3</i>	<i>CLRN1</i>	<i>RBP3</i>	
<i>PRPF4</i>	<i>CNGA1</i>	<i>REEP6</i>	
<i>PRPF6</i>	<i>CNGB1</i>	<i>RGR</i>	
<i>PRPF8</i>	<i>CRB1</i>	<i>RHO</i>	
<i>PRPF31</i>	<i>CYP4V2</i>	<i>RLBP1</i>	
<i>PRPH2</i>	<i>DHDDS</i>	<i>RP1</i>	
<i>RDH12</i>	<i>DHX38</i>	<i>RP1L1</i>	
<i>RHO</i>	<i>EMC1</i>	<i>RPE65</i>	
<i>ROM1</i>	<i>EYS</i>	<i>SAG</i>	
<i>RP1</i>	<i>FAM161A</i>	<i>SAMD11</i>	
<i>RP9</i>	<i>GPR125</i>	<i>SLC7A14</i>	
<i>RPE65</i>	<i>HGSNAT</i>	<i>SPATA7</i>	
<i>SAG</i>	<i>IDH3B</i>	<i>TRNT1</i>	
<i>SEMA4A</i>	<i>IFT140</i>	<i>TTC8</i>	
<i>SNRNP200</i>	<i>IFT172</i>	<i>TULP1</i>	
<i>SPP2</i>	<i>IMPG2</i>	<i>USH2A</i>	
<i>TOPORS</i>	<i>KIAA1549</i>	<i>ZNF408</i>	
	<i>KIZ</i>	<i>ZNF513</i>	
	<i>LRAT</i>		

Table 1.1. List of the 89 RP-associated genes (RetNet), their inheritance mode and the overlap between some genes and inheritance modes. Seven genes (in bold) are associated with either adRP or arRP.

1.1.4. Epidemiology of RP

The prevalence of non-syndromic RP is estimated to be between 1:3,000 to 1:5,000 people (Pagon, 1988; Chizzolini *et al.*, 2011). Haim (2002) calculated that the prevalence of RP in the US and Europe is approximately 1:3,500 to 1:4,000.

The prevalence of RP does not seem to be related to ethnic specificity, however, the range of mutations in a particular gene may be different among populations or due to a high rate of consanguinity, as seen in isolated communities. In these cases,

prevalence can be 1:2,400 or more (Heckenlively *et al.*, 1981; Puech *et al.*, 1991), reaching as high as 1:750, depending on the geographic region (Nangia *et al.*, 2012). Moreover, the frequency of a given recessive or dominant mutant allele in a distinct population may be high due to the founder effect, or it may change as a result of genetic drift (Sullivan *et al.*, 2006).

Mutations in *PRPF31* gene account for 2.5-5% of adRP (Hartong *et al.*, 2006; Sullivan *et al.*, 2006; Fahim *et al.*, 2017), the third most common contributor to adRP behind mutations in rhodopsin and peripherin genes.

1.1.5. Clinical presentation of RP

Age of onset

In the non-syndromic form of RP, the signs and symptoms of the RP are normally related to loss of vision, but the clinical findings can vary a lot due to the large number of genes involved in RP and their several alleles. The age at which individuals acquire, develop or first experience RP can vary greatly. Some patients are diagnosed with RP during childhood, whilst others are affected later in life (Fahim *et al.*, 2017).

Night blindness

The first symptom of RP is generally deficient dark adaptation (called nyctalopia or "night blindness"), as a result of the degeneration of rod photoreceptors. RP is also described as rod-cone dystrophy due to the gradual loss of rod photoreceptors, followed by secondary degeneration of cones. Peripheral vision loss normally occurs early in the disease but since the loss is very gradual, and changes are not obvious during day and artificial light, it is not often recognised as a symptom by the affected individuals. The more severe cases of RP tend to have an earlier age of onset (Hamel, 2006; Fahim *et al.*, 2017; Martin-Merida *et al.*, 2017).

Tunnel vision

The quality of vision in patients with RP usually remains the same in early stages of the disease, but it decreases with time and the field of vision becomes constricted due to the gradual degeneration of rods, leading to what is called as “tunnel vision” (Figure 1.2). At this point, patients find reading too difficult and they can no longer move autonomously. Both eyes are affected in a similar way (Hamel, 2006; Verbakel *et al.*, 2018).



Figure 1.2. Images of a normal visual field (left panel) and tunnel vision (right panel). The blackness surrounding the central image indicates loss of peripheral vision.

Visual acuity

Visual acuity is retained in early stages of the disease. With disease progression, quality of vision is decreased, but central visual acuity is usually preserved until the final stages of the disease. Some mutations affect both rods and cones and cone function can be affected soon after the death of rods around the fovea. In RP patients, the presence of macular lesions, which is estimated to occur in about 10% to 50% of individuals with RP, is also related with loss of central visual acuity (Hamel, 2006; Gandra *et al.*, 2008).

Fundus appearance

The appearance of the ocular fundus in patients with RP is normally related to the stage of the disease. The fundus usually appears normal in the early stages of RP, even if the electroretinogram (a test to measure the electrical responses of retinal cells in response to a light stimulus) reveals defective rod responses. Arteriolar narrowing and waxy pallor of the optic disc nerve head can be observed later on in the disease. In mid stages of RP, it's possible to see bone spicule-shaped pigment deposits in the periphery and/or mid periphery of the retina, which are clumps of melanin from the RPE that detaches from Bruch membrane and migrates to the inner retina (Figure 1.3) (Li *et al.*, 1995). Absence of pigment deposits may also occur and the term *retinitis pigmentosa sine pigmento* has been used to describe a normal appearance of the retina, despite abnormal function of photoreceptors (Hamel, 2006; Ghazawy *et al.*, 2007; Fahim *et al.*, 2017).



Figure 1.3. Photographs of a normal (left) and RP retina (right). Typical features of RP, such as waxy optic disc pallor, retinal vascular narrowing and 'bone spicule' intra-retinal pigmented deposits, are clearly observed in the RP retina. Reproduced from Farrar *et al.* (2002).

Cataract is also common in all forms of RP. The severity of the cataract is normally related with the age of the individual with RP and its cause in the disease is unknown. Almost half of individuals with RP eventually need cataract surgery (Fahim *et al.*, 1993).

1.1.6. Pathophysiology of RP

The pathophysiology of RP starts as a sequence of metabolic abnormalities that initially cause rod photoreceptor degeneration and retinal pigment epithelium (RPE) defects (Berson, 1993; Haim, 2002). Cone degeneration may also follow rod degeneration, causing complete blindness.

Histopathologic and histologic changes in RP have been well documented and have also been associated with specific mutations in RP genes (Daiger *et al.*, 2013). The shortening of the outer segments in rods is the first histologic change noticed in the retina. Since the outer segments gradually shorten, loss of the rod photoreceptor can be detected. As rods are located in the midperipheral retina, cell degeneration in this area leads to peripheral vision loss and night blindness (Milam *et al.*, 1998). The reduction of nuclei in the outer nuclear layer of these regions is a result of cell apoptosis (Figure 1.4). Death of cones can only be seen when rods are decreased to a single row of cells. Punzo *et al.* (2009) suggested that cell density could be the reason for the progressive and late nature of cone degeneration. Another hypothesis claims that cones are dependent on trophic factors produced by the rods (Kolomeyer and Zarbin, 2014). A recent study, however, has shown that increased oxygen levels in the outer retina, after death of rods, leads to progressive oxidative stress and consequent death of cones (Campochiaro and Mir, 2018).

It's still not clear what causes the attenuation of retinal vessels in RP. A plausible hypothesis is that with death of photoreceptors, and consequently death of retinal ganglion cells, the reduced consumption of oxygen leads to vasoconstriction and reduced blood flow in retina vessels (Grunwald *et al.*, 1996; Penn *et al.*, 2000; Yu and Cringle, 2005; Padnick-Silver *et al.*, 2006). Another hypothesis proposes that loss of synaptic input and reduction of trophic factors as a result of death of photoreceptors induces vascular remodeling and vessel attenuation (Stone *et al.*, 1992). Followed by photoreceptors degeneration, the RPE then detaches from the Bruch membrane and migrates into the inner retinal layers forming the bone spicules retinal structures, which names the disease (Li *et al.*, 1995; Shintani *et al.*, 2009). The mechanism that triggers RPE migration is still not know, but it should reflect the dependent correlation between the choroid, RPE and photoreceptors (Jaissle *et al.*, 2010). At this stage, disorganisation of the inner nuclear layer is also noticed. The waxy pallor of the optic

disc is likely caused but the overgrowth of ganglion cells inside the optic disc due to the increased light reflectance (Szamier, 1981; Hwang and Kim, 2012).

Currently, photoreceptor apoptosis is not well understood as the kinetics of rod death is quite distinct for different genes (Punzo *et al.*, 2009). Mutations in RP genes normally result in truncated proteins involved in phototransduction cascades, photoreceptor structure and visual cycle, leading to photoreceptor cell death (Camacho and Wirkus, 2013). Degeneration of photoreceptors associated with RP, although triggered by various processes, is primarily genetic (Shastry, 1994; Hartong *et al.*, 2006; Bowne *et al.*, 2008; Neidhardt *et al.*, 2008; Shastry, 2008; Shintani *et al.*, 2009; Buskamp *et al.*, 2010).

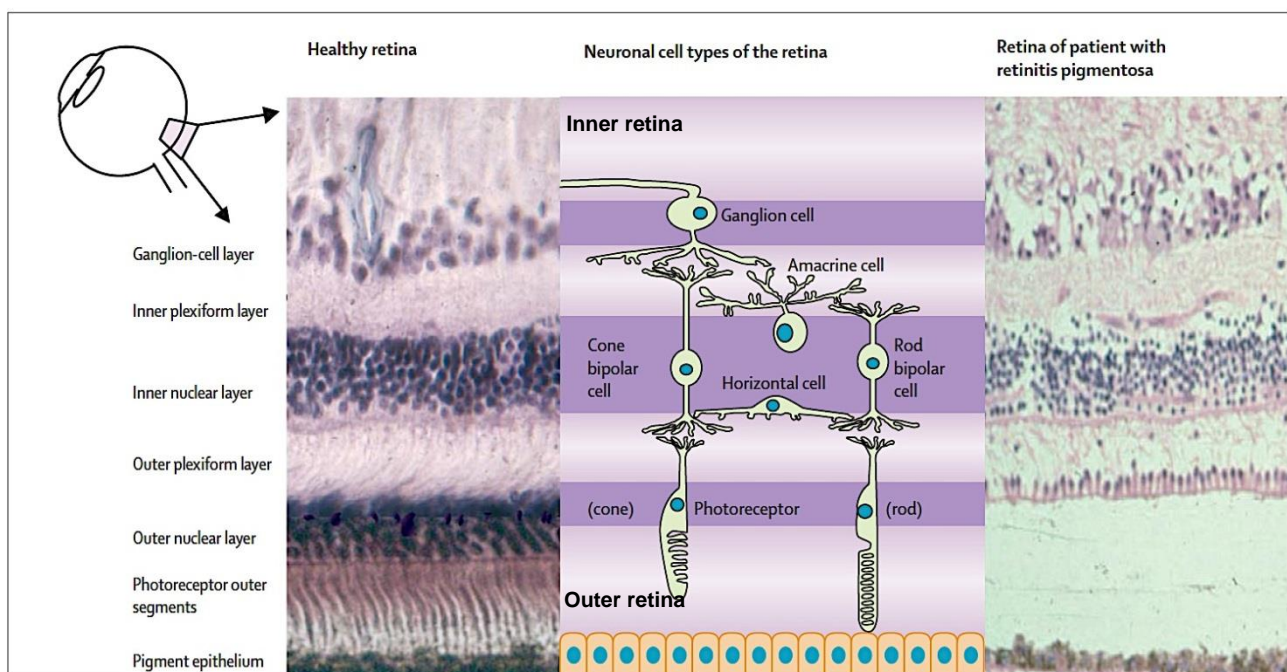


Figure 1.4. Histological appearance of healthy human retina (left) and retina of a patient with retinitis pigmentosa (right). The space between the retinal pigment epithelium and the outer nuclear layer in the diseased retina is a processing artefact. Reproduced from Hartong *et al.* (2006).

To date, over 80 genes have been linked to non-syndromic RP (RetNet). Some of these genes are involved in important processes within photoreceptors and/or RPE, such as pathways related to the visual cycle or phototransduction. Other genes have been linked to an underlying structure, such as primary or connecting cilium, and are ubiquitously expressed (Verbakel *et al.*, 2018). For instance, the autosomal dominant genes *PRPF31*, *PRPF8*, and *PRPF3* encode protein components of the spliceosome, a very important macromolecular machine that removes introns from pre-mRNA

transcripts, joining the exons. These proteins are highly conserved in eukaryotes, so the fact that mutations in these genes lead to retinitis pigmentosa without other evidence of systemic disease in patients is especially intriguing.

It has been demonstrated that high levels of alternative splicing occur in the vertebrate nervous system, being essential for brain development and function. Murine photoreceptors have their own specific splicing programme, starting prior to the development of outer segments, as shown by Murphy et al. (2016). The retina's splicing programme seems to primarily affect transcripts of cilia genes, including photoreceptor connecting cilia and RPE primary cilia, which are required for phototransduction in photoreceptors and maturation of the RPE, respectively (May-Simera et al., 2018).

1.1.7. *PRPF31* gene organisation and protein structure

The *PRPF31* pre-mRNA processing factor 31 gene was identified as an adRP-associated gene and is located in chromosome 19 at position 19q13.42. It spans approximately 16 kB of DNA and encompasses 14 exons (Vithana et al., 2001) (Figure 1.5).

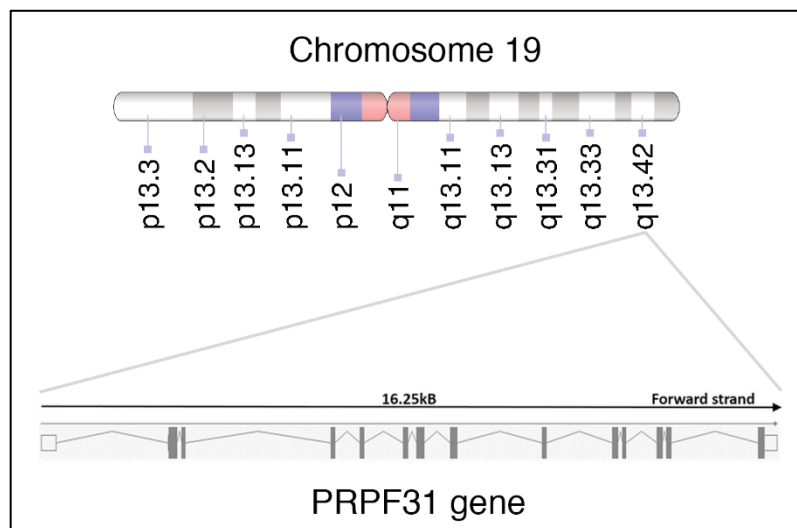


Figure 1.5. Location and structure of *PRPF31* gene. This gene is located in the long arm of chromosome 19 and encompasses 14 exons. Exon-intron arrangements and untranslated regions are shown. Adapted from Rose et al. (2017) and NCBI.

PRPF31 gene encodes a widely expressed pre-mRNA splicing factor, a protein of 499 amino acids and 61 kDa. The initiation and stop codons, ATG and TAG, are

present in exons 2 and 14, respectively (Vithana *et al.*, 2001; Rose *et al.*, 2017). PRPF31 protein has a NOP domain, which is a highly conserved ribonucleoprotein (RNP) binding motif, that contains both RNA and protein binding surfaces (Figure 1.6). During the splicing cycles, NOP domain mediates protein-protein interactions and they may be involved in RNA binding (Liu *et al.*, 2007).

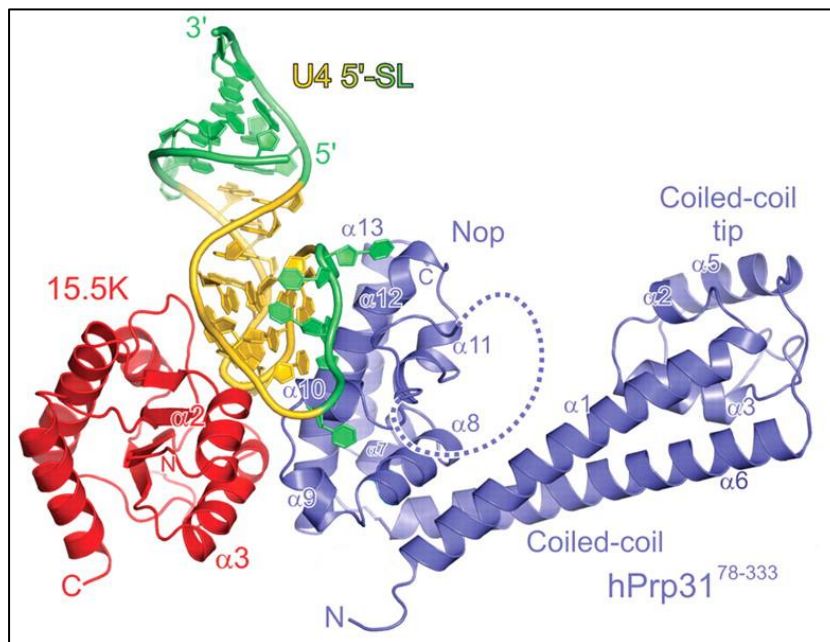


Figure 1.6. Representation of PRPF31 protein. Alpha helical NOP domain (blue), 15.5K/SNU13 (red) and U4/U5 (yellow/green backbone). Adapted from Liu *et al.* (2007).

1.1.8. Role of PRPF31 protein

The *PRPF31* gene, or pre-mRNA processing factor 31, is one of many retinitis pigmentosa-associated genes. This gene encodes a splicing factor required for the formation of U4/U6.U5 tri-small nuclear ribonucleic protein (tri-snRNP) complex, which is a constituent of the pre-mRNA processing spliceosome (Mordes *et al.*, 2006; Linder *et al.*, 2011) (Figure 1.7).

Pre-mRNA splicing is the process in which intervening sequences are removed from the new transcripts, joining the exons together to produce mature messenger RNAs. The spliceosome, a large macromolecular complex, catalyses the splicing in the nuclei of cells and it goes through a dynamic and stepwise process of assembly, activation and catalysis during each splicing cycle (Rose *et al.*, 2017).

During the assembly, U1 snRNP recognizes the 5' splice site of an intron and U2 snRNP targets the other end, the 3' splice site, defining the boundaries of the intron and formation of complex A, or pre-spliceosome (Figure 1.7). At the same time, U4, U6 and U5 snRNP, with PRPF31, preassemble to form the tri-SNP, which is the main component of the spliceosome and it's necessary for the spliceosome activation. The integration between complex A and the tri-RPN forms the pre-catalytic complex B. During the activation step, U1 dissociates from 5' and U4 snRNP dissociates from the complex B, activating the spliceosome through the generation of the catalytic complex B. The catalytic step involves two main reactions. In the first one, a DEAH (Asp-Glu-Ala-His) box helicase catalyses the first splice at the 5' end, forming the catalytic C complex, which then catalyses the splice at the 3' end and the intron is released. The remaining of the snRNP are then disassembled and stored into cajal bodies in the nucleus, to be re-used in other splicing cycles (Zhou *et al.*, 2002; Wahl *et al.*, 2009; Zhao *et al.*, 2009; Rose *et al.*, 2017) (Figure 1.7).

PRPF31 interacts with U4 and is vital during U4/U6.U5 tri-snRNP assembly and maintenance in (Weidenhammer *et al.*, 1997; Liu *et al.*, 2006). Knock-out of *PRPF31* in mammalian cells by RNAi has been shown to stop spliceosome assembly and then splicing, which can lead to cell death by apoptosis (Schaffert *et al.*, 2004).

The splicing reaction can either produce just one type of mRNA or various populations of mRNA transcripts, through the process of alternative splicing. The human genome project has revealed that only 20,000-25,000 genes exist, but there are about four times more proteins in human cells, highlighting the importance of alternative splicing in proteomics (Stetefeld and Ruegg, 2005). It has been shown that out of 20,000-25,000 human protein coding genes, 90-95% undergo some levels of alternative splicing and 37% of all coding genes generate different protein isoforms, suggesting that alternative splicing profoundly contributes to proteome complexity. It has also been established that specific splicing programmes have a big role in cell differentiation, lineage specification; acquisition and maintenance of tissue-identity, and organ development (Kalsotra *et al.*, 2008; Pan *et al.*, 2008; Wang *et al.*, 2008; Kim *et al.*, 2014; Scotti and Swanson, 2016; Baralle and Giudice, 2017).

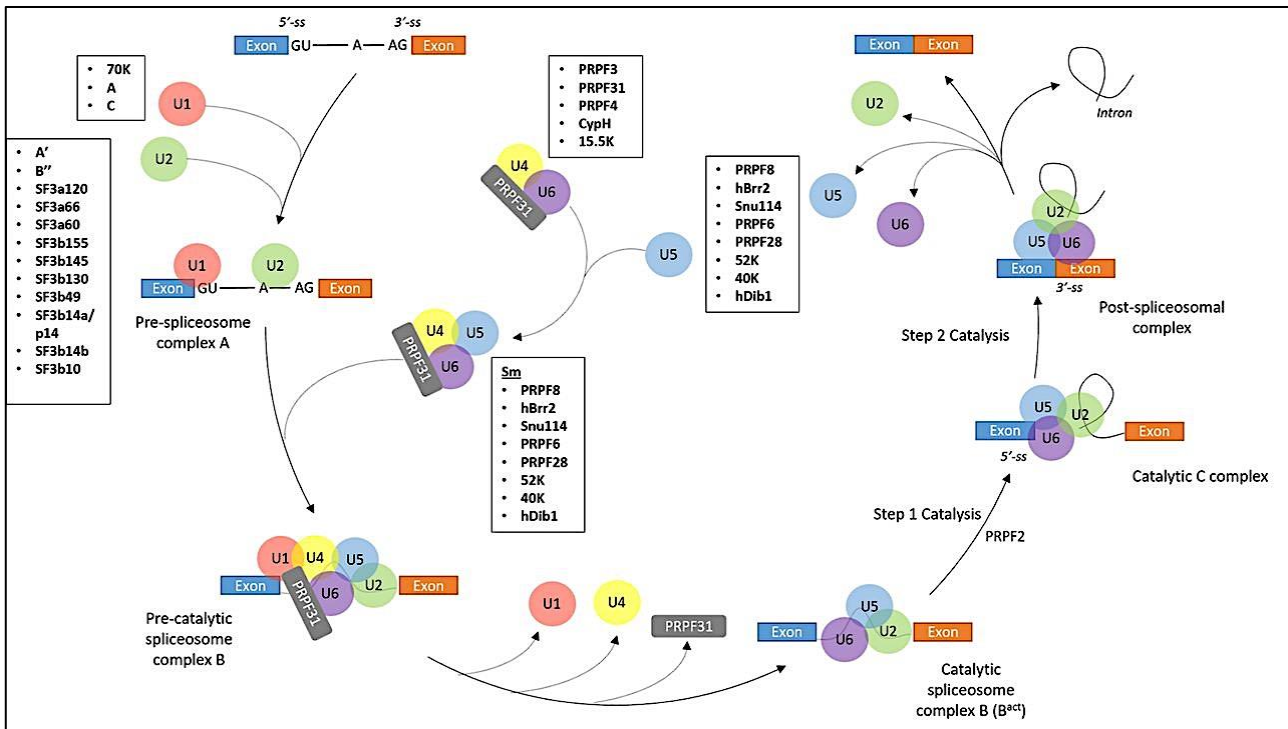


Figure 1.7. Spliceosome assembly and function. PRPF31 (grey box) interacts with U4 and is required during U4/U6.U5 tri-snRNP assembly and maintenance in spliceosomes. Reproduced from Rose *et al.* (2017).

1.1.9. Impact of PRPF31 mutations in the Retina

Mutations in the core components of the spliceosome are known to cause retinal degenerative disorders and cancer (Vithana *et al.*, 2001; Farkas *et al.*, 2014; Kurtovic-Kozaric *et al.*, 2015; Shirai *et al.*, 2015). *PRPF31* gene, which is widely expressed, would be expected to play an important role in mRNA splicing in most tissues. However, until now, *PRPF31* mutations have been only linked to RPE disorders and photoreceptors degeneration, resulting in retinal disease phenotype (Farkas *et al.*, 2014; Villanueva *et al.*, 2014; Martin-Merida *et al.*, 2017; Bhatia *et al.*, 2018).

Some hypotheses have been postulated to explain how mutations in splicing factors affect retina-specific cells. One of them is based on the premise that photoreceptors would be more vulnerable to a reduced splicing activity than any other cell type. According to this hypothesis, splicing deficiency caused by mutations in splicing factors would affect all cell types, but photoreceptors would be more vulnerable because of their high demand for mRNA transcripts. This could be explained due to haplo-insufficiency: only one functional copy of *PRPF31* would not generate enough protein for functional splicing of genes expressed in rods due to the rapid renewal of

outer segments in rod cells. The whole rod outer segment is renewed within 10 days and there are about 120 million rods in the human retina. This model postulates that mRNA levels produced by the retina would exceed the mRNA amount produced by other tissues (Baehr and Chen, 2001).

An alternative hypothesis proposes that those mutations do not affect splicing in all tissues but only impair the splicing patterns in retinal genes. Two plausible explanations for this specificity include the vulnerability of the photoreceptors to defective splicing during its outer segment renewal and the functional consequence of the mutations themselves. Previous studies (Deery *et al.*, 2002) revealed that mutations in *PRPF31* result in reduction of functional protein levels in the nucleus and this could lead to deficiency of splicing function in retina cells. The lack of any effects in other tissues suggests that the protein levels from only one wild-type allele would be sufficient to meet the minimum splicing demand in other cells types, resulting in normal cell function (Vithana *et al.*, 2003).

A third model claims the existence of retina-specific isoforms. These isoforms would be translated into proteins with specific functions in the retinal tissue, and therefore, mutations in *PRPF31* would alter the population or the ratio of expression of those isoforms in the retina (Neidhardt *et al.*, 2007).

Incomplete penetrance has also been reported for PRPF31-RP. The gene called CCR4-NOT transcription complex subunit 3 (*CNOT3*) has been identified as a major modifier gene controlling the penetrance of *PRPF31* mutations. This gene is expressed at low levels in asymptomatic individuals, allowing high expression of the wild-type *PRPF31* allele (Venturini *et al.*, 2012). Heterozygous individuals carrying low and high-expressing alleles or homozygous carriers of low-expressing *CNOT3* alleles are asymptomatic for PRPF31-RP. However, two copies of a higher expressing *CNOT3* allele are necessary to cause symptoms in individuals harbouring *PRPF31* mutations (Figure 1.8) (Rose *et al.*, 2014).

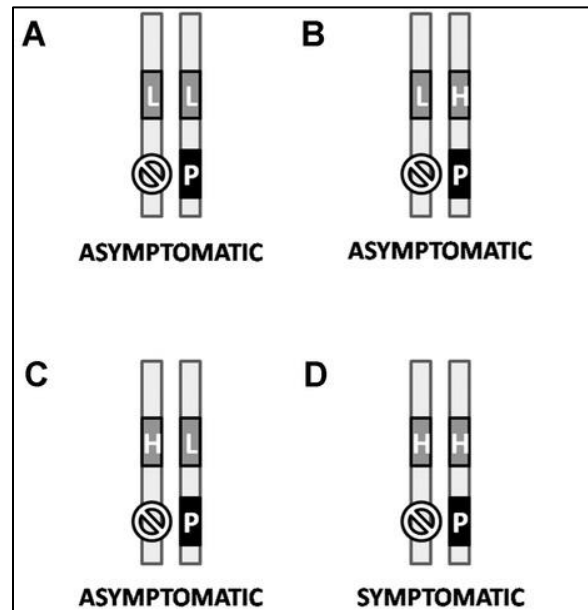


Figure 1.8. *CNOT3* combinations in patients carrying *PRPF31* mutations. L represents a low-expressing *CNOT3* allele, leading to high levels of *PRPF31*; H represents a high-expressing *CNOT3* allele, and due to its repressive nature, leads to lower levels of *PRPF31*; and P represents *PRPF31*. The only symptomatic individual “D” inherits the two copies of high-expressing *CNOT3*, masking *PRPF31* expression. Adapted from Rose *et al.* (2014).

In summary, the pathophysiology of *PRPF31*-RP is poorly understood, and it’s not known why only the retina is affected. Furthermore, the correlation between *PRPF31* and its genetic modifiers, causing different phenotypes for the same mutations, need to be further investigated.

1.1.10. Diagnosis and Management of RP

Usually, RP diagnosis is performed by analysis of electroretinogram and fundus appearance. A multidisciplinary approach combining genotyping and ophthalmology can optimize diagnosis and management of RP. Genotyping can improve the outcome of ophthalmic counselling, since phenotypes can vary greatly within a genetic subtype and even among family members sharing the same mutation. In addition to clinical diagnosis, some centers now perform exome sequencing to identify RP-causing genes, providing a molecular diagnosis in 60-80% of RP patients. The remaining cases that cannot be diagnosed by this method may have specific non-detectable variants including structural rearrangements or mutations in non-coding areas (ie. introns) (Abu-Safieh *et al.*, 2013; Haer-Wigman *et al.*, 2017).

Visual rehabilitation for RP patients with reduced visual acuity is now focusing on the patient's abilities and needs, including mobility and orientation training combined with the use of visual aid such as night goggles and reverse telescopes in order to improve vision. In severe cases, the quality of life of RP-patients can be improved by using text-to-speech software, allowing patients to interpret text, and the use of guide dogs to increase mobility and independence (Verbakel *et al.*, 2018).

Better understanding about genetic causes of RP has been followed by progress in the development of new strategies to treat RP (Scholl *et al.*, 2016). Those strategies can be classified into two groups: genetic approaches, including treatment for gene or mutation-specific; and non-genetic approaches, including therapeutic approaches and transplantation of retinal cells.

Genetic approaches

Genetic-specific approaches are more effective and successful if they are performed in the early stages of the disease, before cell degeneration. In gene-augmentation therapies, constructs containing wild-type copy of cDNA of the gene mutated, are introduced to target cells with the aim of introducing wild type expression to the cells. For RP, recombinant adeno-virus vector is normally the preferred choice to introduce genetic material into the retina. Initial studies using RPE65 gene therapy in patients with LCA and RP were carried out successfully (Bainbridge *et al.*, 2008; Hauswirth *et al.*, 2008; Maguire *et al.*, 2008). Since then, many gene therapy clinical trials phases I and II have been performed including choroideremia (MacLaren *et al.*, 2014), MERTK-RP (Ghazi *et al.*, 2016), CNGA3-achomatopsia, PDE6A-RP, RPGR-xLRP, retinoschisis and Stargardt disease. It's still unclear if this kind of treatment would result in long-lasting benefits for the patients, how much of the genetic content would have to be delivered, or if this would have dominant-negative effects in patient cells. Another genetic approach involves the use of antisense oligonucleotides (ASOs) to inhibit gene expression. ASOs can be designed to bind to specific mRNA sequences, causing them to be cut into pieces, and interfere with protein synthesis (Rinaldi and Wood, 2018). New therapies also combine knockdown of defective gene using short-hairpin RNA (shRNA) with replacement of healthy copies of the protein, resistant to shRNA (Cideciyan *et al.*, 2018).

Non-genetic approaches

Currently, there are no conventional standard treatments for patients with RP. There has been some significant effort on the investigation of the effects of nutritional and drug supplements and their ability to stop degeneration and preserve photoreceptor function. Lutein, vitamin A, docosahexaenoic acid (DHA), ascorbic acid and calcium-channel blockers are among the various supplements that have been found to slow retinal degeneration, reducing the decline of visual acuity and changes in electroretinograms (Bazan *et al.*, 1986; Frasson *et al.*, 1999; Berson, 2000; Zhao *et al.*, 2003; Brito-Garcia *et al.*, 2017). Unfortunately, although some studies have found benefits, others have reported no detectable changes (Organisciak *et al.*, 1992; Frasson *et al.*, 1999; Aleman *et al.*, 2001; Pawlyk *et al.*, 2002; Rayapudi *et al.*, 2013).

Another non genetic approach is cell replacement therapy, which is the transplantation of ocular-derived retinal progenitor cells, such as fetal retinal tissue, or non-ocular-derived retinal progenitor cells, such as embryonic stem cells (ESCs) and induced pluripotent stem cells (iPSCs), in patients, which could integrate and produce normal retinal cells (Tang *et al.*, 2017). Both methods have advantages and disadvantages, as described below.

Cell replacement therapy of ocular-derived retinal progenitor cells can be done by the introduction of fetal retina sheets (Seiler *et al.*, 2005) into the subretinal space to replace photoreceptors and RPE and have been transplanted in pre-clinical retinal degeneration models, showing improvement in visual function. Radtke *et al.* (2002) showed that fetal retina cells transplanted into a patient with adRP can survive one year without clinical evidence of rejection and that improvement in visual acuity could be achieved. Fetal stem cells also have the capacity to produce trophic substances, facilitating retinal connections. This process, however, is very inefficient and immunological rejection is also a risk. Other disadvantages are the scarcity of donor material and the ethical debate and controversy involved in extracting fetal stem cells, as fetal tissues and aborted embryos are necessary for treatments. Although there has been published evidence of cellular reconnection after transplantation of fetal retinal stem cell in animal models (Gouras *et al.*, 1991), there was no demonstration that transplanted cells formed functional synaptic connections in the host retina or restore

visual function. MacLaren and Ali (MacLaren *et al.*, 2006) showed that mouse post-mitotic rod precursors isolated from a specific stage of retinal development have a higher probability of success after transplantation. They showed that donor cells could integrate in murine adult or degenerating retina if they are extracted from the developing retina during rod genesis. Those transplanted cells were able to integrate and differentiate into rod photoreceptors. In 2012, the same group showed that transplanted rod precursors formed synaptic connections and generated visual signals, improving visual function (Pearson *et al.*, 2012). However, recent studies have shown that while integration of murine photoreceptor precursor cells occurs, the majority of donor-reporter-labelled cells in the host appears to be originated from material transfer, including proteins and nucleic acids, between donor and host photoreceptors. It's still not clear how long the host retina will benefit from material transfer, as this depends on the viability of the donor cells as well as the half-life and turnover of the material exchanged (Pearson *et al.*, 2016; Waldron *et al.*, 2018; Gasparini *et al.*, 2019).

Cell replacement of non-ocular-derived retinal precursors, from iPSCs or ESCs, in patients is an alternative method to the one described above. iPSCs are patient-specific cells, allowing autologous transplantation of iPSC-derived RPE or photoreceptors, avoiding immunosuppressive treatment, used in the case of ESC transplantation. Additionally, the disease mutation-causing gene can be corrected before transplantation using genome editing techniques (Li *et al.*, 2016). Those treatments, however, are highly individualized and very expensive. Assawachananont *et al.* (2014) demonstrated that transplanted 3D-differentiated mouse ESC or iPSC-derived retinal sheets can further differentiated into different retinal cell types and mature photoreceptors capable of forming outer segments (OS) or synapses in a model of advanced retinal degeneration with absence of outer nuclear layer (ONL). This study provided a 'proof of concept' for transplantation therapy of retinal sheets as it was shown that the transplanted sheets survived well in the host retina, the sheets could also develop to form structured ONL of mature photoreceptors and these photoreceptors could form synaptic connections with bipolar cells from the host retina. However, electrophysiological examinations are needed to confirm the presence of light responses from the grafted cells and their ability to transmit signals to the host. Zhong *et al.* (2014) showed that human iPSC cells formed fully laminated 3D retinal tissue and begun to develop outer-segment discs *in vitro*, before transplantation, which reached the stage of photosensitivity.

Several transplantations of both fetal-RPE and ESC derived-RPE have been conducted and some are currently in phases I/II of clinical trials (www.clinicaltrials.gov). The most common risk in these clinical trials has been associated with the use of immunosuppressants (Schwartz *et al.*, 2012; Schwartz *et al.*, 2015), thus opening the way for transplantation of autologous RPE cell sheets derived from iPSCs to treat age-related macular degeneration (AMD) (Hirami *et al.*, 2009; Kamao *et al.*, 2014). Serious concerns were raised about the safety of the procedure after reports had linked iPSC genomic instability and tumorigenicity. As a result, the following transplantation of iPSC-derived RPE sheet was cancelled in 2015 (Garber, 2015; Chakradhar, 2016) and re-opened later on, proving the procedure was safe and feasible in the treatment of another patient (Mandai *et al.*, 2017). Phase I/II clinical trials to treat RP are also being carried out for the safety, tolerability and efficacy of human retinal progenitor cells-stem cell therapy in patients with RP. Preliminary results showed a rapid improvement in vision in the treated eye, when compared to the untreated eye (www.reneuron.com).

Another recent approach for end-stages of RP is the use of electronic retinal implants in patients with little or no light perception. Argus II and Alpha AMS (Mills *et al.*, 2017) work by stimulation the inner retinal layer, when it's still intact, the residual retinal ganglion cells directly, or the bipolar cell layer. Despite some promising results regarding light perception, some challenges still have to be overcome including adverse effects, device durability and resolution (Zrenner, 2013; Cheng *et al.*, 2017).

1.2. Pluripotent Stem Cells

Stem cells are classified based on their developmental potential. Unipotent cells can generate a single cell type (Wagers and Weissman, 2004; Jaenisch and Young, 2008); Totipotent cells, found in the zygote and early blastomeres are able to generate both embryonic and extra-embryonic cell types and pluripotent stem cells are capable of indefinite self-renewal and can differentiate into any cell types of the three embryonic germ layers (endoderm, mesoderm and ectoderm). Embryonic and induced pluripotent stem cells are considered pluripotent (Figure 1.9).

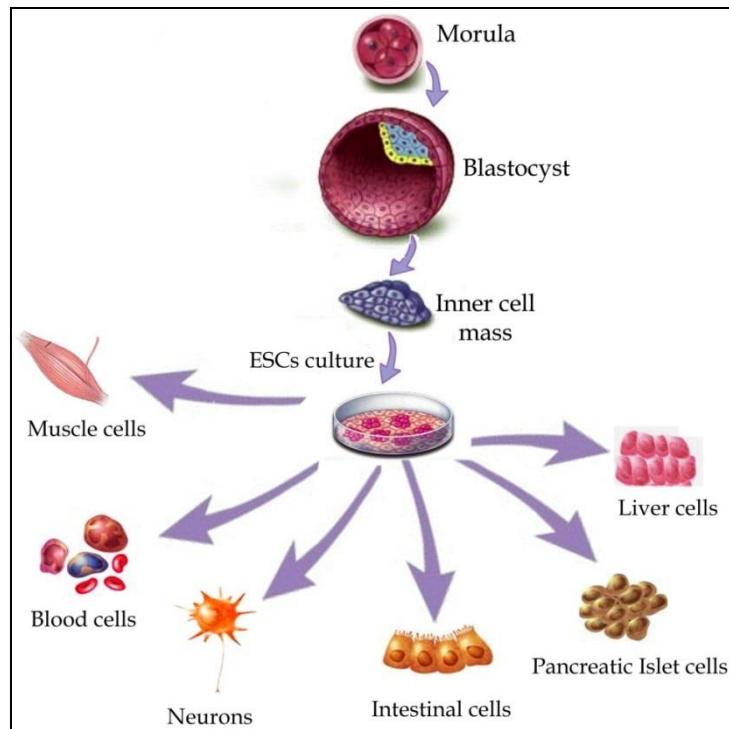


Figure 1.9. Potential of pluripotent embryonic stem cells. The pluripotency is determined by the ability of the cells to differentiate into any cell types belonging to all three germ layers. Reproduced from Meregalli (2011).

1.2.1. Origin of Pluripotent Stem Cells

The first embryonic stem cells (ESCs) were isolated from mouse preimplantation blastocyst-stage embryos in 1981 (Evans and Kaufman, 1981; Martin, 1981). The study of teratocarcinoma, a spontaneous tumour which consists of a mixture of tissues such as hair, muscle, bone and even complete teeth, led to the discovery of embryonic stem cells. In the mid-1970s, it was found that teratocarcinomas contained undifferentiated stem cells and they could be induced in mice by transferring embryos into tissues outside the uterus. These embryonal carcinoma (EC) stem cells have been isolated and grown in culture keeping their undifferentiated status. The work on teratocarcinomas provided the concept of a stem cell that can give rise to the multiple types of tissue (Kleinsmith and Pierce, 1964).

Chromosomal abnormalities, however, were often present in EC cells, limiting their ability to differentiate into a variety of tissue types. Since transferring blastocysts to ectopic sites could induce teratocarcinomas, it was thought that the derivation of

pluripotent cell lines from blastocysts rather than from tumors could also be possible. Martin and Evans did this in 1981 and the result was a stable diploid cell line that could generate all tissues of the adult body, including germ cells.

In 1992 it was shown that mouse primordial germ cells could be directed to form embryonic germ (EG) cells (Matsui *et al.*, 1992). These EG cells have a very similar developmental capacity to that of ESCs, however they show differences in gene expression.

In 1998 James Thomson at the University of Wisconsin-Madison developed a technique to isolate and grow ESCs derived from human blastocysts. This was considered a major breakthrough in embryonic stem cell research and it was achieved by plating the inner cell mass onto a mouse embryonic fibroblast feeder cell layer in the presence of culture media containing bFGF. Following a brief period of attachment and expansion the outgrowth was dissociated and plated onto another feeder cell layer (Thomson *et al.*, 1998). These presented unique features associated with pluripotent stem cells (PSC).

1.2.2. Characteristics of Pluripotent Stem Cells

Pluripotent stem cells, such as ESCs, present some particular features which are always seen in any PSCs. PSCs are derived from a pluripotent cell population; they are diploid and karyotypically normal *in vitro*; they are capable of self-renew in the embryonic state and can differentiate into multiple cell types from all three embryonic germ layers, excluding the extra-embryonic membrane and placental tissue, either in teratomas after grafting or *in vitro* under specific conditions,. The criteria for pluripotency also include derivation of the stem cell line from a single clone. This eliminates the possibility that differentiated products from ESCs are derived from a mixture of heterogeneous cell populations present in the culture (Pera *et al.*, 2000).

Additionally, ESCs express specific markers or characteristics that are similar but not identical to the pluripotent cells present in the inner cell mass. These characteristics include stage specific embryonic antigens (SSEA), enzymatic activities such as alkaline phosphatase (AP), telomerase activity and expression of genes that are down regulated upon differentiation, including *POU5F1* (*OCT4*) and *NANOG*. Under defined conditions, ESCs can proliferate indefinitely maintaining an undifferentiated phenotype

with self-renewing properties. Conventional human ESCs have also been regarded as “primed pluripotent stem cells” (Takahashi *et al.*, 2018).

Naïve pluripotent stem cells, another type of PSCs, can mature into almost any cell type and are more similar to pluripotent cells in the early human embryo than conventional ESCs. Naive PSC state is based on gene expression and genome-wide reduction in methylation levels, which is closer to that of the human cleavage stage embryo (Takahashi *et al.*, 2018).

1.2.3. Induced Pluripotent Stem Cells

In 2006, Takahashi and Yamanaka (2006) demonstrated that stem cells with the same characteristics as ESCs could be generated from mouse fibroblasts by the introduction of four transcription factors at the same time. These cells were designated induced pluripotent stem cells (iPSCs). In 2007, Yamanaka group published another work reporting that human fibroblasts could also be reprogrammed to a pluripotent state by introducing key transcription factors (Takahashi *et al.*, 2007). James Thomson’s group also demonstrated the generation of human iPSCs using a different combination of factors (Yu *et al.*, 2007b).

Three major lines of research led to the discovery and generation of patient specific pluripotent stem cells: the reprogramming by nuclear transfer, the “master” transcription factors and the discovery of ESCs.

First, in 1962, it was shown that unfertilized eggs could receive a nucleus from a frog’s intestinal cell and generate tadpoles (Gurdon, 1962). Three decades later, the birth of Dolly amazed the world as this was the first mammal generated by cloning of mammary epithelial cells (Wilmut *et al.*, 1997). Those two cases demonstrated that even differentiated cells contain all of the genetic information necessary for the development of whole organisms, and that oocytes contain all the factors to reprogram somatic cells.

In 1987, it was demonstrated that a *drosophila* transcription factor could induce the development of legs instead of antennae when expressed ectopically (Schneuwly *et al.*, 1987). Additionally, *MyoD*, a mammalian transcription factor, was shown to convert fibroblasts into myocytes (Davis *et al.*, 1987). Taken together, these results led

to the idea of a “master regulator” that would induce specification of different lineages (Yamanaka and Blau, 2010).

The third line of research involved ESCs. Following the generation of the first mouse ESCs in 1981 (Evans and Kaufman, 1981; Martin, 1981), culture conditions that enabled the long-term maintenance of pluripotency have been established (Smith et al., 1988). Leukemia inhibitory factor (LIF) was found to be a key factor for maintenance of mouse ESCs and later on, fibroblast growth factor (bFGF) was shown to be very important for optimal culture conditions of human ESCs (Thomson et al., 1998).

Yamanaka and Takahashi discovered that the ectopic expression of combined transcription factors (*OCT4*, also known as *POUF51*, *SOX2*, *KLF4*, *C-MYC*, and also *Nanog* and *Lin-28*), were able to reprogram human somatic cells (Takahashi *et al.*, 2007; Yu *et al.*, 2007a). Human iPSCs generated by this cocktail of transcription factors seemed to have all of the features of human ESCs, as well as the ability to grow indefinitely and form all somatic cell types of the body. Unlike ES cells, however, iPSCs dispense the use embryos or the need for somatic cell nuclear transfer to derive pluripotent cells (Figure 1.10).

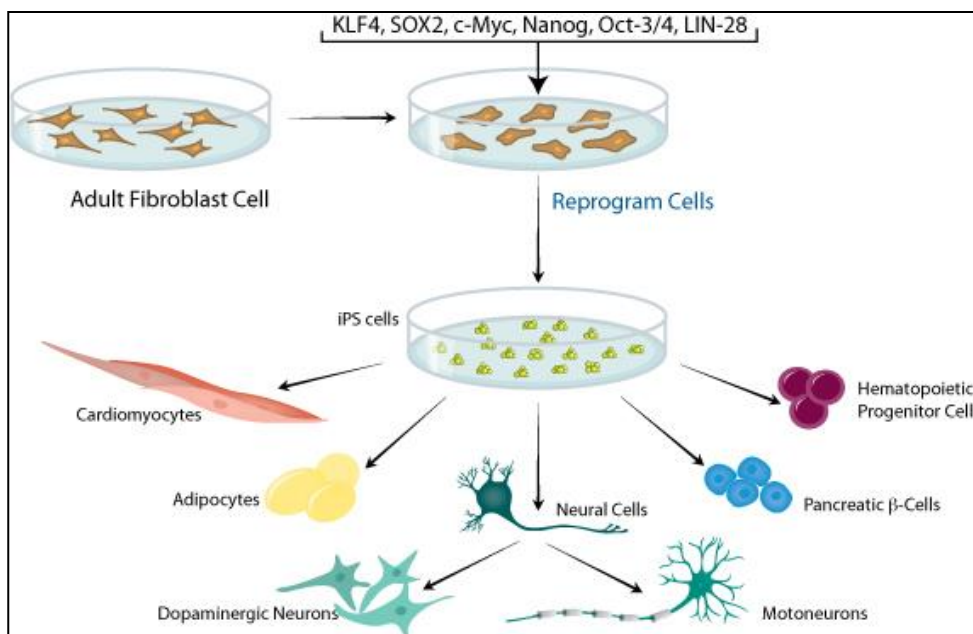


Figure 1.10. Differentiation of iPSCs. Induced pluripotent stem cells are generated by reprogramming adult somatic cells. Reproduced from Amabile and Meissner (2009).

Despite a lot of work done on the understanding of reprogramming, a lot still remains to be investigated. Expression of the reprogramming factors is required for 2-3 weeks, and during this time a complex cascade of events is initiated and culminates in the silencing of endogenous genes related to cell-type identity and activation of genes required for pluripotency and self-renewal (*OCT4*, *SOX2* and *NANOG*). Once properly established, the reprogrammed state appears to be maintained. Therefore, epigenetic modifications of the DNA and histones, as well as the mesenchymal-epithelial transition, which is a reversible biological process that involves the transition from elongated mesenchymal cells to cubical polarised cells called epithelia, appear to be critical for the induction of pluripotency and its maintenance as a consequence of the overexpression of the reprogramming transgenes introduced by viral infection (Marson *et al.*, 2008; Meissner *et al.*, 2008).

The process of generation iPSCs is reproducible; however, the efficiency of this process remains low. Normally less than 1% of transfected fibroblasts become iPSCs. Initially it was thought that iPSCs were derived from a “rare stem” or undifferentiated cells in fibroblast cultures. However subsequent studies showed that iPSCs could be derived from differentiated lymphocytes (Loh *et al.*, 2009) and postmitotic neurons (Kim *et al.*, 2011). Those studies demonstrated that most of somatic cells have a potential to become iPSCs, regardless different efficiencies.

1.2.4. Generation of iPSCs

Reprogramming factors can either be delivered by integrating methods, which could lead to the insertion of the transgenes in their genome, or with non-integrating methods, generating iPSCs without any permanent genetic modification. Integrating reprogramming methods include the use of retroviruses, lentiviruses and transposons.

This transgene integration could lead to mutation within the host genome or could alter expression of neighboring host genes (Hacein-Bey-Abina *et al.*, 2003). There is also the risk of reactivation of these viral transgenes that could result in tumour formation, although integrated proviruses are usually silenced during iPSC generation (Takahashi and Yamanaka, 2006; Okita *et al.*, 2008). Even if the viral transgenes are not silenced properly, leaky expression may inhibit iPSC differentiation and maturation, increasing the risk of immature teratoma formation (Markoulaki *et al.*, 2009).

Non-integrating reprogramming methods include non-viral and viral delivery. Non-viral delivery methods include episomal vectors (Yu *et al.*, 2009), microRNAs (miRNAs) (Miyoshi *et al.*, 2011), reprogramming proteins (Kim *et al.*, 2009; Zhou *et al.*, 2009) and small molecules, such as valproic acid (VPA). All these strategies can be used to reprogram iPSCs, but they present disadvantages such as low efficiency, high cost and technical difficulties.

Viral delivery methods include adenoviruses (Stadtfield *et al.*, 2008b) and Sendai viruses (Fusaki *et al.*, 2009). Sendai viruses, however, show a significant improvement in efficacy over adenoviruses.

The Sendai transduction method

Sendai virus is an RNA virus that only replicates in the host cell cytoplasm and it does not have a DNA phase, so it cannot integrate into the host genome (Kato *et al.*, 1997). An F-deficient SeV vector which contains the fusion protein but not the fusion gene is able to infect cells with high efficiency, including non-dividing cells, but is unable to transmit viral particles (Li *et al.*, 2000). One of the advantages of the use of Sendai virus for reprogramming is that it remains in the cytoplasm of infected cells for a few passages but is cleared out rapidly and it is completely gone by passage ten. (Fusaki *et al.*, 2009). Due to the high reprogramming efficiency in various cell types and its non-integrating approach, Sendai virus is a good method to induce pluripotency (Table 1.2).

Method	Integrating	Time (days)	Efficiency (%)	Multiple cell types reprogrammed
Retroviral	Yes	25–35	0.02–0.08	Yes
Lentiviral	Yes	20–30	0.02–1	Yes
Lentiviral (miRNA)	No	18–26	10.4–11.6	No
miRNA (direct transfection)	No	20	0.002	Yes
Adenoviral	No	25–30	0.0002	No
Sendai virus	No	25	0.5–1.4	Yes
mRNA	No	20	0.6–4.4	No
Protein	No	56	0.001	No
Transposons	Yes	14–28	0.02–0.05	No

Table 1.2. Comparison of published methods for the reprogramming of human somatic cells into iPSCs. Adapted from Rao and Malik (2012).

Stages of Reprogramming

Reprogramming of somatic cells can be divided into 3 distinct phases; initiation, maturation and stabilisation (Samavarchi-Tehrani *et al.*, 2010). During the initiation phase, cells undergo major transcriptional changes, starting just after *OCT4*, *SOX2*, *KLF4* and *C-MYC* (OSKM) expression and peaking around day 3. This is followed by a repression of mesenchymal regulators and it is represented in culture by morphological change from fibroblasts to epithelial-like colonies, termed mesenchymal-epithelial transition (MET). These changes affect cell growth, cytoskeleton organization, metabolism and developmental processes (Khalil *et al.*, 2009; Polo *et al.*, 2012). Early pluripotency genes are upregulated together with DNA replication, cell cycle progression and stress-induced genes (Mikkelsen *et al.*, 2008; Samavarchi-Tehrani *et al.*, 2010; Polo *et al.*, 2012; Hussein *et al.*, 2014). During the

initiation phase cell fate is elastic, and removal of OSKM can result in a reversion of cells to a differentiated state (Samavarchi-Tehrani *et al.*, 2010).

The maturation phase begins around day 8 with expression of *NANOG*, *SALL4*, *ESRRB*, *REX1*, *TCL1*, *CRIP1* and *NODAL*. This is followed by a second wave of transcriptional and proteomic changes between days 9 and 12 (Samavarchi-Tehrani *et al.*, 2010; Hansson *et al.*, 2012; Polo *et al.*, 2012; Hussein *et al.*, 2014). In addition to this, proteins involved in vesicle-mediated transport, cell adhesion and extracellular matrix that were silenced during the initiation phase, are reactivated during this phase. The end of the maturation phase is marked by the establishment of the endogenous pluripotent transcriptional network, led by upregulation of *SOX2*, independent of transgene expression. (Samavarchi-Tehrani *et al.*, 2010; Buganim *et al.*, 2012; Polo *et al.*, 2012).

The stabilisation phase represents the changes occurring after iPSCs have acquired pluripotency. Activation of endogenous pluripotent markers is thought to represent the first step in a sequence which allows the cells to become pluripotent (Buganim *et al.*, 2012; Golipour *et al.*, 2012). The stabilization phase also involves the silencing of OSKM transgenes and it continues with elongation of telomeres, similar to embryonic levels, reactivation of both copies of the X chromosome in female iPSCs and upregulation of genes involved in the regulation of DNA methylation (Stadtfield *et al.*, 2008a; Polo *et al.*, 2012).

1.2.5. Advantages of using iPSC technology

Pluripotent stem cells are capable of indefinite self-renewal and can differentiate into any cell types of all three embryonic germ layers. The use of iPSCs has some advantages over ESCs, which are described below.

Patient Specific

iPSC technology has made it feasible to generate patient-specific models. Patients' cells carrying genetic mutations can be reprogrammed into iPSCs, which can be subjected to genome editing, followed by differentiation in almost every cell type of

the body. Thus, they can be powerful tools for disease modeling, regenerative medicine and drug screening (Sayed *et al.*, 2016).

Avoidance of ethical issues

The use of ESCs has been limited or banned in some countries due to ethical and religious concerns regarding the use of pre-implantation stage embryos for research. Since iPSCs can be generated from adult somatic cells, these cells can be used for research purposes without those ethical concerns (Robertson, 2001; Halevy and Urbach, 2014).

Accessibility of cells for reprogramming

Primary cells from patients can be difficult to expand, hard to access and difficult to obtain, especially from patients with degenerative diseases, such as RP, due to the low number of cells of interest. Primary cultured cells *in vitro* have also limited capacity for division and growth (Shay and Wright, 2006). iPSCs, however, can be generated from available and easily accessible cell types such as skin fibroblasts, peripheral blood, hairs and urine (Raab *et al.*, 2014).

1.2.6. *Challenges in iPSC technology*

Despite all the advantages of iPSCs, there are still some challenges that cannot be overlooked when working with iPSCs.

Viral integration

The potential tumorigenicity of iPSC is a major concern of iPSC technology. Integrating methods of reprogramming can result in multiple random integration sites (Takahashi and Yamanaka, 2006) in the genome and a risk of neoplasia, gene inactivation and dysregulation. It has been shown that iPSC lines generated with

integrating methods display more single nucleotide variations and mosaicism than cells generated by non-integrating iPSC lines (Kang *et al.*, 2015). To overcome potential safety-related concerns, non-integrative methods of reprogramming, such as Sendai virus, are preferable to generate iPSCs (Fusaki *et al.*, 2009).

Incomplete reprogramming

Reprogramming of somatic cells is a process that occurs at different stages. Firstly, delivery of *OCT4*, *KLF4*, *SOX2* and *C-MYC* into the cells results in expression of those transcription factors and opening of the chromatin at enhancers of pluripotency genes, leading to activation of other transcription factors that downregulate somatic gene expression. Cells that fail reprogramming, also fail to downregulate somatic genes. Reprogramming requires the expression of *OCT4*, *KLF4*, *SOX2* and *C-MYC* until the iPSC state is established, otherwise reprogramming fails and cells return to a differentiated state. Absence or defective transcriptional and epigenetic changes during reprogramming can lead to incomplete reprogramming of the cells and clonal variability (Scacheri and Tesar, 2017). Incomplete reprogrammed cells have characteristics that are similar to ESCs, such as morphology, gene expression and are able to form teratomas. However, they exhibit defects such as poor capacity of differentiation, reduced growth rate, abnormal transcription and DNA methylation, and abnormal chromatin regulation (Meissner *et al.*, 2008; Mikkelsen *et al.*, 2008).

Genomic instability

iPSCs frequently acquire chromosomal abnormalities, which often can be gains or losses of whole chromosomes, copy number variants (CNVs), which are sections of the genome of least 1 kb that are repeated and can vary in copy number, through duplications or deletions, among individuals in a specific population, or single nucleotide variants (SNVs), which are common variants of single nucleotides that are frequently observed in the population (Yoshihara *et al.*, 2017).

Genetic variations of iPSCs can have origin in genetic variability of parental cells, being fixed at the cloning picking stage during the process of iPSC generation; at the reprogramming stage; and/or during prolonged culture. CNVs are generally acquired during reprogramming (Hussein *et al.*, 2011), and in prolonged *in vitro* culture (International Stem Cell *et al.*, 2011). Some CNVs are more common than others in iPSCs. CNVs at 1q31.3, 8q24.3 and 17q21.1 (>25% of iPSC samples) were identified as recurrent and unique to iPSC samples, acquired during prolonged periods in culture (Martins-Taylor *et al.*, 2011; Turinetto and Giachino, 2015). Duplications of 20q11.21 (18%) and 2p11.2 (>25%) were also detected in high incidence in ESCs, (Spits *et al.*, 2008). Amplification of 20q11.21 was identified as one of the most recurrent CNVs hotspot in iPSCs and ESCs in several studies (Elliott *et al.*, 2010; Laurent *et al.*, 2011; Martins-Taylor *et al.*, 2011). SNVs are also acquired during prolonged culture, but they generally exist in low frequencies (Gore *et al.*, 2011).

It is crucial to determine if variations in iPSCs are pathogenic or tumorigenic. Giemsa (G)-banding can detect large structural changes, while single nuclear polymorphisms (SNP) array-based analysis, which is a type of DNA microarray used to detect thousands of SNPs across the genome, have a higher resolution and can also be applied to detect CNV (Le Scouarnec and Gribble, 2012). More recently, next generation sequencing (NGS) has enabled the detection of any variants in the genome, including SNVs (Metzker, 2010). Integration free reprogramming and better characterization of iPSCs are crucial in order to generate better models to mimic diseases and for cell therapies.

iPSC variability

Some studies, including one of the largest analysis about genomic stability in iPSCs, found that differences between individuals are responsible for up to 50% of all the variation in iPSC phenotypes, including differentiation capacity and cellular morphology (Carcamo-Orive et al., 2017; Kilpinen et al., 2017). It was also demonstrated that cell type of origin does not impact on differentiation as much as inter-individual genetic variability, as shown by differentiation capability, transcriptomic and epigenetic data of iPSC lines derived from blood and fibroblasts samples from the same donors (Kyttala et al., 2016). Hallam et al. (2018) also demonstrated that variation in RPE differentiation efficiencies are not due solely to disease pathology, as differences were also encountered in unaffected individuals.

1.2.7. The use of iPSCs in disease modeling

Due to their pluripotency nature and their ability to differentiate into any cell type of the three germ layers, ESCs and iPSCs became powerful models to study various degenerative diseases, including retinitis pigmentosa. iPSCs, principally, became the preferred choice for disease modeling, as they are patient-specific and can mimic patients' phenotypes, in addition to the possibility of genome editing via correction of disease-specific mutations, for future cell-based therapies.

ESCs and iPSCs have been used in retinal disease modeling by several research groups. Capowski *et al.* (2014) investigated the expression of human *MITF*, a transcription factor expressed in optic vesicles, in human ESCs at the earliest stages of retinal differentiation and its role in human retinogenesis. It was demonstrated that during human ESC differentiation towards a retinal fate, a population of *MITF* isoforms was expressed in a similar way to that observed in mice. Downregulation of *MITF* reduced optic vesicle cell proliferation, decreased expression of eye field transcription factors and disrupted RPE maturation. This study also showed that human ESCs can mimic complex gene expression profiles and molecular events of retinal development, that could lead to a better understanding of human eye development and improve standardisation and safety of future cellular therapies.

In another study, patient's iPSC-derived RPE cells harboring mutations in *MFRP*, a RPE-specific membrane receptor, causative of autosomal recessive RP, displayed increased b-actin, abnormal morphology, low levels of pigmentation and loss of tight junctions. Introduction of a healthy copy of *MFRP* by adeno-associated virus vector, restored actin organization, levels of pigmentation and transepithelial resistance (Li *et al.*, 2014).

Lukovic *et al.* (2015) reported the successful generation of iPSC-derived RPE from a patient with a severe form of autosomal recessive RP (arRP), harbouring a novel Ser331Cysfs*5 mutation in the *MERTK* gene. iPSC-derived RPE cells had defective phagocytosis, a common phenotype of RP observed in human patients and animal models. *MERTK*-deficient RPE cells, therefore, have been shown to be a faithful cellular model of arRP that can be used for the investigation of the disease mechanism, drug testing and gene-based therapies.

The following year, Leber congenital amaurosis (LCA) patient-specific iPSCs with a mutation in *CEP290*, a cilia related gene, were differentiated towards RPE and photoreceptors, in three-dimensional optic cups, to investigate disease mechanisms and evaluate candidate therapies (Parfitt *et al.*, 2016). Results have shown that the highest levels of aberrant splicing and cilia defects, as a consequence of a mutation in *CEP290*, were observed mainly in optic cups, explaining the retinal degeneration observed in *CEP290*-LCA disease.

Hallam *et al.* (2017) demonstrated that disease modelling of AMD using patient-specific iPSC-derived RPE is a useful tool to assess potential therapeutic agents to treat AMD. In this study, iPSC-derived RPE from high-risk patients displayed distinct cellular, structural and functional deficiencies that mimicked inflammation and cellular stress processes that characterises AMD, when compared to RPE from low-risk patients. Additionally, it has been shown that exposure to intermittent UV light resulted in an improvement of cellular and structural features in high-risk RPE cells, associated with AMD.

In an *in vitro* model of Bietti's crystalline dystrophy, patient-specific iPSC-derived RPE cells were used to demonstrate that accumulation of free cholesterol damages the RPE and leads to cell death through lysosomal dysfunction and impairment of autophagy flux in affected cells (Hata *et al.*, 2018).

Smith *et al.* (2019) also used iPSC-derived RPE to provide a potential mechanism underlying decreased *VEGFA* expression in AMD patients. It was shown that the rs943080 risk allele is associated with regulatory protein binding in iPSC-RPE, causing decreased in *VEGFA* expression.

All these examples of iPSCs modelling retinal diseases show the importance of patient-specific iPSCs for the genetic characterisation of functional variation in RPE and to mimic the development and pathogenesis of retinal degeneration diseases, such as retinitis pigmentosa.

1.3. Retinal Pigment Epithelium

Retinal pigment epithelium is a layer of cells located between photoreceptors and Bruch's membrane and it is responsible for the maintenance and survival of photoreceptors (Figure 1.11).

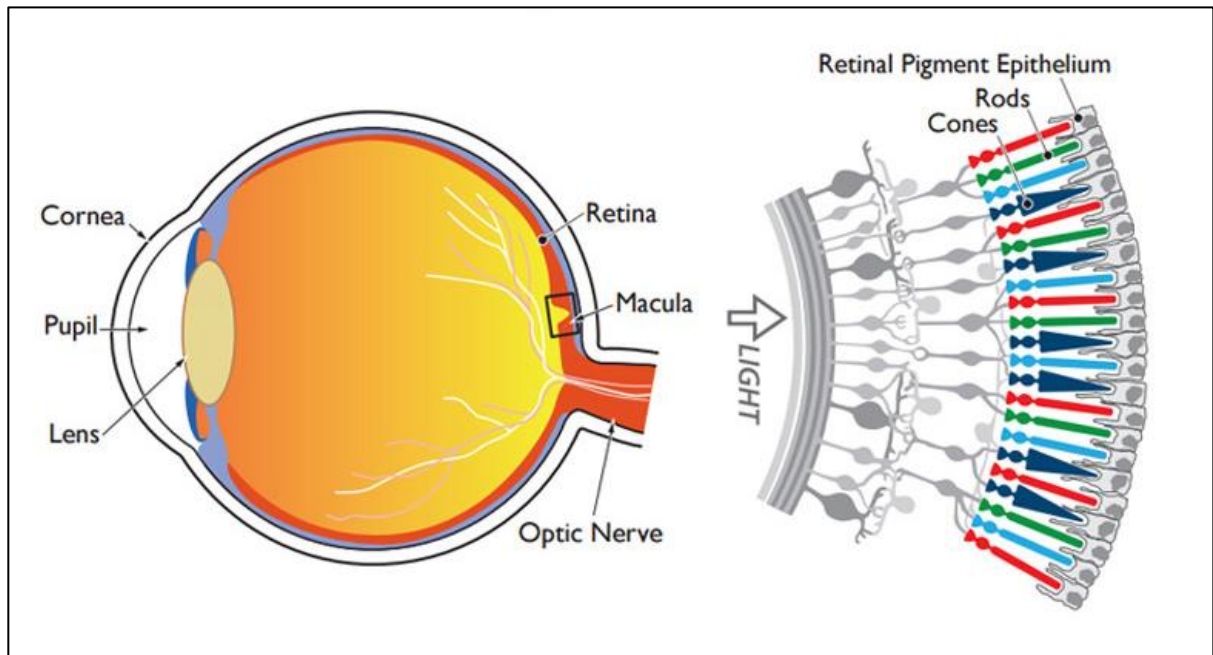


Figure 1.11. Schematic representation of the human eye, retina and location of the RPE. Reproduced from <https://www.closerlookatstemcells.org/stem-cells-medicine/macular-degeneration/>

The RPE acts as a selective barrier, taking up nutrients and fatty acids from the blood and transporting those to the photoreceptors. It also transports water and ions from the subretinal space, at the apical side, to the capillaries, at the basolateral side (Strauss, 2009). The $\text{Na}^+\text{-K}^+\text{-ATPase}$, which is located in the RPE apical membrane, provides the energy for transepithelial transport (Rizzolo, 1999). Tight junctions, between RPE cells, keep cells tightly connected, allowing the control of fluids and solutes through the blood retinal barrier as well as in preventing the entrance of toxic molecules into the retina.

The transport of retinol from the blood to the photoreceptors is crucial for the visual cycle. The visual cycle is the conversion of light into an electrical signal in the retina and occurs via G-protein coupled receptors called opsins which contain 11-cis-retinal (Hargrave, 2001). In the presence of light, 11-cis-retinal is converted into all-trans-

retinal, changing the conformation of the opsins and leading to closure of cation channels, and hyperpolarization of the photoreceptor cells. Photoreceptors don't produce 11-cis-retinal and all-trans-retinal is metabolised into all-trans-retinol and transported to the RPE to be converted to 11-cis-retinal and then redelivered to the photoreceptors (Pang *et al.*, 2006). Three RPE enzymes are crucial for the visual cycle. After entering RPE cells, all-trans retinol is bound to cellular retinoid binding protein (CRBP) and transferred to lecithin retinol acyl transferase (LRAT) to generate all-trans retinyl esters. The esters are then used as a substrate for the regeneration of 11-cis retinal by retinoid isomerohydrolase (RPE65), in the next step of the visual cycle. This cyclical process of exchange of retinoids between the RPE and photoreceptors is crucial for phototransduction (Muniz *et al.*, 2014).

Photoreceptors are exposed to intense light, leading to accumulation of light-induced toxic substances each day (Beatty *et al.*, 2000). To maintain the levels of radicals, photodamaged proteins and lipids to a minimum, allowing normal function of photoreceptors, the RPE engulfs bound photoreceptors outer segments (POSS) through the apical $\alpha\beta 5$ integrin and Mer tyrosine kinase (MerTK) receptors and degrades the POSS (Finnemann and Nandrot, 2006). The final products are recycled, leaving the RPE layer via choroidal capillaries or are redelivered to photoreceptors to rebuild light-sensitive outer segments (Bibb and Young, 1974; Bok, 1993). Through the coordination between phagocytosis and the formation of new POS, the length of the POS is maintained.

Due to intense light exposure and constant renewal of optic discs, the retina is one of the parts of the body that consumes more oxygen, thus producing more oxidative stress (Girotti and Kriska, 2004). The RPE also protects the retina against oxidative stress by absorbing scattered light with its melanin granules, producing antioxidants and repairing or replacing damaged proteins (Beatty *et al.*, 2000; Beatty *et al.*, 2001).

The RPE also secretes a variety of growth factors including pigment epithelium-derived factor (PEDF) and vascular endothelial growth factor (VEGF) (Simo *et al.*, 2006). PEDF, which is secreted to the apical side of the RPE, helps to maintain the retinal structure by protecting neurons against glutamate or hypoxia-induced apoptosis (Cao *et al.*, 1999; Cao *et al.*, 2001; Ogata *et al.*, 2001). It also acts as an antiangiogenic factor to stabilise the endothelium of the choriocapillaris and inhibit endothelial cell proliferation (Adamis *et al.*, 1993; Lopez *et al.*, 1996; Simo *et al.*, 2006). Generation of PEDF-deficient mouse models confirmed that PEDF is a modulator of early postnatal

retinal vascularization and the lack of PEDF promotes faster retinal vascularization (Huang *et al.*, 2008). VEGF, as opposed to PEDF, is mostly secreted to the basal side of the RPE where it acts on the choroidal endothelium, preventing endothelial cell apoptosis and promoting an intact endothelium of the choriocapillaris (Burns and Hartz, 1992; Roberts and Palade, 1995).

In summary, the RPE nourishes and protects the photoreceptors by transporting nutrients, ions and waste products from and to the neuroretina, recycling the spent tips of the POSs, defending the retina against oxidative stress and producing molecules that support the survival of photoreceptors, ensuring an optimal circulation and supply of nutrients (Figure 1.12).

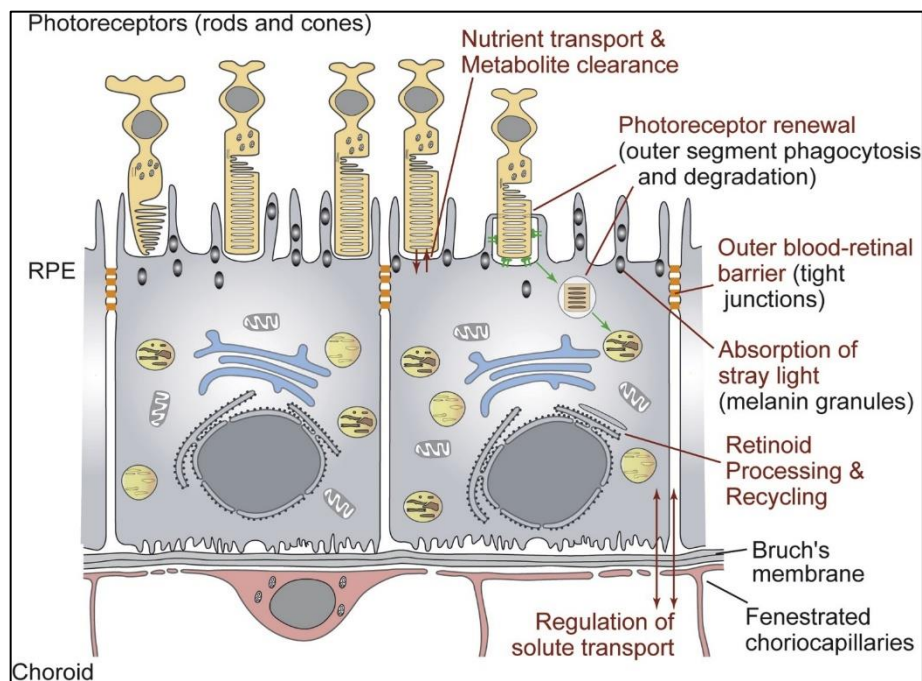


Figure 1.12. Schematic representation of the RPE cells and its support functions. Reproduced from Lehmann *et al.* (2014).

1.3.1. The role of primary cilia in RPE

It has been shown that RPE requires a functional primary cilium to fully mature and maturation defects in RPE precede photoreceptors degeneration. Primary cilium also regulates polarisation of human RPE through canonical Wnt suppression and PKC δ activation. Therefore, defects in primary cilia result in structural defects and function, such as decreased barrier properties, apical activity and fluid transport (Bharti, 2014; Bharti, 2015; May-Simera *et al.*, 2018).

Defects in primary cilia function are collectively known as ciliopathies (Braun and Hildebrandt, 2017) and can affect different parts of the body (Lee and Gleeson, 2011). Retinal degeneration is the most frequent phenotype found in ciliopathy patients (Wheway *et al.*, 2014; Bujakowska *et al.*, 2017), mainly caused by functional and developmental defects in photoreceptors due to impaired development of outer segments. Defects in other non-photoreceptor ocular cell types, such as the RPE cells, are now being investigated, since previous work suggested that development of photoreceptor outer segment is dependent on complete maturation of the RPE (Nasonkin *et al.*, 2013). As mentioned above, photoreceptors health and function are dependent on functional and metabolic support from the RPE in an entwined manner (Bharti *et al.*, 2011).

The presence of cilia in human RPE cells was first reported in 1965 (Allen, 1965) from electron microscopy images of an exenterated human eye. Since then other observations of a single cilium in RPE cells supported previous reports (Allen, 1965; Fisher and Steinberg, 1982) that cilia are common and can be found in human RPE cells *in vivo*. They are present on the apical surface of RPE cells they vary between 1-10 μm in length (Nishiyama *et al.*, 2002). They are anchored to the cell through a basal body derived from the mother centriole and are composed of nine microtubule doublets extending from microtubule triplets of the basal body (Reiter *et al.*, 2012). Another type of cilia, the motile cilia, has the same structural arrangement plus an additional central pair of microtubules that is required for generation of movement. (Figure 1.13). The main role of primary cilia is to act as a signalling antenna of the cells, regulating ubiquitous developmental pathways such as Wnt, Sonic Hedgehog (SHH) and transforming growth factor β (TGF- β). The signalling molecules composition varies from cell type and cell stage (Rachel *et al.*, 2012; Sasai and Briscoe, 2012).

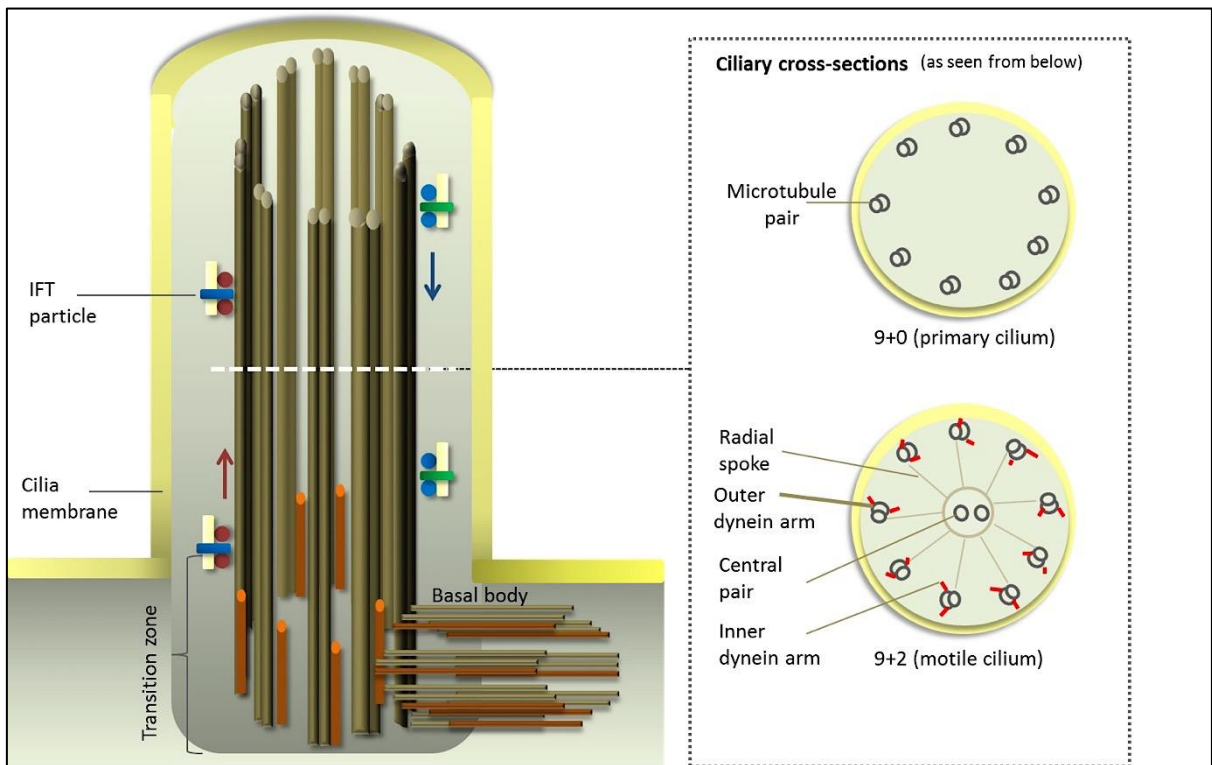


Figure 1.13. Schematic representation of primary cilium. The cilium is made of a basal body and microtubular backbone, the axoneme, arranged in a typical '9+0' architecture with nine outer microtubules doublets. The motile cilium has a '9+2' architecture with a central pair of microtubules. Ciliary proteins, synthesized in the cell body, are transported to the tip of the axoneme by the intraflagellar transport (IFT), comprised of polypeptide complexes (IFT particles) that move along the length of the ciliary axoneme. Reproduced from <https://ciliopathyalliance.org/cilia>.

Ciliation in human RPE cells is regulated by cell cycle mechanisms that are not fully understood. It has been demonstrated in adult RPE1 cells that the primary cilium is assembled after cell division, in late G1 phase and disassembled just before cell cycle entry, although a second wave of deciliation can be observed in S phase. Usually primary cilia are not present during mitosis, perhaps because the mother centriole of the centrosomes attaches to the cell membrane during the cilia formation and it needs to be released to carry out its role in mitotic spindle formation. It's also possible that deciliation is coupled to DNA synthesis. Disruption of cell cycle, cilia structure and function are consequence of many human genetic disorders, including retinal ciliopathies (Spalluto *et al.*, 2013).

1.3.2. RPE development in vivo

RPE is formed by the ectoderm lineage of embryonic development. Following fertilisation, the human embryo starts to divide and around the fourth day after fertilisation, it forms a blastocyst consisting of an inner cell mass (ICM) surrounded by an epithelial layer known as the trophoblast. The ICM forms the embryo whilst the trophoblast forms the extraembryonic tissues including part of the placenta. Prior to the implantation, the ICM divides into two layers of cells known as the epiblast and hypoblast. The epiblast undergoes gastrulation during the third week of embryogenesis to form the three embryonic germ layers; ectoderm, endoderm, and mesoderm (Niakan *et al.*, 2012).

The anterior neuroectoderm, which forms the eye field and the forebrain, is specified into the optic neuroepithelium. FGF, BMP, Wnt and retinoic acid pathways play important roles during gastrulation and early neural development, but their exact role in the specification of the anterior neural plate, including the eye field, is still poorly understood (Fuhrmann *et al.*, 2014). A combination of eye development transcription factors such as RX, PAX6, SIX3, SIX6 and LHX2 characterises the eye field and the integration of those transcription factors has an important role in the arrangement of cells in an organised and coordinated pattern to generate retina, RPE and lens, leading to the evagination of the optic vesicles (Bailey *et al.*, 2004; Kwan *et al.*, 2012) (Figure 1.14A).

The distal layer of the optic vesicles touches the surface ectoderm and invaginates forming the optic cup. The close proximity of the inner layer of the optic cup with the surface ectoderm promotes the formation the neural retina whilst the outer layer, in contact with the surrounding extracellular mesenchyme, differentiates to the RPE (Figure 1.14B). The RPE becomes morphologically different to the neural retina by the switch from a pseudo-stratified organisation to an epithelial monolayer with the presence of pigment granules (Nguyen and Arnheiter, 2000; Martinez-Morales *et al.*, 2004; Pearson *et al.*, 2005).

One of the earliest indicators of RPE specification is the expression of Melanocyte Inducing Transcription Factor (*MITF*), which promotes the activation of genes related to terminal RPE differentiation and function such as tyrosinase, tyrosinase-related protein, melanosomal proteins and the Ca-dependent chloride channel protein

bestrophin (Best1) (Adijanto *et al.*, 2012; Li *et al.*, 2012). *OTX2*, which is initially expressed throughout the optic vesicle, becomes restricted to the RPE in the optic cup and its expression is required for RPE development (Martinez-Morales *et al.*, 2004).

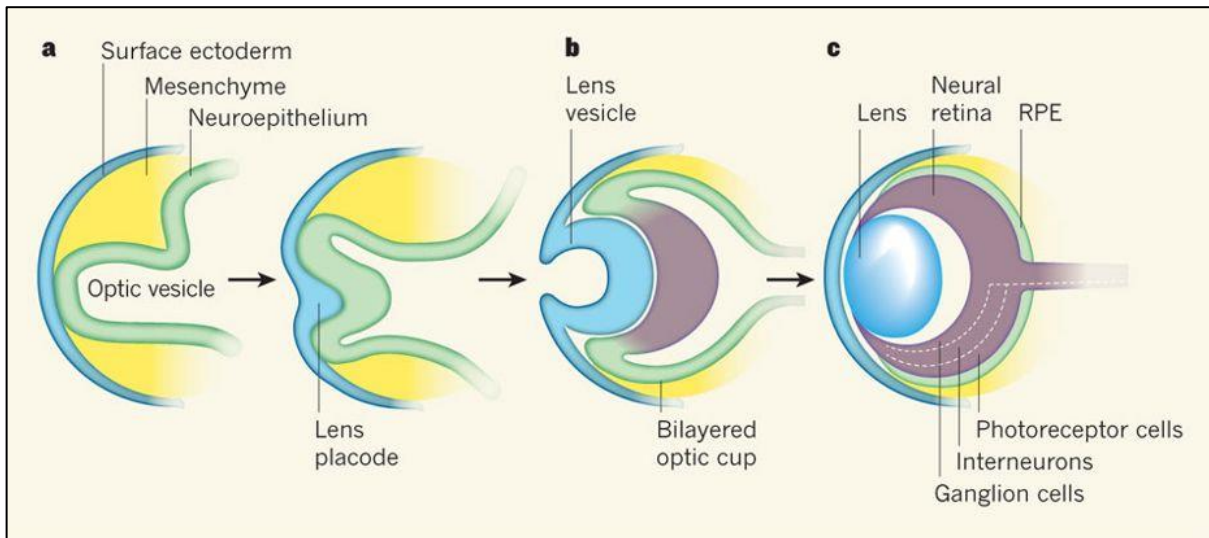


Figure 1.14. Stages of eye development and RPE specification. A: during early stages of eye development, the neuroepithelium invaginates together with the surface ectoderm forming the optic vesicle. B: The inner layer of the optic cup gives rise to neural retina and the outer layer gives rise to the RPE. C: The lens, neural retina and RPE. Reproduced from Ali and Sowden (2011).

1.3.3. Differentiation of human iPSCs into RPE cells

Several protocols have reported the direct differentiation of iPSCs towards RPE, including spontaneous differentiation after removal of basic fibroblast growth factor (bFGF) from the culture medium (Klimanskaya *et al.*, 2004; Buchholz *et al.*, 2009), serum-free floating culture of embryoid body-like aggregates (SFEB) which are plated on to extracellular matrix to encourage neuroectoderm fate (Watanabe *et al.*, 2005), and directed methods using drugs and cytokines such as Nicotinamide (NIC) and Activin A (Idelson *et al.*, 2009; Krohne *et al.*, 2012).

More recently published protocols use defined factors in a stepwise method to drive RPE differentiation in a manner which recapitulates embryonic eye development. (Buchholz *et al.*, 2013; Zhu *et al.*, 2013; Leach *et al.*, 2015). A combination of directed differentiation methods by mediation of signalling pathways, such as nicotinamide, Dkk-1 and Lefty-A to induce neuralisation, with formation of embryoid bodies has been shown to improve efficiency of RPE differentiation (Idelson *et al.*, 2009; Meyer *et al.*,

2009; Osakada *et al.*, 2009; Zhu *et al.*, 2013). Buchholz *et al.* (2013) reported a directed differentiation protocol to generate RPE from human ESC in only 14 days, which was later modified with Wnt activation to improve efficiency without manual selection or enrichment at day 14 (Leach *et al.*, 2015).

Although directed differentiation became the preferred choice to generate RPE due to the improved efficiency and reduction of costs as a result of standardisation of production, RPE generated by different methods do not show differences in terms of transcription levels of RPE markers, protein localisation or functional analysis. Leach *et al.* (2016) compared iPSC-derived RPE derived from five different iPSC lines using spontaneous and guided differentiation methods. The results showed there was no significant differences between iPSC-derived RPE derived from both differentiation methods. Differences in expression levels of *RPE65* and *BEST1* were observed between cell lines as an indication of internal lineage-specific differences.

Successful RPE differentiation enables the generation of pure populations of functional RPE cells with key RPE features, including the four 'Ps' (pigmented, polygonal, phagocytic and polarized), with the ability to mimic the behaviour of native RPE cells and respond to normal and disease-associated stimuli (Bharti *et al.*, 2011; Mazzoni *et al.*, 2014). The characterisation of RPE cells is essential to confirm all these features of typical RPE cells. Structural and ultrastructural RPE characteristics including pigmentation, polarity and tight junctions, can be verified with transmission and scanning electron microscopy. Expression of typical RPE markers such as MERTK, chloride channel encoded BEST1, retinoid cycle-associated RPE65 and CRALBP can be analysed by RT-PCR, immunostaining and/or western blot. Functional analyses of RPE include measurement of cytokines secretion such as VEGF, PEDF, and phagocytic capability assay using purified POSs (Kamao *et al.*, 2014).

1.3.4. Attempts to explore disease pathogenesis in PRPF31-RP

Attempts have been made to explore disease pathogenesis in PRPF31-RP. Deery *et al.* (2002) used yeast models to introduce human *PRPF31* wild-type into a defective-PRPF31 yeast strain, incapable of growing at the restrictive temperature of 37°C. This resulted in only partial rescue of growth at the restrictive temperature, suggesting that splicing function was not completely restored. Yuan *et al.* (2005) and

Mordes *et al.* (2007) examined the relationship between *PRPF31* and pre-mRNA splicing of photoreceptor-specific genes in mouse primary cell cultures, using *RHO*, *PRPH2* and *FSCN2* minigenes. Transfection of cells with minigenes showed that intron 3 of *RHO*, intron 1 of *PRPH2* and intron 3 of *FSCN2* are spliced out in the presence of wild-type *PRPF31* protein, whereas mutant *PRPF31* protein inhibit those events, linking widely expressed *PRPF31* protein and expression of retina-specific genes. On the other hand, Wilkie *et al.* (2008) demonstrated that splicing of *RHO* intron 3 in mini-gene templates was inefficient, with both spliced and unspliced products clearly detected, in a study of A216P-*PRPF31* missense mutation using human embryonic kidney 293 (HEK293) cells. The effect of the mutation was also not noticed on a full-length human *RHO* gene template. In another study, Yin *et al.* (2011) showed that different *PRPF31* mutations affect zebrafish retinas through distinct mechanisms such as loss-of-function and dominant-negative effect.

Even though the examples cited above provided valuable contribution towards the elucidation of disease pathogenesis in *PRPF31*-RP, the use of non-human models or other non-retina human cells do not reflect or recapitulate the human retina physiology, or do not faithfully mimic the phenotypes present in *PRPF31*-RP.

Likewise, generation of knock-in and knock-out mouse models failed to display retinal degeneration and they did not present any visual defect until 18 months of age (Bujakowska *et al.*, 2009). Those models, however, showed that *prpf31* knockout mice developed changes in the retinal pigment epithelium (RPE), such as presence of vacuoles and amorphous deposits between the RPE and Bruch's membrane, and loss of basal infoldings. Death of retinal photoreceptor cells, however, which is the most striking pathological change in human RP disease, was not seen in those animals and change in retinal function was not detected. Therefore those animals cannot be considered a faithful model for *PRPF31*-RP disease (Graziotto *et al.*, 2011).

Large animals such as pigs and monkeys can also be used as models for retinal diseases, however knock-in and knock-out animal models are very expensive and difficult to obtain due to ethical issues. Additionally, the successes seen in animal models for disease modeling and gene therapy moves in a very slow pace to a fully approved treatment that could be commercially viable to anyone who needs it (Tucker *et al.*, 2014).

To date, iPSCs are the best models of PRPF31-RP, as these cells can be matched to the individuals and they can differentiate into various retinal cell types. iPSCs not only mimic the pathogenesis of the disease but can also help to distinguish phenotypes of *PRPF31* patients with same mutation but various clinical manifestations, due to the incomplete penetrance of the disease.

1.4. Aims

The aims of this thesis were:

- To generate and characterise controls and PRPF31-patient-specific induced pluripotent stem cells (iPSCs);
- To differentiate controls and PRPF31-patient-specific iPSCs towards retinal pigment epithelium (RPE) and validate the iPSC-derived RPE model;
- To investigate the pathogenesis of the *PRPF31* form of RP using the PRPF31-RPE patient-specific disease models.

Chapter 2 - Methods

All methods were extracted from Buskin *et al.* (2018).

2.1. Human Subjects

All samples used in this study were obtained with informed consent according to the protocols approved by Yorkshire & the Humber Research Ethics Committee (REC ref. no. 03/362).

2.2. iPSC Generation

Two age-matched unaffected controls (WT1 and WT3) and seven RP11 dermal skin fibroblasts (severe RP11S1, moderate RP11M, very severe RP11VS, asymptomatic RP11A, severe RP11S2, severe RP11S3 and severe RP11S4) (Table 3.1) were cultured with Advanced Dulbecco's Modified Eagle Medium (Thermo-Fisher, Waltham, MA, USA) containing 10% FBS (Thermo Fisher Scientific), 1% Glutamax (Thermo Fisher Scientific) and 1% penicillin/streptomycin (Thermo Fisher Scientific) at 37°C and 5% CO₂ in a humidified incubator. These fibroblasts were transduced at a density of 30,000 cells/cm² using the CytoTune™-iPS 2.0 Reprogramming Kit (Life Technologies, A16517) following the manufacturer's instructions. iPSC colonies were established on inactivated primary mouse embryonic fibroblasts feeder layer and then adapted to the feeder-free system described below.

2.3. iPSC Culture

Human iPSCs were cultured in 6-well plates coated with Matrigel™ GFR (Corning, 354230) using mTeSR™1 (StemCell Technologies, 05850) media supplemented with 1% penicillin/streptomycin (Gibco, 15140). Cell culture medium was replaced on a daily basis. Cells were allowed to grow for 4-5 days prior to passaging or induction of differentiation. Passaging was carried out using Versene

(EDTA 0.02%) (Lonza, BE17-771E) solution at 37°C for 3-5 minutes and cells were transferred to fresh matrigel plates in a 1:3 – 1:6 ratio. All cultures were maintained at 37°C, in a humidified environment, with 5% CO₂. Cells were cryopreserved with freezing media containing 90% Fetal Bovine Serum (Gibco, 10270) and 10% Dimethyl Sulfoxide (Sigma, D2650).

2.4. Mutation validation

10 ng of DNA of primary dermal fibroblast and iPSCs from control and patients was amplified by standard PCR (40 cycles of 95°C for 30 seconds, 64°C for 30 seconds, 72°C for 30 seconds) using primers described in Dong *et al.* (2013) for the specific exons where the *PRPF31* mutations were located. The amplified products were purified using the QIAquick Purification kits (Qiagen, 28104 and 28704) and quantified using the Qubit® 2.0 Fluorometer. The sequencing files were analysed in the SeqScape v.2.5 software and forward and reverse sequences from both fibroblasts and iPSCs were aligned and compared with the *PRPF31* reference sequence gene (NG_009759.1) from Genbank to identify the *PRPF31* mutations. The consensus sequences from the forward and reverse sequences were then extracted from the software and pairwise aligned against the coding *PRPF31* sequence. The nucleotide designated as 1 commences at position 36 of GenBank accession number AL050369. All primer details are shown in Table 2.2.

2.5. RNA isolation and reverse transcription

iPSC and iPSC-derived RPE cell pellets were washed with PBS before being lysed with RNA Lysis buffer provided by the RNA extraction kit ReliaPrep™ RNA Cell Miniprep System (Promega, Z6010). The manufacturer's instructions were followed, including a DNase incubation step to the extracted RNA. The products were then passed through a column and resuspended in nuclease-free water. RNA was stored at -80°C or immediately used for cDNA synthesis. RNA was measured with a NanoDrop 2000 Spectrophotometer (Thermo Scientific) and 1 µg of extracted RNA

was converted into cDNA using GoScript™ Reverse Transcription System (Promega, A5000) following manufacturer's instructions.

2.6. Polymerase chain reaction (PCR)

For detection of any residual expression of the ectopically applied Yamanaka factors, PCR was carried out with primers that were complimentary to part of the Sendai vector as well as the transgenes. For the detection of mRNA transcripts as a result of c.1115_1125 del11 mutation, primers to detect wild type, long and short mutant transcripts of *PRPF31* gene were designed. All primers are listed on Table 2.2. The housekeeping gene (*GAPDH*) was used as a positive control. For the PCR reaction mixture, cDNA produced from 1 µg of RNA was amplified using primers at the concentration of 10 µM each in addition to 10 µM dNTP mix, 5X Green GoTaq® Reaction Buffer and GoTaq® DNA Polymerase (5 U/µl) (Promega, M3175). The PCR consisted of a 35-cycle program of 95°C for 30 seconds, 55°C for 30 seconds followed by 72°C for 30 seconds and was carried out using a Mastercycler® thermal cycler. Following the reactions, the samples were analysed using a 2% agarose gel electrophoresis mixed with GelRed™ Nucleic Acid Stain (Biotium, 41003). A 100 bp ladder was run against the samples.

2.7. Quantitative real time polymerase chain reaction (qRT-PCR)

qRT-PCR was performed using the GoTaq™ qPCR Master (Promega) according to the manufacturer's instructions. Each reaction contained 5 µl GoTaq qPCR Master Mix (Promega), 0.5 µl cDNA sample, nuclease-free water, and 0.6 µl primers (10 µM). All amplified products ranged from 100 to 200 bp in size. The plates were run on an Applied Biosystems 7500 fast Real Time PCR machine. The cycling program consisted of a hot-start activation at 95°C for 5 minutes, followed by 45 cycles of denaturation at 95°C for 10 seconds, annealing/extension at 60°C for 30 seconds, and denaturation 95°C for 1 minute. Following amplification, a melt-curve analysis was performed from 65°C to 95°C with 0.5°C increments every 10 seconds. Each sample was run in triplicates, and the average quantification cycle (C_q) value was determined. Control

reactions were run with water instead of template for each primer pair to check for primer-dimers and reagent contamination. Normalised gene expression values (against *GAPDH*) were obtained using the $\Delta\Delta CT$ method. All primer details are shown in Table 2.1.

2.8. Detection of pluripotency markers by immunocytochemistry

iPSC colonies were fixed in 4% paraformaldehyde (Sigma, 47608) for 15 minutes at room temperature and permeabilised with 0.25% Triton-X-100 (Sigma, T8787) for 40 minutes. Blocking solution was applied (10% FBS + 1% Bovine Serum Albumin - Sigma, A3311) for 45 minutes at room temperature before proceeding with addition of anti-human SSEA4 conjugated with Alexa Fluor® 555 (BD Biosciences) and anti-human OCT4 primary antibody (R&D). Secondary staining was performed with the antibody anti-goat IgG with FITC (Sigma) diluted in blocking solution, followed by nuclear counterstaining with DAPI (Partec, 05-5005). Colonies were imaged using a Bioscience Axiovert microscope in combination with the associated Carl Zeiss software, AxioVision. All antibody details are shown in Table 2.1.

2.9. Detection of pluripotency markers by flow cytometry analysis

iPSCs were treated with accutase (Gibco, A1110501) for 3 minutes at 37°C to dissociate the colonies. The suspension was collected in Phosphate Buffer Saline (PBS) and centrifuged for 3 minutes at 300xg. Supernatant was removed and replaced with PBS with 0.1% BSA containing TRA-1-60 conjugated FITC (Millipore) and NANOG conjugated with Alexa Fluor® 647 (Cell Signaling). Samples were incubated in the dark at room temperature for 60 minutes on a shaker. Cells were washed with PBS and resuspended in FACS buffer (PBS with 2% FBS). At least 10,000 events were analysed using a FACS Canto II flow cytometer. Results were analysed using the FACSDiva software.

2.10. *In vitro* and *in vivo* three germ layers differentiation assay

iPSCs were detached from 6-well plates (20-30 colonies per well) using 1 ml of 1 µg/ml Collagenase type IV (Gibco 17104-019) and 0.5 µg/ml Dispase II (Gibco, 17105-041) solutions. The colony suspension was transferred to a 50 ml conical tube until the colonies settled in the bottom of the tube. The supernatant was carefully aspirated and 2 ml of differentiation media, containing DMEM-F12 (Gibco 11330), 20% FBS (Gibco, 10270), 1% Penicillin/Streptomycin (Gibco, 15140), 1% Non-Essential Amino acids (Gibco, 11140), was added per well. The colony suspension was then transferred to a 10 cm petri dish and media was changed every day. After 7 days, the embryoid bodies (EBs) were transferred to a gelatin coated 24-well plate or a chamber slide. After an additional 7 days colonies were fixed and stained with anti-human SMA, TUJ1, AFP, FOXA2, HAND1 and PAX6. Details of all specific antibodies for the three germ layers and also secondary antibodies are shown in Table 2.1. As a negative control, cells were stained only with secondary antibodies.

For the teratoma assay, iPSC colonies were dissociated with EDTA and 1 million cells were resuspended in a 200 µl solution of PBS (Gibco, 14190) + 2% FBS (Gibco, 10270). The samples were injected intraperitoneally in immunosuppressed mice at the Comparative Biology Centre, at the Medical School, Newcastle University. Each injection consisted of 0.5 million cells mixed with 100 µl Matrigel (BD, 354230). Following a period of 10 weeks, the mice were euthanized and the teratomae were excised, processed and sectioned according to standard procedures and stained for Weigert's haematoxylin, Masson's trichrome and Mayer's haematoxylin and eosin histological analysis. Sections (5-8 µm) were examined using brightfield microscopy and stained tissue photographed as appropriate.

2.11. Genomic DNA Extraction

Genomic DNA was extracted from pelleted cell cultures following cell lysis, isolation, cleaning and elution of DNA, using the QIAamp DNA Mini Kit (Qiagen, 56304).

2.12. SNP array

DNA samples from the iPSCs and corresponding parental fibroblasts were analysed using the Infinium HumanCytoSNP-12 (Illumina, WG-320-2101) SNP array following the manufacturer's instructions. Around 300.000 SNPs were analysed, and SNP genotypes (B allele frequency) and physical copy number (R ratios) were determined by BlueFuse Multi 4.3 software (Illumina, San Diego, USA).

2.13. iPSC Differentiation to Retinal Pigment Epithelium (RPE)

iPSC colonies were grown to 80-95% confluency and all differentiation areas were removed. MTeSR™1 media was replaced with 2 ml of differentiation medium [Advanced RPMI 1640, (12633, Gibco), GlutaMAX-1 (35050, Gibco), penicillin/streptomycin (Gibco, 15140) and B-27 (Gibco, 17504)] supplemented with 10 µM SB431542 (STEMCELL™, 72232) and 10 ng/ml Noggin (R&D Systems, 6057-NG-025) from days 0 to 5. From days 6-9 only 10 ng/ml Noggin (R&D Systems, 6057-NG-025) was added to the medium. From days 10-15, the medium was supplemented with 5 ng/ml Activin A (PeproTech, 120-14A) and from days 16-21 Activin A was replaced with 3 µM CHIR99021 (Sigma, SML1046). The cells were then fed every two days until the first RPE patches appeared, normally by week 4 of differentiation. RPE patches were mechanically picked and placed in TryPLE Express (Gibco, 12604013) for 30 minutes to dissociate the cells, agitated by gentle pipetting at 10, 20 and 30 minutes. Cells were sieved using a 100 µm cell strainer and re-plated at 4.5×10^5 cells per cm² on 24 well plates or 0.33 cm² PET hanging cell culture inserts (Merck Millipore; Billerica, United States) coated with Matrigel™ GFR (Corning, 354230).

2.14. Counting of pigmented areas and measurement of pigment intensity

Original plates with pigmented patches were scanned at days 30, 60, 90 and 120. ImageJ (ImageJ 1.49, National Institutes of Health-USA) was used to count the number of pigmented foci and measure the intensity of pigmentation in images from a well of a 6-well plate for each experiment. The images were converted to 8-bit greyscale and

the function “find edges” was applied to detect and highlight the pigmented areas. The function “analyze particles” was then used on the images to detect and count pigmented areas by contrast, equal or greater than 18 pixels in size. The intensity of pigmentation was assessed by ImageJ through the measurement of grey areas in the images, where the higher values were associated with the decrease of white/grey areas and increase of dark pigmentation. The average number of foci and intensity of pigmentation values were divided by the area of the well.

2.15. Measurement of Trans-Epithelial Resistance (TER)

TER was performed using a Millicell ERS-2 Voltohmmeter (Millipore, MERS00002) by measuring the resistance of the blank transwell insert with PBS (Gibco, 14190) and the insert with RPE cells. The shorter and longer tips of the electrode were inserted in the transwell apical and in the basolateral chambers, respectively. The resistance was measured twice in each transwell insert. The resistance reading of the blank was then subtracted from the resistance reading of the cells for each measurement. The results were multiplied by the membrane area value using the formula: Unit area resistance = Resistance (Ω) x Effective Membrane Area (cm^2), where the final value was given in ohms (Ω).

2.16. Transmission Electron Microscopy (TEM)

RPE samples were fixed with 2% glutaraldehyde in 0.1M sodium cacodylate buffer and sent to the Transmission Electron Microscopy facilities at Newcastle University, where samples were post-fixed in 1% osmium tetroxide, dehydrated in gradient acetone and embedded in epoxy resin. Ultrathin sections (70 nm) were picked up on copper grids, stained with uranyl acetate and lead citrate and imaged using a Philips CM100 transmission electron microscope with high resolution digital image capture.

2.17. Serial Block Face SEM (SBFSEM)

Cells were fixed overnight in 2% glutaraldehyde in 0.1M sodium cacodylate buffer. Once fixed, the samples were processed using the heavy metal staining protocol adapted from Deerinck *et al.* (2018). Briefly, samples were incubated in a series of heavy metal solutions -3% potassium ferrocyanide in 2% osmium tetroxide, 10% thiocarbohydrazide, 2% osmium tetroxide again, 1% uranyl acetate overnight, and finally lead aspartate solution. Between each step the samples were rinsed thoroughly in several changes of deionised water. Samples were dehydrated through a graded series of acetone and then impregnated with increasing concentrations of Taab 812 hard resin, with several changes of 100% resin. The samples were embedded in 100% resin and left to polymerise at 60°C for a minimum of 36 hours. The resin blocks were trimmed to approximately 0.75 mm by 0.5 mm and glued onto an aluminium pin. In order to reduce sample charging within the SEM, the block was painted with silver glue and sputter-coated with a 5 nm layer of gold. The pin was placed into a Zeiss Sigma SEM incorporating the Gatan 3view system, which allows sectioning of the block *in situ* and the collection of a series of images in the z-direction. Multiple regions of interest were imaged at x2000 magnification, 3000 x 1500 pixels scan, which gave a pixel resolution of approximately 15 nm. Section thickness was 50 nm in the z-direction. In the resulting z-stacks, cilia were identified and segmented manually using Microscopy Image Browser (MIB, University of Helsinki). The segmentations were imported into Amira (FEI) for construction of the 3D models.

2.18. Phagocytosis Assay

Bovine Rod Photoreceptor Outer Segments (POS) (InVisionBioResources, 98740) were centrifuged at 2600xg for 4 minutes and the pellet was resuspended in 100 µl of Advanced RPMI 1640 medium (12633, Gibco). The POS were incubated with 0.4 mg/ml FITC for 1 hour at room temperature and agitated in the dark. POS were centrifuged at 2600xg for 4 minutes and washed three times with PBS (Gibco, 14190). Then, they were resuspended in AdRPMI 1640 (12633, Gibco) supplemented with B-27 (Gibco, 17504) and 10% Fetal Bovine Serum (FBS) (Gibco, 10270) and the staining was confirmed under a Bioscience Axiovert microscope. RPE cells were treated with

1 x 10⁶ POS-FITC per cm² and incubated for 4 hours at 37°C. Control RPE cells were treated with the same number of non-stained POS and incubated for the same time. Controls treated with stained POS and incubated at 4°C were also set up. Cells were rinsed with PBS supplemented with calcium and were detached from the wells using 200 µl of TrypLE Express (Gibco, 12604013) for 5-8 minutes. TrypLE was neutralised by the addition of 500 µl of AdRPMI 1640 medium with 10% FBS and POS were centrifuged at 300xg. Cells were washed with 0.2% Trypan Blue Solution (Sigma, T8154) to quench fluorescence from bound POS, washed with PBS and suspended in FACS buffer (PBS with 2% FBS). 5 mM DRAQ5 (Biostatus, DR50200; 1:2500) was used to distinguish cells from debris and outer segments. Samples were analysed immediately on a LSRII flow cytometer and 10,000 events were collected per sample. Results were analysed using FACS Diva software.

2.19. RPE Cytokine Secretion Studies

Medium from basal and apical chambers of transwell inserts were collected from RPE cells of healthy controls and patients. The levels of PEDF and VEGF secretion were measured by using human PEDF-ELISA Kit (Cusabio, CSB-E08818h) and human VEGF-ELISA Kit (Life technologies KHG0111) according to manufacturer's instructions.

2.20. RPE Characterisation by Immunocytochemistry

Cells were fixed in 4% paraformaldehyde (Sigma, 47608) for 15 minutes at room temperature and permeabilised with 0.25% Triton-X-100 (Sigma, T8787) for 15 minutes, followed by treatment with blocking solution (3% BSA in PBS, Sigma, A3311) for 30 minutes at room temperature. Cells were treated with primary antibodies Anti-Bestrophin (Abcam, 1:300), Anti-Sodium Potassium ATPase (Alexa Fluor® 488 conjugate) (Abcam, 1:50), Pericentrin (Abcam, 1:500), MERTK (Bethyl, 1:200), ARL13B (Proteintech, 1:500), Collagen IV (Abcam, 1:200), PRPF31 (Abnova, 1:500) and SNRPB Monoclonal Antibody (Y12) (Thermo, 1:500), overnight at 4°C, and with secondary antibodies anti-rabbit FITC (Sigma, 1:500) or anti mouse FITC (Jackson

Immuno Research, 1:500) and anti-mouse Cy3 (Jackson Immuno Research, 1:500) or anti-rabbit Cy3 (Jackson Immuno Research 1:500) diluted in PBS for 1 hour at room temperature. Washes with PBS were carried out between and after treatments. Finally, cells were treated with the nuclear stain-DAPI (Partec, 05-5005), and imaged using a Nikon A1R Confocal microscope in combination with the associated NIS Elements software. All antibody details are shown in Table 2.1.

2.21. Inhibition of nonsense-mediated mRNA decay (NMD)

Inhibition of NMD was achieved by incubating 10×10^4 cells per cm^2 with 300 $\mu\text{g/ml}$ of puromycin (Sigma-Aldrich) for 6 hours. All negative controls were treated with a relevant volume of DMSO alone. Cells were pelleted and RNA was extracted for semi-quantitative RT-PCR analysis.

2.22. Western blot analysis

Cells were washed with PBS and lysed in lysis buffer (40 mM HEPES pH 7.4, 150 mM NaCl, 1% Triton X-100, 1 mM phenylmethylsulfonylfluoride, 1 mM sodium orthovanadate and 0.5 mM DTT) supplemented with phosphatase inhibitor and EDTA-free protease inhibitor cocktails (Roche). The concentration of total protein in cleared lysates was measured by Bradford assay and about 20 μg of each sample was analysed by western blotting followed by immunostaining using antibodies against SART1, PRPF8, Snu114, PRPF31 (against its N terminus or C terminus), PRPF4 and SF3b155, and the Amersham ECL detection kit (GE Healthcare). All antibody details are shown in Table 2.1.

2.23. E1A alternative splicing assays

Total RNA was extracted from cells transduced with the E1A lentivirus using an RNA extraction kit (Macherey Nagel). E1A alternative splicing was analysed by RT-PCR with 1 µg of the total RNA sample using the high-capacity cDNA reverse transcription kit (Applied Biosystems) and GoTaq DNA polymerase (Promega). PCR was performed with the 5'-end radiolabelled exon 1 forward primer (5'-GTTTTCTCCTCCGAGCCGCTCCGA) and the exon 2 reverse primer (5'-CTCAGGCTCAGGTTTCAGACACAGG) by using the following programme: 95 °C for 2 min, 30 cycles of 95 °C for 30 s, 64 °C for 30 s, 72 °C for 1 min, and a final step of 72 °C for 5 min. PCR products were separated by denaturing polyacrylamide gel electrophoresis (PAGE), visualised by autoradiography using a Typhoon Trio plus scanner (GE Healthcare) and quantified using Quantity One software (Bio-Rad).

2.24. RNA Sequencing

Total RNA was extracted from tissue using TRIzol (ThermoFisher Scientific Inc). RNA samples were treated with a TURBO DNA-free™ Kit (Ambion Inc.) using conditions recommended by the manufacturers, and then cleaned with an RNA Clean & Concentrator™-5 spin column (Zymo Research Corp.) RNA was tested for quality and yield using a NanoDrop 1000 spectrophotometer and an Agilent 2100 Bioanalyzer. RNA-seq analysis was performed for all patients and all controls as triplicate biological repeats. To minimize bubble PCR artefacts, 100 ng of purified total RNA was used for library preparation, following the “TruSeq” Illumina protocol. In brief, RNA was polyA-selected, chemically fragmented to about 200 nt in size, and cDNA synthesized using random hexamer primers. Each individual library received a unique Illumina barcode. RNA-seq was performed on an Illumina HiSeq 2000 or HiSeq2500 instrument with six or eight libraries multiplexed per flow-cell lane using 100 bp paired-end reads. This resulted in an average of 250 million reads per lane, with an average of 40 million reads per sample. Raw reads were aligned to the human (*Homo sapiens*) full genome (GRCm38, UCSC mm10) using STAR, a splice-aware aligner (Dobin *et al.*, 2013). GTF transcript annotation files were downloaded from Ensembl. Transcripts were assembled using STAR, followed by estimates of raw gene counts using HTSeq (Anders *et al.*, 2015). Differential gene expression was analysed using DESeq2 (Love

et al., 2014) with statistical significance expressed as a p-value adjusted for a false discovery rate of 0.01 using Benjamini-Hochberg correction for multiple-testing.

Alternative splicing analysis was then carried out using rMATS (Park *et al.*, 2013). For each comparison being made we used the sorted BAM files produced by STAR to run rMATS using default unpaired settings. Reported splicing changes were considered significant if they had a p-value less than 0.05 and a change in inclusion level difference of more than 5%. GO Enrichment Analysis was carried out on the genes found to have significant splicing changes via clusterProfiler (Yu *et al.*, 2012). Multiple testing corrections were carried out using the Benjamini-Hochberg method with an adjusted p-value < 0.05 denoting significantly enriched gene ontology.

2.25. Cilia Length and Frequency Measurements in RPE Cells

The length of cilia was measured by a 3D method using Imaris 8.3 Software (Bitplane Inc). Immunocytochemistry Z-stacks images of RPE samples from patients and controls were uploaded to Imaris. Surfaces were created to cover all the length of the cilia across the bottom and top of the stacks. The values were given in μm and a minimum of 150 cilia were independently measured for each sample. The cilia incidence was calculated by counting the number of cilia per cell in each image. Z-stacks were uploaded to Imaris software and spots were created for the blue (DAPI) and green (FITC) channels to cover all nuclei and cilia of cells. The percentage of cilia spots per nuclei spots was calculated and a minimum of 300 cells were counted per sample.

2.26. CRISPR/Cas9 Correction of PRPF31 Mutation in the RP11VS

Correction of *PRPF31* mutation in the RP11VS iPSCs was achieved by using the CRISPR/Cas9 system in combination with ssODNs as homologous templates covering the mutation site. The online design tool (<http://tools.genome-engineering.org>) was used to design the sgRNA sequences and predict off-targets. The sgRNA (Table 2.2), which targets only mutant but not wild-type *PRPF31* sequences and predicted to have low off-targets, was chosen. The sgRNA was cloned into the CRISPR/Cas9 vector

(pSpCas9(BB)-2A-Puro) following the protocol from Ran *et al.* (2013). The ssODN template with wildtype *PRPF31* sequences was designed manually with 91bp homology arms on each side of the mutation region (Table 2.2). The sgRNA-CRISPR/Cas9 vector and ssODN were co-transfected into the RP11VS iPSCs by using Lipofectamine-3000 (Invitrogen) according to the manufacturer's instructions. 24 hours after transfection, puromycin (0.2 µg/ml) was added for 2 days. 4-5 days after selection, the resistant iPSCs were dissociated into single cells using Accutase (Gibco, A1110501). 100,000 cells in mTeSR1 media supplemented with ROCK inhibitor (Y-27632, Chemdea, CD0141, 20 µM) were plated on a 10 cm Matrigel-coated dish. After 7 days, the colonies were picked and transferred to a cell culture 96-well plate. When the wells became confluent, iPSCs were split in two 24-well plates for further expansion and DNA isolation. Genomic DNA (gDNA) was isolated using QIAamp DNA Mini Kit (Qiagen, 56304). Subsequently, PCR were performed with the primers including *PRPF31*-mutation specific primers; *PRPF31*-WT specific primers; *PRPF31*-mutation/WT primers (Table 2.2). The positive clones, which are negative for *PRPF31*-mutation specific primers and positive for *PRPF31*-WT specific primers were sequenced to confirm *in situ* gene-editing of *PRPF31*.

sgRNA off-target sequences were predicted using the online design tool (<http://tools.genome-engineering.org>). Each sgRNA off target sequence was blasted against the human genome reference (<https://blast.ncbi.nlm.nih.gov/Blast.cgi>). Capture intervals were expanded by approximately 500 bp in both the 5' and 3' directions. Primers were designed for this region (Table 2.2). The PCR products were then sequenced to check the off-target effects of sgRNA.

2.27. Quantification and Statistical Analysis

p-values were calculated of normally distributed data sets using a two-tailed Student's *t* test, or One-way ANOVA with Dunnett's post-hoc test, or two-way ANOVA with Bonferroni post-hoc tests using GraphPad Prism Software Inc. (San Diego, CA, USA). Statistical analyses represent the mean of at least three independent experiments, error bars represent standard error of mean (s.e.m.) or as otherwise indicated. The statistical significance of pairwise comparisons shown on bar graphs is indicated by: n.s. not significant, * $p < 0.05$, ** $p < 0.01$, *** $p < 0.001$, and **** $p < 0.0001$.

For cell populations, a minimum of 100 cells were counted from >10 separate fields of view.

Name	Dilution	Clone	Company/ number	Catalogue
Anti-ARL13B	1 in 500-1000	Rabbit polyclonal, IgG	Proteintech/	17711-1-AP
Anti-PRPF31	1 in 100-500	Goat polyclonal	Abnova/	PAB7154
Anti-SNRPB (Y12)	1 in 500	Mouse monoclonal IgG3, F-2	ThermoFisher/	MA5-13449
Anti-Bestrophin [E6-6]	1 in 300	Mouse monoclonal IgG1, kappa [E6-6]	Abcam/	ab2182
Anti-Sodium Potassium ATPase (Alexa Fluor® 488 conjugate)	1 in 50	Rabbit monoclonal [EP1845Y]	Abcam/	ab197713
Anti-NANOG (Alexa Fluor® 647 conjugate)	1 in 150	Rabbit monoclonal	Cell Signalling Technology/	5448S
Anti-TRA-1-60 (FITC conjugate)	1 in 60	Mouse monoclonal	Merck Millipore/	FCMAB115F
Anti-SMA	1 in 100	Mouse IgG2a	Thermofisher/	A25538
Anti-TUJ1	1 in 500	Rabbit	Thermofisher/	A25538
Anti-AFP	1 in 500	Mouse IgG2a	Thermofisher/	A25538
Anti-FOXA2	1 in 250	Mouse monoclonal	Abcam/	ab60721
Anti-HAND1	1 in 350	Rabbit polyclonal	Abcam/	ab46822
Anti-PAX6	1 in 350	Rabbit polyclonal	Convance/	PRB-278P
Anti-SSEA4 (Alexa Fluor®555 conjugate)	1 in 200	Mouse IgG1	BD Biosciences/	560218
Anti-OCT4	1 in 200	Polyclonal Goat IgG	R&D/	AF1759
Anti-Pericentrin	1 in 500	Mouse Monoclonal IgG1	Abcam/	ab28144
Anti-MERTK	1 in 200	Rabbit	Bethyl/	A300-222A
Anti-Collagen IV	1 in 200	Rabbit polyclonal	Abcam/	ab6586
Anti-PRPF8	1 in 2500	Rabbit polyclonal	Homemade	
Anti-SF3b155	1 in 2000	Rabbit polyclonal	Homemade	
Anti-Snu114	1 in 5000	Rabbit polyclonal	Homemade	
Anti-PRPF4	1 in 1000	Rabbit polyclonal	Homemade	
Anti-SART1	1 in 1000	Rabbit polyclonal	Homemade	
Anti-PRPF31 (against C-terminus)	1 in 1000	Rabbit polyclonal	Homemade	
SECONDARY ANTIBODIES				
Name	Dilution		Company/ number	Catalogue
Goat anti-Mouse IgG, Alexa Fluor 488	1 in 2000		Life Technologies Ltd/	A11029
Goat anti-Mouse IgG, Alexa Fluor 568	1 in 2000		Life Technologies Ltd/	A11031
Goat anti-Rabbit IgG, Alexa Fluor 488	1 in 2000		Life Technologies Ltd/	A11034
Goat anti-Rabbit IgG, Alexa Fluor 568	1 in 2000		Life Technologies Ltd/	A11011
Anti-Mouse-IgG-FITC	1 in 500		Jackson Immuno Research/	715-095-151
Anti-Mouse-IgG-Cy3	1 in 500		Jackson Immuno Research/	115-165-003
Anti-Rabbit-IgG-Cy3	1 in 500		Jackson Immuno Research/	111-165-003
Anti-Goat-IgG-FITC	1 in 500		Jackson Immuno Research/	705-096-147

Table 2.1. List of antibodies used for ICC and their dilutions.

MUTATION VALIDATION			
	Forward	Reverse	Size of Products
c.522_527 +10del exons 6,7	GTTCCCGAGCCTCCCCTATCTTCT	CGCTCCAGCTCCTCCTCCGACA G	320 bp
c.1115_1125 del11 exons 10,11	GTGGCGGTGAGGCAGCATTAGGT G	CTGGCTGGCTGTGGGGTTGAG GA	430 bp
GAPDH	GGCATGGACTGTGGTCATGAG	TGCACCACCAACTGCTTAGC	81 bp
SENDAI CLEARANCE PRIMERS			
SeV	GGATCACTAGGTGATATCGAGC	ACCAGACAAGAGTTTAAGAGAT ATGTATC	181 bp
KOS	ATGCACCGCTACGACGTGAGCGC	ACCTTGACAATCCTGATGTGG	528 bp
Klf4	TTCCTGCATGCCAGAGGAGCCC	AATGTATCGAAGGTGCTCAA	410 bp
c-Myc	TAAGTACTAGCAGGCTTGTGCG	TCCACATACAGTCTGGATGAT GATG	532 bp
GAPDH	GGCATGGACTGTGGTCATGAG	TGCACCACCAACTGCTTAGC	81 bp
PRPF31-EXON11-WT.LM.SM			
h-prpf_ex10F- to-EX12R	TGGATGGACAGCGGAAGAAG	CTCGTTTACCTGTGTCTGCC	203 bp (WT) 192 bp (LM) 130 bp (SM)
gRNA, ssODN, PRIMERS FOR CRISPR-CAS9			
PRPF31- exon11- gRNA	GAGATCCAACCGTATGAGCTT		
PRPF31- exon11- ssODN	GTCCTCCTCCCAGCCGACTCCCTGGCGCCGCCACCCACCCGTCGCCAGGTACCGCAAGAT GAAGGAGCGGCTGGGGCTGACGGAGATCCGGAAGCAGGCCAACCGTATGAGCTTCGGAGA GGTCAGACTCCCAGAGCGCCCTCCTCAACCCACAGCCAGCCAGCCGCCACCGCCCTCTGC CTCCTGCCA		
sgRNA OFF-TARGET SEQUENCES		PCR PRIMERS FOR OFF-TARGET REGION	
Offtarget- 1	CAGGCCAACCGTATGAGCTT CGG	CGCAAATTCGACAAGTGCC A	GCTTTGGGGCTGAACGG ATG
Offtarget- 2	AGAAACTACAGTATGAGCTTA GG	GGAGATTGTGCCTCAGTGC T	TCTTGAGCACTTCACCAT TCTT
Offtarget- 3	ACAACCAAAGGTATGAGCTTC AG	TGGGTCTTCTTTGTCCTGAC T	GCATAGGCTGCTTGGCAA AT
Offtarget- 4	CTATCCAAGTGAATGAGCTTG GG	TGCTGGGAGGGTCTTACAC T	TGGCCAGCTACATCCAAG AA
Offtarget- 5	AGAGTCAGCCGTCTGAGCTT TGG	CACGGCCTGGGATAACATA CT	GGCCATACTGCCTATCAC ACA
Offtarget- 6	AGACCCTACTCTATGAGCTTA GG	AGTTATTGGGCCGAACCTG G	CAACAGCCAGTTACGGTT GC
Offtarget- 7	ACATCAAAGGGTATGAGCTTT AG	GAAATGACCTGGGTGGAAG C	TACTCTGTGAACACATGA GCCAG
Offtarget- 8	AGATCCATCTGTATGTGCTTG GG	CCTCCACACCGCACA	TGCCTGTCAGTAGGAGAG AGG
Offtarget- 9	AGCTACAACCAGATGAGCTTC AG	AGGTTGACAAACATGGCTT GG	AAGTCAAGCTGGTGCCTA AG
Offtarget- 10	AGAACTAACAGTATGAGCTCC AG	AGTTCAGGCCAAGCAGATC A	AAATGCCTAGCCTGAGGT CTG
Offtarget- 11	GGATCTAACAGTTTGAGCTTG AG	CCTGGGATTCAAACTCCAC CT	ACTGCATGCCAGGCAATA TG
MUTATION SPECIFIC PRIMERS			
	Forward	Reverse	
PRPF31-exon11-Mutation Specific Primer	CGCAAATTCGACAAGTGCCA	TCCGAAGCTCATACGGTTGGATC	
PRPF31-exon11-WT Specific Primer	CGCAAATTCGACAAGTGCCA	GAAGCTCATACGGTTGGCCTGCTT	
PRPF31-exon11-Mutation/WT Primer	CGCAAATTCGACAAGTGCCA	GCTTTGGGGCTGAACGGATG	

Table 2.2. List of primers used for PCR and Q-PCR.

Chapter 3 - Generation and characterisation of iPSCs

3.1. Introduction

The ability to generate patient-specific induced pluripotent stem cells and the great potential of iPSCs to differentiate into disease-relevant cell types, make these cells excellent models for *in vitro* disease modelling (Tucker *et al.*, 2013; Capowski *et al.*, 2014; Sternecker *et al.*, 2014; Yoshida *et al.*, 2014). Unlike primary cultures, iPSCs are capable of self-renew, providing unlimited cell source to investigate diseases at molecular, cellular, and functional levels. This is particularly useful for PRPF31-RP, since its phenotype is restricted to clinically relevant cells, such as RPE cells and photoreceptors.

The reprogramming into iPSCs is initially directed by the expression of the reprogramming transgenes, which are required by the transduced cells for 2-3 weeks, and during this time a cascade of events is initiated in the cells of origin which culminates in the silencing of cell type-specific genes and in the activation of endogenous genes required for pluripotency and self-renewal such as *OCT4*, *SOX2* and *NANOG* (Takahashi *et al.*, 2007). Once properly established, the pluripotency state is maintained, and the cells exhibit expression of pluripotency genes and the ability to give rise to any cell types from the three germ layers (Chan *et al.*, 2009).

The differential potential of iPSCs, however, can be affected by some limitations that are still inherent to iPSC technology. This includes incomplete reprogramming, integration of reprogramming transgenes to the host's genome and introduction of genetic variation during the course of reprogramming or continuous passaging, especially in long-term cultures (Figure 3.1). Therefore, the iPSC characterisation process is essential to ensure the generation of bona fide iPSC lines, suitable for downstream applications (Liang and Zhang, 2013a).

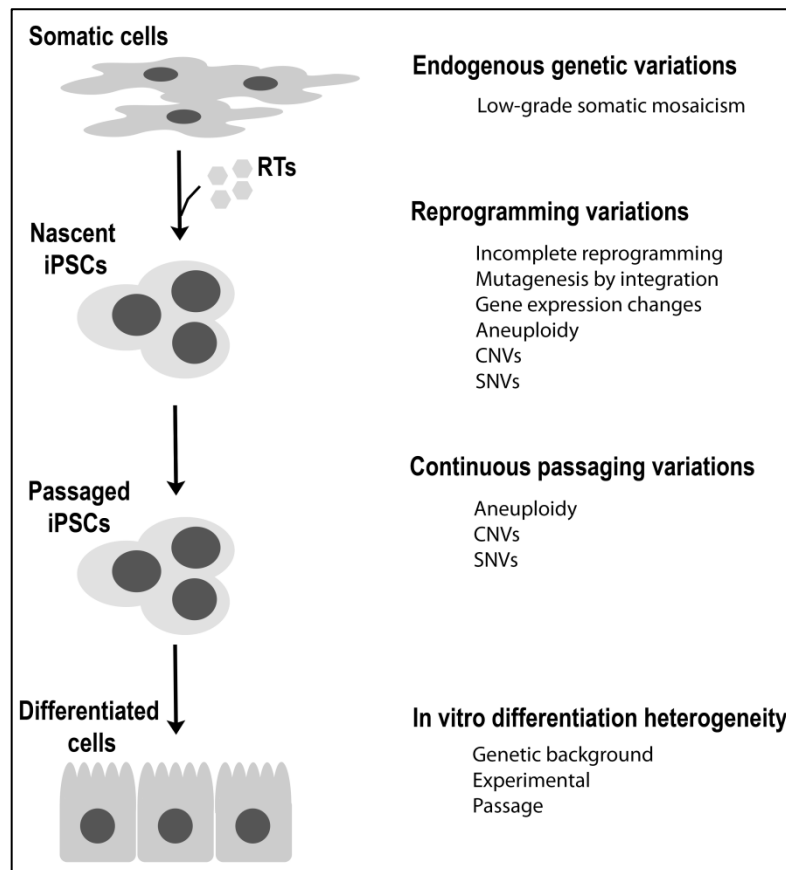


Figure 3.1. Sources of genetic variation throughout the process of iPSC generation and differentiation. Transduction of iPSCs with reprogramming transgenes (RTs) can lead to mutagenesis by integration of transgenes to the host's genomes. Incomplete reprogramming can result in genetic variation due to failure of the removal of somatic epigenetic marks in the reprogrammed cells. CNVs: copy number variants, SNVs: single nucleotide variants.

3.2. Aims

This chapter aims to describe the process of generation and characterisation of control and PRPF31-iPSCs generated for this study as follows:

- Mutation validation of control and PRPF31-mutant cell lines
- Generation of iPSCs by transduction of controls and PRPF31-mutant fibroblasts with Sendai vectors containing reprogramming transgenes
- Detection of residual expression of Sendai genome and reprogramming transgenes in controls and PRPF31-mutant iPSC lines
- Assessment of pluripotency of controls and PRPF31-mutant iPSCs by expression of pluripotency markers and *in vitro* and *in vivo* differentiation potential
- Analysis of chromosomal abnormalities and confirmation of genetic identity of controls and PRPF31-mutant iPSCs, as well as parental fibroblasts

3.3. Control and patient's samples

Seven patients with *PRPF31* mutations were identified in collaboration with Mr. Martin McKibbin, Mr. David Steel and Prof. Chris Inglehearn at St James University Hospital, Leeds. Skin biopsies were deposited at the Newcastle's University Biobank, which was able to derive dermal skin fibroblasts following appropriate ethics consent. Three patients from the same family harboured a deletion at exon 11 (c.1115_1125 del11), another three patients from other unrelated family harboured a deletion at exon 6 in *PRPF31* gene (c.522_527+10del) and one patient had a single point mutation in exon 3 (c.201delT) (Figure 3.2). The age and phenotypes of the patients are shown in table 3.1.

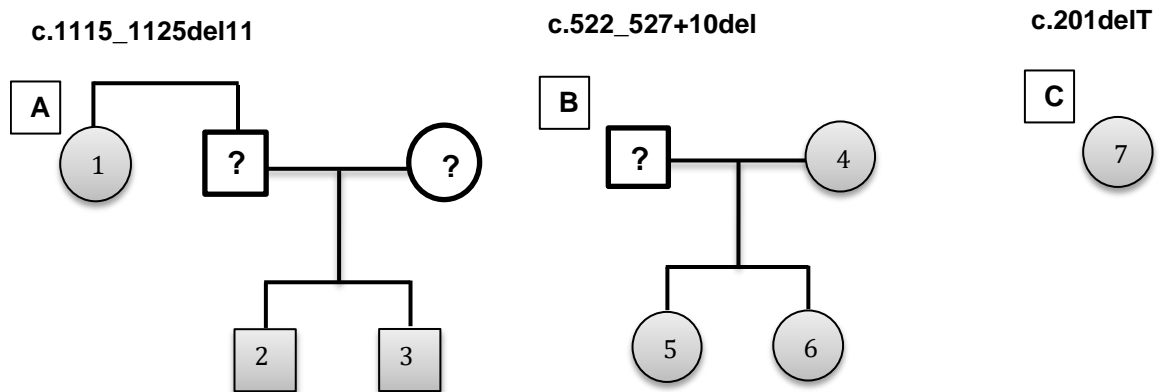


Figure 3.2. Family pedigrees of RP-*PRPF31* patients and their respective mutations. A: Paternal aunt and two siblings harbouring mutation c.1115_1125del11. B: Mother and two siblings harbouring mutation c.522_527+10del. C: Single patient harbouring mutation c.201delT. Question marks represent unknown genotypes/phenotypes

Case No.	Sample No.	Lab ID.	Initials	Age (biopsy)	Age (onset of symptoms)	Sex	Type	Genotype	Phenotype
Control	WT1	AD2	-	51	-	M	-	-	Unaffected [LONZA, 0000293971]
Control	WT3	AD4	-	68	-	M	-	-	Unaffected [LONZA, 0000268030]
1	RP11S1	F116	MR	69	10	F	PRPF31	c.1115_1125 del11	Severe - Presented with night blindness aged 10yrs old with decreased central vision by 30yrs. Cataract requiring surgery in 50s. Current visual acuity 6/60 and 6/24. Bilateral extensive bone spicular fundal pigmentation, attenuated arterioles and pale optic discs with small preserved islands of RPE in macula.
2	RP11M	F118	RH	52	10	M	PRPF31	c.1115_1125 del11	Moderate - Presented with night blindness aged 10yrs old. Cataracts requiring surgery at early age. Current. Acuity 6/9 both eyes and still meeting legal requirements for driving. Ring of bone spiculation (about 4 Optic Disc Diameters wide) anterior to arcades, maculae normal.
3	RP11VS	F119	SH	45	10	M	PRPF31	c.1115_1125 del11	Very Severe - Presented with night blindness aged 10yrs old with decreased central vision by 30yrs. Also has right optic nerve hypoplasia. Current visual acuity - No perception of light right eye and 6/18 left. Bilateral extensive bone spicular fundal pigmentation, attenuated arterioles and pale optic discs and visual field restricted to around 5 degrees from fixation.
4	RP11A	F149	RW	78	Asymptomatic	F	PRPF31	c.522_527+10del	Mild - Asymptomatic patient and mother of cases 2 and 3. No visual symptoms but subtle intra retinal pigment migration peripherally in both fundi. Visual acuity 6/9 bilaterally.
5	RP11S2	F255	HD	49	15	F	PRPF31	c.522_527+10del	Severe - Presented with night blindness aged 15yrs old with decreased central vision by 30yrs. Current visual acuities 6/18 and 6/36 with a refraction of -2 and bilateral posterior subcapsular cataracts. Bilateral extensive bone spicular fundal pigmentation, attenuated arterioles and pale optic discs.
6	RP11S3	F150	AW	50	15	F	PRPF31	c.522_527+10del	Severe - very similar clinical phenotype and age of onset to sister, patient RP11S2.
7	RP11S4	F117	CW	52	18	F	PRPF31	c.201delT	Severe - Presented with night blindness aged 10yrs old and reduced central vision from 20 years old. Cataracts requiring surgery at early age. Current visual acuity Hand movements bilaterally. Bilateral extensive bone spicular fundal pigmentation, attenuated arterioles and pale optic discs with central macular atrophy also. Visual field constricted to <5 degrees from fixation.

Table 3.1. Age matched controls and PRPF31-mutant patients used in this study. All patients, shown in column 'Sample No.', are named as RP11 followed by A (asymptomatic), M (moderate), S (severe) and VS (very severe) and two unaffected controls are referred to as WT1 and WT3.

3.4. Confirmatory mutation screening analysis

To confirm the genotype of the fibroblasts, the regions harboring the mutations were amplified by PCR with primers that flanked mutated regions and submitted to Sanger sequencing. This was also performed in fibroblast derived-iPSCs to ensure that all iPSCs generated had the same mutations of the parental fibroblasts.

Three patients, harboring the mutation c.1115_1125 del11 were screened for *PRPF31* exon 11, where the mutation was located. Screening of this sequence in patients RP11S1, RP11M and RP11VS (Figure 3.2A, Table 3.1) revealed a 11 bp deletion in exon 11, present in fibroblasts and iPSCs (Figure 3.3). One of the predicted effects of this mutation is the inactivation of an exonic splicing enhancer, leading to the skipping of exon 11 during splicing and out of phase premature termination codon (PTC) in exon 12 (Vithana *et al.*, 2001). This could then result in a short mRNA transcript encoding 387 amino acids, which would be sensitive to nonsense-mediated mRNA decay (NMD), or it could result in the formation of a long mRNA transcript containing the deletion in exon 11 and a PTC before the natural termination codon in exon 14, encoding 469 amino acids (Figure 3.4) (Rio Frio *et al.*, 2008). The effects of the mutations were confirmed, and results are shown in Chapter 5.

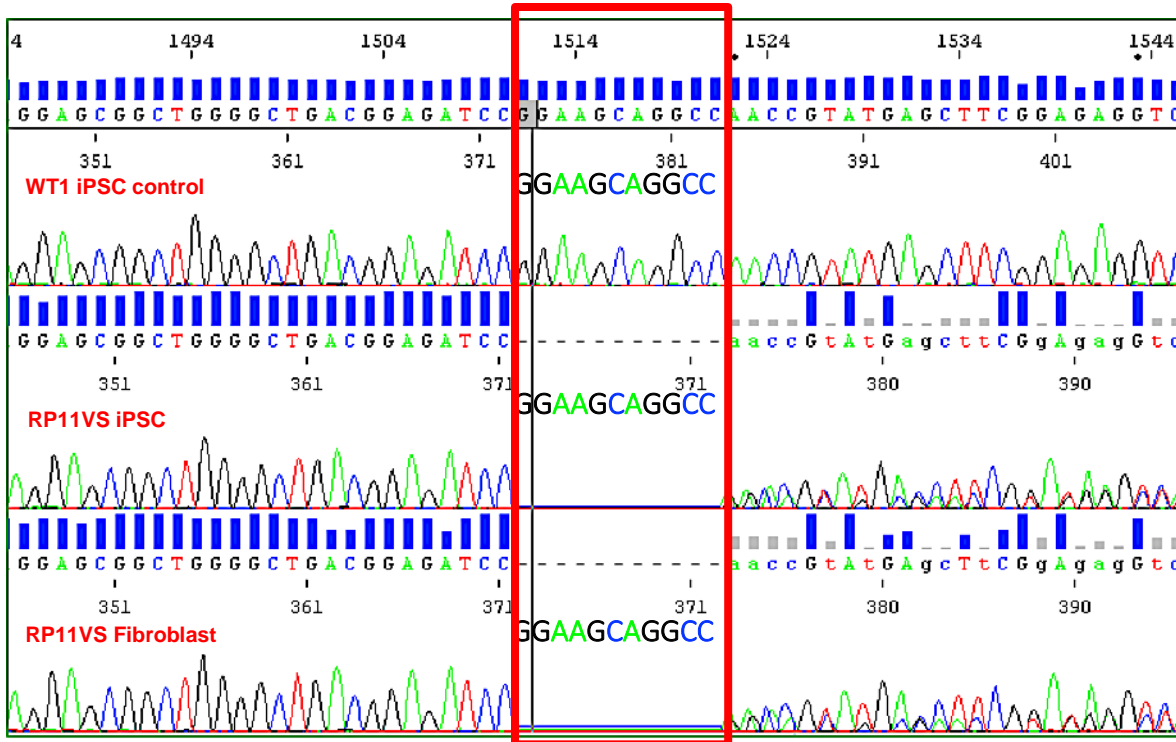


Figure 3.3. Sequences of *PRPF31* exon 11 from WT1 control iPSC (upper), RP11VS iPSC (middle) and RP11VS fibroblast (lower). As the mutation is heterozygous, the middle and lower images show both the mutated and normal sequences superimposed after the deletion. The spaces inside the red box were created to facilitate the view of the deletion and the alignment of the control and *PRPF31*-RP sequences. The other two patients of the same family showed the same deletion.

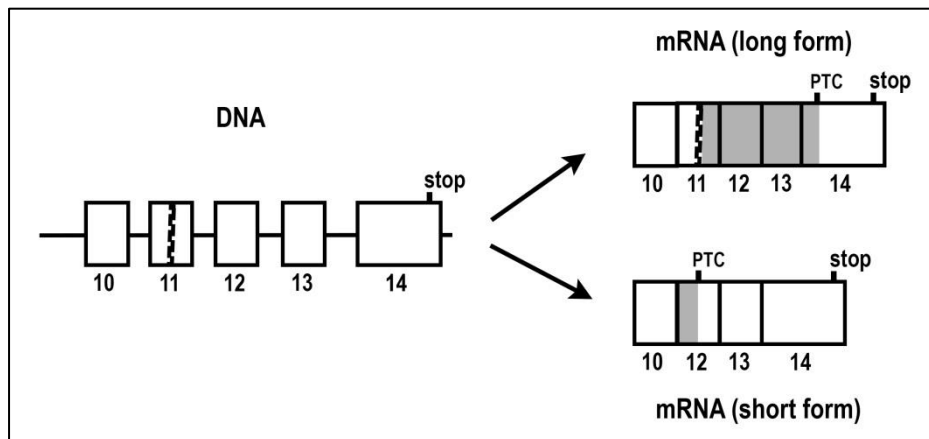


Figure 3.4. Predicted effects of the *PRPF31* c.1115_1125del mutation on its own transcripts. The mutation, represented by the vertical dotted bar, result in either a long mRNA transcript containing the deletion in exon 11 and a PTC just before the termination codon in exon 14, or a short mRNA transcript formed by the skipping of exon 11 during splicing and a PTC in exon 12.

Three patients (RP11A, RP11S2 and RP11S3) harboring the mutation c.522_527+10del were screened for *PRPF31* exon 6, where this mutation was located (Figure 3.2B, Table 3.1). The sequences confirmed the mutation was present in fibroblasts and iPSCs (Figure 3.5). This mutation consists of a 16 bp deletion starting at the end of exon 6 and ending at the beginning of intron 6 and delete codons 175 and 176, which encode glutamine and glycine residues. It also deletes the first 10 bp of intron 6, including the exon 6/intron 6 boundary and splice donor site. The new mRNA transcript may include intron 6, encoding 7 novel amino acids, or exclude exon 6 entirely (Ghazawy *et al.*, 2007) (Figure 3.6).

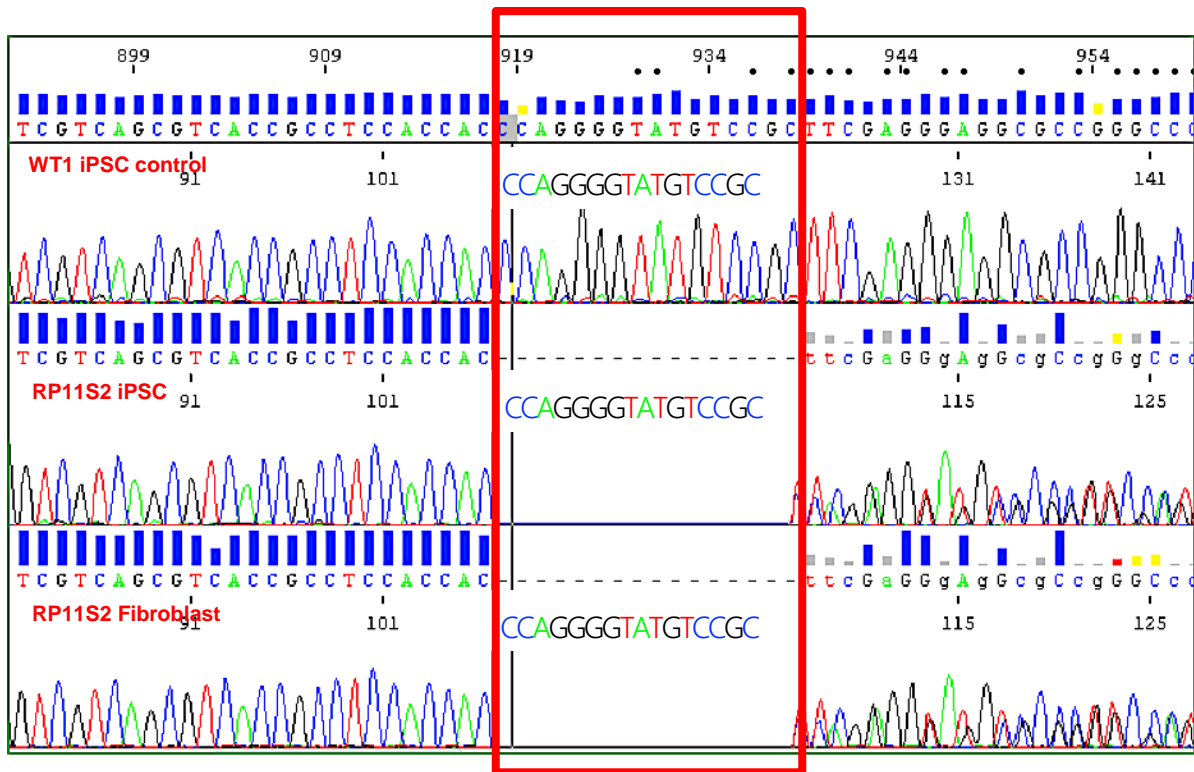


Figure 3.5. Sequences of *PRPF31* exon 6 from WT1 control iPSC (upper), RP11S2 iPSC (middle) and RP11S2 fibroblast (lower). As the mutation is heterozygous, the middle and lower images show both the mutated and normal sequences superimposed after the deletion. The spaces inside the red box were created to facilitate the view of the deletion and the alignment of the control and *PRPF31*-RP sequences. The other two patients of the same family showed the same deletion.

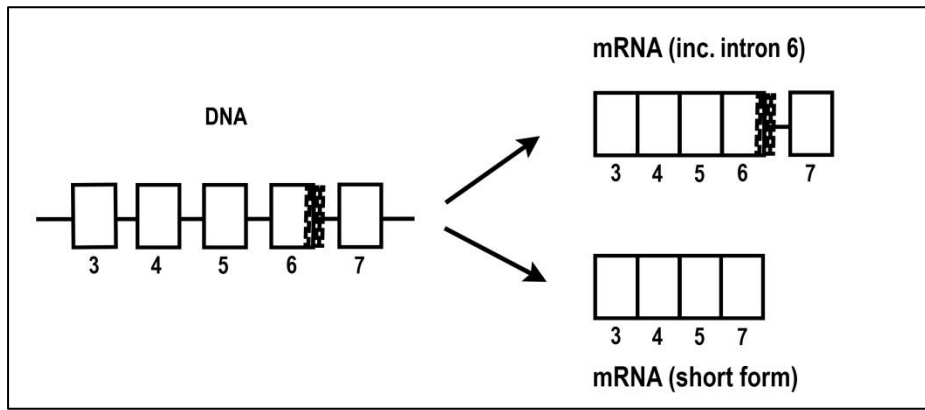


Figure 3.6. Predicted effects of the *PRPF31* c.522_527+10del mutation on its own transcripts. The mutation, represented by the vertical dotted bar, result in either a mRNA transcript containing the deletion in exon 6, including intron 6, or a short mRNA transcript formed by the skipping of exon 6 entirely.

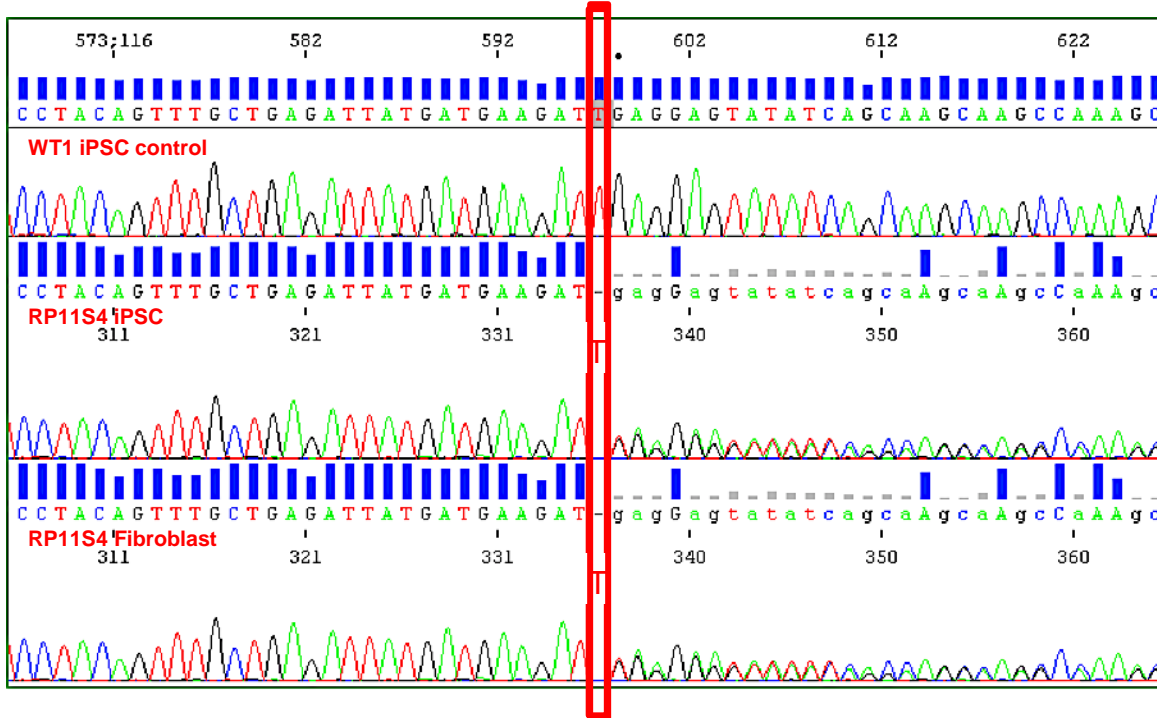


Figure 3.7. Sequences of *PRPF31* exon 3 from control iPSC (upper), RP11S4 iPSC (middle) and RP11S4 fibroblast (lower). As the mutation is heterozygous, the middle and lower images show both the mutated and normal sequences superimposed after the deletion. The single space inside the red box was created to facilitate the view of the deletion and the alignment of the control and patient sequences.

The other sequence screened was *PRPF31* encompassing exons 2 and 3 together. The screening of this sequence in the patient RP11S4 (Table 3.1) revealed a single base pair deletion in exon 3 (Figure 3.7). This sequence mutation is denoted c.201delT and it is a frameshift mutation, resulting in 13 novel amino acids with a stop codon at exon 4. The patient bearing this mutation has a severe RP phenotype. The patient is presented with night blindness in the first decade of life and reduced central vision in the second decade.

3.5. Generation of control and *PRPF31* patient-specific iPSC

Fibroblasts from the unaffected controls and *PRPF31*-mutant patients were reprogrammed using the non-integrative Sendai viral particles encoding the reprogramming factors KOS (*KLF4*, *OCT3/4* and *SOX2*), *C-MYC* and *KLF4*. The main steps required for reprogramming human fibroblast cells to generate iPSCs are shown in figure 3.8A.

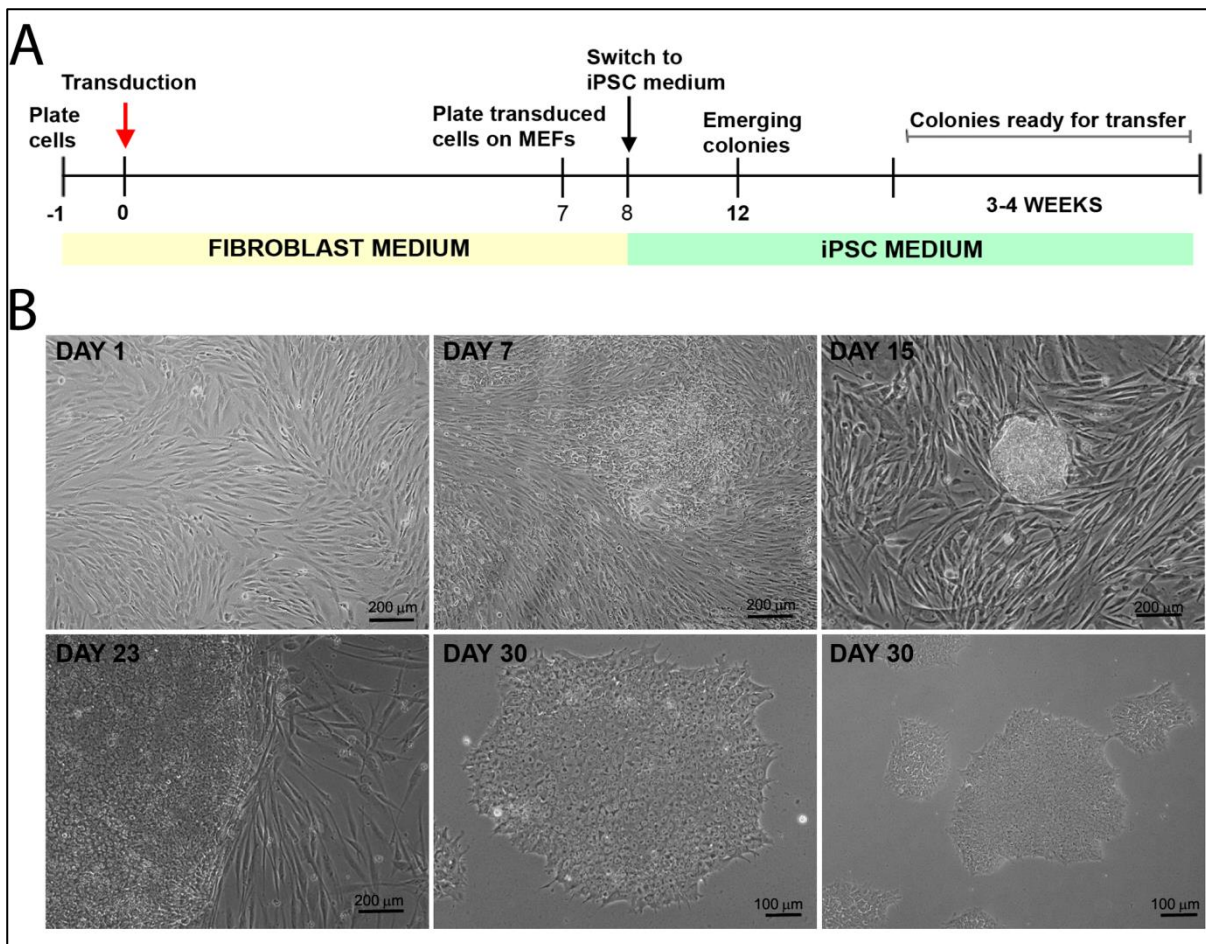


Figure 3.8. Overview of the reprogramming process. A: Reprogramming timeline for generation of iPSCs. B: Microscope images showing changes from patient-specific RP11S2-PRPF31 fibroblasts to induced pluripotent stem cells. Day 1: Fibroblasts of passage 5. Day 7: Cells changing morphology. Day 15: Observation of the first colonies. Day 23: Colonies showing typical iPSC morphology, ready to be picked and transferred to matrigel. Day 30: Colonies on matrigel passage 1 show typical morphology of iPSCs.

On day 1 of the reprogramming protocol the fibroblast cultures were transduced with the vectors containing reprogramming transgenes. Following a 7-day period, the morphology of fibroblasts began to change from a long, elongated form to a small and circular conformation with reduced cytoplasm and large nuclei, typical of iPSC morphology (Figure 3.8B). Over the following three weeks, fully reprogrammed cells formed compact thin colonies, delimited by distinct borders (Figure 3.8B: DAY30). The reprogramming efficiencies of all iPSC lines are shown on Table 3.2. Mature colonies from each cell line, representing one clone each, were manually picked from their original plate and passaged onto MEF feeder plates. Three clones from each patient were isolated and expanded in feeder free cultures prior the analysis.

Characterization of iPSCs consisted of detection of residual expression of Sendai genome and reprogramming transgenes, assessment of pluripotency, ability to give

rise to the three germ layers, chromosomal integrity and identity of the iPSC lines used in this project.

Cell line	Number of cells transduced	Number of transduced cells after 7 days	Number of clones picked	Number of clones generated	Reprogramming efficiency
Control WT1	100.000	1,012,500	65	286	0.29%
Control WT3	100.000	800,000	46	245	0.25%
RP11S1	100.000	760,000	89	294	0.29%
RP11M	100.000	1,612,500	72	505	0.50%
RP11VS	100.000	1,025,000	54	241	0.24%
RP11A	100.000	937,500	39	159	0.16%
RP11S2	100.000	1,050,000	56	256	0.26%
RP11S3	100.000	900,000	48	188	0.19%
RP11S4	100.000	2,087,500	47	427	0.43%

Table 3.2. Reprogramming efficiencies of control and PRPF31 lines. The number of clones generated is an estimate of the total number of clones that were originated from the transduced cells plated on MEF feeder plates (230.000 cells per plate) over a period of 30 days. The reprogramming efficiency for each cell line was calculated using the number of clones generated and the original number of fibroblasts that were transduced with Sendai containing reprogramming transgenes.

3.6. Detection of Sendai virus genome and reprogramming transgenes

Detection of vector-free iPSCs was done by reverse transcription PCR (RT-PCR). Primers used to detect vectors KOS (containing reprogramming factors KLF4, OCT3/4, SOX2), KLF4 and C-MYC, were also complimentary to Sendai vector genome. The analysis of the PCR products showed expression of Sendai vector and reprogramming transgenes in positive control cells (transduced fibroblasts collected at day 7) but non-detectable residual expression of both Sendai vector genome and reprogramming transgenes in iPSC controls and PRPF31-mutant iPSC lines (Figure 3.9).

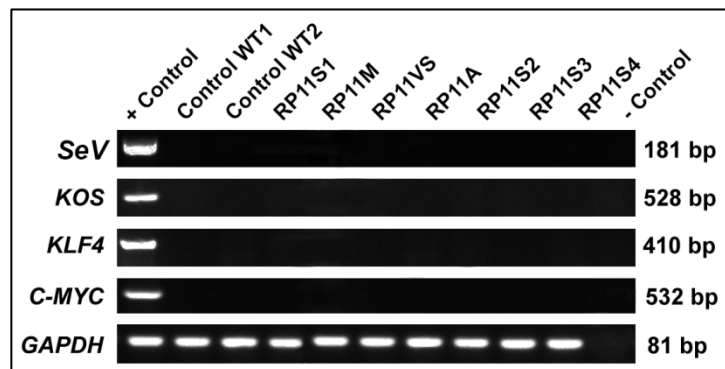


Figure 3.9. Detection of residual expression of Sendai (SeV) genome and reprogramming transgenes in controls and PRPF31-iPSC lines by RT-PCR. At passage 15, controls and PRPF31-iPSC lines did not express Sendai and reprogramming vectors KOS (KLF4, OCT3/4, SOX2) KLF4 and C-MYC. Positive controls consisted of RNA that was extracted from fibroblasts at day-7 post transduction. Nuclease-free water was used as negative control to confirm absence of contamination in the PCR reagents or primer-dimer formation.

3.7. *In vitro* assessment of pluripotency

In addition to the examination of typical iPSC morphology, *in vitro* assessment of pluripotency was performed to detect expression of pluripotency markers by different methods. Both controls and PRPF31-iPSC lines showed a positive staining of pluripotency-associated markers OCT4 and stage specific embryonic antigen-4 (SSEA-4) by immunocytochemistry. The images show localisation of the SSEA-4 marker on the cell membrane and OCT4 staining in the cell's nuclei, associated with DAPI nuclear stain (Figure 3.10).

Quantification of the double-positive cell population expressing the nuclear transcription factor NANOG and the surface marker tumour-rejection antigen 1-60 (TRA-1-60) was carried out by flow cytometry. All iPSC lines showed a high percentage of positive cell population co-expressing NANOG and TRA-1-60 pluripotency-associated markers (Figure 3.11).

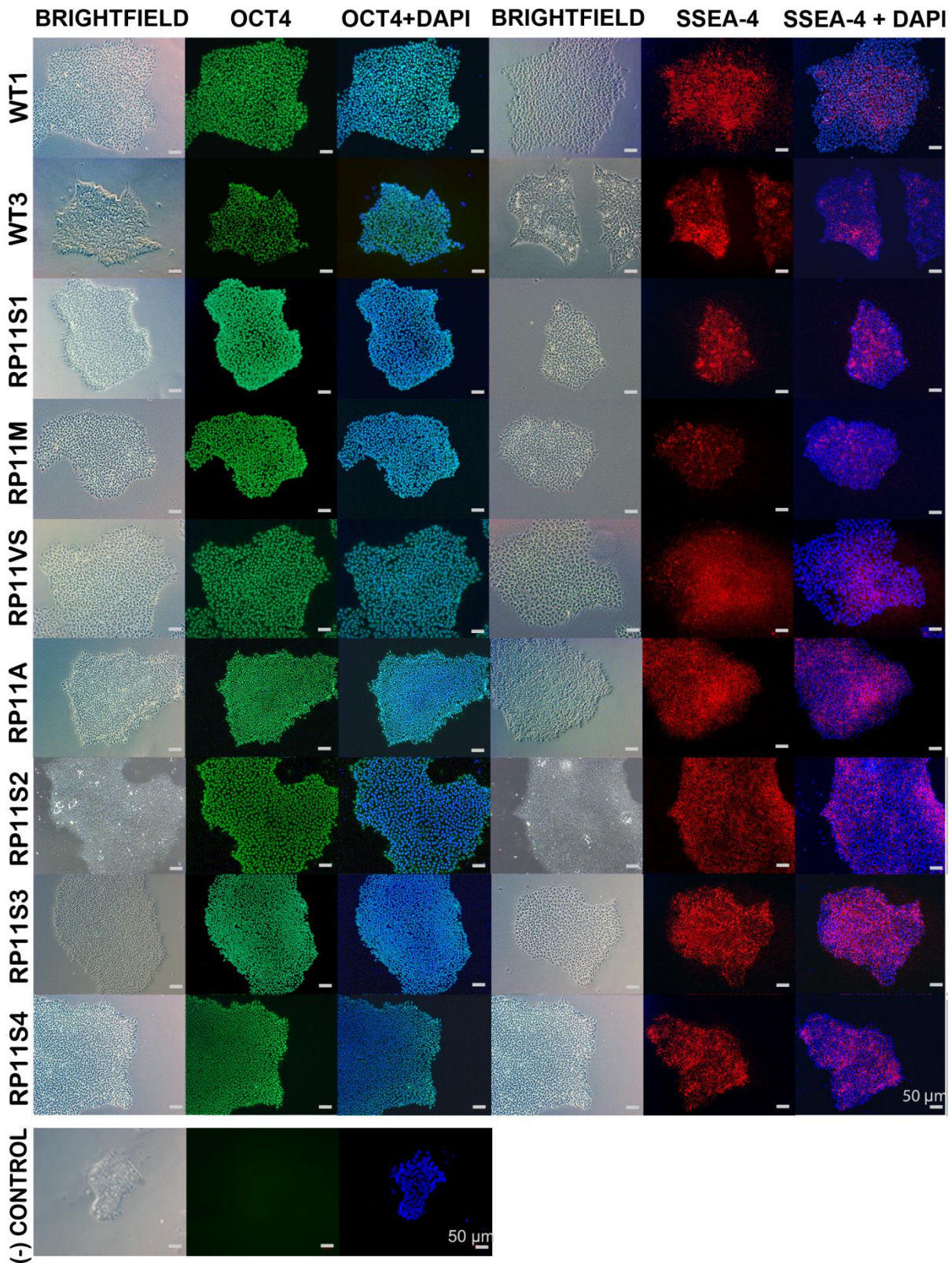


Figure 3.10. Detection of pluripotency-associated markers by immunocytochemistry. Brightfield and Immunocytochemistry images showing expression of OCT4 (green) and SSEA-4 (red) in control and PRPF31-iPSC lines. Nuclei were stained with DAPI. Negative control of SSEA-4 antibody was not performed because it is conjugated.

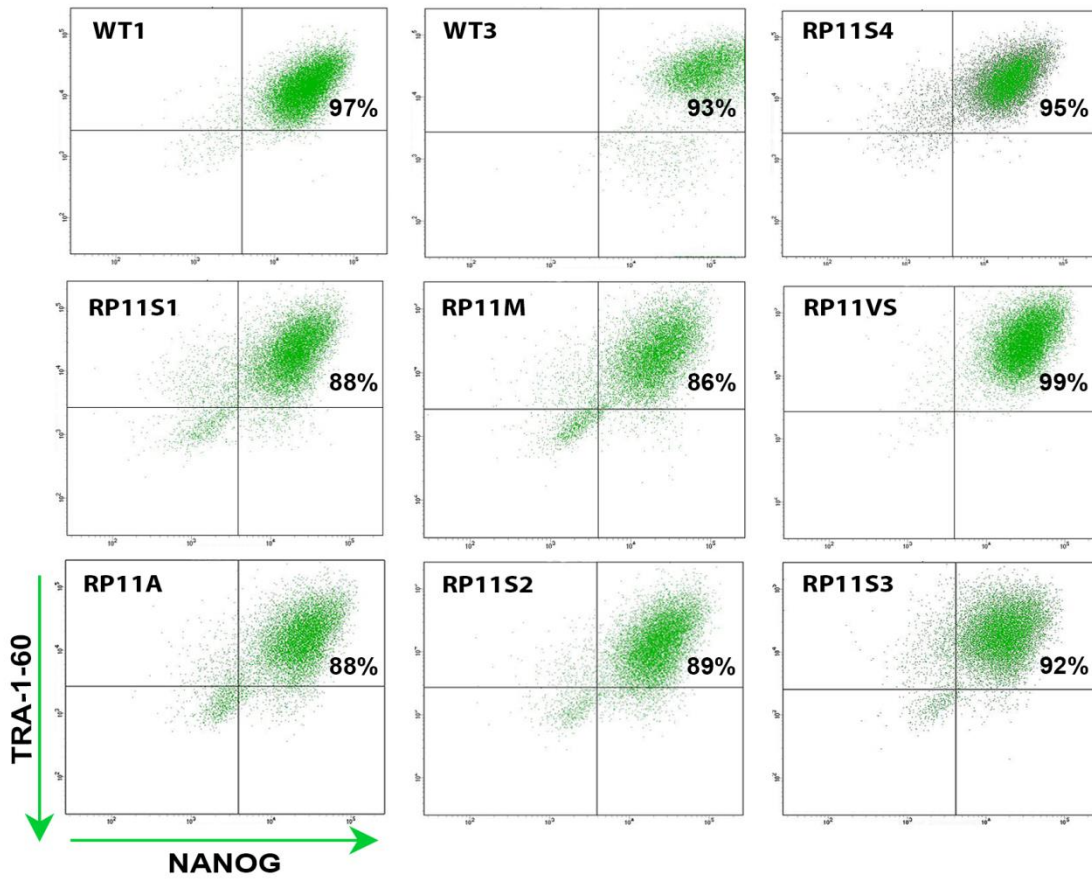


Figure 3.11. Quantification of pluripotency-associated markers by flow cytometry. Representative images showing double-positive cell population of NANOG and TRA-1-60 in controls and PRPF31-iPSC lines.

3.8. Three Germ Layers and Teratoma Assays

One of the key characteristics of iPSCs is the ability to potentially differentiate into any cell types of the three germ layers, endoderm, mesoderm and ectoderm. This capability can be assessed *in vitro* by the three germ layers differentiation assay, via embryoid bodies (EBs) formation, and/or *in vivo*, by the teratoma assay.

For the three germ layers differentiation assay, two markers of each germ layer were selected. Alpha-fetoprotein (AFP) and forkhead box protein A2 (FOXA2) were selected for endoderm; Smooth muscle actin (SMA) and heart- and neural crest derivatives-expressed protein 1 (HAND1) were selected for mesoderm; and paired box-6 (PAX6) and β III tubulin (TuJ1) were selected for ectoderm. Following immunocytochemistry, cells belonging to three germ layers were found in all controls and PRPF31- iPSC lines (Figures 3.12).

Teratoma experiments, carried out by Professor Stefan Pryzborski's group, showed that one control and four PRPF31-iPSC lines were able to induce teratoma formation in severe combined immunodeficient (SCID) mice. The teratoma tumours were removed and analysed after 6 weeks post injection of iPSCs in SCID mice and contained heterogenic tissues from endoderm, mesoderm and ectoderm lineages, such as such as gut, cartilage, connective and neural tissue (Figure 3.13).

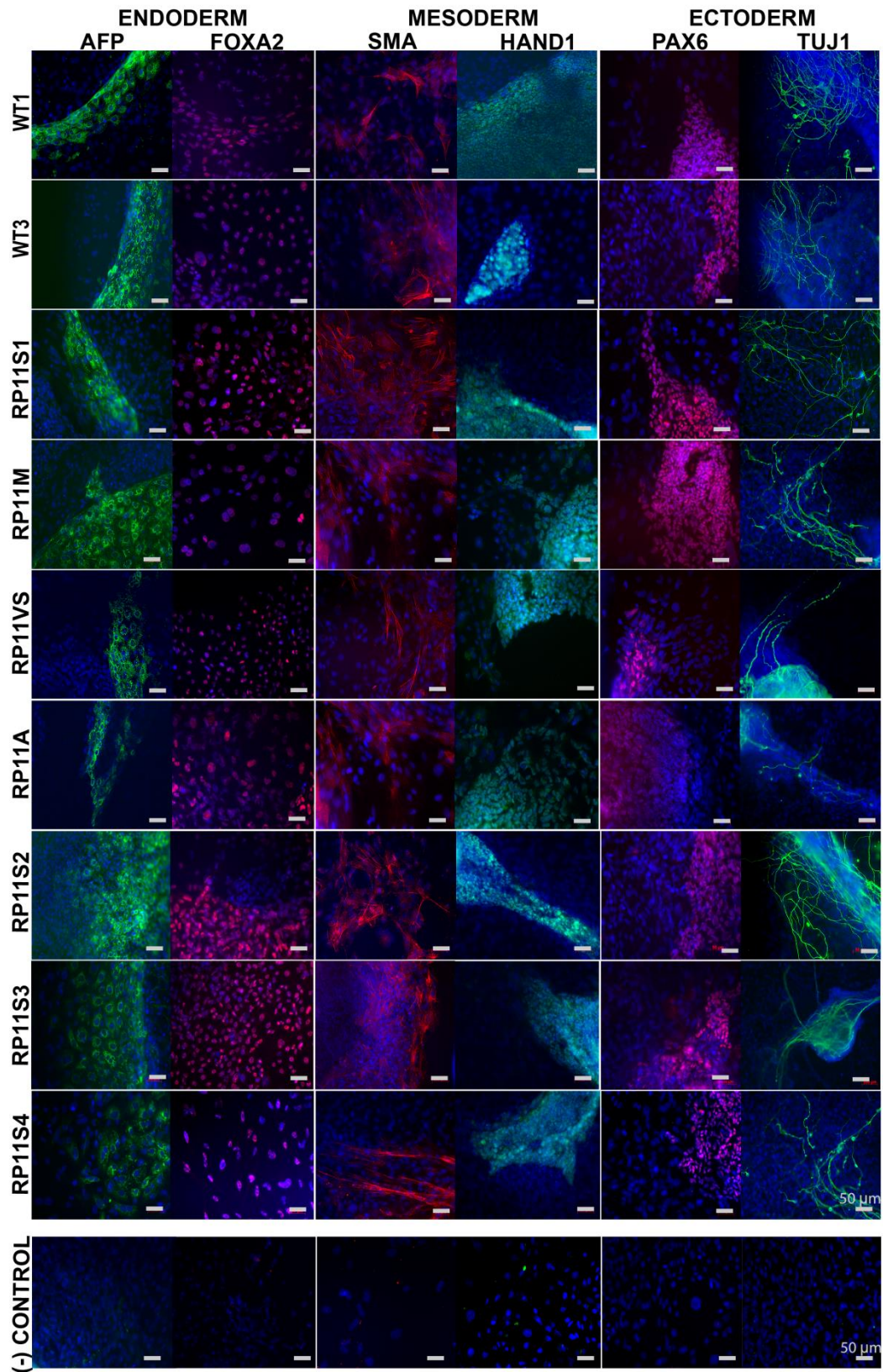


Figure 3.12. Three germ-layer assay by immunocytochemistry. Differentiated cells from controls and PRPF31-mutated lines showing positive staining for two markers of each germ layer. Endoderm: AFP (green) and FOXA2 (red). Mesoderm: SMA (red) and HAND1 (green). Ectoderm: PAX6 (red) and TUJ1 (green).

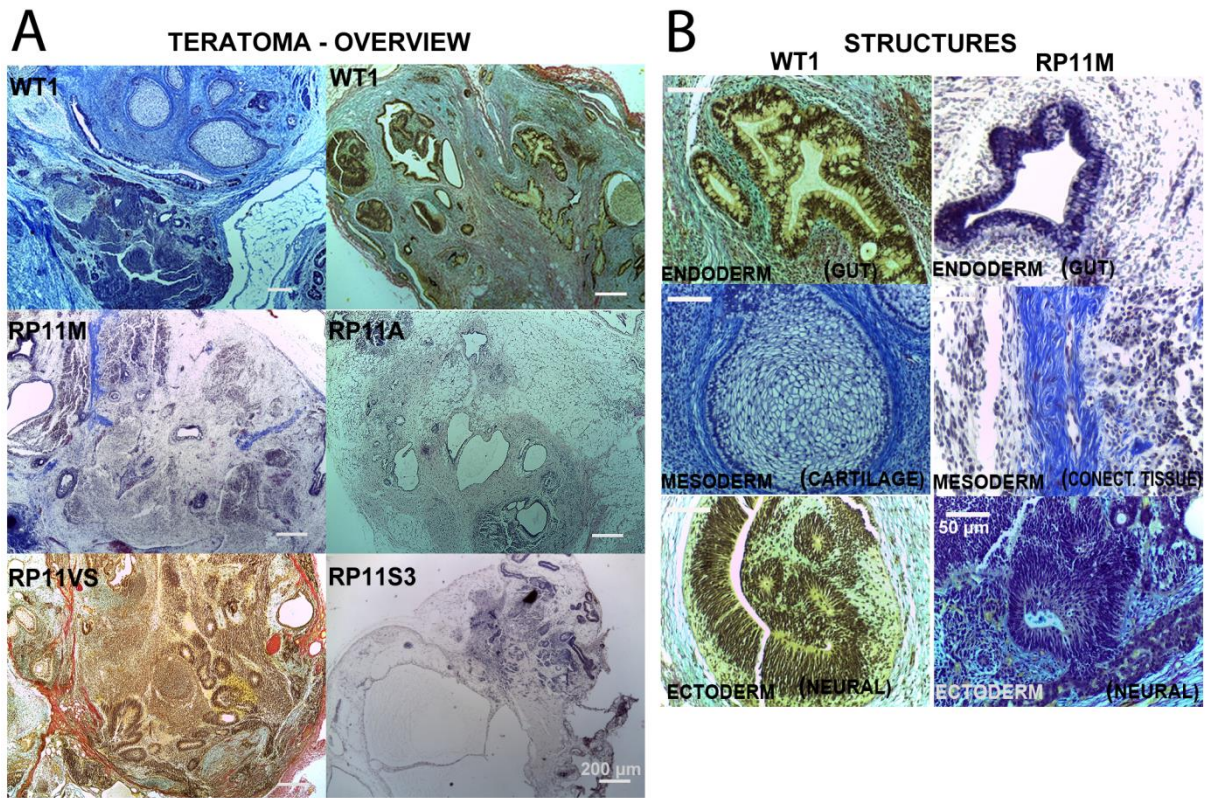


Figure 3.13. Teratoma formation assay in SCID mice. A: Representative images of tumours generated from control and PRPF31-iPSC lines. B: Structures found in the tumours of endodermal, mesodermal and ectodermal origin.

3.9. Cytogenetic Analysis

Genomic SNP array, performed by our collaborator, Dr. Hussein Sheek, showed that none of the parental fibroblasts or iPSCs from controls and PRPF31-mutated lines displayed major chromosomal abnormalities associated to the reprogramming process or variations introduced by long term culture when compared to a human reference genome (hg38) (Table 3.3). Additionally, SNP analysis confirmed that parental fibroblast and iPSCs had the same genetic profile, proving the authenticity of the iPSC lines generated for this study (Figure 3.14).

Sample No.	Cell type	Passage number	Alteration (size in Mb)	OMIM Disease-causing	Karyotype
WT1	Fibroblast	5	-	-	46XY
	iPSC	20	-	-	
WT3	Fibroblast	5	-	-	46XY
	iPSC	15	-	-	
RP11S1	Fibroblast	5	-	-	46XX
	iPSC	15	-	-	
RP11M	Fibroblast	5	-	-	46XY
	iPSC	15	-	-	
RP11VS	Fibroblast	5	-	-	46XY
	iPSC	15	-	-	
RP11A	Fibroblast	5	-	-	46XX
	iPSC	15	-	-	
RP11S2	Fibroblast	5	-	-	46XX
	iPSC	15	-	-	
RP11S3	Fibroblast	5	-	-	46XX
	iPSC	15	-	-	
RP11S4	Fibroblast	5	-	-	46XX
	iPSC	20	-	-	

Table 3.3. Summary of cytogenetic analysis of controls and PRPF31-mutated cells lines by SNP array. No abnormalities were detected in the controls and PRPF31-iPSC lines.

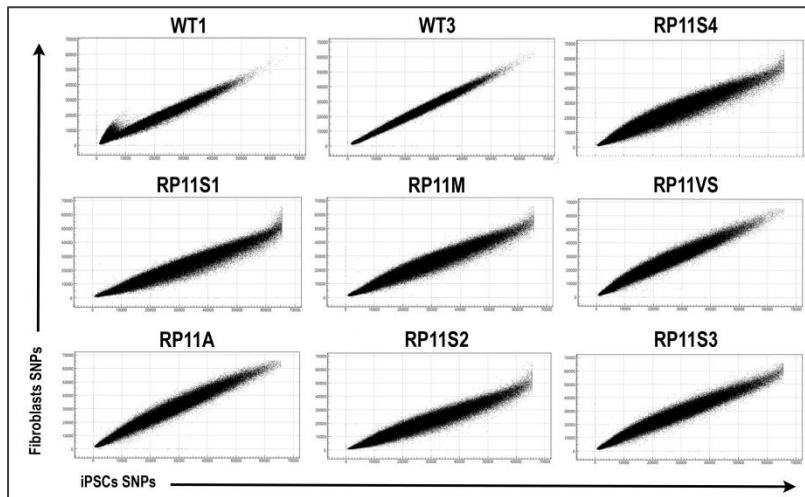


Figure 3.14. Confirmation of genetic Identity of parental fibroblasts and iPSCs by SNP microarray. SNP patterns revealed correlation of the genetic identity profile from parental fibroblasts and iPSCs, confirming the authenticity of the lines used in this study.

3.10. Discussion

The iPSC technology has emerged as an alternative modelling method to primary cell culture, providing unlimited cells of the same genetic type as the donor source, as well as the ability to observe the development of pathological features of some diseases, such as RP. This chapter provides evidence of successful generation and characterisation of controls and PRPF31-iPSCs to be further used as models for the study of PRPF31-RP.

All RP patient fibroblasts were screened for *PRPF31* mutations to confirm their presence. The same screening was done later to all fibroblast derived-iPSCs and it was verified that the reprogramming process had no effect on the sites where the mutations were located.

The success or efficiency of cellular reprogramming is dependent on the reorganisation of the cellular memory disc (CMD), which functions to maintain cell identity during development and to preserve gene silencing. The CMD is mostly formed by reprogramming-resistance memory, a group of repressing multiprotein complexes that may inhibit chromatin remodelling, make some genes inaccessible to the transcriptional machinery and preserve the topology of chromosome domains (Anjamrooz, 2013). Therefore, the efficiency of cellular reprogramming, although reproducible, remains low. Normally less than 1% of transfected fibroblasts become iPSCs. Transduction of cells by Sendai vectors has been proved to be more efficient than other methods, with capability to transduce a wide range of cell types in proliferative and quiescent states (Fusaki *et al.*, 2009; Rao and Malik, 2012). The differences of reprogramming efficiencies between controls and PRPF31-mutated fibroblasts were small, demonstrating that sex, age or *PRPF31* mutations of the donors had no impact on the derivation of iPSCs. Successfully reprogramming of PRPF31-mutated fibroblast has also been previously reported in the literature (Terray *et al.*, 2017).

Another feature of this method of reprogramming is that it is non-integrative. Sendai virus replicates its genome in the cytoplasm of the host cells, and it's expected to remain in the cytoplasm of infected cells for a few passages, until it is cleared out by the host's cells. The chance of integration, which could jeopardize the differentiation process or result in insertional mutations in iPSCs, still had to be investigated (Fusaki

et al., 2009). Controls and PRPF31-iPSCs showed no residual expression of Sendai vector genome and reprogramming transgenes at passage 15, indicating the cells were able to maintain regulation of endogenous pluripotency genes after clearance of exogenous transgenes.

The expression of pluripotency markers was used to demonstrate that the derived iPSCs were indeed pluripotent. The cells were stained with SSEA-4, an embryonic stem cell marker, and OCT4, which maintains pluripotency in murine and primate cells. Not only iPSC colonies showed the typical cell colony morphology characteristic of human pluripotent stem cells lines, but also stained positive for those markers. SSEA4 was present to the cell membrane and OCT4 stained the cells nuclei in a slightly punctuate pattern, characteristic of those antibodies. In addition to the immunocytochemistry, the analysis of expression of pluripotency markers was also done by flow cytometry. Controls and PRPF31-iPSCs showed a high percentage of positive cell population co-expressing TRA-1-60 and NANOG pluripotency-associated markers. Expression of all four pluripotency markers together provide strong evidence of pluripotency in iPSCs, as described before in the literature (Draper *et al.*, 2002; Henderson *et al.*, 2002; International Stem Cell *et al.*, 2007), and have been shown in all controls and PRPF31-iPSCs.

Another key characteristic of iPSCs is the ability to differentiate into any cell types of the three germ layers – endoderm, mesoderm and ectoderm. This capability can be assessed *in vitro* by the Three Germ Layers differentiation assay, via EBs formation, and/or *in vivo*, by the Teratoma assay. For the Three Germ Layers differentiation assay, specific markers of each lineage were selected. Alpha-fetoprotein (AFP) is a marker of early endoderm commitment and is produced by the yolk sac and liver cells. Definitive endodermal lineages, which give rise to organs such as the liver and pancreas and the inner lining cells of the gut, depends on the activity of transcription factors, such as Forkhead domain families, including the FOXA2 marker (Kwon *et al.*, 2006; Wong *et al.*, 2010). The mesoderm lineage is originated during gastrulation, like the other germ layers, and it forms the muscles, blood cells and the mesenchyme. Two early markers for mesodermal lineage fate were selected. Smooth muscle actin (SMA) is a conserved protein that is involved in cells movements, structure and integrity of muscular tissues, and Heart- and neural crest derivatives-expressed protein 1, or HAND1 protein, which is present in the developing ventricular chambers and cardiac neural crest (Kruithof *et al.*, 2003; Barnes *et al.*, 2010).

Pluripotent cells can also commit to an ectodermal fate, forming cells of the nervous system, epidermis and lining cells of the mucosa. For the early ectoderm differentiation the selected markers were the Paired box-6 (PAX6) transcription factor, expressed in some neuroprogenitors cells of the neural tube, and β III Tubulin (TuJ1), present in both immature and mature neurons and in some mitotically active neuronal precursors (Dimanlig *et al.*, 2001; Mizuseki *et al.*, 2003). Following spontaneous differentiation and staining, cells belonging to three germ layers were found in all controls and PRPF31-iPSCs.

To demonstrate the pluripotency of iPSCs *in vivo*, cells are injected into SCID mice to potentially develop into an experimental tumour. Cells are considered pluripotent if the tumour is proven to contain differentiated structures from all three germ layers (Brivanlou *et al.*, 2003). One control and four PRPF31-iPSCs successfully induced tumours in SCID mice. Some tumours however, failed to display tri-lineage differentiation according to results from histological analysis. The lack of structures from a specific germ layer observed in these teratomaes does not necessarily entail the cells are not pluripotent since only two mice were used for each cell line in this assay. This technique, however, is not easily repeated as it's regarded as time, cost, and labour intensive. The use of minimal animal numbers due to ethical concerns and lack of standardisation described by Muller *et al.* (2010) are additional hurdles in performing this assay.

Finally, cytogenetic analysis was performed to detect genetic abnormalities and confirm cell identity of the iPSCs generated. It is known that even transgene-free iPSCs can acquire genetic variations, which can arise from the heterogeneous genetic background of original cells, even at low frequencies, due to low efficiency and clonal nature of iPSC derivation. Variations can also be introduced during reprogramming, long-term culture or innate genetic instabilities of the *in vitro* pluripotent state (Liang and Zhang, 2013b). Cytogenetic analysis of the iPSCs becomes paramount to detect any likely genetic variation prior to their differentiation. In this case, none of controls and PRPF31-iPSCs, as well as their respective parental fibroblasts, displayed genetic abnormalities qualified as pathogenic or that would affect downstream analyses. Additionally, this analysis has also confirmed that all the iPSC generated had the same genetic profile of their correspondent parental fibroblasts, corroborating the origin of iPSCs in this study.

All the results, collectively, provide evidence of the successful generation of fully reprogrammed controls and PRPF31-iPSC lines suitable for further differentiation into RPE, to be used as disease model for PRPF31-RP.

Chapter 4 - Differentiation and Characterisation of Retinal Pigment Epithelium (RPE) Cells

4.1. Introduction

In retinitis pigmentosa (RP) pathology, the cells of interest are the retinal pigment epithelium (RPE) and the photoreceptors. These retinal cells are not easily accessible from the patients but can be supplied through iPSC technology (Jin et al., 2012; Deng et al., 2018).

This project focused on the study of iPSC-derived RPE cells to investigate the pathophysiology of PRPF31-RP. iPSC-derived RPE have been successfully used to elucidate degenerative eyes diseases including RP, as seen in Chapter 01, and they have been proved to be a powerful research tool (Mead et al., 2015; Nguyen et al., 2015; Bracha et al., 2017).

To this day, several protocols have reported the direct differentiation of iPSCs towards RPE, including spontaneous differentiation after removal of basic fibroblast growth factor (bFGF) from the culture medium (Klimanskaya et al., 2004; Buchholz et al., 2009), serum-free floating culture of embryoid body-like aggregates (SFEB) (Watanabe et al., 2005), and directed methods using drugs and cytokines such as Nicotinamide (NIC) and Activin A (Idelson et al., 2009; Krohne et al., 2012). More recently published protocols use a stepwise method that tends to mimic the events involved in the development of the eye to enhance the efficiency of differentiation (Buchholz et al., 2013; Zhu et al., 2013; Leach et al., 2015).

Successful RPE differentiation enables the generation of pure populations of functional RPE cells with key RPE features, including the four 'Ps' (pigmented, polygonal, polarized and phagocytic), with the ability to mimic the behaviour of native RPE cells in responding to normal and disease-associated stimuli (Bharti et al., 2011; Mazzoni et al., 2014).

4.2. Aims

This chapter aims to describe the process of differentiation of iPSCs into RPEs and validate the iPSC-derived RPE model through:

- The capacity of iPSC to generate pigmented cells with typical RPE morphology under differentiation conditions
- Analysis of RPE morphology through transmission electron microscopy (TEM)
- Functional analysis of RPE cell monolayers by measuring their trans-epithelial resistance and phagocytosis capability
- Expression of RPE markers by immunocytochemistry (ICC)
- Assessment of RPE polarity via measurement of VEGF and PEDF levels and expression of RPE apical and basal markers by ICC

4.3. Retinal Pigment Epithelium Differentiation

Clonal variance experiments were performed to determine the differentiation capacity of three individual clones from the same patient, generated during the reprogramming of iPSCs, under the same differentiation conditions. Three clones of the control iPSC-WT1 were selected and differentiated into RPE cells, and the degree of pigmentation was measured at different time points. The experiments showed that there were no significant differences between all iPSC clones and thus, only one clone of each cell line was selected for differentiation experiments (Figure 4.1).

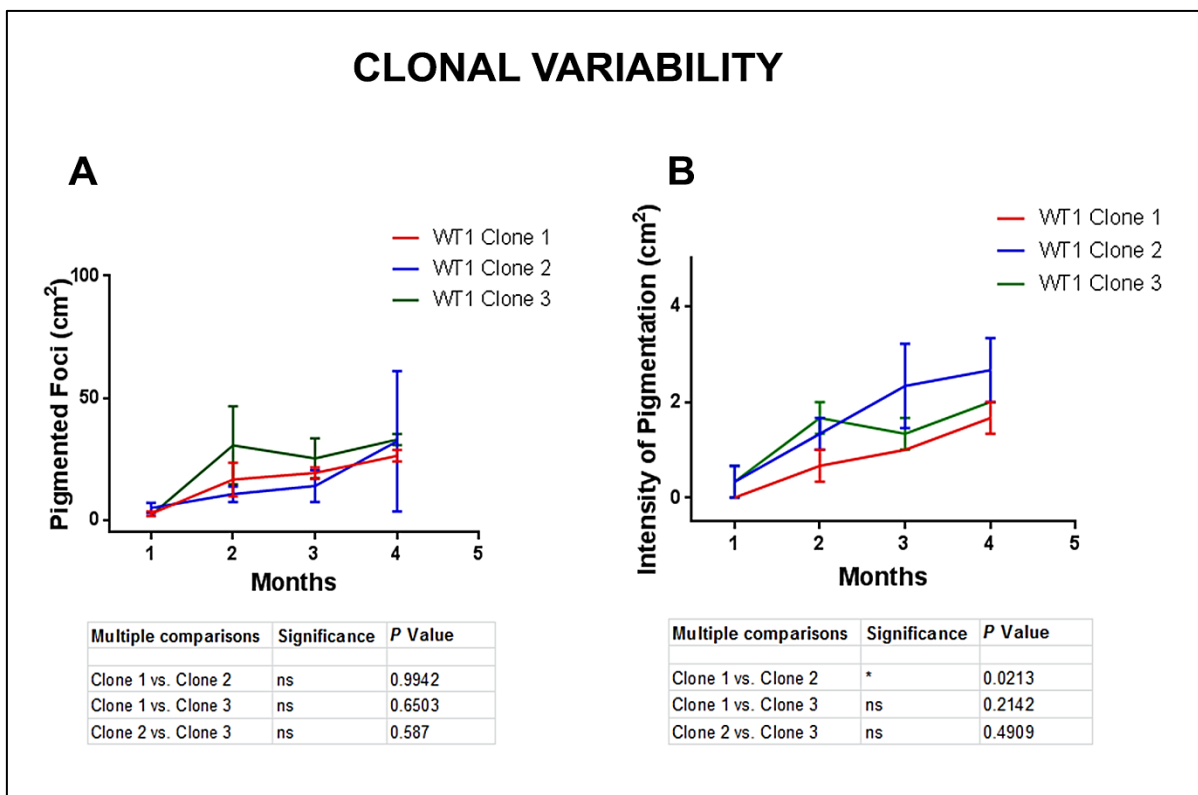


Figure 4.1. Differentiation capacities of clones 1, 2 and 3 of control WT1-iPSC. The mean of the number of pigmented foci and intensity of pigmentation per cm² of each clone is not significantly different from one another, except for intensity of pigmentation between clones 1 and 2. Data shown as mean \pm SEM, n = 3.

For the differentiation experiments two control iPSCs were selected, WT1 and WT3, and three PRPF31-iPSCs (RP11S1, RP11M and RP11VS), with the same *PRPF31* mutation in exon 11 (Chapter 3: Table 3.1). Embryonic stem cells H9 were used as an internal control for the differentiation protocol following previous experiments performed in our group using the same conditions (Chichagova *et al.*,

2017). The process of differentiation from iPSC to RPE cells is lengthy and the first pigmented areas can be seen after six weeks, if the differentiation is successful. Small pigmented patches expand over time and after 10-15 weeks (>3 months) they are large enough to be mechanically dissected and seeded onto 24-wells and/or transwell inserts (Figures 4.2).

The initial differentiation experiments, using only basal media (supplemented with B27, which allows proliferation of neuronal lineages in defined serum-free medium), revealed that the differences in pigment formation between control and patient specific cell lines were significant and did not relate to disease severity or phenotype (Figure 4.3).

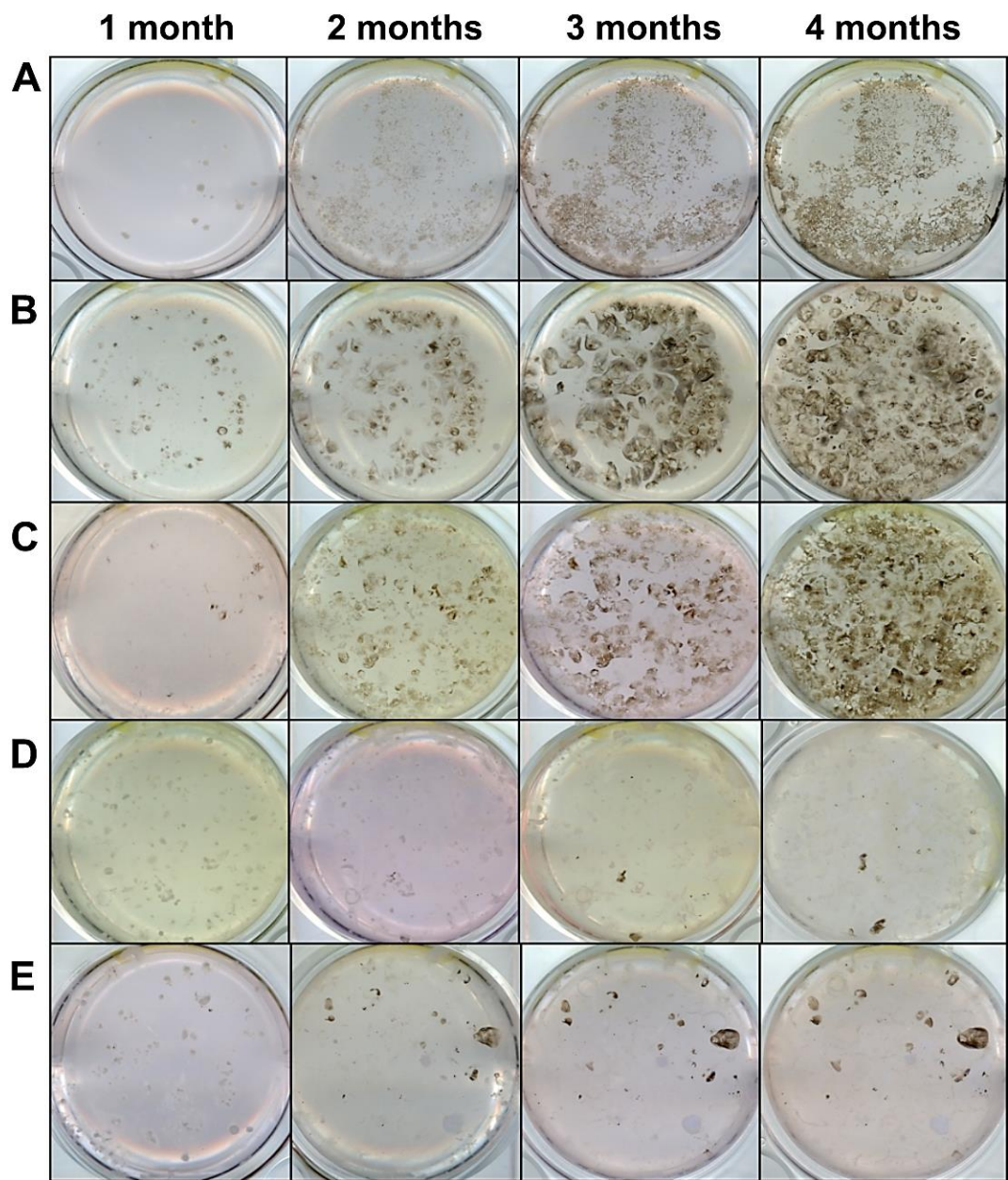
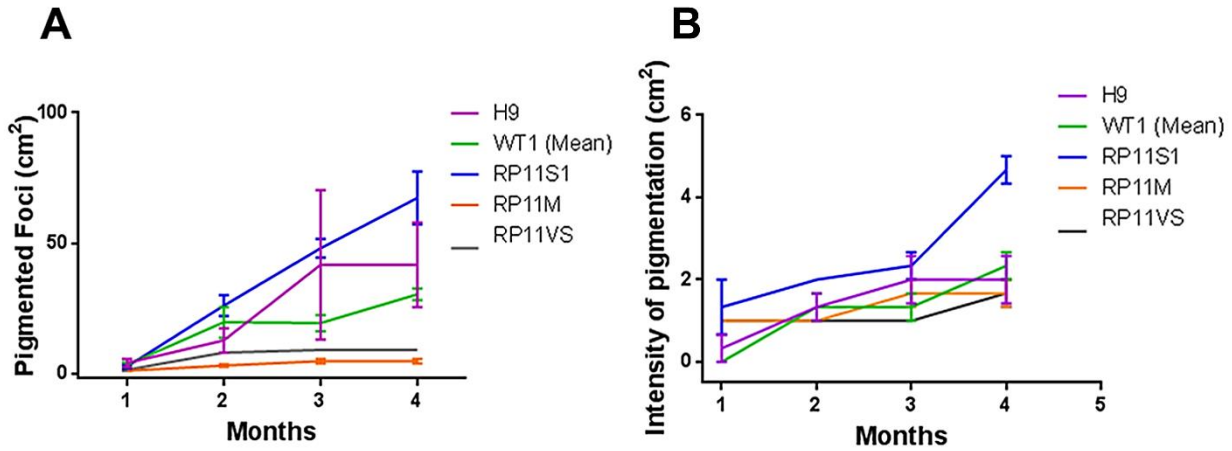


Figure 4.2. Representative images of RPE differentiation with only base medium, derived from controls and PRPF31-iPSCs. The images were scanned from 6-well plates. A: H9-hESC. B: WT1-iPSC. C: RP11S1-iPSC. D: RP11M-iPSC. E: RP11VS-iPSC. Examples are representative of at least three independent experiments.

RPE DIFFERENTIATION EFFICIENCY



Multiple comparisons	Significance	P value
H9 vs. WT1	ns	0.7516
H9 vs. RP11S1	ns	0.3181
H9 vs. RP11M	**	0.0041
H9 vs. RP11VS	*	0.022
WT1 vs. RP11S1	*	0.0255
WT1 vs. RP11M	ns	0.0888
WT1 vs. RP11VS	ns	0.2895
RP11S1 vs. RP11M	****	<0.0001
RP11S1 vs. RP11VS	****	<0.0001
RP11M vs. RP11VS	ns	0.972

Multiple comparisons	Significance	P value
H9 vs. WT1	ns	0.9537
H9 vs. RP11S1	***	0.0001
H9 vs. RP11M	ns	0.9965
H9 vs. RP11VS	ns	0.8252
WT1 vs. RP11S1	****	<0.0001
WT1 vs. RP11M	ns	0.9965
WT1 vs. RP11VS	ns	0.9965
RP11S1 vs. RP11M	****	<0.0001
RP11S1 vs. RP11VS	****	<0.0001
RP11M vs. RP11VS	ns	0.9537

Figure 4.3. RPE differentiation efficiency. A: Formation of pigmented foci per cm² in controls H9-hESC and WT1-iPSC (Mean of all clones) and PRPF31-iPSCs (RP11S1, RP11M and RP11VS). The differences between the mean of all time points of H9 vs RP11M and RP11VS and between WT1 vs RP11S1 were significant. RP11S1 is also significantly different from RP11M and RP11VS. B: Intensity of pigmentation per cm² in controls H9-hESC and WT1-iPSC (Mean of all clones) and PRPF31-iPSCs (RP11S1, RP11M and RP11VS). The differences between H9 vs RP11S1, WT1 vs RP11S1, and between RP11S1 vs RP11M and RP11VS were significant. Data shown as mean \pm SEM, n = 3.

In order to improve the efficiency of the differentiation technique and generate more pigmented patches, especially from *PRPF31*-mutated lines RP11M and RP11VS, different combinations of small molecules were added to the media at temporal windows to mimic the events involved in the formation of RPE (Figures 4.4 and 4.5; see discussion for rationale).

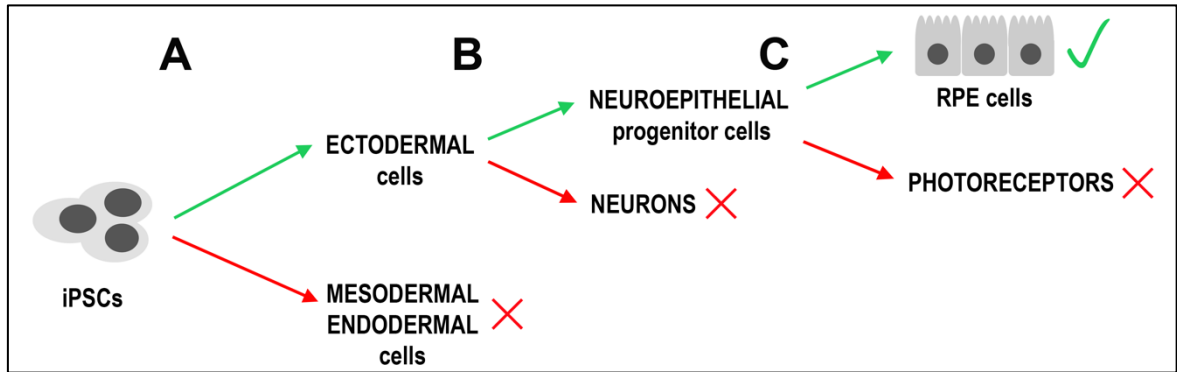


Figure 4.4. Representation of directed stem cells differentiation to RPE cells. A: Inhibition of transforming growth factor beta (TGF- β) and bone morphogenic protein (BMP) pathways suppresses differentiation towards mesodermal and endodermal lineages, leading the cells to an ectodermal fate. B: Cells were directed to become retinal precursors. C: Wnt pathway was stimulated to further direct the cells to RPE.

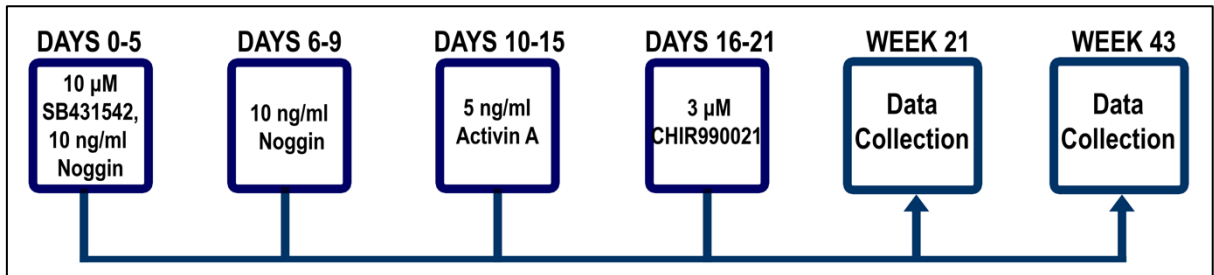


Figure 4.5. Timing of factor addition directing pluripotent cells toward RPE fate. From days 0-5, SB431542 (TGF- β inhibitor) and Noggin (BMP inhibitor) were added to the differentiation media followed by the addition of Noggin from days 6-9. Activin A was added to the differentiation media from days 10-15. CHIR990021 (Wnt agonist) was added to the media from days 16-21. After day 21 the cultures were fed with only base medium containing B27 and pigmented patches were picked and expanded to form RPE monolayers until they were used for analysis around week 21 (~6months) and further on, around week 43 (~11 months).

The new differentiation protocol using small molecules generated pigmented areas that appeared around week 8 (~02 months). The patches were mechanically dissected and dissociated as single cells after week 15 (~04 months) and seeded onto 24-wells and transwell inserts.

Since some of pigmented patches were observed on the edges of the wells in most of the iPSCs lines, especially in iPSC control WT3 and PRPF31-RP11VS, and it was not possible to count the pigmented patches and make a direct comparison of all the lines. It was possible, however, to determine the efficiency of the new differentiation protocol compared to the previous protocol using PRPF31-RP11M, as this line developed even pigmentation across the wells. The new protocol using small molecules has been shown to generate considerably more pigmentation for this line than the previous protocol (Figure 4.6).

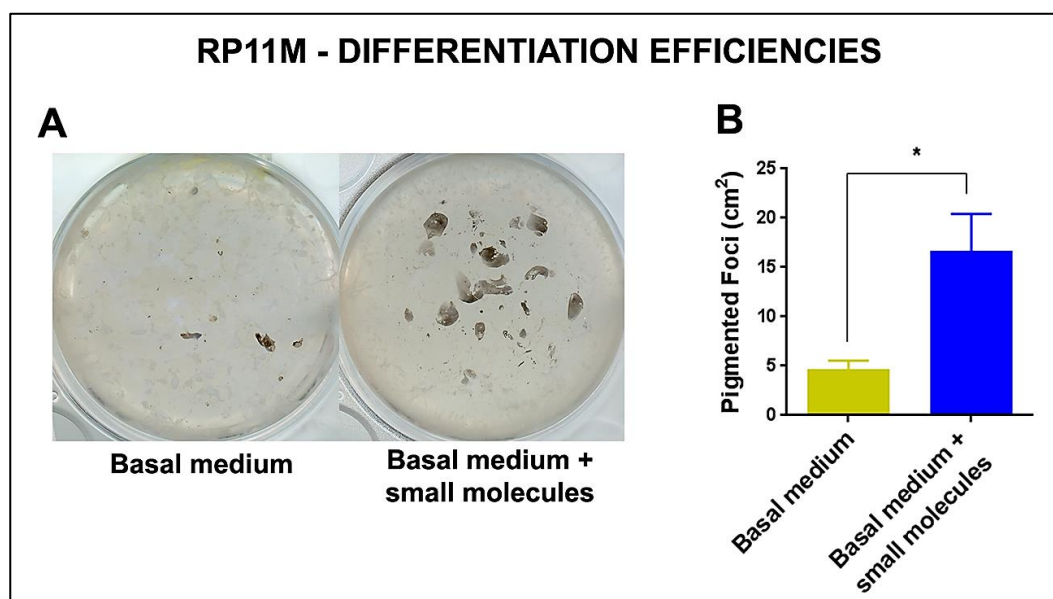


Figure 4.6. Comparison of RPE differentiation protocols with and without small molecules using RP11M at week 16 (~04 months). A: Pigmented patches at week 15 (~04 months) of differentiation with only basal medium and basal medium supplemented with small molecules. B: A significant difference was seen between the two protocols ($P < 0.05$). Data shown as mean \pm SEM, $n = 3$.

4.4. Measurement of trans-epithelial resistance

Through trans-epithelial resistance (TER) analysis, it is possible to measure the barrier strength of the RPE monolayer, as consequence of formation of tight junctions between the RPE cells. A high TER value requires formation of functional tight junctions between RPE cells to minimize the paracellular flow of ions. Wells containing no cells have low resistance to passage of ionic current between electrodes placed in the inner and outer wells.

Trans-epithelial resistance was measured from transwell inserts at week 21 to assess the barrier properties of RPE cells derived from controls and PRPF31-iPSCs. This time point was chosen based on the maturation of RPE cells (Buchholz et al., 2009; Brandl et al., 2014; Weed and Mills, 2017). All cell lines formed cobblestone monolayer, but there was a significant difference between TER values of controls and PRPF31-RPE cells (Figure 4.7).

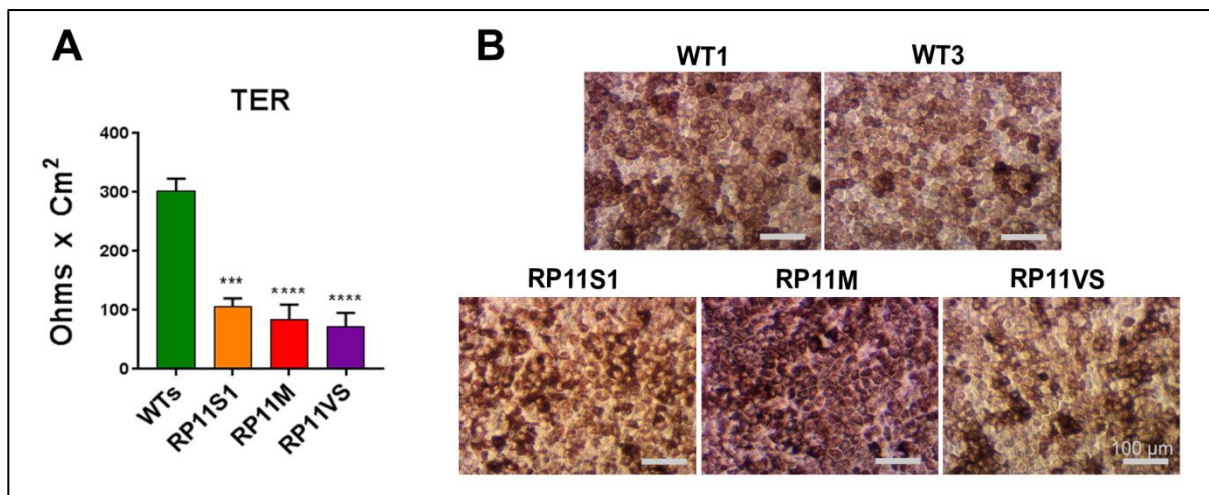


Figure 4.7. Trans-epithelial resistance of controls and PRPF31-RPE cells. A: TER values show that there is a significant difference between the mean of controls (WTs) and PRPF31-mutant lines. Data shown as mean \pm SEM, $n = 3$. B: All PRPF31-RPE cells formed a cobblestone monolayer, with polygonal cells, typical of RPE morphology.

4.5. Transmission Electron Microscopy

The transmission electron microscopy (TEM) performed on the RPE derived from controls iPSC at week 21 revealed healthy cells, typical RPE structures and organelles such as mitochondria, melanosomes and tight junctions. The images also show very active cells with abundant microvilli, and secreting exosomes and extracellular matrix (Figure 4.8).

In contrast to controls, TEM images of RPE cells derived from patient-specific PRPF31-iPSCs at weeks 21 and 43 showed a general disorganisation, loss of basal infoldings and over 2-fold shorter apical microvilli (average length of $3.1 \mu\text{m} \pm 0.49$ SEM in WT3 and $1.4 \mu\text{m} \pm 0.33$ SEM in RP11S1) (Figure 4.8).

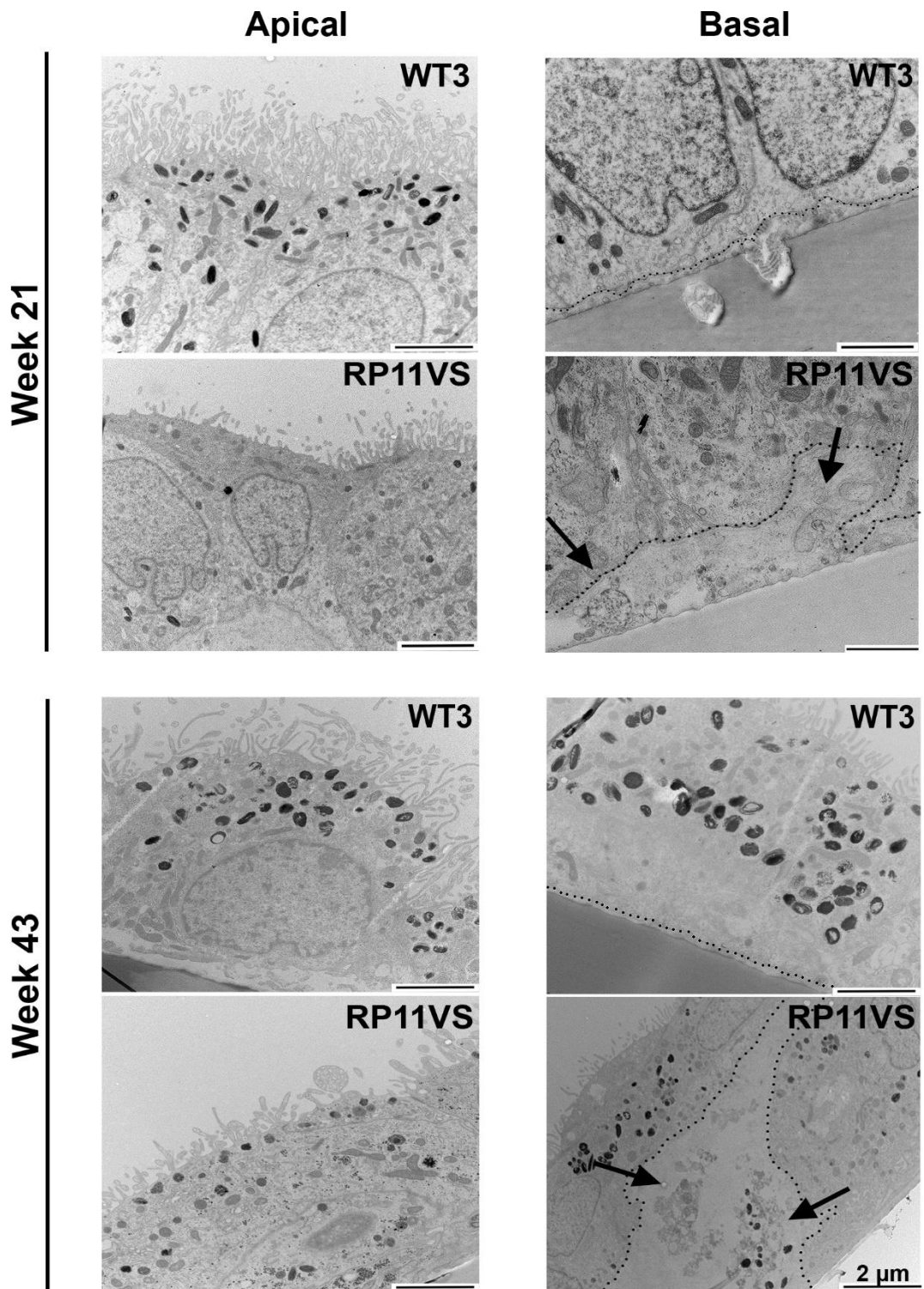


Figure 4.8. Abnormal ultrastructural features of RPE PRPF31-mutant cells. TEM of PRPF31-RPE cells at 21 and 43 weeks shows shorter and fewer microvilli in PRPF31-RPE cells (average length of $3.1 \mu\text{m} \pm 0.49 \text{ SEM}$ in WT3 and $1.4 \mu\text{m} \pm 0.33 \text{ SEM}$ in RP11S1) and large basal deposits that were not observed in controls. Representative images of at least three independent experiments.

4.6. Phagocytosis Assay

One of the most important roles of RPE cells is to phagocytose outer segment fragments shed from photoreceptors, which is essential for the maintenance of photoreceptors and consequently, vision.

The immunocytochemistry assays to assess the RPE phagocytosis *in vitro* are not sufficiently standardised or quantitative. Fluorescence-activated cell sorting (FACS) can be an alternative method to quantify the internalisation of FITC-labelled POSs. To achieve this, it is important to quench any extracellular fluorescence from bound and free POSs with trypan blue but not from internalised POSs (Westenskow *et al.*, 2012). Several control experiments using iPSC-derived RPE were set up in our group to ensure the robustness of the data including treatment of cells with FITC-labelled POSs at 4°C to block their ability to phagocytosis, treatment of cells with FITC-labelled POSs followed by quenching the fluorescence from non-internalised POSs with Trypan blue, and treatment of cells with unlabeled POSs to assess background fluorescence (Chichagova *et al.*, 2017).

Controls and PRPF31-RPE cells were analysed and the results of three independent experiments were expressed as percentage of cells within the population with internalised POSs, and median fluorescence intensity (MFI), which represents the total amount of FITC-labelled POSs internalised by individual cells as an indication of cell-surface receptor density involved in phagocytosis (Figure 25). Both severe PRPF31-RPE phenotypes (RP11S1 and RP11VS) are significantly different from controls in regard to the number of POSs that were internalised (MFI) per cell and are likely to have a deficiency in phagocytosis (Figure 4.9).

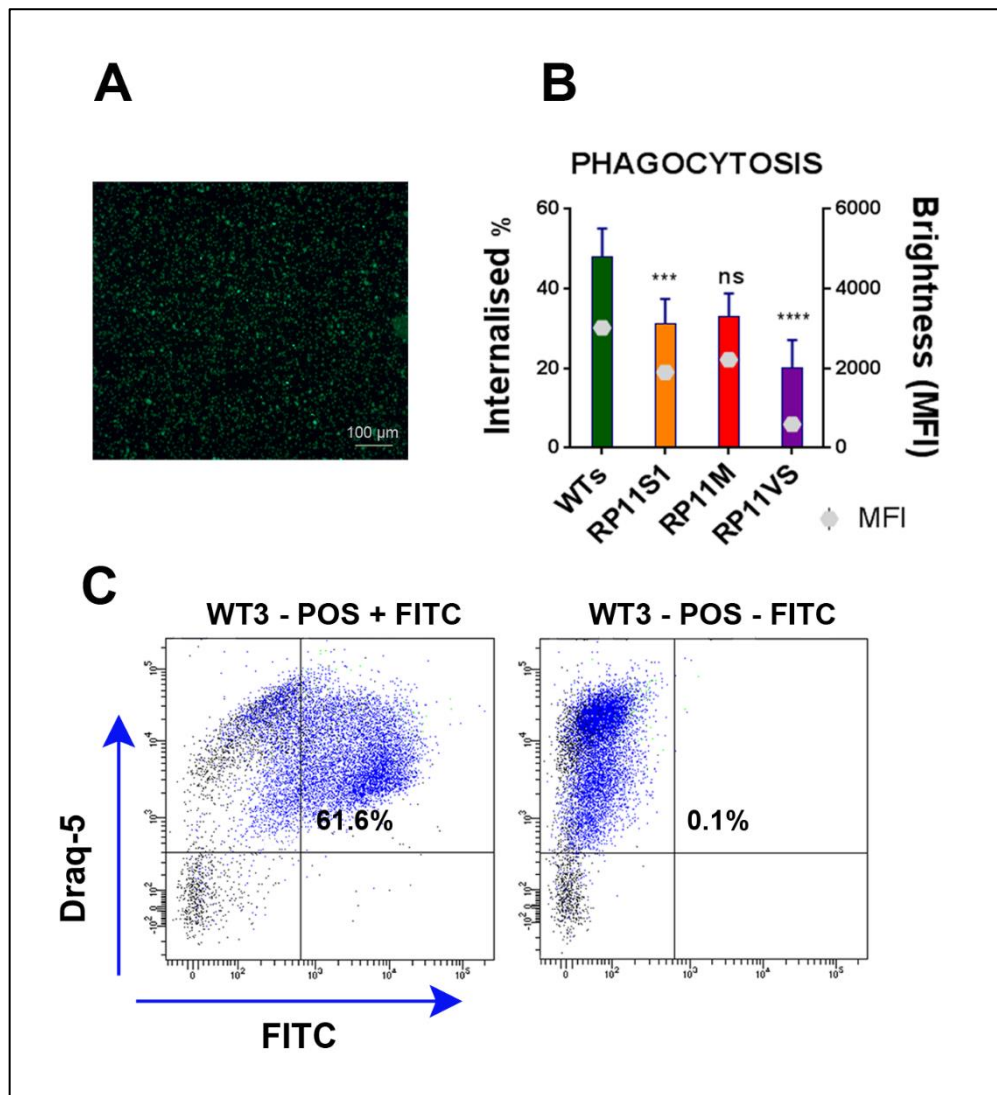


Figure 4.9. Photoreceptor outer segments phagocytosis assay of iPSC-derived RPE cells by flow cytometry. A: FITC-labelled POSs. B: The results of the phagocytosis assay demonstrated that iPSC-derived RPE were able to phagocytose but PRPF31-severe patients showed deficiency in the ability of ingesting more POSs per cell, as determined by median fluorescence intensity values. All cells were age-matched with regards to the length of differentiation time (~6 months). Data shown as mean \pm SEM, $n = 3$. C: Example of the results with cells fed with FITC-labelled POSs and non-labelled POSs.

4.7. RPE Polarity studies

The RPE cell layer is strategically located between the neural retina and choroid capillaries, and its polarised organisation is essential for the RPE's role as a selective blood-retinal barrier, involving the vectorial transport of ions, nutrients and waste into and from the retina and also the secretion of growth factors such as pigment epithelium-derived factor (PEDF) and vascular endothelial growth factor (VEGF) (Bonilha, 2014; Lehmann et al., 2014). The levels of PEDF and VEGF, which are

associated with barrier function and choroidal neovascularisation, were analysed by enzyme-linked immunosorbent assay (ELISA). Expression of RPE polarity markers Na⁺/K⁺-ATPase, BEST1, MERTK and Collagen IV, involved in transport of ions, phagocytosis and secretion of extracellular matrix, were analysed by immunocytochemistry (ICC).

4.7.1. PEDF and VEGF protein levels

Cytokine secretion assays revealed a significantly higher apical PEDF and basal VEGF expression in the severe and very severe PRPF31-RPE in comparison to control RPE (Figure 4.10).

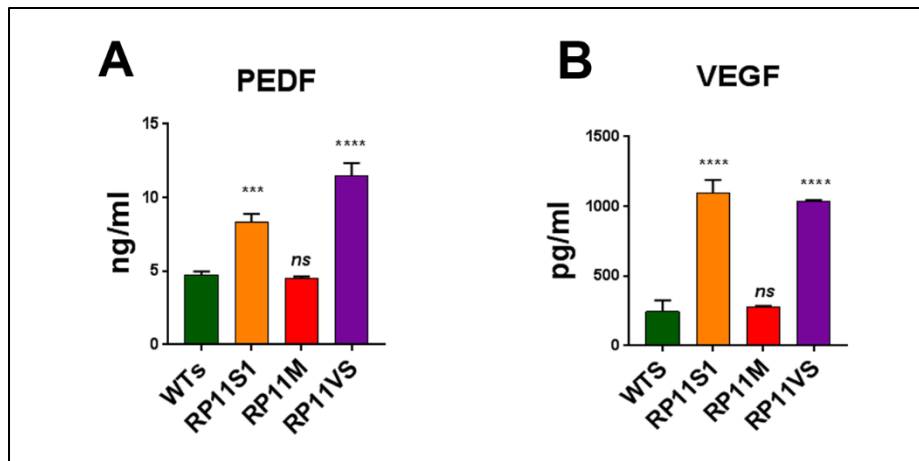


Figure 4.10. ELISA assays for apical and basal secretion of PEDF and VEGF, respectively, in controls and PRPF31-RPE cells. Data of three independent experiments obtained from RPE at week 21 of differentiation. Data shown as mean \pm SEM, n = 3.

4.7.2. Detection of polarity markers by immunocytochemistry

Immunocytochemistry images, taken with the same exposure time, revealed that PRPF31-RPE levels of apical Na⁺/K⁺-ATPase, also known as sodium-potassium-pump, were similar to controls. Expression of the basolateral marker BEST1, however, was reduced in the severe and very severe PRPF31-mutant lines RP11S1 and RP11VS (Figure 4.11A).

PRPF31-RPE expression of MERTK, a phagocytic protein, located the apical layer and Collagen IV, in the basal layer, were reduced in both markers compared to controls (Figure 4.11B).

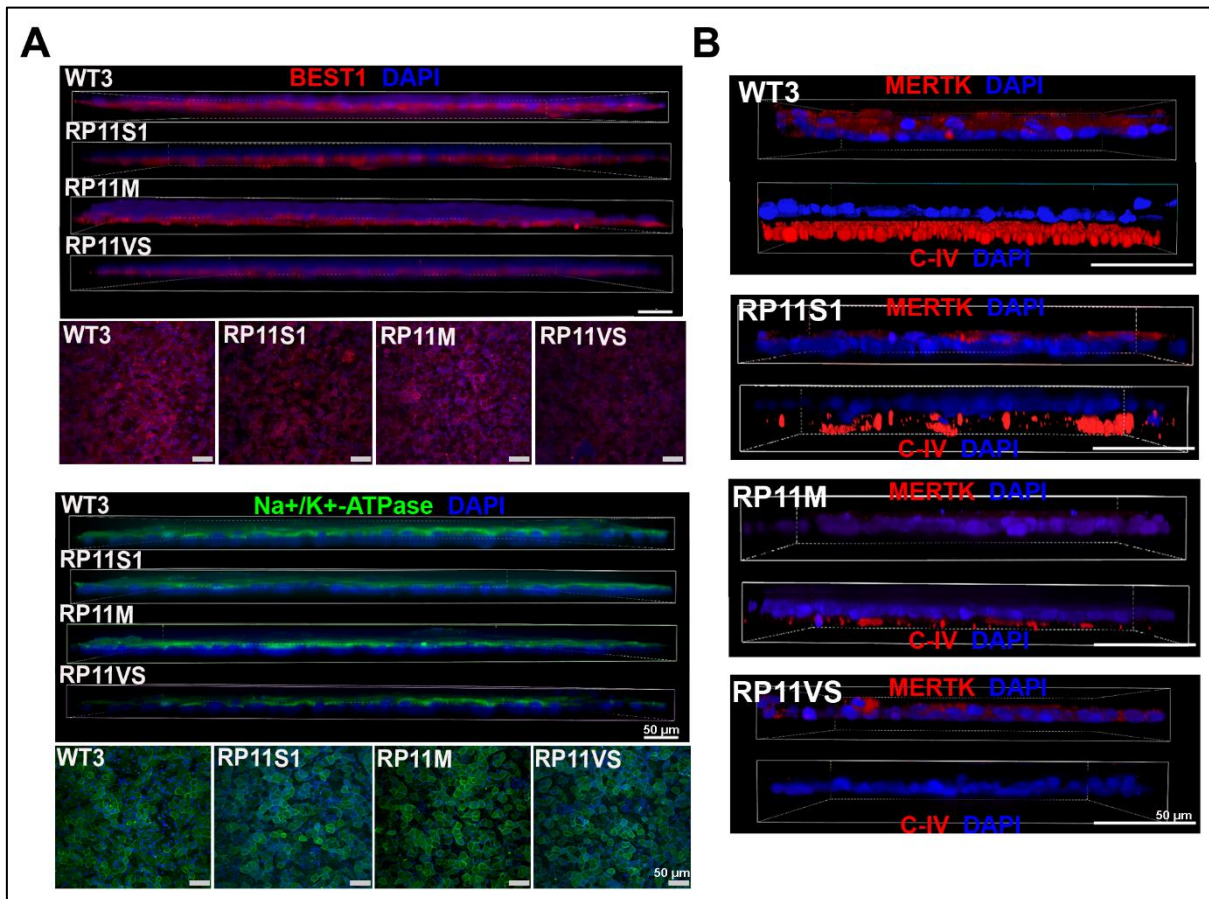


Figure 4.11. Detection of polarity markers by immunocytochemistry. A: Immunostaining for basolateral markers BEST1 and apical Na⁺/K⁺-ATPase. B: Correct basolateral distribution of collagen IV (C-IV) and apical MERTK was seen in unaffected control (WT3) but not in RP11 RPE cells. Representative images from three independent experiments.

4.8. Discussion

The efficacy of RPE differentiation protocols has been shown to be very variable between cell lines. The differences are likely to be cell line specific, related to a particular cell line's innate responses and cannot be attributed only to disease severity or phenotype as it has been previously demonstrated that even iPSC lines from unaffected individuals exhibit such differences (Lane *et al.*, 2014; Hallam *et al.*, 2018), and iPSC inter-individual differences are bigger than cell type of origin or clonal variances of the same IPSC due to a larger proportion of gene regulatory variation (Burrows *et al.*, 2016).

To enhance the differentiation of iPSC towards RPE cells, a stepwise method was used to mimic the events involved in the development of the eye. It is known that inhibition of Transforming Growth Factor-Beta (TGF- β) and Bone Morphogenetic Proteins (BMPs) pathways enhance differentiation of iPSCs to neuroectodermal lineages and suppresses the differentiation towards mesodermal and endodermal lineages (Zhang and Li, 2005; Chambers *et al.*, 2009). Thus, from days 0-5, SB431542 (TGF- β inhibitor) and Noggin (BMP inhibitor) were added to the differentiation media followed by the addition of Noggin from days 6-9. Activin A was shown to promote and maintain RPE fate (Idelson *et al.*, 2009; Buchholz *et al.*, 2013) by acting mainly in the induction of RPE transcription factors (Ikeda *et al.*, 2005) during the stages of optic vesicle to optic cup of eye development (Martinez-Morales *et al.*, 2004; Idelson *et al.*, 2009; Meyer *et al.*, 2009). Activin A was added to the differentiation media from days 10-15. To further direct the cells to RPE from a neural retina point, Wnt pathway was stimulated to generate RPE cells. Treatment with the Wnt agonist CHIR99021 has been shown to induce the formation of epithelial cells expressing Melanogenesis Associated Transcription Factor (MITF) that further developed into RPE with high pigmentation (Nakano *et al.*, 2012). The addition of Wnt agonist from days 16-21, added to the differentiation cultures after the cells are committed to the retinal fate, has also been reported in mouse in vivo and in vitro studies (Fuhrmann, 2008; Fujimura *et al.*, 2009; Gorges *et al.*, 2009).

Despite of all differences seen in our differentiation experiments, all cultures generated pigmented patches containing cells with typical RPE morphology that were dissected out the plates, dissociated into single cells and expanded in 24-wells. All iPSC-derived RPE lines formed a cobblestone monolayer of RPE cells, however PRPF31-RPE monolayers were not as tightly packed as controls RPE and there was a significant difference in the TER values between controls and PRPF31-RPE lines, at week 21 of differentiation. This suggests PRPF31-RPE had leaky tight junctions. Controls reached TER values above 200 Ω , which is considered as a sign of functionality in RPE cells as it has been demonstrated that cells with TER values of 200 Ω are able to clear outer segments within 5 hours after phagocytosis (Sonoda *et al.*, 2009; Toops *et al.*, 2014).

RPE phagocytosis is highly depended on cell-receptor density and an abnormal balance of receptor densities affects the tendency of RPE cells to phagocytose photoreceptors outer segments (POSs). This is very important during differentiation

when there is a change in the dynamic of surface receptors and the RPE gradually become more efficient at phagocytosing POSs, alongside with the development of typical hexagonal morphology and pigmentation. The cell surface receptors that are involved in RPE phagocytosis are $\alpha V\beta 5$ Integrin, possibly being the primary binding site (Finnemann *et al.*, 1997; Lin and Clegg, 1998), MerTK (D'Cruz *et al.*, 2000) and CD36 (Ryeom *et al.*, 1996). The results of the phagocytosis assay indicated RPE derived from patients RP11S1 and RP11VS, with severe and very severe phenotypes, have reduced functional ability to phagocytose rod outer segments. This has confirmed a previous study that showed that primary RPE cultures of *Prpf31*^{+/-} mice and shRNA-mediated knockdown of *PRPF31* in human ARPE-19 cells had decreased phagocytosis (Farkas *et al.*, 2014).

TEM images of RPE cells derived from patient-specific PRPF31-RPEs at weeks 21 and 43 of differentiation showed cells with over 2-fold shorter and fewer microvilli in contrast to RPE cells derived from control iPSCs. Microvilli, which are about 3-7 μm long, are composed of microfilaments containing actin-associated proteins, such as myosin, fimbrin, and α -actin, is directly involved in phagocytosis of photoreceptors outer segments, transport of nutrients and removal of waste products from photoreceptor cells (Bok, 1993; Bonilha *et al.*, 2004; Lamb and Pugh, 2004; Bonilha, 2014). Both controls and PRPF31-RPE displayed pigmented melanosomes and exosomes. Dark colour of melanosomes, as seen in all samples, is characteristic of the late stages of melanosome maturation, which are essential for the absorption of scattered light, protecting the retina against free radicals. Exosomes are small membranous vesicles released into the extracellular medium carrying genetic material and proteins (Atienzar-Aroca *et al.*, 2016). It is thought exosomes are a way of communication between the RPE and the outer retina (Locke *et al.*, 2014)

It was also noticed that PRPF31-RPE had a general disorganisation of basal infoldings, containing large amorphous deposits underneath the RPE. The basal surface of healthy RPE cells is highly infolded, to increase absorption and secretion area, and interacts with the underlying Bruch's membrane. The folds form narrow compartments containing numerous mitochondria which provide energy to pump ions located in the plasma membrane. Control RPE cells also showed the presence of extracellular matrix on the basal surface of cells, which was not obvious on TEM images of PRPF31-RPE. The formation of collagen-like fibrils in the basal ECM of cultured RPE cells has been observed in cells from chick embryos and adult cats

(Newsome and Kenyon, 1973; Li *et al.*, 1984). It has also been demonstrated that RPE cells in culture mainly secrete collagen types IV and V producing its own cellular matrix between the basal surface of RPE cells and the culture plates (Kigasawa *et al.*, 1998).

Disorganisation and loss of basal infoldings as well as atrophy of apical microvilli, disappearance of melanin granules and accumulation of oxidized lipids residues are a sign of RPE aging or stress and consequently death (Bonilha, 2008; Gu *et al.*, 2012). The TEM of RPE cells from *prpf31* knockout mice revealed loss of the basal infoldings, vacuolisation and accumulation of amorphous deposits between the RPE and Bruch's membrane at one year of age, corroborating the results of this project (Graziotto *et al.*, 2011).

The polarised organisation of the RPE is essential for proper functioning of the neural retina. RPE cells produce high levels of pigment epithelium-derived factor (PEDF), associated with RPE polarisation and maturation (Karakousis *et al.*, 2001; Becerra *et al.*, 2004; Kozulin *et al.*, 2010). In the retina, PEDF is found in the apical surface of RPE cells, in the subretinal space, and in rods and cones. Furthermore, PEDF has been shown to support proliferation and differentiation of cones and inhibit rod development [30]. Vascular endothelial growth factor (VEGF), also secreted by RPE cells, is important for the survival of Müller cells and photoreceptors, in addition to its role in the stimulation and formation of blood vessels (Volpert *et al.*, 2009). Studies also revealed that the balance between VEGF and PEDF maintain the barrier function of endothelial cells (Ablonczy and Crosson, 2007). This study demonstrated that severe and very severe PRPF31-RPE phenotypes overexpressed PEDF and VEGF. Elevated levels of such important cytokines could therefore impair RPE polarity, cell proliferation, adhesion, migration, tight junction formation, and vascular permeability with further functional consequences for rod survival. Although overexpression of VEGF has been strongly implicated in the development of choroidal neovascularization found in age-related macular degeneration (Spilisbury *et al.*, 2000), no neovascularisation was observed in PRPF31-mutant patients.

Control and PRPF31-RPE cells showed a similar expression of the apical RPE marker Na⁺/K⁺-ATPase, also known as sodium-potassium-pump. Na⁺/K⁺-ATPase is found on the apical surface of the RPE cells and it is vital for several RPE cell functions such as vectorial transport of ions and nutrients from the choroid to the photoreceptors and to maintain a high concentration of Na⁺ in the subretinal space for regulation of

the charge across the photoreceptor plasma in the light-dark cycle of phototransduction (Hodson *et al.*, 1994; Kaplan, 2002). Expression of the basolateral marker Bestrophin-1, or Best-1, which is involved in ion channel function as well as its calcium regulatory capabilities (Hartzell *et al.*, 2008), was reduced in the severe (RP11S1) and very severe (RP11VS) patients.

Additionally, expression of apical MERTK and Collagen IV in the basolateral layer was also reduced in PRPF31-RPE lines in comparison to controls. MERTK is involved in the redistribution of myosin II (Strick *et al.*, 2008) for the formation and closure of the phagocytic cup (Olazabal *et al.*, 2002; Araki, 2006). It also acts in conjunction with $\alpha\beta 5$ integrin to enable normal binding and uptake of POSs (Finnemann and Nandrot, 2006; Nandrot *et al.*, 2012). A mutation in this gene result in the inability of RPE to phagocytise shed photoreceptor outer segments leading to a degeneration of the photoreceptors, a phenotype seen in the Royal College of Surgeons (RCS) rats (Burstyn-Cohen *et al.*, 2012). MERTK-deficient mouse (Duncan *et al.*, 2003) as well as double-knockout mice have been shown to mimic the retinal phenotype of the RCS rats and therefore the reduced expression of MERTK in the apical surface of RPE also confirms the deficiency of those cells in phagocytose POSs. Collagen IV, which is one of the components of the extracellular matrix plays a role in retinal adhesion, differentiation, growth and prevention of neovascularisation (Campochiaro *et al.*, 1986).

Taken together, the results indicate a loss of apical/basal polarity in patient-derived PRPF31-RPE, suggesting that the RPE cells are affected in the pathogenesis of PRPF31-retinitis pigmentosa, which could later contribute with the degeneration of the photoreceptors.

Furthermore, the variation observed between the three disease phenotypes is very interesting and although the data of more PRPF31 phenotypes is needed to confirm these findings, analysis of expression of *PRPF31* gene in the study cell lines will be described in the next chapter.

Chapter 5 - Molecular Pathogenesis of Splicing Factor *PRPF31*

5.1. Introduction

Retinitis pigmentosa (RP) is characterised by progressive retinal degeneration and can be inherited by different inheritance patterns. More than 80 genes are known for causing RP and most of those genes are expressed only in the retina and /or have a distinct biochemical or structural role within the retina or the retinal pigment epithelium (RPE) (RetNet, the Retinal Information Network). Other RP causing genes, such as the pre-mRNA processing factors (PRPFs), are widely expressed in all cell types, although most clinical phenotypes have been described in the retina (Vithana *et al.*, 2001; Yuan *et al.*, 2005; Sullivan *et al.*, 2006; Xu *et al.*, 2012). Mutations in *PRPF8*, a large component of the spliceosome, have also been reported to cause blood cancers and *PRPF8* is likely to have a tumour suppressor role in myeloid malignancies (Kurtovic-Kozaric *et al.*, 2015).

The human *PRPF31* gene is ubiquitously expressed and it encodes a protein of 499 amino acids that acts as a 'bridge' between the U4/U6 di-snRNP and U5 snRNP forming the tri-snRNP, which is the pre-catalytic spliceosome that is remodelled into the active spliceosome. *PRPF31* protein, therefore, is essential for splicing in all cell types, although mutations in *PRPF31* have been reported to cause only RP, without evidence of systemic symptoms (Teigelkamp *et al.*, 1998; Makarova *et al.*, 2002) (Figure 5.1).

Many hypotheses have been proposed on how defects in splicing genes lead to RP. Most of those hypotheses can be incorporated into two main models. The first one proposes mis-splicing events affect mRNAs that are retina-specific. The second model postulates that mis-splicing events would affect widely expressed transcripts, but only the retina would be susceptible to those effects (Ivings *et al.*, 2008; Wilkie *et al.*, 2008; Cao *et al.*, 2011; Linder *et al.*, 2011; Tanackovic *et al.*, 2011). Recently, it has been demonstrated that mouse photoreceptors express a unique splicing program, with high inclusion of alternative exons that are absent outside of the retina, and affects the transcripts of several genes, which is more in line with the second model. Some of those ubiquitously expressed genes are implicated in the formation and function of

primary cilia, having specific isoforms in the photoreceptors related to the connecting cilium and the formation of outer-segments (Murphy *et al.*, 2016).

It has also been proposed that PRPF31-RP is a ciliopathy. Ciliopathy is a genetic disorder of the cilia or its anchoring components that affects ciliary function and retinal degeneration is the most common phenotype of ciliopathy patients. The primary cilium is involved in the maturation and polarisation of RPE cells, which in turn are essential for photoreceptor development and function (Whewey *et al.*, 2015; May-Simera *et al.*, 2018).

The aim of this chapter is to investigate the pathogenesis of the *PRPF31* form of RP using the PRPF31 patient-specific disease model described in chapters 3 and 4.

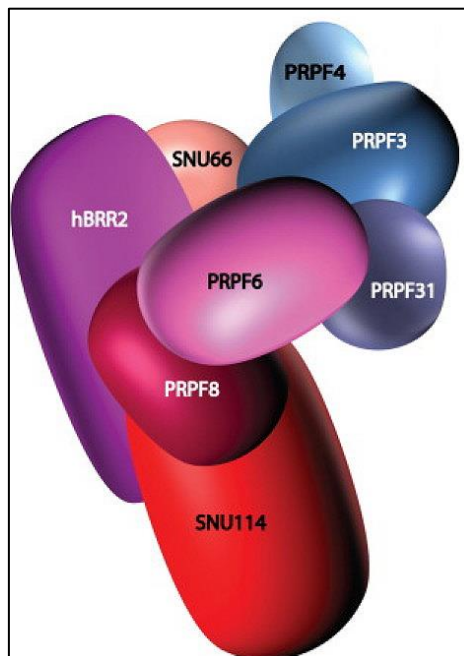


Figure 5.1. Schematic representation of the tri-snRNP component of the spliceosome and proteins associated with adRP. Elements of the U5 snRNP are presented in different shades of red, and those belonging to the U4/U6 snRNP are in shades of blue. Adapted from Tanackovic *et al.* (2011).

5.2. Description and effects of *PRPF31* mutation c.1115_1125 del11

The three patients RP11S1, RP11M and RP11VS, harbouring the mutation c.1115_1125del11, were sequenced for *PRPF31* exon 11, where the mutation is located. Screening of this sequence (Chapter 3, Figure 3.2A, Table 3.1) revealed a 11 bp deletion in exon 11, which is present in both fibroblasts and iPSCs.

Previous *in silico* analysis predicted that one of the effects of this mutation would be the inactivation of an exonic splicing enhancer, leading to the skipping of exon 11 during splicing and inclusion of premature termination codon (PTC) in out-of-phase exon 12 (Rio Frio *et al.*, 2008). This would then result in a short mRNA transcript encoding 387 amino acids, which would be sensitive to nonsense-mediated mRNA decay (NMD). Another predicted result of this mutation would be the formation of a long mRNA transcript containing the deletion in exon 11, which would cause a frame shift after amino acid 371 and a PTC in the last exon of *PRPF31* gene, exon 14, encoding 469 amino acids. Therefore, this isoform would be NMD-insensitive (Vithana *et al.*, 2001; Rio Frio *et al.*, 2008) (Chapter 3, Figure 3.4).

Nonsense-mediated mRNA decay (NMD) is a conserved post-transcriptional cellular mechanism that checks new mRNA transcripts and destroys those that have premature termination codons (PTCs) before their translation into truncated proteins (Hentze and Kulozik, 1999; Chang *et al.*, 2007; Rio Frio *et al.*, 2008).

NMD pathway can be inhibited in cultured cells by puromycin, a drug that affects the function of ribosomes, which proofreads the nascent mRNAs, resulting in inhibition of NMD and stabilisation of nonsense transcripts (Carter *et al.*, 1995). To distinguish between *PRPF31*-RP11VS wild-type (WT), long mutant (LM) NMD-insensitive transcripts, and short mutant (SM) NMD-sensitive transcripts, drug-induced expression changes were measured by semi-quantitative RT-PCR in primary fibroblasts, iPSCs, iPSC-derived RPE and retinal organoids (generated by Dr. Lili Zhu) from WT3 control and patient *PRPF31*-RP11VS.

The results showed that only *PRPF31*-RP11VS displayed LM and SM isoforms in all cell types. Importantly, SM isoforms were only seen by NMD inhibition upon drug treatment, confirming SM transcripts were sensitive to NMD (Figure 5.2A). It was also

demonstrated that expression levels of *PRPF31*-exon 11 were reduced more significantly in RPE cells compared to other cell types (Figure 5.2B).

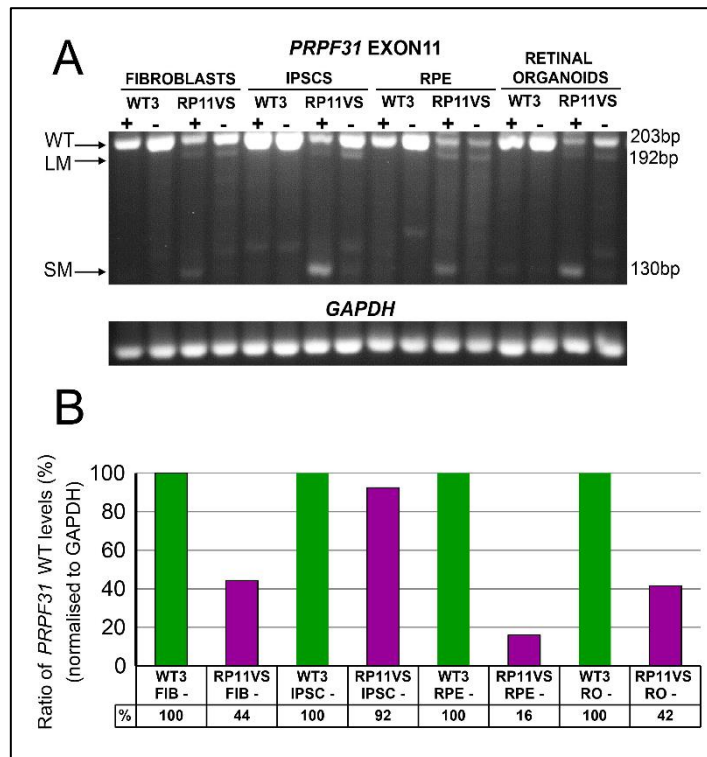


Figure 5.2. *PRPF31* expression in patient-specific cells. A: Short mutant (SM) isoform of 130 bp is only present upon inhibition of NMD with puromycin (indicated by +). B: Quantification of *PRPF31* mRNA in patient cells relative to *GAPDH*. Data are representative of at least three independent repeats. RO: retinal organoids.

Both long and short alleles were confirmed in this study by Sanger sequencing of semi-quantitative RT-PCR of *PRPF31* cDNA containing exon 11 using control WT3 and RP11VS-RPE. The 11 bp deletion was absent in WT3, but present in RP11VS long mutant (LM) and short mutant (SM) alleles, which was 73 bp shorter than LM (Figure 5.3).

Samples	Alleles
WT3	WT- <pre> -----TTGGAT GGACAGCGGAAGAAGCGAGGCGGCCGCAGGTACCGCAAGATGAAGGAGCGGCTGGGGCTGACGGAGATCCGGAAGCAGGC CAACCGTATGAGCTTCGGAGAGATCGAGGAGGACGCCACAGGAGGACCTGGGATTCAGCCTGGGCCACCTGGGCAAGT CGGGCAGTGGGCGTGTGCGGCAGACACAGGTAACGAGA----- </pre>
	RP11VS LM- <pre> -----TTGGAT GGACAGCGGAAGAAGCGAGGCGGCCGCAGGTACCGCAAGATGAAGGAGCGGCTGGGGCTGACGGAGATCC----- -AACCGTATGAGCTTCGGAGAGATCGAGGAGGACGCCACAGGAGGACCTGGGATTCAGCCTGGGCCACCTGGGCAAGT CGGGCAGTGGGCGTGTGCGGCAGACACAGGTAACGAGA----- </pre>
RP11VS	SM- <pre> -----TTGGAT GGACAGCGGAAGAAGCGAGGCGGCCGCAG----- -----ATCGAGGAGGACGCCACAGGAGGACCTGGGATTCAGCCTGGGCCACCTGGGCAAGT CGGGCAGTGGGCGTGTGCGGCAGACACAGGTAACGAGA----- </pre>

Figure 5.3. Sequences of *PRPF31*-exon 11 cDNA in WT3-RPE and RP11VS-RPE samples. WT allele: absence of the mutation, 203 bp; LM allele: 192 bp; SM allele: 130 bp.

The amino acid sequences translated from the cDNA sequences confirmed that c.1115_1125del11 deletion results in a long mutant (LM) isoform with a frameshift after amino acid 371. The other isoform generated by this mutation was an NMD-sensitive short mutant (SM) transcript, where exon 11 was skipped entirely (Figure 5.4).

Samples	Isoforms	EXON 10	EXON 11	EXON 12	aa 371
WT3	WT- <pre> LDGQRKKRGGRRYRKMetKERLGLTEIRKQANRMet SFGEIEEDAYQEDLGFSLGHLGKSGSGRVVRQTQVNE </pre>	█	█	█	█
	RP11VS LM- <pre> LDGQRKKRGGRRYRKMetKERLGLTEIQPYELR RDRGGRLPGGPGIQPGPGVQVQWACAADTGKR </pre>	█	█	█	█
RP11VS	SM- <pre> LDGQRKKRGGRRSRRTPTRRTWDSAWATWASRAV GVCGRHR Stop TR </pre>	█	█	█	█

Figure 5.4. *PRPF31*-exon 11 amino acid sequences in WT3-RPE and RP11VS-RPE samples. WT isoform: presence of exon 11; LM isoform: a frame shift after amino acid 371 creates a long mutant (LM) transcript; SM isoform: skipping of exon 11 leads to a truncated NMD-sensitive short mutant (SM) transcript. Met: open reading frame AUG; Stop codon: UAA.

5.3. Modulators of *PRPF31* expression & Penetrance

The penetrance of a mutation is related to the percentage of individuals carrying an allele of a gene that express traits of a genetic disease. The term incomplete penetrance indicates that a dominant allele, such as in the case of dominant RP *PRPF31*, does not always “penetrate” into the phenotype of the individual. It is now known that CCR4-NOT Transcription Complex Subunit 3 (*CNOT3*), also located in chromosome 19, is a genetic modifier that is responsible for the penetrance of *PRPF31* mutations and acts as a negative regulator of *PRPF31* by binding to its promoter and modulating *PRPF31* transcription (Venturini et al., 2012). Asymptomatic carriers of *PRPF31* mutations express *CNOT3* at low levels, allowing higher amounts of wild-type *PRPF31* transcripts to be produced and preventing retinal degeneration. This mechanism is likely dependent on the presence of polymorphic DNA variants in *CNOT3* sequence (Venturini et al., 2012; Rose et al., 2014).

Preliminary results based on RNA-seq analyses in primary fibroblasts, iPSCs, iPSC-derived RPE and retinal organoids from WT3 control and patient RP11VS showed that the combined total expression of *CNOT3* in triplicate samples was higher in patient’s cells, potentially masking *PRPF31* expression and leading to the development of symptoms (Figure 5.5).

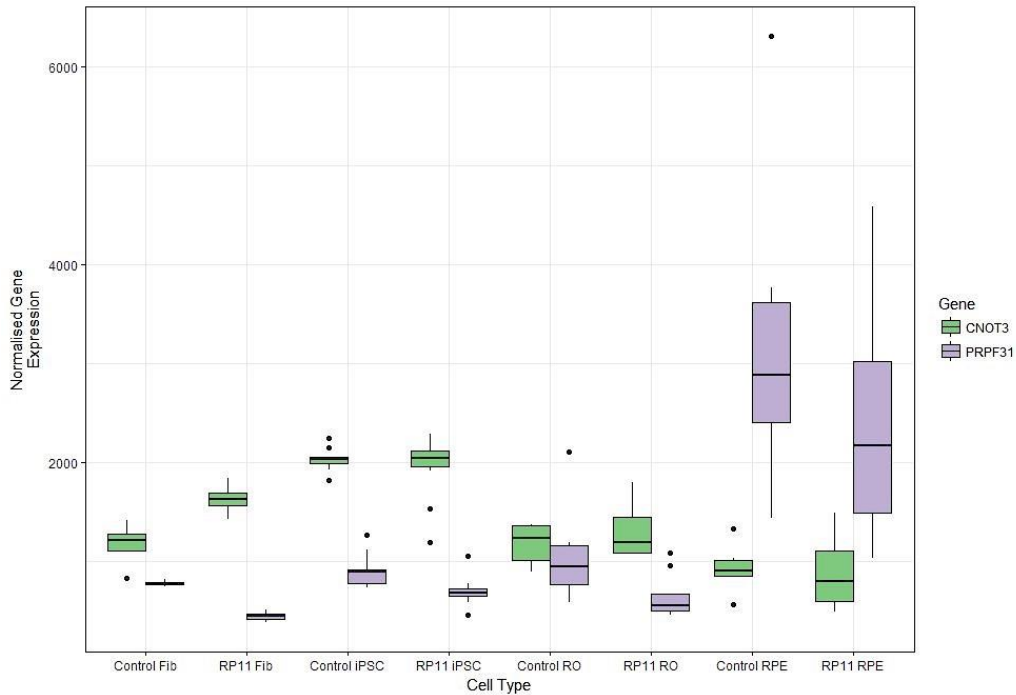


Figure 5.5. Expression of *PRPF31* and *CNOT3* in primary fibroblasts, iPSCs, iPSC-derived RPE and retinal organoids from WT3 control and patient RP11VS by RNA sequencing. In patient's cells, the combined total *CNOT3* expression of biological triplicates was higher than in controls, whilst *PRPF31* was lower in patient's cells. Data from three independent replicates. Graph courtesy of Mr David Dolan.

Another study has shown that variation in the number of a minisatellite repeat element (MSR1) flanking the *PRPF31* core promoter could also be the cause of RP incomplete penetrance (Rose et al., 2016). Three copies of the MSR1 element would repress gene transcription by 50 to 115-fold and four copies of the alleles, which were not observed in symptomatic patients, would correlate with rate of asymptomatic carriers in different populations. Sequencing of MSR1 region did not show any variation in the number of repeats between iPSCs derived from unaffected controls and *PRPF31*-mutant patients (appendix 1), suggesting that MSR1 is not a controller of *PRPF31* gene expression.

5.4. *PRPF31* expression by Immunocytochemistry

To confirm the localisation of PRPF31 protein in RPE cells, iPSCs-derived RPEs were stained with PRPF31 and Y12, a specific marker of Sm proteins, components of the spliceosomal snRNPs (Urlaub et al., 2001). Following immunostaining, PRPF31 was only found in the nuclei of the cells, where it co-localized with Y12 (Figure 5.6).

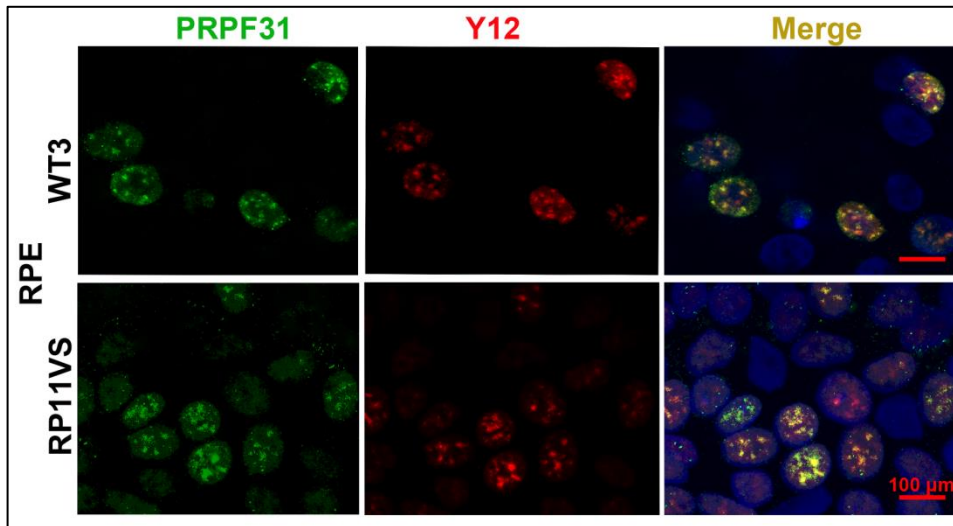


Figure 5.6. Colocalisation of PRPF31 with spliceosomal component (Y12) in iPSC-derived RPE. These are representative examples of at least three independent experiments.

5.5. Splicing & RNA-Seq analysis

Splicing assays and transcriptome analysis were performed in collaboration with research groups led by Prof. Colin A. Johnson, Prof. Reinhard Lührmann and Dr Sushma Grellscheid.

Levels of relevant proteins involved in the assembly of the spliceosome, PRPF8 (assembly of U4/U6-U5 tri-snRNP), SF3b155 (component of U2 snRNP), Snu114 (component of U5 snRNP), SART1 (recruiter Of U4/U6.U5 Tri-SnRNP), PRPF4 (binding of U4, U5, and U6) and PRPF31 (assembly of U4/U6-U5 tri-snRNP) were checked by western blot and it was demonstrated that wild-type PRPF31 is significantly reduced in patient RPE cells when compared to other cell types. The LM form and reduced SART1 were observed only in patient RPE cells (Figure 5.7A). The quantification of wild-type *PRPF31* in patient cells normalized to SF3b155 is shown in Figure 5.7B.

In order to assess the splicing efficiency in patient-specific cells and unaffected controls, an E1A minigene reporter with multiple 5'-splice sites was introduced to the cells via lentiviral transduction (Zerler et al., 1986; Caceres et al., 1994). It is believed that the ability to regulate splicing is generally mediated by splicing factors that interact with cis-elements either promoting or hindering splicing at adjacent splice sites (Bourgeois et al., 2004; Ladd et al., 2004; Underwood et al., 2005). The EA1 minigene reporter can be alternatively spliced into at least five mRNA isoforms (sizes 13S, 12S, 11S, 10S and 9S; Figure 5.7C), depending on the intracellular variation and combination of splicing factors in different cell types. Both PRPF31-RPE and retinal organoids showed accumulation of pre-mRNA, reduction of the 9S and 10S isoforms in RPE, and reduction the 12S isoform in retinal organoids compared to unaffected controls, PRPF31-fibroblasts and iPSCs (Figure 5.7D).

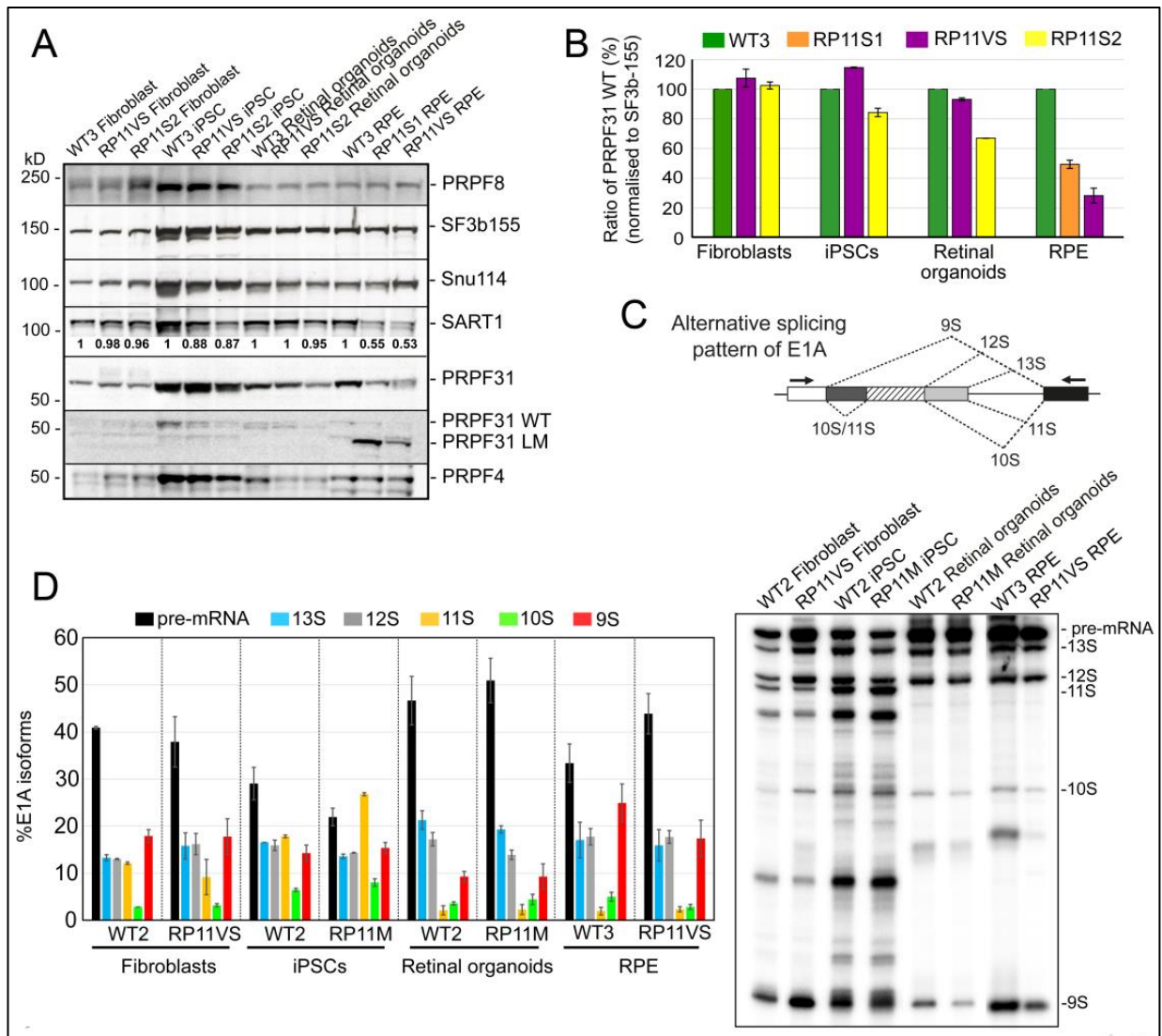


Figure 5.7. PRPF31 expression in patient-specific cells and effects on pre-mRNA splicing. A: Wild-type PRPF31 is significantly reduced in patient RPE cells. The LM form and reduced SART1 is observed only in the patient RPE cells. B: The bar graph shows wild-type PRPF31 levels in patient cells normalized to SF3b15. C: Schematic representation of alternative splice variants of E1A minigene reporter. D: Patient RPE cells showed a notable defect in the alternative splicing of E1A minigene reporter, with reduction of the 9S and 10S isoforms and accumulation of pre-mRNA.

RNA sequencing analysis was performed to identify differences in gene expression and splicing profiles between PRPF31-mutant patients and unaffected controls in primary fibroblasts, iPSCs, RPE and retinal organoids, in biological triplicates (Buskin *et al.*, 2018). Following the differentially expressed genes analysis, there were no significantly enriched pathways in PRPF31-RPE. PRPF31-retinal organoids, however, were enriched for Gene Ontology (GO) categories related to cilium, ciliary membrane, actin cytoskeleton, photoreceptor inner and outer segments, axon terminals and phototransduction. Fibroblasts showed significant differentially expressed genes for lysosome and endosomal processes, focal adhesion, cell-

substrate junctions and extracellular matrix organisation. There were no notable-enriched pathways in RP11-iPSCs.

Since PRPF31-RPE and retinal organoids showed impaired pre-mRNA splicing (Figure 5.7C, D), transcripts in all four cell types were analysed by replicate Multivariate Analysis of Transcript Splicing (rMATS) for differential exon usage (retained introns, alternative 5' and 3' splice sites, mutually exclusive exons, retained introns and skipped exons, Figure 5.8A). It was revealed by differential exon usage analysis that PRPF31-RPE had the highest level of transcripts with retained introns and alternative 3' splice sites compared to other cell types (Figure 5.8B).

PRPF31-fibroblasts also had enriched GO biological processes for cilium formation and genes involved in microtubules and cytokinesis. iPSCs had enriched processes for DNA repair pathways, with centrosome, centrioles and microtubule organising centre highlighted as main cellular components. PRPF31-retinal organoids were enriched for centrosome, microtubules and centrioles, whilst RPE had genes involved in cells-to-substrate adherens junctions, focal adhesions, and mitochondrial inner membrane (Figure 5.8C).

Importantly, both PRPF31-RPE and retinal organoids, but not the fibroblasts or iPSCs had significantly enriched GO biological processes for RNA splicing via the spliceosome (Figure 5.8C).

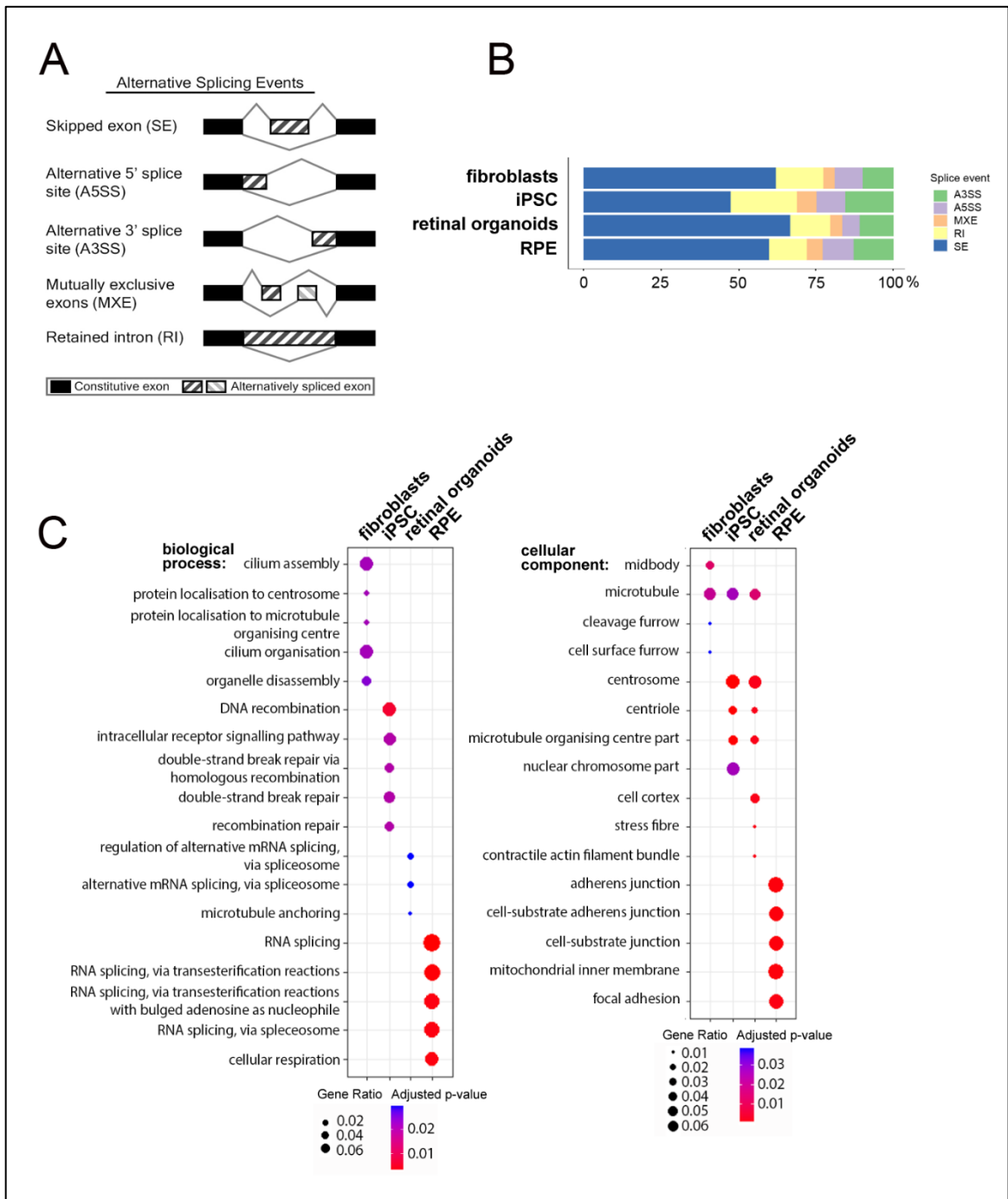


Figure 5.8. Differential alternative splicing analysis from RNA sequencing data of fibroblasts, iPSC, retinal organoids and RPE. A: Schematic representation of alternative splicing events, adapted from Park *et al.* (2013). B: rMATS analysis showing that PRPF31-RPE have the highest percentage of transcripts containing retained introns (RI) and alternative 3' splice sites (A3SS). C: Gene Ontology enrichment analysis showing biological and cellular processes affected by alternative splicing, in all four cell types.

5.6. Cilia length and incidence

Since cilia or its anchoring components were enriched in some GO categories following RNA sequencing results, we hypothesised that primary cilia may have been affected in PRPF31-RPE cells.

Controls and PRPF31-RPEs were stained with ARL13B, a marker of ciliary axoneme, and pericentrin, a marker of the basal body complex located at the base of the cilia, followed by cilia measurement and counting of ciliated cells.

Results showed that there was a significant difference in cilia length and incidence between controls and PRPF31-RPE (Figure 5.9A, B). The average cilia length in RPE cells derived from iPSC controls was $3.3 \mu\text{m} \pm \text{SEM } 0.04$, whilst the average cilia length in RPE cells derived from PRPF31-patient's cells was $2.12 \mu\text{m} \pm \text{SEM } 0.02$. The number of control cells showing cilia was 84% compared to 63% of cells from PRPF31-patient (Figure 5.9B). Cells from both controls and PRPF31-RPE were found at G0/G1 phase, in a post-mitotic state characteristic of RPE (appendix 2).

Transmission electron microscopy (TEM) analysis showed the presence of long cilia with aligned microtubules in control RPE cells, whereas PRPF31-RPE had short, bulbous cilia with misaligned microtubules (Figure 5.9C). Structural defects in cilia, such as bulbous tips and misaligned microtubules were further confirmed by serial block face scanning electron microscopy (SBFSEM, Figure 5.9D).

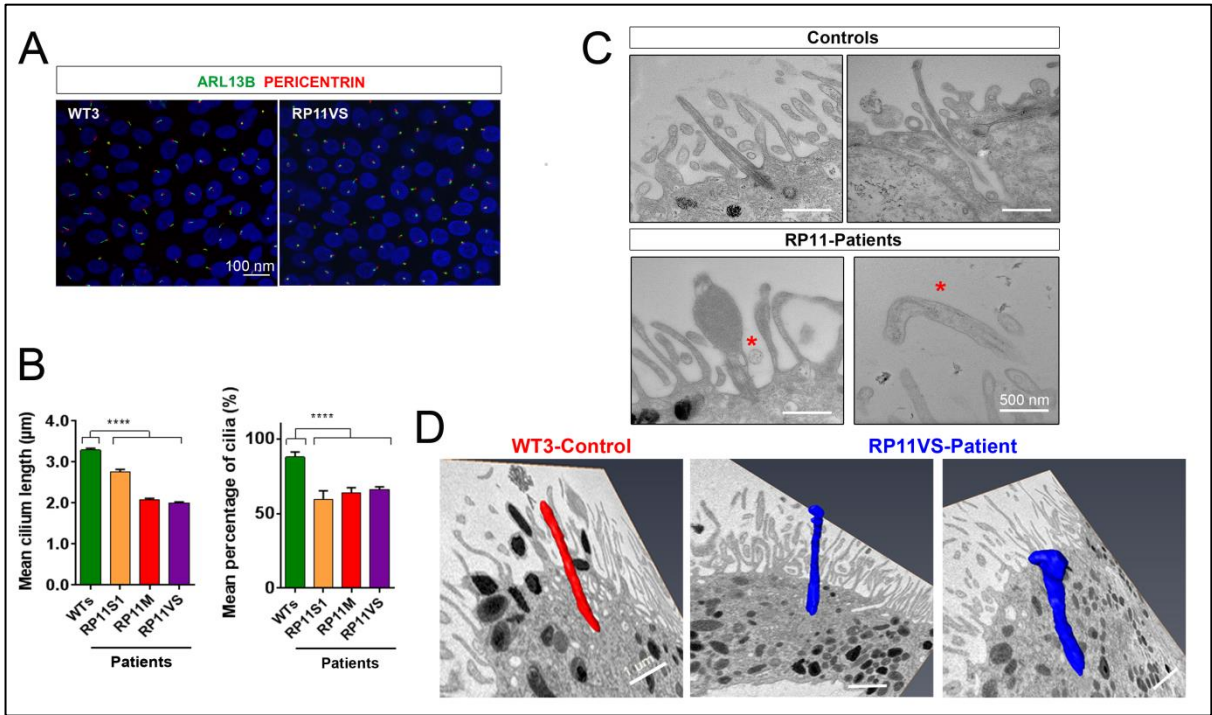


Figure 5.9. PRPF31-RPE cells have defects in cilia formation and structure. A: Immunostaining of RPE cells with cilia markers ARL13B (green) and Pericentrin (red). Representative images from $n = 3$ independent experiments. B: Quantification of cilia length and incidence showing the decrease of both parameters in PRPF31-mutant patients; C, D: TEM and 3D SBFSEM images showing shorter cilia in PRPF31-RPE cells with bulbous tip.

5.7. Crispr-Cas9 correction of *PRPF31* mutation

CRISPR/Cas9 genome editing was performed in collaboration with Dr. Lili Zhu and Dr. Joseph Collin to correct the *PRPF31* c.1115_1125del11 genetic mutation in the cell line with the most severe phenotype (RP11VS). For this purpose, a single-stranded oligodeoxynucleotide (ssODN) template with the wild-type *PRPF31* sequence was designed with 91bp homology arms on each side of the mutation region.

Two hundred iPSC clones were selected, tested by quantitative RT-PCR for expression of wild type *PRPF31* (Figure 10A), and clones expressing *PRPF31* were sequenced to confirm the presence of correction site (Figure 10B). Quantitative RT-PCR analysis confirmed the increased expression of *PRPF31* in the CRISPR/Cas9 corrected clone when compared to uncorrected iPSCs (Figure 10C). Potential off-target effects were excluded and lack of genomic abnormalities and genetic identity were also confirmed by CytoSNP analysis (Buskin *et al.*, 2018).

One CRISPR/Cas9-corrected iPSC clone was then differentiated to RPE, in parallel with uncorrected *PRPF31*-iPSCs using the protocol described in Chapter 4. Quantification of cilia length and incidence in Cas9-RP11VS-RPE showed that both parameters were significantly increased in corrected RPE (Figure 10D, E). Long cilia with aligned axonemal microtubules were also observed by TEM analysis in corrected cells, instead of aberrant morphology seen in the *PRPF31*-RPE (Figure 10F). Correction of RP11VS-RPE line also restored phagocytic capacity, in contrast to the impaired phagocytosis in *PRPF31*-RPE showed by flow cytometry (Figure 10G). PEDF/VEGF secretion assays also revealed normal levels of cytokine secretion, in addition to normal expression of basal collagen IV and apical MERTK, confirmed by immunostaining (Figure 10H-J).

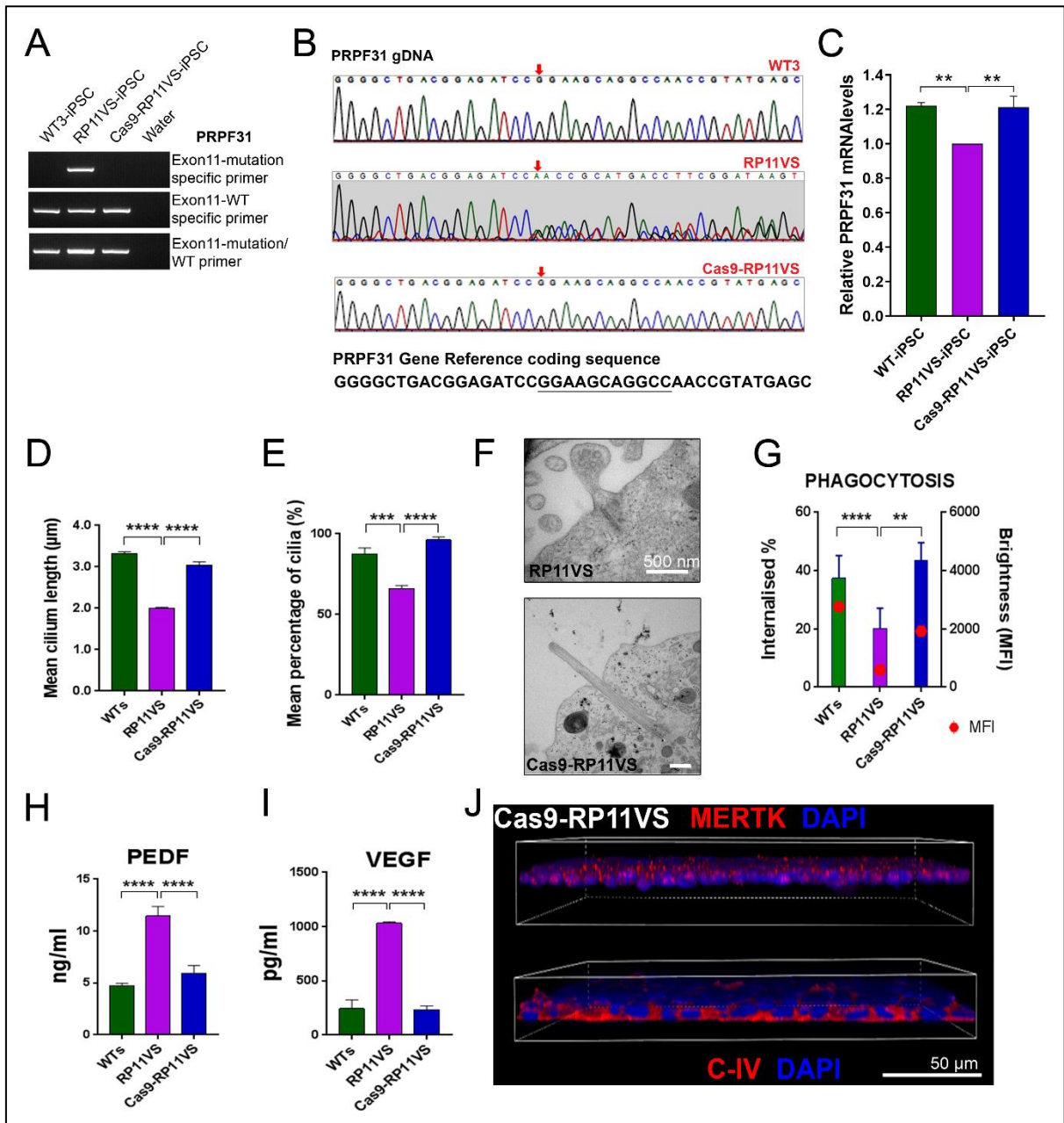


Figure 5.10. Correction of *PRPF31* mutation results in reversal of cellular and functional phenotypes in *PRPF31*-RPE. A: Quantitative RT-PCR analysis confirming the increased expression of *PRPF31* in CRISPR/Cas9 corrected clone. B: Presence of the correction site in Cas9-RP11VS-iPSC sequence. C: Quantification of *PRPF31* expression in corrected cell line. D,E: Quantification of cilia length and incidence in controls, *PRPF31*-RPE and Cas9-RP11VS-RPE. F: TEM images of Cas9-RP11VS-RPE showing morphologically normal cilia, compared to uncorrected *PRPF31*-RPE. G: Rescued phagocytic capacity in Cas9-RP11VS-RPE. H,I,J: Restoration of apical-basal polarity in Cas9-RP11VS-RPE.

5.8. Discussion

Mutations in the ubiquitously expressed splicing factor gene *PRPF31* cause Retinitis Pigmentosa, a hereditary form of retinal degeneration. One of those mutations, c.1115_1125 del11 in exon 11, was first found in a large family from the north of England, diagnosed as having adRP with incomplete penetrance (Moore *et al.*, 1993). The mutation c.1115_1125 del11 was later characterised by Vithana *et al.* (2001) and predicted to result in a short mRNA transcript, which is sensitive to NMD, or in a long NMD-insensitive mRNA transcript containing the deletion in exon 11 and out-of-phase PTC in the last exon of *PRPF31* gene, exon 14. Those two isoforms generated as a result of c.1115_1125 del11 mutation in *PRPF31* gene were confirmed in this study by the sequencing of cDNA products encompassing exons 10, 11 and 12 in a patient with severe phenotype RP11VS in *PRPF31*-primary fibroblasts, iPSCs, RPE and retinal organoids. It was also confirmed that only the SM isoform was sensitive to NMD as seen by NMD inhibition upon drug treatment. Most importantly, *PRPF31* was more reduced in *PRPF31*-RPE cells, compared to other cell types.

The main difference between a PTC and a bona-fide termination codon is that the PTC lies upstream of an intron whilst a real termination codon lies in the terminal exon of a gene. Most mutations producing PTCs are equivalent to null alleles because the pre-mRNA produced by them is proofread and quickly degraded in the nucleus by NMD, before the mRNA transcripts are translated into proteins in the cytoplasm of cells. In a case where the PTC generated by the mutation occurs in the last exon of a gene, the mutant pre-mRNA is insensitive to NMD and can be translated in the cytoplasm into a truncated protein (Hentze and Kulozik, 1999; Chang *et al.*, 2007; Rio Frio *et al.*, 2008). Since the mutation c.1115_1125 del11 results in null alleles and reduction of *PRPF31* functional protein, heterozygous patients bearing the mutation can be considered functional hemizygotes (Rio Frio *et al.*, 2008). It's interesting, however, the fact that members of the same family bearing the same mutation have different phenotypes. In this study, it was observed that phagocytic activity was not significantly reduced in the patient with moderate RP phenotype, RP11M. *CNOT3* has been shown to modulate *PRPF31* gene expression in a transcriptional level by direct binding to *PRPF31* promoter. Studies in ARPE-19 cell lines have demonstrated that silencing of *CNOT3* by siRNA leads to an increase of *PRPF31* expression (Venturini *et al.*, 2012). The correlation between both *PRPF31* and *CNOT3* expressions

corroborate the phenotypic differences seen in *PRPF31* patients bearing c.1115_1125 del11 mutation, although the inclusion of only three patients makes it difficult to evaluate such correlations.

Even though *PRPF31*-RPE patients showed decreased level of *PRPF31* expression, nuclear localisation of that protein by immunohistochemistry was the same as in controls, which can be an indicative of normal functioning of the hemizygote allele. Colocalisation with Y12, a Sm protein that is part of the small nuclear RNAs U1, U2, U4, U5, and U6, provided evidence that *PRPF31* interacts directly with those snRNPs and are compartmentalised in the same nuclear bodies.

Further western blotting analysis using an anti-*PRPF31* C terminus antibody confirmed that *PRPF31* is more significantly reduced in patient RPE cells compared to other cell types. Interestingly, mutant *PRPF31*-LM protein isoform, detected by using an anti-*PRPF31* N terminus antibody, was only seen in *PRPF31*-RPE cells and it's not known whether the presence of those proteins would have a dominant-negative effect on RPE cells (Figure 6.7D). *SART1*, a U5 snRNP protein important for the formation of the pre-catalytic spliceosomal B complex, was reduced only in patient RPE cells, but no changes in the expression of the U5 protein *PRPF8* or the U4/U6 protein *PRPF4* were observed. Splicing was impaired in both *PRPF31*-RPE and retinal organoids, as it was shown by the accumulation of pre-mRNA and decrease of some isoforms, as shown in the E1A minigene reporter assays, compared to other cell types.

Differential exon usage, which detects differential alternative splicing from replicate RNA-Seq data, revealed that *PRPF31*-RPE had the highest level of transcripts with retained introns and alternative 3'splice sites compared to other cell types, confirming the impaired of splicing showed by the minigene assay. Intron removal by the spliceosome occurs through a succession of sequential events that involve the assembly and disassembly of snRNP complexes. Within each round of splicing, the U4/U6.U5 tri-snRNP complex is assembled through the mediation of splicing factors *PRPF31* and *PRPF6* (Makarov et al., 2000; Schaffert et al., 2004). Therefore, mutations in splicing factor genes, associated with adRP, affect the function of tri-snRNP and impair the process of intron excision for specific pre-mRNA transcripts (Boon et al., 2007; Gonzalez-Santos et al., 2008; Huranová et al., 2009; Maeder et al., 2009; Tanackovic et al., 2011). This could have a bigger impact on cell types with the highest levels of alternative splicing and specific splicing variants, such as retinal cell types (Murphy *et al.*, 2016).

Differential exon usage analysis also revealed that PRPF31-RPE have genes involved in cells-to-substrate adherens junctions and focal adhesions, confirmed by the RPE phenotypes described in Chapter 4. Possible mitochondrial processes affected by mutation c.1115_1125 del11 still remain to be investigated. Both PRPF31-RPE and retinal organoids had significantly enriched GO biological processes for RNA splicing via the spliceosome, suggesting that disrupted alternative splicing programmes in the retina result in an increase of splicing deficiencies, leading to disruption of specific biological processes that cause the unique phenotypes observed in RP-PRPF31.

PRPF31-mutant fibroblasts had enriched GO biological processes for cilium formation and genes involved in microtubules and cytokinesis, suggesting PRPF31 is involved in fibroblasts ciliogenesis as previously demonstrated by data on decreased cilia length and incidence in PRPF31-mutant primary fibroblasts (Whewey *et al.*, 2015). Despite of those ciliary defects, primary fibroblasts were reprogrammed into iPSCs with similar efficiencies to control cells. Although the role of cilia in iPSCs still remains uncertain, generation of iPSCs from patients with ciliopathies have been reported (Nathwani *et al.*, 2014; Hey *et al.*, 2018). This suggests that impaired mRNA splicing is the primary cause of RP, followed by cilia deficiencies as secondary defects resulted from splicing deficiencies. PRPF31-retinal organoids were also enriched for cilia processes and related organelles; therefore, it was relevant to check cilia length and incidence in PRPF31-RPE cells.

The presence of primary cilia in human RPE cells was first reported in 1965 (Allen, 1965) from electron microscopy images of an exenterated human eye. Since then other observations of a single cilium in RPE cells supported previous reports (Allen, 1965; Fisher and Steinberg, 1982) that cilia are common and can be found in human RPE cells *in vivo*. They are present on the apical surface of RPE cells and vary between 1-10 μm in length (Nishiyama *et al.*, 2002). Retinal ciliopathies are a group of retinal diseases, in which many proteins implicated in retinal degeneration have been found to be localised in the retinal cilia, basal bodies and adjacent centrioles. In this study, both cilia length and incidence were significantly reduced in all PRPF31-RPEs when compared to controls. Additionally, structural defects were noticed by TEM images, such as bulbous tips and misaligned microtubules.

Primary cilia are essential for complete maturation of RPE cells, and lack of maturation combined with defects in apical processes are strongly linked to defects in ciliogenesis. It has been previously demonstrated that iPSC-derived RPE from a patient with Joubert syndrome, a ciliopathy, harbouring *CEP290* mutations, had a lack of structural and functional maturity (Parfitt *et al.*, 2016). Additionally, studies have shown the knockdown of cilia component IFT88, an intraflagellar transport protein, in wild type iPSC-derived RPE results in RPE with leaky tight junctions and severe maturation and polarization defects (May-Simera *et al.*, 2018). Indeed, *PRPF31* knockdown in hTERT-RPE1 cells caused significant mislocalisation of IFT88 to the ciliary tip, partially elucidating the bulbous ciliary tip phenotype seen in *PRPF31*-RPE cells (Buskin *et al.*, 2018).

RPE function such as phagocytosis and secretion of growth factors, are fundamentally vital for photoreceptors development and function. Studies with *BBS8*^{-/-} mice with abnormal cilia have shown that RPE maturation defects temporally precede photoreceptors maturation and degeneration. In mice, photoreceptor outer segments begin to develop around post-natal day 5, with complete maturation at day 21. In contrast, RPE maturation is completed by post-natal day 0 (Bharti *et al.*, 2012; Nasonkin *et al.*, 2013). This study showed the impairment of important cellular and functional characteristics in RPE cells, such as phagocytic activity and loss of apical/basal polarity, described in Chapter 4, in addition to the lowest levels of wild type *PRPF31* compared to other cell types and presence of mutant transcripts. Taken together, these results indicate that RPE is the most affected cell type in the pathogenesis of *PRPF31*-RP, corroborating the *PRPF31*-RPE phenotype in mouse models (Graziotto *et al.*, 2011).

Most importantly, combined ‘double hit’ defects in human RPE and photoreceptors, characterised by incomplete maturation and impaired polarisation of RPE, and defects in photoreceptor connecting cilium, both caused by splicing deficiencies and disruption of splicing programmes for ciliary genes in *PRPF31*-mutant patients, are likely to underlie the mechanism for *PRPF31*-retinal ciliopathy.

Finally, the correction of the mutation c.1115_1125del11 in the most severe clinical phenotype rescued all cellular and functional phenotypes in *PRPF31*-RPE, including cilia length and incidence, phagocytic capacity, secretion of cytokines and

expression of typical RPE markers, without any off-targets effects, demonstrating proof of concept for future gene therapies.

Chapter 6 - Discussion and Conclusions

Retinal degenerative disorders are a vast and varied group of diseases caused by degeneration of retinal cells. As individuals suffer the loss of their sight, this understandably affects their mental well-being. They also require support from society to carry out their daily lives. This can include financial, health and mobility resources. Partial and complete blindness can restrict their ability to work, travel and to interact socially and professionally with friends, colleagues and family.

Retinitis pigmentosa (RP) is a genetic condition in which degeneration of photoreceptors and retinal pigment epithelium (RPE) gradually leads to visual loss. RP affects approximately 1.5 million people worldwide and it's a leading cause of blindness in young people (Herse, 2005). Pre-mRNA processing factor 31, *PRPF31*, an RP-associated gene, encodes a splicing factor required for the formation of U4/U6.U5 tri-small nuclear ribonucleic protein (tri-snRNP) complex, which is a constituent of the pre-mRNA processing spliceosome (Mordes et al., 2006; Linder et al., 2011). Although *PRPF31* is ubiquitously expressed, it solely causes retinal phenotype.

Traditional models to study RP are normally difficult to obtain or fail to faithfully mimic the pathophysiology of the disease. Primary cells from patients are hard to access and difficult to obtain and expand, especially from patients with degenerative diseases, such as RP, due to the low number of cells of interest. Although *PRPF31*-RP animal models developed changes in the RPE, they failed to display retinal degeneration and they did not present any visual defect until 18 months of age (Bujakowska *et al.*, 2009; Graziotto *et al.*, 2011).

Large animals such as pigs and monkeys can also be used as models for retinal diseases, but they are very expensive and difficult to obtain due to ethical issues. Additionally, the successes seen in animals models for disease modelling and gene therapy are not translated well into fully approved treatments that could be commercially viable to anyone who needs it (Tucker et al., 2014).

One attractive alternative method to generate disease models is the use of stem cells. Pluripotent stem cells have special features including indefinite self-renew and ability to differentiate into multiple cell types from all three embryonic germ layers *in vitro* or *in vivo*, under specific conditions (Thomson et al., 1998). Induced pluripotent

stem cells (iPSCs), which can be reprogrammed to a pluripotent state by introduction of key transcription factors, possess all the features of pluripotent stem cells and can be derived from available and easily accessible cell types such as skin fibroblasts, peripheral blood, hairs and urine from unaffected donors and patients, (Raab *et al.*, 2014). For those reasons iPSCs became the preferred choice for disease modeling, as they can be patient-specific and mimic disease phenotypes, in addition to the possibility of genome editing via correction of disease-specific mutations.

For this project, fibroblasts from the unaffected controls and PRPF31-mutant patients, including moderate, severe and very severe phenotypes (RP11M, RP11S1 and RP11VS, respectively), were reprogrammed into iPSC and PRPF31 mutations were validated. The differences of reprogramming efficiencies between controls and PRPF31-mutant fibroblasts were small, demonstrating that sex, age or *PRPF31* mutations of the donors had no impact on the derivation of iPSCs. Successfully reprogramming of PRPF31-fibroblast has also been reported in the literature (Terray *et al.*, 2017). The iPSCs were fully reprogrammed and bone fide, as shown by absence of reprogramming transgenes, expression of pluripotency markers and ability to differentiate into any cell type of the three germ layers *in vitro* and *in vivo*. Additionally, none of controls and PRPF31-iPSCs, as well as their respective parental fibroblasts, displayed genetic abnormalities qualified as pathogenic or that would affect downstream analysis. iPSCs also had the same genetic profile of their correspondent parental fibroblasts, corroborating the origin of iPSCs in this project.

iPSCs were differentiated into RPE using a stepwise method to enhance RPE differentiation in a manner which recapitulates eye development. In this method, cells were directed to ectodermal lineage to form neuroepithelial progenitor cells and then to RPE cells, using a combination of small molecules. All iPSC selected lines generated RPE despite of the severity of the phenotypes. Indeed, differentiation efficiencies were likely to be cell line specific, related to a particular cell line's innate responses and cannot be attributed only to disease severity or phenotype as it has been previously demonstrated that even iPSC lines from unaffected individuals exhibit such differences (Lane *et al.*, 2014; Hallam *et al.*, 2018).

Although iPSC-derived RPE lines formed a cobblestone monolayer of RPE cells, PRPF31-RPE monolayers were not as tightly packed and mature as controls RPE and displayed leaky tight junctions at week 21 of differentiation, as shown by

measurements of transepithelial electrical resistance (TER) in the monolayers. The RPE derived from patients RP11S1 and RP11VS, with severe and very severe phenotypes, also had reduced functional ability to phagocytose rod outer segments, corroborating a previous study that showed that primary RPE cultures of *Prpf31*^{+/-}-mice and shRNA-mediated knockdown of *PRPF31* in human ARPE-19 cells had decreased phagocytosis (Farkas *et al.*, 2014). Defects in RPE polarity were also detected by overexpression levels of PEDF and VEGF and reduction of expression of apical RPE marker MerTK and basolateral markers BEST1 and Collagen IV in severe and very severe PRPF31-RPE phenotypes. Disruption of polarity has been shown to impact cell proliferation, adhesion, migration, tight junction formation, and vascular permeability with further functional consequences for rod survival (Farnoodian *et al.*, 2015). In an ultrastructural level, severe PRPF31-RPE showed cells with over 2-fold shorter and fewer microvilli in contrast to RPE cells derived from control iPSCs, at weeks 21 and 43 of differentiation. It was also noticed that PRPF31-RPE had a general disorganization of basal infoldings, containing large deposits underneath the RPE. Loss of basal infoldings as well as atrophy of apical microvilli, disappearance of melanin granules and accumulation of oxidized lipids residues are a sign of RPE aging or stress, and consequently death (Bonilha, 2008; Gu *et al.*, 2012). Furthermore, RPE cells from *prpf31* knockout mice have shown loss of the basal infoldings, vacuolization and accumulation of amorphous deposits between the RPE and Bruch's membrane at one year of age, corroborating the results of this project (Rio Frio *et al.*, 2008; Graziotto *et al.*, 2011).

The *PRPF31* mutation present in patients RP11M, RP11S1 and RP11VS, named as c.1115_1125 del11, at exon 11, is a deletion of 11 bp. This mutation was predicted to result in a short mRNA transcript (SM) sensitive to non-mediated decay (NMD), or in a long NMD-insensitive mRNA transcript (LM) containing the deletion in exon 11 and out-of-phase premature termination codon (PTC) in the last exon of *PRPF31* gene (Vithana *et al.*, 2001; Rio Frio *et al.*, 2008), which was confirmed in this study. Since the mutation c.1115_1125 del11 results in null alleles and reduction of PRPF31 functional protein, heterozygous patients bearing the mutation can be considered functional hemizygotes (Rio Frio *et al.*, 2008). Members of the same family bearing the same mutation, however, have different phenotypes, as exemplified in this study by significantly reduced phagocytic activity in the patients with severe and very severe phenotypes, but not moderate RP phenotype. One possible explanation for this is the

interaction between *PRPF31* and *CNOT3* genes. *CNOT3* has been shown to modulate *PRPF31* gene expression in a transcriptional level by direct binding to *PRPF31* promoter and masking *PRPF31* expression (Venturini *et al.*, 2012). The correlation between both *PRPF31* and *CNOT3* expressions corroborated the phenotypic differences seen in *PRPF31*-mutant patients bearing c.1115_1125 del11 mutation, although the inclusion of only three patients makes it difficult to evaluate such correlations.

PRPF31 protein was localised in the nuclei of the cells and *PRPF31*-RPE patients showed the lowest levels of protein when compared to primary fibroblasts, iPSCs and 3D retinal organoids generated in Professor Majlinda Lako's group. Interestingly, mutant *PRPF31*-LM protein isoform, was only seen in *PRPF31*-RPE cells and it's not known whether the presence of those proteins would have a dominant-negative effect in RPE cells. Splicing was impaired in both *PRPF31*-RPE and retinal organoids, as it was shown by the accumulation of pre-mRNA and decrease of some isoforms, as shown in the E1A minigene reporter assays, compared to other cell types. Differential exon usage, which detects differential alternative splicing from replicate RNA-Seq data, revealed that *PRPF31*-RPE had the highest level of transcripts with retained introns and alternative 3'splice sites compared to other cell types, confirming the impaired of splicing showed by the minigene assay. Mutations in splicing factor genes have been shown to affect the function of tri-snRNP and impair the process of intron excision for specific pre-mRNA transcripts (Boon *et al.*, 2007; Gonzalez-Santos *et al.*, 2008; Huranová *et al.*, 2009; Maeder *et al.*, 2009; Tanackovic *et al.*, 2011). This can cause a bigger impact on cell types with the highest levels of alternative splicing and specific splicing variants, such as retinal cell types (Murphy *et al.*, 2016).

Both *PRPF31*-RPE and retinal organoids, but not primary fibroblast or iPSCs, had significantly enriched GO biological processes for RNA splicing via the spliceosome, suggesting that disrupted alternative splicing programme in the retina result in an increase of splicing deficiencies, leading to disruption of specific biological processes that cause the unique phenotypes observed in RP-*PRPF31*.

Additionally, *PRPF31*-mutant fibroblasts had enriched GO biological processes for cilium formation, suggesting *PRPF31* is involved in fibroblasts ciliogenesis as previously demonstrated by data on decreased cilia length and incidence in *PRPF31*-mutant primary fibroblasts (Wheway *et al.*, 2015). Despite of those ciliary defects, primary fibroblasts were reprogrammed into iPSCs with similar efficiencies to control

cells, suggesting that impaired mRNA splicing is the primary cause of RP, followed by cilia deficiencies as secondary defects resulted from splicing deficiencies. PRPF31-retinal organoids were also enriched for cilia processes and related organelles.

Primary cilia have been shown to be essential for complete maturation of RPE cells (May-Simera *et al.*, 2018). Therefore impairment of important cellular and functional characteristics in RPE cells such as phagocytic activity and loss of apical/basal polarity, possibly caused by observed structural defects in RPE primary cilia, in addition to the lowest levels of wild type *PRPF31* and presence of mutant transcripts, indicate that RPE is the most affected cell type in the pathogenesis of PRPF31-RP. PRPF31 phenotype seen in mouse models also corroborate those results (Graziotto *et al.*, 2011).

Incomplete maturation and impaired polarisation of RPE, and defects in photoreceptor connecting cilium, both caused by disruption of splicing programmes for ciliary genes in PRPF31-mutant patients, are likely to underlie the mechanism for PRPF31-retinal ciliopathy. Finally, the correction of the mutation c.1115_1125 del11 in the most affected RPE phenotype rescued all cellular and functional phenotypes in PRPF31-RPE, without off-targets effects, demonstrating proof of concept for future gene therapies.

6.1. Conclusions and future directions

In summary, iPSCs are a great model to study complex retinal degeneration conditions, such as RP. We have shown successful generation of iPSCs from primary fibroblasts of RP patients with different clinical phenotypes. These iPSCs expressed typical pluripotency markers and were capable to differentiate into cells from the three embryonic germ layers *in vitro* and *in vivo*. We were also able to differentiate PRPF31-iPSCs into RPE, using a stepwise protocol in a manner that recapitulates eye development, to interrogate the pathophysiology of the disease. We found that PRPF31-RPE had functional and ultrastructural defects, implicating in loss of apical/basal polarity, when compared to wild type RPE. PRPF31-RPE also had pronounced defects in primary cilia, the lowest levels of wild type PRPF31 protein and presence of mutant transcripts. Additionally, PRPF31-RPE had impaired splicing and the highest level of isoforms with retained introns and alternative 3'splice sites, when compared to other cell types, indicating that RPE is the most affected cell type in the pathogenesis of PRPF31-RP. Finally, we showed that the correction of the mutation c.1115_1125 del11 in the most affected RPE phenotype rescued all cellular and functional phenotypes in PRPF31-RPE.

To address the complexity of RP and the existence of different clinical phenotypes originated from the same mutation, more samples would need to be investigated. Modulation of *CNOT3* expression via the use of repressors or knock out of one high-expressing alleles in severe clinical phenotypes can be an interesting way to investigate incomplete penetrance of RP. Modulation of cilia growth upon use of known compounds could restore primary cilia, and therefore rescue some of PRPF31-RPE phenotype. It has been found that many common drugs have the ability to restore primary cilium in cancer cell line models and most of those compounds have already been tested for safety in humans, paving the way for clinical translation (Khan *et al.*, 2016). Additionally, delivery of wild type *PRPF31* into retina cells using adeno-virus vectors can be an interesting method for cell-based therapies.

Chapter 7 - Appendices

7.1. Appendix 1

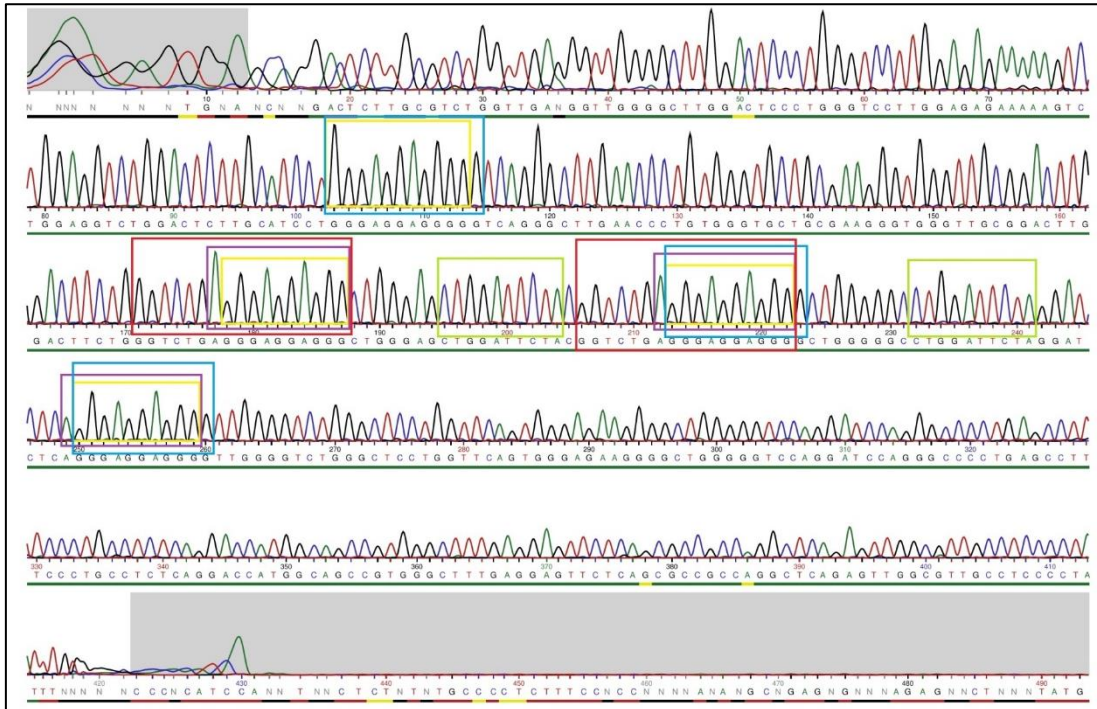


Figure 7.1. Sequencing of a MSR1 region adjacent to *PRPF31* core promoter in control WT3 iPSC. All cell lines showed the same sequence. Work performed by Ms Kasia Bialas.

7.2. Appendix 2

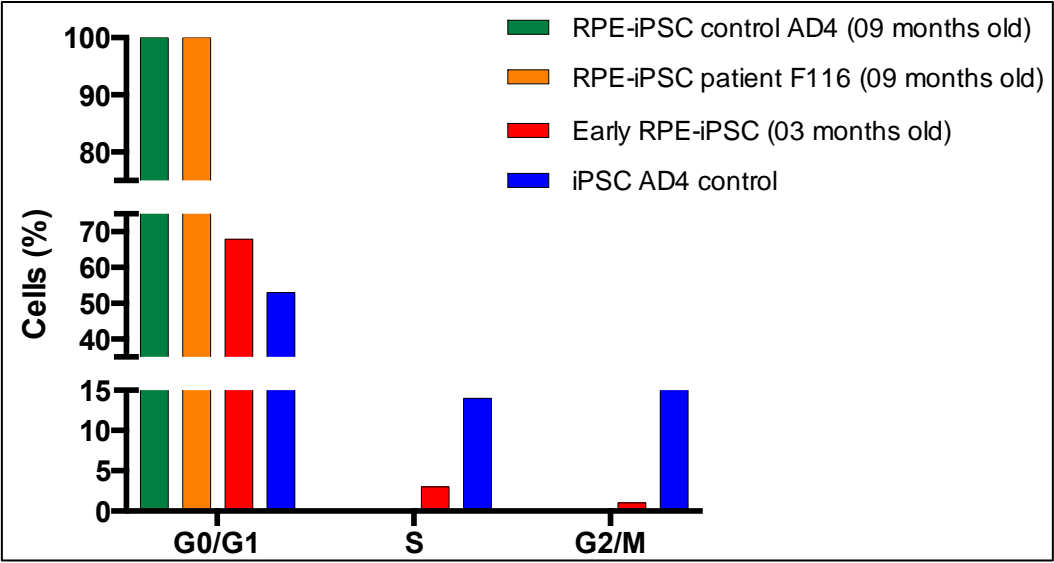


Figure 7.2. Distribution of RPE cells derived from iPSC control WT3 (AD4), RPE-iPSC patient RP11S1 (F116), early RPE-iPSC and control iPSC WT3 (AD4).

Publications:

Buskin, A., Zhu, L., Chichagova, V., Basu, B., Mozaffari-Jovin, S., Dolan, D., Droop, A., Collin, J., Bronstein, R., Mehrotra, S., Farkas, M., Hilgen, G., White, K., Pan, K.T., Treumann, A., Hallam, D., Bialas, K., Chung, G., Mellough, C., Ding, Y., Krasnogor, N., Przyborski, S., Zwolinski, S., Al-Aama, J., Alharthi, S., Xu, Y., Wheway, G., Szymanska, K., McKibbin, M., Inglehearn, C.F., Elliott, D.J., Lindsay, S., Ali, R.R., Steel, D.H., Armstrong, L., Sernagor, E., Urlaub, H., Pierce, E., Luhrmann, R., Grellscheid, S.N., Johnson, C.A. and Lako, M. (2018) 'Disrupted alternative splicing for genes implicated in splicing and ciliogenesis causes PRPF31 retinitis pigmentosa', *Nat Commun*, 9(1), p. 4234.

Chichagova, V., Hallam, D., Collin, J., **Buskin, A.**, Saretzki, G., Armstrong, L., Yu-Wai-Man, P., Lako, M. and Steel, D.H. (2017) 'Human iPSC disease modelling reveals functional and structural defects in retinal pigment epithelial cells harbouring the m.3243A > G mitochondrial DNA mutation', *Sci Rep*, 7(1), p. 12320.

Hallam, D., Collin, J., Bojic, S., Chichagova, V., **Buskin, A.**, Xu, Y., Lafage, L., Otten, E.G., Anyfantis, G., Mellough, C., Przyborski, S., Alharthi, S., Korolchuk, V., Lotery, A., Saretzki, G., McKibbin, M., Armstrong, L., Steel, D., Kavanagh, D. and Lako, M. (2017) 'An Induced Pluripotent Stem Cell Patient Specific Model of Complement Factor H (Y402H) Polymorphism Displays Characteristic Features of Age-Related Macular Degeneration and Indicates a Beneficial Role for UV Light Exposure', *Stem Cells*, 35(11), pp. 2305-2320.

Neganova, I., Tilgner, K., **Buskin, A.**, Paraskevopoulou, I., Atkinson, S.P., Peberdy, D., Passos, J.F. and Lako, M. (2014) 'CDK1 plays an important role in the maintenance of pluripotency and genomic stability in human pluripotent stem cells', *Cell Death Dis*, 5, p. e1508.

Chapter 8 - References

- Ablonczy, Z. and Crosson, C.E. (2007) 'VEGF modulation of retinal pigment epithelium resistance', *Exp Eye Res*, 85(6), pp. 762-71.
- Abu-Safieh, L., Alrashed, M., Anazi, S., Alkuraya, H., Khan, A.O., Al-Owain, M., Al-Zahrani, J., Al-Abdi, L., Hashem, M., Al-Tarimi, S., Sebai, M.A., Shamia, A., Ray-Zack, M.D., Nassan, M., Al-Hassnan, Z.N., Rahbeeni, Z., Waheeb, S., Alkharashi, A., Abboud, E., Al-Hazzaa, S.A. and Alkuraya, F.S. (2013) 'Autozygome-guided exome sequencing in retinal dystrophy patients reveals pathogenetic mutations and novel candidate disease genes', *Genome Res*, 23(2), pp. 236-47.
- Adamis, A.P., Shima, D.T., Yeo, K.T., Yeo, T.K., Brown, L.F., Berse, B., D'Amore, P.A. and Folkman, J. (1993) 'Synthesis and secretion of vascular permeability factor/vascular endothelial growth factor by human retinal pigment epithelial cells', *Biochem Biophys Res Commun*, 193(2), pp. 631-8.
- Adijanto, J., Castorino, J.J., Wang, Z.X., Maminishkis, A., Grunwald, G.B. and Philp, N.J. (2012) 'Microphthalmia-associated transcription factor (MITF) promotes differentiation of human retinal pigment epithelium (RPE) by regulating microRNAs-204/211 expression', *J Biol Chem*, 287(24), pp. 20491-503.
- Aleman, T.S., Duncan, J.L., Bieber, M.L., de Castro, E., Marks, D.A., Gardner, L.M., Steinberg, J.D., Cideciyan, A.V., Maguire, M.G. and Jacobson, S.G. (2001) 'Macular pigment and lutein supplementation in retinitis pigmentosa and Usher syndrome', *Invest Ophthalmol Vis Sci*, 42(8), pp. 1873-81.
- Ali, R.R. and Sowden, J.C. (2011) 'Regenerative medicine: DIY eye', *Nature*, 472(7341), pp. 42-3.
- Allen, R.A. (1965) 'Isolated cilia in inner retinal neurons and in retinal pigment epithelium', *J Ultrastruct Res*, 12(5), pp. 730-47.
- Amabile, G. and Meissner, A. (2009) 'Induced pluripotent stem cells: current progress and potential for regenerative medicine', *Trends Mol Med*, 15(2), pp. 59-68.
- Anders, S., Pyl, P.T. and Huber, W. (2015) 'HTSeq--a Python framework to work with high-throughput sequencing data', *Bioinformatics*, 31(2), pp. 166-9.
- Anjamrooz, S.H. (2013) 'The cellular memory disc of reprogrammed cells', *Stem Cell Rev*, 9(2), pp. 190-209.
- Assawachananont, J., Mandai, M., Okamoto, S., Yamada, C., Eiraku, M., Yonemura, S., Sasai, Y. and Takahashi, M. (2014) 'Transplantation of Embryonic and Induced Pluripotent Stem Cell-Derived 3D Retinal Sheets into Retinal Degenerative Mice', *Stem Cell Reports*, 2(5), pp. 662-74.
- Atienzar-Aroca, S., Flores-Bellver, M., Serrano-Heras, G., Martinez-Gil, N., Barcia, J.M., Aparicio, S., Perez-Cremades, D., Garcia-Verdugo, J.M., Diaz-Llopis, M., Romero, F.J. and Sancho-Pelluz, J. (2016) 'Oxidative stress in retinal pigment epithelium cells increases exosome secretion and promotes angiogenesis in endothelial cells', *J Cell Mol Med*, 20(8), pp. 1457-66.
- Baehr, W. and Chen, C.K. (2001) 'RP11 and RP13: unexpected gene loci', *Trends Mol Med*, 7(11), pp. 484-6.
- Bailey, T.J., El-Hodiri, H., Zhang, L., Shah, R., Mathers, P.H. and Jamrich, M. (2004) 'Regulation of vertebrate eye development by Rx genes', *Int J Dev Biol*, 48(8-9), pp. 761-70.

- Bainbridge, J.W., Smith, A.J., Barker, S.S., Robbie, S., Henderson, R., Balaggan, K., Viswanathan, A., Holder, G.E., Stockman, A., Tyler, N., Petersen-Jones, S., Bhattacharya, S.S., Thrasher, A.J., Fitzke, F.W., Carter, B.J., Rubin, G.S., Moore, A.T. and Ali, R.R. (2008) 'Effect of gene therapy on visual function in Leber's congenital amaurosis', *N Engl J Med*, 358(21), pp. 2231-9.
- Baralle, F.E. and Giudice, J. (2017) 'Alternative splicing as a regulator of development and tissue identity', *Nat Rev Mol Cell Biol*, 18(7), pp. 437-451.
- Barnes, R.M., Firulli, B.A., Conway, S.J., Vincentz, J.W. and Firulli, A.B. (2010) 'Analysis of the Hand1 cell lineage reveals novel contributions to cardiovascular, neural crest, extra-embryonic, and lateral mesoderm derivatives', *Dev Dyn*, 239(11), pp. 3086-97.
- Bazan, N.G., Scott, B.L., Reddy, T.S. and Pelias, M.Z. (1986) 'Decreased content of docosahexaenoate and arachidonate in plasma phospholipids in Usher's syndrome', *Biochem Biophys Res Commun*, 141(2), pp. 600-4.
- Beatty, S., Koh, H., Phil, M., Henson, D. and Boulton, M. (2000) 'The role of oxidative stress in the pathogenesis of age-related macular degeneration', *Surv Ophthalmol*, 45(2), pp. 115-34.
- Beatty, S., Murray, I.J., Henson, D.B., Carden, D., Koh, H. and Boulton, M.E. (2001) 'Macular pigment and risk for age-related macular degeneration in subjects from a Northern European population', *Invest Ophthalmol Vis Sci*, 42(2), pp. 439-46.
- Becerra, S.P., Fariss, R.N., Wu, Y.Q., Montuenga, L.M., Wong, P. and Pfeiffer, B.A. (2004) 'Pigment epithelium-derived factor in the monkey retinal pigment epithelium and interphotoreceptor matrix: apical secretion and distribution', *Exp Eye Res*, 78(2), pp. 223-34.
- Berson, E.L. (1993) 'Retinitis pigmentosa. The Friedenwald Lecture', *Invest Ophthalmol Vis Sci*, 34(5), pp. 1659-76.
- Berson, E.L. (2000) 'Nutrition and retinal degenerations', *Int Ophthalmol Clin*, 40(4), pp. 93-111.
- Bharti, H.M.-S.S.D.M.K.M.L.M. (2014) 'Primary Cilium Regulates iPS Cell Derived RPE Maturation', *ARVO. Investigative Ophthalmology & Visual Science*.
- Bharti, K., Gasper, M., Ou, J., Brucato, M., Clore-Gronenborn, K., Pickel, J. and Arnheiter, H. (2012) 'A regulatory loop involving PAX6, MITF, and WNT signaling controls retinal pigment epithelium development', *PLoS Genet*, 8(7), p. e1002757.
- Bharti, K., Miller, S.S. and Arnheiter, H. (2011) 'The new paradigm: retinal pigment epithelium cells generated from embryonic or induced pluripotent stem cells', *Pigment Cell Melanoma Res*, 24(1), pp. 21-34.
- Bharti, W.H.M.K.D.M. (2015) 'Primary Cilia Regulates the Polarization and Maturation of hiPSC-RPE through PKC-delta Activation', *ARVO. Investigative Ophthalmology & Visual Science*.
- Bhatia, S., Goyal, S., Singh, I.R., Singh, D. and Vanita, V. (2018) 'A novel mutation in the PRPF31 in a North Indian adRP family with incomplete penetrance', *Doc Ophthalmol*, 137(2), pp. 103-119.
- Bibb, C. and Young, R.W. (1974) 'Renewal of fatty acids in the membranes of visual cell outer segments', *J Cell Biol*, 61(2), pp. 327-43.
- Bok, D. (1993) 'The retinal pigment epithelium: a versatile partner in vision', *J Cell Sci Suppl*, 17, pp. 189-95.
- Bonilha, V.L. (2008) 'Age and disease-related structural changes in the retinal pigment epithelium', *Clin Ophthalmol*, 2(2), pp. 413-24.
- Bonilha, V.L. (2014) 'Retinal pigment epithelium (RPE) cytoskeleton in vivo and in vitro', *Exp Eye Res*, 126, pp. 38-45.
- Bonilha, V.L., Bhattacharya, S.K., West, K.A., Crabb, J.S., Sun, J., Rayborn, M.E., Nawrot, M., Saari, J.C. and Crabb, J.W. (2004) 'Support for a proposed retinoid-

processing protein complex in apical retinal pigment epithelium', *Exp Eye Res*, 79(3), pp. 419-22.

Boon, K.L., Grainger, R.J., Ehsani, P., Barrass, J.D., Auchynnikava, T., Inglehearn, C.F. and Beggs, J.D. (2007) 'prp8 mutations that cause human retinitis pigmentosa lead to a U5 snRNP maturation defect in yeast', *Nat Struct Mol Biol*, 14(11), pp. 1077-83.

Bourgeois, C.F., Lejeune, F. and Stevenin, J. (2004) 'Broad specificity of SR (serine/arginine) proteins in the regulation of alternative splicing of pre-messenger RNA', *Prog Nucleic Acid Res Mol Biol*, 78, pp. 37-88.

Bowne, S.J., Sullivan, L.S., Gire, A.I., Birch, D.G., Hughbanks-Wheaton, D., Heckenlively, J.R. and Daiger, S.P. (2008) 'Mutations in the TOPORS gene cause 1% of autosomal dominant retinitis pigmentosa', *Mol Vis*, 14, pp. 922-7.

Bracha, P., Moore, N.A. and Ciulla, T.A. (2017) 'Induced pluripotent stem cell-based therapy for age-related macular degeneration', *Expert Opin Biol Ther*, 17(9), pp. 1113-1126.

Brandl, C., Zimmermann, S.J., Milenkovic, V.M., Rosendahl, S.M., Grassmann, F., Milenkovic, A., Hehr, U., Federlin, M., Wetzel, C.H., Helbig, H. and Weber, B.H. (2014) 'In-depth characterisation of Retinal Pigment Epithelium (RPE) cells derived from human induced pluripotent stem cells (hiPSC)', *Neuromolecular Med*, 16(3), pp. 551-64.

Braun, D.A. and Hildebrandt, F. (2017) 'Ciliopathies', *Cold Spring Harb Perspect Biol*, 9(3).

Brito-Garcia, N., Del Pino-Sedeno, T., Trujillo-Martin, M.M., Coco, R.M., Rodriguez de la Rua, E., Del Cura-Gonzalez, I. and Serrano-Aguilar, P. (2017) 'Effectiveness and safety of nutritional supplements in the treatment of hereditary retinal dystrophies: a systematic review', *Eye (Lond)*, 31(2), pp. 273-285.

Buchholz, D.E., Hikita, S.T., Rowland, T.J., Friedrich, A.M., Hinman, C.R., Johnson, L.V. and Clegg, D.O. (2009) 'Derivation of functional retinal pigmented epithelium from induced pluripotent stem cells', *Stem Cells*, 27(10), pp. 2427-34.

Buchholz, D.E., Pennington, B.O., Croze, R.H., Hinman, C.R., Coffey, P.J. and Clegg, D.O. (2013) 'Rapid and efficient directed differentiation of human pluripotent stem cells into retinal pigmented epithelium', *Stem Cells Transl Med*, 2(5), pp. 384-93.

Buganim, Y., Faddah, D.A., Cheng, A.W., Itskovich, E., Markoulaki, S., Ganz, K., Klemm, S.L., van Oudenaarden, A. and Jaenisch, R. (2012) 'Single-cell expression analyses during cellular reprogramming reveal an early stochastic and a late hierarchic phase', *Cell*, 150(6), pp. 1209-22.

Bujakowska, K., Maubaret, C., Chakarova, C.F., Tanimoto, N., Beck, S.C., Fahl, E., Humphries, M.M., Kenna, P.F., Makarov, E., Makarova, O., Paquet-Durand, F., Ekstrom, P.A., van Veen, T., Leveillard, T., Humphries, P., Seeliger, M.W. and Bhattacharya, S.S. (2009) 'Study of gene-targeted mouse models of splicing factor gene Prpf31 implicated in human autosomal dominant retinitis pigmentosa (RP)', *Invest Ophthalmol Vis Sci*, 50(12), pp. 5927-33.

Bujakowska, K.M., Liu, Q. and Pierce, E.A. (2017) 'Photoreceptor Cilia and Retinal Ciliopathies', *Cold Spring Harb Perspect Biol*, 9(10).

Burns, M.S. and Hartz, M.J. (1992) 'The retinal pigment epithelium induces fenestration of endothelial cells in vivo', *Curr Eye Res*, 11(9), pp. 863-73.

Burrows, C.K., Banovich, N.E., Pavlovic, B.J., Patterson, K., Gallego Romero, I., Pritchard, J.K. and Gilad, Y. (2016) 'Genetic Variation, Not Cell Type of Origin, Underlies the Majority of Identifiable Regulatory Differences in iPSCs', *PLoS Genet*, 12(1), p. e1005793.

Burstyn-Cohen, T., Lew, E.D., Traves, P.G., Burrola, P.G., Hash, J.C. and Lemke, G. (2012) 'Genetic dissection of TAM receptor-ligand interaction in retinal pigment epithelial cell phagocytosis', *Neuron*, 76(6), pp. 1123-32.

Buskin, A., Zhu, L., Chichagova, V., Basu, B., Mozaffari-Jovin, S., Dolan, D., Droop, A., Collin, J., Bronstein, R., Mehrotra, S., Farkas, M., Hilgen, G., White, K., Pan, K.T., Treumann, A., Hallam, D., Bialas, K., Chung, G., Mellough, C., Ding, Y., Krasnogor, N., Przyborski, S., Zwolinski, S., Al-Aama, J., Alharthi, S., Xu, Y., Wheway, G., Szymanska, K., McKibbin, M., Inglehearn, C.F., Elliott, D.J., Lindsay, S., Ali, R.R., Steel, D.H., Armstrong, L., Sernagor, E., Urlaub, H., Pierce, E., Luhrmann, R., Grellscheid, S.N., Johnson, C.A. and Lako, M. (2018) 'Disrupted alternative splicing for genes implicated in splicing and ciliogenesis causes PRPF31 retinitis pigmentosa', *Nat Commun*, 9(1), p. 4234.

Buskamp, V., Duebel, J., Balya, D., Fradot, M., Viney, T.J., Siegert, S., Groner, A.C., Cabuy, E., Forster, V., Seeliger, M., Biel, M., Humphries, P., Paques, M., Mohand-Said, S., Trono, D., Deisseroth, K., Sahel, J.A., Picaud, S. and Roska, B. (2010) 'Genetic reactivation of cone photoreceptors restores visual responses in retinitis pigmentosa', *Science*, 329(5990), pp. 413-7.

Caceres, J.F., Stamm, S., Helfman, D.M. and Krainer, A.R. (1994) 'Regulation of alternative splicing in vivo by overexpression of antagonistic splicing factors', *Science*, 265(5179), pp. 1706-9.

Camacho, E.T. and Wirkus, S. (2013) 'Tracing the progression of retinitis pigmentosa via photoreceptor interactions', *J Theor Biol*, 317, pp. 105-18.

Campochiaro, P.A., Jerdon, J.A. and Glaser, B.M. (1986) 'The extracellular matrix of human retinal pigment epithelial cells in vivo and its synthesis in vitro', *Invest Ophthalmol Vis Sci*, 27(11), pp. 1615-21.

Campochiaro, P.A. and Mir, T.A. (2018) 'The mechanism of cone cell death in Retinitis Pigmentosa', *Prog Retin Eye Res*, 62, pp. 24-37.

Cao, H., Wu, J., Lam, S., Duan, R., Newnham, C., Molday, R.S., Graziotto, J.J., Pierce, E.A. and Hu, J. (2011) 'Temporal and tissue specific regulation of RP-associated splicing factor genes PRPF3, PRPF31 and PRPC8--implications in the pathogenesis of RP', *PLoS One*, 6(1), p. e15860.

Cao, W., Tombran-Tink, J., Chen, W., Mrazek, D., Elias, R. and McGinnis, J.F. (1999) 'Pigment epithelium-derived factor protects cultured retinal neurons against hydrogen peroxide-induced cell death', *J Neurosci Res*, 57(6), pp. 789-800.

Cao, W., Tombran-Tink, J., Elias, R., Sezate, S., Mrazek, D. and McGinnis, J.F. (2001) 'In vivo protection of photoreceptors from light damage by pigment epithelium-derived factor', *Invest Ophthalmol Vis Sci*, 42(7), pp. 1646-52.

Capowski, E.E., Simonett, J.M., Clark, E.M., Wright, L.S., Howden, S.E., Wallace, K.A., Petelinsek, A.M., Pinilla, I., Phillips, M.J., Meyer, J.S., Schneider, B.L., Thomson, J.A. and Gamm, D.M. (2014) 'Loss of MITF expression during human embryonic stem cell differentiation disrupts retinal pigment epithelium development and optic vesicle cell proliferation', *Hum Mol Genet*.

Carcamo-Orive, I., Hoffman, G.E., Cundiff, P., Beckmann, N.D., D'Souza, S.L., Knowles, J.W., Patel, A., Papatsenko, D., Abbasi, F., Reaven, G.M., Whalen, S., Lee, P., Shahbazi, M., Henrion, M.Y.R., Zhu, K., Wang, S., Roussos, P., Schadt, E.E., Pandey, G., Chang, R., Quertermous, T. and Lemischka, I. (2017) 'Analysis of Transcriptional Variability in a Large Human iPSC Library Reveals Genetic and Non-genetic Determinants of Heterogeneity', *Cell Stem Cell*, 20(4), pp. 518-532 e9.

Carter, M.S., Doskow, J., Morris, P., Li, S., Nhim, R.P., Sandstedt, S. and Wilkinson, M.F. (1995) 'A regulatory mechanism that detects premature nonsense codons in T-cell receptor transcripts in vivo is reversed by protein synthesis inhibitors in vitro', *J Biol Chem*, 270(48), pp. 28995-9003.

Chakradhar, S. (2016) 'An eye to the future: Researchers debate best path for stem cell-derived therapies', *Nat Med*, 22(2), pp. 116-9.

Chambers, S.M., Fasano, C.A., Papapetrou, E.P., Tomishima, M., Sadelain, M. and Studer, L. (2009) 'Highly efficient neural conversion of human ES and iPS cells by dual inhibition of SMAD signaling', *Nat Biotechnol*, 27(3), pp. 275-80.

Chan, E.M., Ratanasirintrao, S., Park, I.H., Manos, P.D., Loh, Y.H., Huo, H., Miller, J.D., Hartung, O., Rho, J., Ince, T.A., Daley, G.Q. and Schlaeger, T.M. (2009) 'Live cell imaging distinguishes bona fide human iPS cells from partially reprogrammed cells', *Nat Biotechnol*, 27(11), pp. 1033-7.

Chang, Y.F., Imam, J.S. and Wilkinson, M.F. (2007) 'The nonsense-mediated decay RNA surveillance pathway', *Annu Rev Biochem*, 76, pp. 51-74.

Cheng, D.L., Greenberg, P.B. and Borton, D.A. (2017) 'Advances in Retinal Prosthetic Research: A Systematic Review of Engineering and Clinical Characteristics of Current Prosthetic Initiatives', *Curr Eye Res*, 42(3), pp. 334-347.

Chichagova, V., Hallam, D., Collin, J., Buskin, A., Saretzki, G., Armstrong, L., Yu-Wai-Man, P., Lako, M. and Steel, D.H. (2017) 'Human iPSC disease modelling reveals functional and structural defects in retinal pigment epithelial cells harbouring the m.3243A > G mitochondrial DNA mutation', *Sci Rep*, 7(1), p. 12320.

Chizzolini, M., Galan, A., Milan, E., Sebastiani, A., Costagliola, C. and Parmeggiani, F. (2011) 'Good epidemiologic practice in retinitis pigmentosa: from phenotyping to biobanking', *Curr Genomics*, 12(4), pp. 260-6.

Cideciyan, A.V., Sudharsan, R., Dufour, V.L., Massengill, M.T., Iwabe, S., Swider, M., Lisi, B., Sumaroka, A., Marinho, L.F., Appelbaum, T., Rossmiller, B., Hauswirth, W.W., Jacobson, S.G., Lewin, A.S., Aguirre, G.D. and Beltran, W.A. (2018) 'Mutation-independent rhodopsin gene therapy by knockdown and replacement with a single AAV vector', *Proc Natl Acad Sci U S A*, 115(36), pp. E8547-E8556.

D'Cruz, P.M., Yasumura, D., Weir, J., Matthes, M.T., Abderrahim, H., LaVail, M.M. and Vollrath, D. (2000) 'Mutation of the receptor tyrosine kinase gene *Mertk* in the retinal dystrophic RCS rat', *Hum Mol Genet*, 9(4), pp. 645-51.

Daiger, S.P., Bowne, S.J. and Sullivan, L.S. (2007) 'Perspective on genes and mutations causing retinitis pigmentosa', *Arch Ophthalmol*, 125(2), pp. 151-8.

Daiger, S.P., Sullivan, L.S. and Bowne, S.J. (2013) 'Genes and mutations causing retinitis pigmentosa', *Clin Genet*, 84(2), pp. 132-41.

Daiger, S.P., Sullivan, L.S., Gire, A.I., Birch, D.G., Heckenlively, J.R. and Bowne, S.J. (2008) 'Mutations in known genes account for 58% of autosomal dominant retinitis pigmentosa (adRP)', *Adv Exp Med Biol*, 613, pp. 203-9.

Davis, R.L., Weintraub, H. and Lassar, A.B. (1987) 'Expression of a single transfected cDNA converts fibroblasts to myoblasts', *Cell*, 51(6), pp. 987-1000.

Deerinck, T.J., Shone, T.M., Bushong, E.A., Ramachandra, R., Peltier, S.T. and Ellisman, M.H. (2018) 'High-performance serial block-face SEM of nonconductive biological samples enabled by focal gas injection-based charge compensation', *J Microsc*, 270(2), pp. 142-149.

Deery, E.C., Vithana, E.N., Newbold, R.J., Gallon, V.A., Bhattacharya, S.S., Warren, M.J., Hunt, D.M. and Wilkie, S.E. (2002) 'Disease mechanism for retinitis pigmentosa (RP11) caused by mutations in the splicing factor gene *PRPF31*', *Hum Mol Genet*, 11(25), pp. 3209-19.

Deng, W.L., Gao, M.L., Lei, X.L., Lv, J.N., Zhao, H., He, K.W., Xia, X.X., Li, L.Y., Chen, Y.C., Li, Y.P., Pan, D., Xue, T. and Jin, Z.B. (2018) 'Gene Correction Reverses Ciliopathy and Photoreceptor Loss in iPSC-Derived Retinal Organoids from Retinitis Pigmentosa Patients', *Stem Cell Reports*, 10(6), p. 2005.

- Dimanlig, P.V., Faber, S.C., Auerbach, W., Makarenkova, H.P. and Lang, R.A. (2001) 'The upstream ectoderm enhancer in Pax6 has an important role in lens induction', *Development*, 128(22), pp. 4415-24.
- Dobin, A., Davis, C.A., Schlesinger, F., Drenkow, J., Zaleski, C., Jha, S., Batut, P., Chaisson, M. and Gingeras, T.R. (2013) 'STAR: ultrafast universal RNA-seq aligner', *Bioinformatics*, 29(1), pp. 15-21.
- Dong, B., Chen, J., Zhang, X., Pan, Z., Bai, F. and Li, Y. (2013) 'Two novel PRP31 premessenger ribonucleic acid processing factor 31 homolog mutations including a complex insertion-deletion identified in Chinese families with retinitis pigmentosa', *Mol Vis*, 19, pp. 2426-35.
- Draper, J.S., Pigott, C., Thomson, J.A. and Andrews, P.W. (2002) 'Surface antigens of human embryonic stem cells: changes upon differentiation in culture', *J Anat*, 200(Pt 3), pp. 249-58.
- Dryja, T.P., McGee, T.L., Hahn, L.B., Cowley, G.S., Olsson, J.E., Reichel, E., Sandberg, M.A. and Berson, E.L. (1990) 'Mutations within the rhodopsin gene in patients with autosomal dominant retinitis pigmentosa', *N Engl J Med*, 323(19), pp. 1302-7.
- Duncan, J.L., LaVail, M.M., Yasumura, D., Matthes, M.T., Yang, H., Trautmann, N., Chappelow, A.V., Feng, W., Earp, H.S., Matsushima, G.K. and Vollrath, D. (2003) 'An RCS-like retinal dystrophy phenotype in mer knockout mice', *Invest Ophthalmol Vis Sci*, 44(2), pp. 826-38.
- Elliott, A.M., Elliott, K.A. and Kammesheidt, A. (2010) 'High resolution array-CGH characterization of human stem cells using a stem cell focused microarray', *Mol Biotechnol*, 46(3), pp. 234-42.
- Evans, M.J. and Kaufman, M.H. (1981) 'Establishment in culture of pluripotential cells from mouse embryos', *Nature*, 292(5819), pp. 154-6.
- Fahim, A.T., Daiger, S.P. and Weleber, R.G. (1993) 'Retinitis Pigmentosa Overview', in Pagon, R.A., Adam, M.P., Bird, T.D., Dolan, C.R., Fong, C.T., Smith, R.J.H. and Stephens, K. (eds.) *GeneReviews(R)*. Seattle (WA).
- Fahim, A.T., Daiger, S.P. and Weleber, R.G. (2017) 'Nonsyndromic Retinitis Pigmentosa Overview', in Adam, M.P., Ardinger, H.H., Pagon, R.A., Wallace, S.E., Bean, L.J.H., Stephens, K. and Amemiya, A. (eds.) *GeneReviews((R))*. Seattle (WA).
- Farkas, M.H., Lew, D.S., Sousa, M.E., Bujakowska, K., Chatagnon, J., Bhattacharya, S.S., Pierce, E.A. and Nandrot, E.F. (2014) 'Mutations in pre-mRNA processing factors 3, 8, and 31 cause dysfunction of the retinal pigment epithelium', *Am J Pathol*, 184(10), pp. 2641-52.
- Farnoodian, M., Kinter, J.B., Yadranji Aghdam, S., Zaitoun, I., Sorenson, C.M. and Sheibani, N. (2015) 'Expression of pigment epithelium-derived factor and thrombospondin-1 regulate proliferation and migration of retinal pigment epithelial cells', *Physiol Rep*, 3(1).
- Farrar, G.J., Kenna, P.F. and Humphries, P. (2002) 'On the genetics of retinitis pigmentosa and on mutation-independent approaches to therapeutic intervention', *EMBO J*, 21(5), pp. 857-64.
- Ferrari, S., Di Iorio, E., Barbaro, V., Ponzin, D., Sorrentino, F.S. and Parmeggiani, F. (2011) 'Retinitis pigmentosa: genes and disease mechanisms', *Curr Genomics*, 12(4), pp. 238-49.
- Finnemann, S.C., Bonilha, V.L., Marmorstein, A.D. and Rodriguez-Boulan, E. (1997) 'Phagocytosis of rod outer segments by retinal pigment epithelial cells requires alpha(v)beta5 integrin for binding but not for internalization', *Proc Natl Acad Sci U S A*, 94(24), pp. 12932-7.
- Finnemann, S.C. and Nandrot, E.F. (2006) 'MerTK activation during RPE phagocytosis in vivo requires alphaVbeta5 integrin', *Adv Exp Med Biol*, 572, pp. 499-503.

Fisher, S.K. and Steinberg, R.H. (1982) 'Origin and organization of pigment epithelial apical projections to cones in cat retina', *J Comp Neurol*, 206(2), pp. 131-45.

Frasson, M., Sahel, J.A., Fabre, M., Simonutti, M., Dreyfus, H. and Picaud, S. (1999) 'Retinitis pigmentosa: rod photoreceptor rescue by a calcium-channel blocker in the rd mouse', *Nat Med*, 5(10), pp. 1183-7.

Fuhrmann, S. (2008) 'Wnt signaling in eye organogenesis', *Organogenesis*, 4(2), pp. 60-7.

Fuhrmann, S., Zou, C. and Levine, E.M. (2014) 'Retinal pigment epithelium development, plasticity, and tissue homeostasis', *Exp Eye Res*, 123, pp. 141-50.

Fujimura, N., Taketo, M.M., Mori, M., Korinek, V. and Kozmik, Z. (2009) 'Spatial and temporal regulation of Wnt/beta-catenin signaling is essential for development of the retinal pigment epithelium', *Dev Biol*, 334(1), pp. 31-45.

Fusaki, N., Ban, H., Nishiyama, A., Saeki, K. and Hasegawa, M. (2009) 'Efficient induction of transgene-free human pluripotent stem cells using a vector based on Sendai virus, an RNA virus that does not integrate into the host genome', *Proc Jpn Acad Ser B Phys Biol Sci*, 85(8), pp. 348-62.

Gandra, M., Anandula, V., Authiappan, V., Sundaramurthy, S., Raman, R., Bhattacharya, S. and Govindasamy, K. (2008) 'Retinitis pigmentosa: mutation analysis of RHO, PRPF31, RP1, and IMPDH1 genes in patients from India', *Mol Vis*, 14, pp. 1105-13.

Garber, K. (2015) 'RIKEN suspends first clinical trial involving induced pluripotent stem cells', *Nat Biotechnol*, 33(9), pp. 890-1.

Gasparini, S.J., Llonch, S., Borsch, O. and Ader, M. (2019) 'Transplantation of photoreceptors into the degenerative retina: Current state and future perspectives', *Prog Retin Eye Res*, 69, pp. 1-37.

Ghazawy, S., Springell, K., Gauba, V., McKibbin, M.A. and Inglehearn, C.F. (2007) 'Dominant retinitis pigmentosa phenotype associated with a new mutation in the splicing factor PRPF31', *Br J Ophthalmol*, 91(10), pp. 1411-3.

Ghazi, N.G., Abboud, E.B., Nowilaty, S.R., Alkuraya, H., Alhommedi, A., Cai, H., Hou, R., Deng, W.T., Boye, S.L., Almaghami, A., Al Saikhan, F., Al-Dhibi, H., Birch, D., Chung, C., Colak, D., LaVail, M.M., Vollrath, D., Erger, K., Wang, W., Conlon, T., Zhang, K., Hauswirth, W. and Alkuraya, F.S. (2016) 'Treatment of retinitis pigmentosa due to MERTK mutations by ocular subretinal injection of adeno-associated virus gene vector: results of a phase I trial', *Hum Genet*, 135(3), pp. 327-43.

Girotti, A.W. and Kriska, T. (2004) 'Role of lipid hydroperoxides in photo-oxidative stress signaling', *Antioxid Redox Signal*, 6(2), pp. 301-10.

Golipour, A., David, L., Liu, Y., Jayakumaran, G., Hirsch, C.L., Trcka, D. and Wrana, J.L. (2012) 'A late transition in somatic cell reprogramming requires regulators distinct from the pluripotency network', *Cell Stem Cell*, 11(6), pp. 769-82.

Gonzalez-Santos, J.M., Cao, H., Duan, R.C. and Hu, J. (2008) 'Mutation in the splicing factor Hprp3p linked to retinitis pigmentosa impairs interactions within the U4/U6 snRNP complex', *Hum Mol Genet*, 17(2), pp. 225-39.

Gore, A., Li, Z., Fung, H.L., Young, J.E., Agarwal, S., Antosiewicz-Bourget, J., Canto, I., Giorgetti, A., Israel, M.A., Kiskinis, E., Lee, J.H., Loh, Y.H., Manos, P.D., Montserrat, N., Panopoulos, A.D., Ruiz, S., Wilbert, M.L., Yu, J., Kirkness, E.F., Izpisua Belmonte, J.C., Rossi, D.J., Thomson, J.A., Eggan, K., Daley, G.Q., Goldstein, L.S. and Zhang, K. (2011) 'Somatic coding mutations in human induced pluripotent stem cells', *Nature*, 471(7336), pp. 63-7.

Gorges, M., Markewitz, B.A. and Westenskow, D.R. (2009) 'Improving alarm performance in the medical intensive care unit using delays and clinical context', *Anesth Analg*, 108(5), pp. 1546-52.

Gouras, P., Du, J., Gelanze, M., Lopez, R., Kwun, R., Kjeldbye, H. and Krebs, W. (1991) 'Survival and synapse formation of transplanted rat rods', *J Neural Transplant Plast*, 2(2), pp. 91-100.

Graziotto, J.J., Farkas, M.H., Bujakowska, K., Deramandt, B.M., Zhang, Q., Nandrot, E.F., Inglehearn, C.F., Bhattacharya, S.S. and Pierce, E.A. (2011) 'Three gene-targeted mouse models of RNA splicing factor RP show late-onset RPE and retinal degeneration', *Invest Ophthalmol Vis Sci*, 52(1), pp. 190-8.

Grover, S., Fishman, G.A., Anderson, R.J. and Lindeman, M. (2000) 'A longitudinal study of visual function in carriers of X-linked recessive retinitis pigmentosa', *Ophthalmology*, 107(2), pp. 386-96.

Grunwald, J.E., Maguire, A.M. and Dupont, J. (1996) 'Retinal hemodynamics in retinitis pigmentosa', *Am J Ophthalmol*, 122(4), pp. 502-8.

Gu, X., Neric, N.J., Crabb, J.S., Crabb, J.W., Bhattacharya, S.K., Rayborn, M.E., Hollyfield, J.G. and Bonilha, V.L. (2012) 'Age-related changes in the retinal pigment epithelium (RPE)', *PLoS One*, 7(6), p. e38673.

Gurdon, J.B. (1962) 'The developmental capacity of nuclei taken from intestinal epithelium cells of feeding tadpoles', *J Embryol Exp Morphol*, 10, pp. 622-40.

Hacein-Bey-Abina, S., de Saint Basile, G. and Cavazzana-Calvo, M. (2003) 'Gene therapy of X-linked severe combined immunodeficiency', *Methods Mol Biol*, 215, pp. 247-59.

Haer-Wigman, L., van Zelst-Stams, W.A., Pfundt, R., van den Born, L.I., Klaver, C.C., Verheij, J.B., Hoyng, C.B., Breuning, M.H., Boon, C.J., Kievit, A.J., Verhoeven, V.J., Pott, J.W., Salleveld, S.C., van Hagen, J.M., Plomp, A.S., Kroes, H.Y., Lelieveld, S.H., Hehir-Kwa, J.Y., Castelein, S., Nelen, M., Scheffer, H., Lugtenberg, D., Cremers, F.P., Hoefsloot, L. and Yntema, H.G. (2017) 'Diagnostic exome sequencing in 266 Dutch patients with visual impairment', *Eur J Hum Genet*, 25(5), pp. 591-599.

Haim, M. (2002) 'Epidemiology of retinitis pigmentosa in Denmark', *Acta Ophthalmol Scand Suppl*, (233), pp. 1-34.

Halevy, T. and Urbach, A. (2014) 'Comparing ESC and iPSC-Based Models for Human Genetic Disorders', *J Clin Med*, 3(4), pp. 1146-62.

Hallam, D., Collin, J., Bojic, S., Chichagova, V., Buskin, A., Xu, Y., Lafage, L., Otten, E.G., Anyfantis, G., Mellough, C., Przyborski, S., Alharthi, S., Korolchuk, V., Lotery, A., Saretzki, G., McKibbin, M., Armstrong, L., Steel, D., Kavanagh, D. and Lako, M. (2017) 'An Induced Pluripotent Stem Cell Patient Specific Model of Complement Factor H (Y402H) Polymorphism Displays Characteristic Features of Age-Related Macular Degeneration and Indicates a Beneficial Role for UV Light Exposure', *Stem Cells*, 35(11), pp. 2305-2320.

Hallam, D., Hilgen, G., Dorgau, B., Zhu, L., Yu, M., Bojic, S., Hewitt, P., Schmitt, M., Uteng, M., Kustermann, S., Steel, D., Nicholds, M., Thomas, R., Treumann, A., Porter, A., Sernagor, E., Armstrong, L. and Lako, M. (2018) 'Human-Induced Pluripotent Stem Cells Generate Light Responsive Retinal Organoids with Variable and Nutrient-Dependent Efficiency', *Stem Cells*, 36(10), pp. 1535-1551.

Hamel, C. (2006) 'Retinitis pigmentosa', *Orphanet J Rare Dis*, 1, p. 40.

Hansson, J., Rafiee, M.R., Reiland, S., Polo, J.M., Gehring, J., Okawa, S., Huber, W., Hochedlinger, K. and Krijgsveld, J. (2012) 'Highly coordinated proteome dynamics during reprogramming of somatic cells to pluripotency', *Cell Rep*, 2(6), pp. 1579-92.

Hargrave, P.A. (2001) 'Rhodopsin structure, function, and topography the Friedenwald lecture', *Invest Ophthalmol Vis Sci*, 42(1), pp. 3-9.

Hartong, D.T., Berson, E.L. and Dryja, T.P. (2006) 'Retinitis pigmentosa', *Lancet*, 368(9549), pp. 1795-809.

Hartzell, H.C., Qu, Z., Yu, K., Xiao, Q. and Chien, L.T. (2008) 'Molecular physiology of bestrophins: multifunctional membrane proteins linked to best disease and other retinopathies', *Physiol Rev*, 88(2), pp. 639-72.

Hata, M., Ikeda, H.O., Iwai, S., Iida, Y., Gotoh, N., Asaka, I., Ikeda, K., Isobe, Y., Hori, A., Nakagawa, S., Yamato, S., Arita, M., Yoshimura, N. and Tsujikawa, A. (2018) 'Reduction of lipid accumulation rescues Bietti's crystalline dystrophy phenotypes', *Proc Natl Acad Sci U S A*, 115(15), pp. 3936-3941.

Hauswirth, W.W., Aleman, T.S., Kaushal, S., Cideciyan, A.V., Schwartz, S.B., Wang, L., Conlon, T.J., Boye, S.L., Flotte, T.R., Byrne, B.J. and Jacobson, S.G. (2008) 'Treatment of leber congenital amaurosis due to RPE65 mutations by ocular subretinal injection of adeno-associated virus gene vector: short-term results of a phase I trial', *Hum Gene Ther*, 19(10), pp. 979-90.

Heckenlively, J., Friederich, R., Farson, C. and Pabalis, G. (1981) 'Retinitis pigmentosa in the Navajo', *Metab Pediatr Ophthalmol*, 5(3-4), pp. 201-6.

Henderson, J.K., Draper, J.S., Baillie, H.S., Fishel, S., Thomson, J.A., Moore, H. and Andrews, P.W. (2002) 'Preimplantation human embryos and embryonic stem cells show comparable expression of stage-specific embryonic antigens', *Stem Cells*, 20(4), pp. 329-37.

Hentze, M.W. and Kulozik, A.E. (1999) 'A perfect message: RNA surveillance and nonsense-mediated decay', *Cell*, 96(3), pp. 307-10.

Herse, P. (2005) 'Retinitis pigmentosa: visual function and multidisciplinary management', *Clin Exp Optom*, 88(5), pp. 335-50.

Hey, C.A.B., Saltokowa, K.B., Larsen, L.J., Tumer, Z., Brondum-Nielsen, K., Gronskov, K., Hjortshoj, T.D. and Moller, L.B. (2018) 'Generation of induced pluripotent stem cells, KCi001-A derived from a Bardet-Biedl syndrome patient compound heterozygous for the BBS1 variants c.1169T>G/c.1135G>C', *Stem Cell Res*, 31, pp. 235-239.

Hirami, Y., Osakada, F., Takahashi, K., Okita, K., Yamanaka, S., Ikeda, H., Yoshimura, N. and Takahashi, M. (2009) 'Generation of retinal cells from mouse and human induced pluripotent stem cells', *Neurosci Lett*, 458(3), pp. 126-31.

Hodson, S., Armstrong, I. and Wigham, C. (1994) 'Regulation of the retinal interphotoreceptor matrix Na by the retinal pigment epithelium during the light response', *Experientia*, 50(5), pp. 438-41.

Huang, Q., Wang, S., Sorenson, C.M. and Sheibani, N. (2008) 'PEDF-deficient mice exhibit an enhanced rate of retinal vascular expansion and are more sensitive to hyperoxia-mediated vessel obliteration', *Exp Eye Res*, 87(3), pp. 226-41.

Huranová, M., Hnilicová, J., Fleischer, B., Cvacková, Z. and Stanek, D. (2009) 'A mutation linked to retinitis pigmentosa in HPRP31 causes protein instability and impairs its interactions with spliceosomal snRNPs', *Hum Mol Genet*, 18(11), pp. 2014-23.

Hussein, S.M., Batada, N.N., Vuoristo, S., Ching, R.W., Autio, R., Narva, E., Ng, S., Sourour, M., Hamalainen, R., Olsson, C., Lundin, K., Mikkola, M., Trokovic, R., Peitz, M., Brustle, O., Bazett-Jones, D.P., Alitalo, K., Lahesmaa, R., Nagy, A. and Otonkoski, T. (2011) 'Copy number variation and selection during reprogramming to pluripotency', *Nature*, 471(7336), pp. 58-62.

Hussein, S.M., Puri, M.C., Tonge, P.D., Benevento, M., Corso, A.J., Clancy, J.L., Mosbergen, R., Li, M., Lee, D.S., Cloonan, N., Wood, D.L., Munoz, J., Middleton, R., Korn, O., Patel, H.R., White, C.A., Shin, J.Y., Gauthier, M.E., Le Cao, K.A., Kim, J.I., Mar, J.C., Shakiba, N., Ritchie, W., Rasko, J.E., Grimmond, S.M., Zandstra, P.W., Wells, C.A., Preiss, T., Seo, J.S., Heck, A.J., Rogers, I.M. and Nagy, A. (2014) 'Genome-wide characterization of the routes to pluripotency', *Nature*, 516(7530), pp. 198-206.

Hwang, Y.H. and Kim, Y.Y. (2012) 'Macular thickness and volume of myopic eyes measured using spectral-domain optical coherence tomography', *Clin Exp Optom*, 95(5), pp. 492-8.

Idelson, M., Alper, R., Obolensky, A., Ben-Shushan, E., Hemo, I., Yachimovich-Cohen, N., Khaner, H., Smith, Y., Wisner, O., Gropp, M., Cohen, M.A., Even-Ram, S., Berman-Zaken, Y., Matzrafi, L., Rechavi, G., Banin, E. and Reubinoff, B. (2009) 'Directed differentiation of human embryonic stem cells into functional retinal pigment epithelium cells', *Cell Stem Cell*, 5(4), pp. 396-408.

Ikeda, H., Osakada, F., Watanabe, K., Mizuseki, K., Haraguchi, T., Miyoshi, H., Kamiya, D., Honda, Y., Sasai, N., Yoshimura, N., Takahashi, M. and Sasai, Y. (2005) 'Generation of Rx+/Pax6+ neural retinal precursors from embryonic stem cells', *Proc Natl Acad Sci U S A*, 102(32), pp. 11331-6.

International Stem Cell, I., Adewumi, O., Aflatoonian, B., Ahrlund-Richter, L., Amit, M., Andrews, P.W., Beighton, G., Bello, P.A., Benvenisty, N., Berry, L.S., Bevan, S., Blum, B., Brooking, J., Chen, K.G., Choo, A.B., Churchill, G.A., Corbel, M., Damjanov, I., Draper, J.S., Dvorak, P., Emanuelsson, K., Fleck, R.A., Ford, A., Gertow, K., Gertsenstein, M., Gokhale, P.J., Hamilton, R.S., Hampl, A., Healy, L.E., Hovatta, O., Hyllner, J., Imreh, M.P., Itskovitz-Eldor, J., Jackson, J., Johnson, J.L., Jones, M., Kee, K., King, B.L., Knowles, B.B., Lako, M., Lebrin, F., Mallon, B.S., Manning, D., Mayshar, Y., McKay, R.D., Michalska, A.E., Mikkola, M., Mileikovsky, M., Minger, S.L., Moore, H.D., Mummery, C.L., Nagy, A., Nakatsuji, N., O'Brien, C.M., Oh, S.K., Olsson, C., Otonkoski, T., Park, K.Y., Passier, R., Patel, H., Patel, M., Pedersen, R., Pera, M.F., Piekarczyk, M.S., Pera, R.A., Reubinoff, B.E., Robins, A.J., Rossant, J., Rugg-Gunn, P., Schulz, T.C., Semb, H., Sherrer, E.S., Siemen, H., Stacey, G.N., Stojkovic, M., Suemori, H., Szatkiewicz, J., Turetsky, T., Tuuri, T., van den Brink, S., Vintersten, K., Vuoristo, S., Ward, D., Weaver, T.A., Young, L.A. and Zhang, W. (2007) 'Characterization of human embryonic stem cell lines by the International Stem Cell Initiative', *Nat Biotechnol*, 25(7), pp. 803-16.

International Stem Cell, I., Amps, K., Andrews, P.W., Anyfantis, G., Armstrong, L., Avery, S., Baharvand, H., Baker, J., Baker, D., Munoz, M.B., Beil, S., Benvenisty, N., Ben-Yosef, D., Biancotti, J.C., Bosman, A., Brena, R.M., Brison, D., Caisander, G., Camarasa, M.V., Chen, J., Chiao, E., Choi, Y.M., Choo, A.B., Collins, D., Colman, A., Crook, J.M., Daley, G.Q., Dalton, A., De Sousa, P.A., Denning, C., Downie, J., Dvorak, P., Montgomery, K.D., Feki, A., Ford, A., Fox, V., Fraga, A.M., Frumkin, T., Ge, L., Gokhale, P.J., Golan-Lev, T., Gourabi, H., Gropp, M., Lu, G., Hampl, A., Harron, K., Healy, L., Herath, W., Holm, F., Hovatta, O., Hyllner, J., Inamdar, M.S., Irwanto, A.K., Ishii, T., Jaconi, M., Jin, Y., Kimber, S., Kiselev, S., Knowles, B.B., Kopper, O., Kukhareenko, V., Kuliev, A., Lagarkova, M.A., Laird, P.W., Lako, M., Laslett, A.L., Lavon, N., Lee, D.R., Lee, J.E., Li, C., Lim, L.S., Ludwig, T.E., Ma, Y., Maltby, E., Mateizel, I., Mayshar, Y., Mileikovsky, M., Minger, S.L., Miyazaki, T., Moon, S.Y., Moore, H., Mummery, C., Nagy, A., Nakatsuji, N., Narwani, K., Oh, S.K., Oh, S.K., Olson, C., Otonkoski, T., Pan, F., Park, I.H., Pells, S., Pera, M.F., Pereira, L.V., Qi, O., Raj, G.S., Reubinoff, B., Robins, A., Robson, P., Rossant, J., et al. (2011) 'Screening ethnically diverse human embryonic stem cells identifies a chromosome 20 minimal amplicon conferring growth advantage', *Nat Biotechnol*, 29(12), pp. 1132-44.

Ivings, L., Towns, K.V., Matin, M.A., Taylor, C., Ponchel, F., Grainger, R.J., Ramesar, R.S., Mackey, D.A. and Inglehearn, C.F. (2008) 'Evaluation of splicing efficiency in lymphoblastoid cell lines from patients with splicing-factor retinitis pigmentosa', *Mol Vis*, 14, pp. 2357-66.

Jaissle, G.B., May, C.A., van de Pavert, S.A., Wenzel, A., Claes-May, E., Giessl, A., Szurman, P., Wolfrum, U., Wijnholds, J., Fischer, M.D., Humphries, P. and Seeliger,

M.W. (2010) 'Bone spicule pigment formation in retinitis pigmentosa: insights from a mouse model', *Graefes Arch Clin Exp Ophthalmol*, 248(8), pp. 1063-70.

Jin, Z.B., Okamoto, S., Xiang, P. and Takahashi, M. (2012) 'Integration-free induced pluripotent stem cells derived from retinitis pigmentosa patient for disease modeling', *Stem Cells Transl Med*, 1(6), pp. 503-9.

Kajiwara, K., Berson, E.L. and Dryja, T.P. (1994) 'Digenic retinitis pigmentosa due to mutations at the unlinked peripherin/RDS and ROM1 loci', *Science*, 264(5165), pp. 1604-8.

Kalsotra, A., Xiao, X., Ward, A.J., Castle, J.C., Johnson, J.M., Burge, C.B. and Cooper, T.A. (2008) 'A postnatal switch of CELF and MBNL proteins reprograms alternative splicing in the developing heart', *Proc Natl Acad Sci U S A*, 105(51), pp. 20333-8.

Kamao, H., Mandai, M., Okamoto, S., Sakai, N., Suga, A., Sugita, S., Kiryu, J. and Takahashi, M. (2014) 'Characterization of human induced pluripotent stem cell-derived retinal pigment epithelium cell sheets aiming for clinical application', *Stem Cell Reports*, 2(2), pp. 205-18.

Kang, X., Yu, Q., Huang, Y., Song, B., Chen, Y., Gao, X., He, W., Sun, X. and Fan, Y. (2015) 'Effects of Integrating and Non-Integrating Reprogramming Methods on Copy Number Variation and Genomic Stability of Human Induced Pluripotent Stem Cells', *PLoS One*, 10(7), p. e0131128.

Kaplan, J.H. (2002) 'Biochemistry of Na,K-ATPase', *Annu Rev Biochem*, 71, pp. 511-35.

Karakousis, P.C., John, S.K., Behling, K.C., Surace, E.M., Smith, J.E., Hendrickson, A., Tang, W.X., Bennett, J. and Milam, A.H. (2001) 'Localization of pigment epithelium derived factor (PEDF) in developing and adult human ocular tissues', *Mol Vis*, 7, pp. 154-63.

Kato, A., Kiyotani, K., Sakai, Y., Yoshida, T. and Nagai, Y. (1997) 'The paramyxovirus, Sendai virus, V protein encodes a luxury function required for viral pathogenesis', *EMBO J*, 16(3), pp. 578-87.

Khalil, A.M., Guttman, M., Huarte, M., Garber, M., Raj, A., Rivea Morales, D., Thomas, K., Presser, A., Bernstein, B.E., van Oudenaarden, A., Regev, A., Lander, E.S. and Rinn, J.L. (2009) 'Many human large intergenic noncoding RNAs associate with chromatin-modifying complexes and affect gene expression', *Proc Natl Acad Sci U S A*, 106(28), pp. 11667-72.

Khan, N.A., Willemarck, N., Talebi, A., Marchand, A., Binda, M.M., Dehairs, J., Rueda-Rincon, N., Daniels, V.W., Bagadi, M., Thimiri Govinda Raj, D.B., Vanderhoydonc, F., Munck, S., Chaltin, P. and Swinnen, J.V. (2016) 'Identification of drugs that restore primary cilium expression in cancer cells', *Oncotarget*, 7(9), pp. 9975-92.

Kigasawa, K., Ishikawa, H., Obazawa, H., Minamoto, T., Nagai, Y. and Tanaka, Y. (1998) 'Collagen production by cultured human retinal pigment epithelial cells', *Tokai J Exp Clin Med*, 23(3), pp. 147-51.

Kilpinen, H., Goncalves, A., Leha, A., Afzal, V., Alasoo, K., Ashford, S., Bala, S., Bensaddek, D., Casale, F.P., Culley, O.J., Danecek, P., Faulconbridge, A., Harrison, P.W., Kathuria, A., McCarthy, D., McCarthy, S.A., Meleckyte, R., Memari, Y., Moens, N., Soares, F., Mann, A., Streeter, I., Agu, C.A., Alderton, A., Nelson, R., Harper, S., Patel, M., White, A., Patel, S.R., Clarke, L., Halai, R., Kirton, C.M., Kolb-Kokocinski, A., Beales, P., Birney, E., Danovi, D., Lamond, A.I., Ouwehand, W.H., Vallier, L., Watt, F.M., Durbin, R., Stegle, O. and Gaffney, D.J. (2017) 'Common genetic variation drives molecular heterogeneity in human iPSCs', *Nature*, 546(7658), pp. 370-375.

Kim, D., Kim, C.H., Moon, J.I., Chung, Y.G., Chang, M.Y., Han, B.S., Ko, S., Yang, E., Cha, K.Y., Lanza, R. and Kim, K.S. (2009) 'Generation of human induced pluripotent stem cells by direct delivery of reprogramming proteins', *Cell Stem Cell*, 4(6), pp. 472-6.

Kim, J., Lengner, C.J., Kirak, O., Hanna, J., Cassady, J.P., Lodato, M.A., Wu, S., Faddah, D.A., Steine, E.J., Gao, Q., Fu, D., Dawlaty, M. and Jaenisch, R. (2011) 'Reprogramming of postnatal neurons into induced pluripotent stem cells by defined factors', *Stem Cells*, 29(6), pp. 992-1000.

Kim, M.S., Pinto, S.M., Getnet, D., Nirujogi, R.S., Manda, S.S., Chaerkady, R., Madugundu, A.K., Kelkar, D.S., Isserlin, R., Jain, S., Thomas, J.K., Muthusamy, B., Leal-Rojas, P., Kumar, P., Sahasrabudde, N.A., Balakrishnan, L., Advani, J., George, B., Renuse, S., Selvan, L.D., Patil, A.H., Nanjappa, V., Radhakrishnan, A., Prasad, S., Subbannayya, T., Raju, R., Kumar, M., Sreenivasamurthy, S.K., Marimuthu, A., Sathe, G.J., Chavan, S., Datta, K.K., Subbannayya, Y., Sahu, A., Yelamanchi, S.D., Jayaram, S., Rajagopalan, P., Sharma, J., Murthy, K.R., Syed, N., Goel, R., Khan, A.A., Ahmad, S., Dey, G., Mudgal, K., Chatterjee, A., Huang, T.C., Zhong, J., Wu, X., Shaw, P.G., Freed, D., Zahari, M.S., Mukherjee, K.K., Shankar, S., Mahadevan, A., Lam, H., Mitchell, C.J., Shankar, S.K., Satishchandra, P., Schroeder, J.T., Sirdeshmukh, R., Maitra, A., Leach, S.D., Drake, C.G., Halushka, M.K., Prasad, T.S., Hruban, R.H., Kerr, C.L., Bader, G.D., Iacobuzio-Donahue, C.A., Gowda, H. and Pandey, A. (2014) 'A draft map of the human proteome', *Nature*, 509(7502), pp. 575-81.

Kleinsmith, L.J. and Pierce, G.B., Jr. (1964) 'Multipotentiality of Single Embryonal Carcinoma Cells', *Cancer Res*, 24, pp. 1544-51.

Klimanskaya, I., Hipp, J., Rezai, K.A., West, M., Atala, A. and Lanza, R. (2004) 'Derivation and comparative assessment of retinal pigment epithelium from human embryonic stem cells using transcriptomics', *Cloning Stem Cells*, 6(3), pp. 217-45.

Kolomeyer, A.M. and Zarbin, M.A. (2014) 'Trophic factors in the pathogenesis and therapy for retinal degenerative diseases', *Surv Ophthalmol*, 59(2), pp. 134-65.

Kozulin, P., Natoli, R., Bumsted O'Brien, K.M., Madigan, M.C. and Provis, J.M. (2010) 'The cellular expression of antiangiogenic factors in fetal primate macula', *Invest Ophthalmol Vis Sci*, 51(8), pp. 4298-306.

Krohne, T.U., Westenskow, P.D., Kurihara, T., Friedlander, D.F., Lehmann, M., Dorsey, A.L., Li, W., Zhu, S., Schultz, A., Wang, J., Siuzdak, G., Ding, S. and Friedlander, M. (2012) 'Generation of retinal pigment epithelial cells from small molecules and OCT4 reprogrammed human induced pluripotent stem cells', *Stem Cells Transl Med*, 1(2), pp. 96-109.

Kruithof, B.P., Van Den Hoff, M.J., Tesink-Taekema, S. and Moorman, A.F. (2003) 'Recruitment of intra- and extracardiac cells into the myocardial lineage during mouse development', *Anat Rec A Discov Mol Cell Evol Biol*, 271(2), pp. 303-14.

Kurtovic-Kozaric, A., Przychodzen, B., Singh, J., Konarska, M.M., Clemente, M.J., Otroock, Z.K., Nakashima, M., Hsi, E.D., Yoshida, K., Shiraishi, Y., Chiba, K., Tanaka, H., Miyano, S., Ogawa, S., Boultonwood, J., Makishima, H., Maciejewski, J.P. and Padgett, R.A. (2015) 'PRPF8 defects cause missplicing in myeloid malignancies', *Leukemia*, 29(1), pp. 126-36.

Kwan, K.M., Otsuna, H., Kidokoro, H., Carney, K.R., Saijoh, Y. and Chien, C.B. (2012) 'A complex choreography of cell movements shapes the vertebrate eye', *Development*, 139(2), pp. 359-72.

Kwon, G.S., Fraser, S.T., Eakin, G.S., Mangano, M., Isern, J., Sahr, K.E., Hadjantonakis, A.K. and Baron, M.H. (2006) 'Tg(Afp-GFP) expression marks primitive and definitive endoderm lineages during mouse development', *Dev Dyn*, 235(9), pp. 2549-58.

Kyttala, A., Moraghebi, R., Valensisi, C., Kettunen, J., Andrus, C., Pasumarthy, K.K., Nakanishi, M., Nishimura, K., Ohtaka, M., Weltner, J., Van Handel, B., Parkkonen, O., Sinisalo, J., Jalanko, A., Hawkins, R.D., Woods, N.B., Otonkoski, T. and Trokovic, R. (2016) 'Genetic Variability Overrides the Impact of Parental Cell Type and Determines iPSC Differentiation Potential', *Stem Cell Reports*, 6(2), pp. 200-12.

- Ladd, A.N., Nguyen, N.H., Malhotra, K. and Cooper, T.A. (2004) 'CELF6, a member of the CELF family of RNA-binding proteins, regulates muscle-specific splicing enhancer-dependent alternative splicing', *J Biol Chem*, 279(17), pp. 17756-64.
- Lamb, T.D. and Pugh, E.N., Jr. (2004) 'Dark adaptation and the retinoid cycle of vision', *Prog Retin Eye Res*, 23(3), pp. 307-80.
- Lane, A., Philip, L.R., Ruban, L., Fynes, K., Smart, M., Carr, A., Mason, C. and Coffey, P. (2014) 'Engineering efficient retinal pigment epithelium differentiation from human pluripotent stem cells', *Stem Cells Transl Med*, 3(11), pp. 1295-304.
- Laurent, L.C., Ulitsky, I., Slavin, I., Tran, H., Schork, A., Morey, R., Lynch, C., Harness, J.V., Lee, S., Barrero, M.J., Ku, S., Martynova, M., Semechkin, R., Galat, V., Gottesfeld, J., Izpisua Belmonte, J.C., Murry, C., Keirstead, H.S., Park, H.S., Schmidt, U., Laslett, A.L., Muller, F.J., Nievergelt, C.M., Shamir, R. and Loring, J.F. (2011) 'Dynamic changes in the copy number of pluripotency and cell proliferation genes in human ESCs and iPSCs during reprogramming and time in culture', *Cell Stem Cell*, 8(1), pp. 106-18.
- Le Scouarnec, S. and Gribble, S.M. (2012) 'Characterising chromosome rearrangements: recent technical advances in molecular cytogenetics', *Heredity (Edinb)*, 108(1), pp. 75-85.
- Leach, L.L., Buchholz, D.E., Nadar, V.P., Lowenstein, S.E. and Clegg, D.O. (2015) 'Canonical/ss-catenin Wnt Pathway Activation Improves Retinal Pigmented Epithelium Derivation from Human Embryonic Stem Cells', *Invest Ophthalmol Vis Sci*.
- Leach, L.L., Croze, R.H., Hu, Q., Nadar, V.P., Clevenger, T.N., Pennington, B.O., Gamm, D.M. and Clegg, D.O. (2016) 'Induced Pluripotent Stem Cell-Derived Retinal Pigmented Epithelium: A Comparative Study Between Cell Lines and Differentiation Methods', *J Ocul Pharmacol Ther*, 32(5), pp. 317-30.
- Lee, J.E. and Gleeson, J.G. (2011) 'Cilia in the nervous system: linking cilia function and neurodevelopmental disorders', *Curr Opin Neurol*, 24(2), pp. 98-105.
- Lehmann, G.L., Benedicto, I., Philp, N.J. and Rodriguez-Boulan, E. (2014) 'Plasma membrane protein polarity and trafficking in RPE cells: past, present and future', *Exp Eye Res*, 126, pp. 5-15.
- Li, H.O., Zhu, Y.F., Asakawa, M., Kuma, H., Hirata, T., Ueda, Y., Lee, Y.S., Fukumura, M., Iida, A., Kato, A., Nagai, Y. and Hasegawa, M. (2000) 'A cytoplasmic RNA vector derived from nontransmissible Sendai virus with efficient gene transfer and expression', *J Virol*, 74(14), pp. 6564-9.
- Li, W., Stramm, L.E., Aguirre, G.D. and Rockey, J.H. (1984) 'Extracellular matrix production by cat retinal pigment epithelium in vitro: characterization of type IV collagen synthesis', *Exp Eye Res*, 38(3), pp. 291-304.
- Li, W.B., Zhang, Y.S., Lu, Z.Y., Dong, L.J., Wang, F.E., Dong, R. and Li, X.R. (2012) 'Development of retinal pigment epithelium from human parthenogenetic embryonic stem cells and microRNA signature', *Invest Ophthalmol Vis Sci*, 53(9), pp. 5334-43.
- Li, Y., Chan, L., Nguyen, H.V. and Tsang, S.H. (2016) 'Personalized Medicine: Cell and Gene Therapy Based on Patient-Specific iPSC-Derived Retinal Pigment Epithelium Cells', *Adv Exp Med Biol*, 854, pp. 549-55.
- Li, Y., Wu, W.H., Hsu, C.W., Nguyen, H.V., Tsai, Y.T., Chan, L., Nagasaki, T., Maumenee, I.H., Yannuzzi, L.A., Hoang, Q.V., Hua, H., Egli, D. and Tsang, S.H. (2014) 'Gene therapy in patient-specific stem cell lines and a preclinical model of retinitis pigmentosa with membrane frizzled-related protein defects', *Mol Ther*, 22(9), pp. 1688-97.
- Li, Z.Y., Possin, D.E. and Milam, A.H. (1995) 'Histopathology of bone spicule pigmentation in retinitis pigmentosa', *Ophthalmology*, 102(5), pp. 805-16.
- Liang, G. and Zhang, Y. (2013a) 'Embryonic stem cell and induced pluripotent stem cell: an epigenetic perspective', *Cell Res*, 23(1), pp. 49-69.

Liang, G. and Zhang, Y. (2013b) 'Genetic and epigenetic variations in iPSCs: potential causes and implications for application', *Cell Stem Cell*, 13(2), pp. 149-59.

Lin, H. and Clegg, D.O. (1998) 'Integrin alphavbeta5 participates in the binding of photoreceptor rod outer segments during phagocytosis by cultured human retinal pigment epithelium', *Invest Ophthalmol Vis Sci*, 39(9), pp. 1703-12.

Linder, B., Dill, H., Hirmer, A., Brocher, J., Lee, G.P., Mathavan, S., Bolz, H.J., Winkler, C., Lagerbauer, B. and Fischer, U. (2011) 'Systemic splicing factor deficiency causes tissue-specific defects: a zebrafish model for retinitis pigmentosa', *Hum Mol Genet*, 20(2), pp. 368-77.

Liu, S., Li, P., Dybkov, O., Nottrott, S., Hartmuth, K., Lührmann, R., Carlomagno, T. and Wahl, M.C. (2007) 'Binding of the human Prp31 Nop domain to a composite RNA-protein platform in U4 snRNP', *Science*, 316(5821), pp. 115-20.

Liu, S., Rauhut, R., Vornlocher, H.P. and Luhrmann, R. (2006) 'The network of protein-protein interactions within the human U4/U6.U5 tri-snRNP', *RNA*, 12(7), pp. 1418-30.

Locke, C.J., Congrove, N.R., Dismuke, W.M., Bowen, T.J., Stamer, W.D. and McKay, B.S. (2014) 'Controlled exosome release from the retinal pigment epithelium in situ', *Exp Eye Res*, 129, pp. 1-4.

Loh, Y.H., Agarwal, S., Park, I.H., Urbach, A., Huo, H., Heffner, G.C., Kim, K., Miller, J.D., Ng, K. and Daley, G.Q. (2009) 'Generation of induced pluripotent stem cells from human blood', *Blood*, 113(22), pp. 5476-9.

Lopez, P.F., Sippy, B.D., Lambert, H.M., Thach, A.B. and Hinton, D.R. (1996) 'Transdifferentiated retinal pigment epithelial cells are immunoreactive for vascular endothelial growth factor in surgically excised age-related macular degeneration-related choroidal neovascular membranes', *Invest Ophthalmol Vis Sci*, 37(5), pp. 855-68.

Love, M.I., Huber, W. and Anders, S. (2014) 'Moderated estimation of fold change and dispersion for RNA-seq data with DESeq2', *Genome Biol*, 15(12), p. 550.

Lukovic, D., Artero Castro, A., Delgado, A.B., Bernal Mde, L., Luna Pelaez, N., Diez Lloret, A., Perez Espejo, R., Kamenarova, K., Fernandez Sanchez, L., Cuenca, N., Corton, M., Avila Fernandez, A., Sorkio, A., Skottman, H., Ayuso, C., Erceg, S. and Bhattacharya, S.S. (2015) 'Human iPSC derived disease model of MERTK-associated retinitis pigmentosa', *Sci Rep*, 5, p. 12910.

MacLaren, R.E., Groppe, M., Barnard, A.R., Cottrill, C.L., Tolmachova, T., Seymour, L., Clark, K.R., Durning, M.J., Cremers, F.P., Black, G.C., Lotery, A.J., Downes, S.M., Webster, A.R. and Seabra, M.C. (2014) 'Retinal gene therapy in patients with choroideremia: initial findings from a phase 1/2 clinical trial', *Lancet*, 383(9923), pp. 1129-37.

MacLaren, R.E., Pearson, R.A., MacNeil, A., Douglas, R.H., Salt, T.E., Akimoto, M., Swaroop, A., Sowden, J.C. and Ali, R.R. (2006) 'Retinal repair by transplantation of photoreceptor precursors', *Nature*, 444(7116), pp. 203-7.

Maeder, C., Kutach, A.K. and Guthrie, C. (2009) 'ATP-dependent unwinding of U4/U6 snRNAs by the Brr2 helicase requires the C terminus of Prp8', *Nat Struct Mol Biol*, 16(1), pp. 42-8.

Maguire, A.M., Simonelli, F., Pierce, E.A., Pugh, E.N., Jr., Mingozzi, F., Bennicelli, J., Banfi, S., Marshall, K.A., Testa, F., Surace, E.M., Rossi, S., Lyubarsky, A., Arruda, V.R., Konkle, B., Stone, E., Sun, J., Jacobs, J., Dell'Osso, L., Hertle, R., Ma, J.X., Redmond, T.M., Zhu, X., Hauck, B., Zeleniaia, O., Shindler, K.S., Maguire, M.G., Wright, J.F., Volpe, N.J., McDonnell, J.W., Auricchio, A., High, K.A. and Bennett, J. (2008) 'Safety and efficacy of gene transfer for Leber's congenital amaurosis', *N Engl J Med*, 358(21), pp. 2240-8.

Makarov, E.M., Makarova, O.V., Achsel, T. and Luhrmann, R. (2000) 'The human homologue of the yeast splicing factor prp6p contains multiple TPR elements and is

stably associated with the U5 snRNP via protein-protein interactions', *J Mol Biol*, 298(4), pp. 567-75.

Makarova, O.V., Makarov, E.M., Liu, S., Vornlocher, H.P. and Lührmann, R. (2002) 'Protein 61K, encoded by a gene (PRPF31) linked to autosomal dominant retinitis pigmentosa, is required for U4/U6*U5 tri-snRNP formation and pre-mRNA splicing', *EMBO J*, 21(5), pp. 1148-57.

Mandai, M., Watanabe, A., Kurimoto, Y., Hiram, Y., Morinaga, C., Daimon, T., Fujihara, M., Akimaru, H., Sakai, N., Shibata, Y., Terada, M., Nomiya, Y., Tanishima, S., Nakamura, M., Kamao, H., Sugita, S., Onishi, A., Ito, T., Fujita, K., Kawamata, S., Go, M.J., Shinohara, C., Hata, K.I., Sawada, M., Yamamoto, M., Ohta, S., Ohara, Y., Yoshida, K., Kuwahara, J., Kitano, Y., Amano, N., Umekage, M., Kitaoka, F., Tanaka, A., Okada, C., Takasu, N., Ogawa, S., Yamanaka, S. and Takahashi, M. (2017) 'Autologous Induced Stem-Cell-Derived Retinal Cells for Macular Degeneration', *N Engl J Med*, 376(11), pp. 1038-1046.

Markoulaki, S., Hanna, J., Beard, C., Carey, B.W., Cheng, A.W., Lengner, C.J., Dausman, J.A., Fu, D., Gao, Q., Wu, S., Cassady, J.P. and Jaenisch, R. (2009) 'Transgenic mice with defined combinations of drug-inducible reprogramming factors', *Nat Biotechnol*, 27(2), pp. 169-71.

Marson, A., Levine, S.S., Cole, M.F., Frampton, G.M., Brambrink, T., Johnstone, S., Guenther, M.G., Johnston, W.K., Wernig, M., Newman, J., Calabrese, J.M., Dennis, L.M., Volkert, T.L., Gupta, S., Love, J., Hannett, N., Sharp, P.A., Bartel, D.P., Jaenisch, R. and Young, R.A. (2008) 'Connecting microRNA genes to the core transcriptional regulatory circuitry of embryonic stem cells', *Cell*, 134(3), pp. 521-33.

Martin, G.R. (1981) 'Isolation of a pluripotent cell line from early mouse embryos cultured in medium conditioned by teratocarcinoma stem cells', *Proc Natl Acad Sci U S A*, 78(12), pp. 7634-8.

Martin-Merida, I., Sanchez-Alcudia, R., Fernandez-San Jose, P., Blanco-Kelly, F., Perez-Carro, R., Rodriguez-Jacy da Silva, L., Almoguera, B., Garcia-Sandoval, B., Lopez-Molina, M.I., Avila-Fernandez, A., Carballo, M., Corton, M. and Ayuso, C. (2017) 'Analysis of the PRPF31 Gene in Spanish Autosomal Dominant Retinitis Pigmentosa Patients: A Novel Genomic Rearrangement', *Invest Ophthalmol Vis Sci*, 58(2), pp. 1045-1053.

Martinez-Morales, J.R., Rodrigo, I. and Bovolenta, P. (2004) 'Eye development: a view from the retina pigmented epithelium', *Bioessays*, 26(7), pp. 766-77.

Martins-Taylor, K., Nisler, B.S., Taapken, S.M., Compton, T., Crandall, L., Montgomery, K.D., Lalande, M. and Xu, R.H. (2011) 'Recurrent copy number variations in human induced pluripotent stem cells', *Nat Biotechnol*, 29(6), pp. 488-91.

Matsui, Y., Zsebo, K. and Hogan, B.L. (1992) 'Derivation of pluripotential embryonic stem cells from murine primordial germ cells in culture', *Cell*, 70(5), pp. 841-7.

May-Simera, H.L., Wan, Q., Jha, B.S., Hartford, J., Khristov, V., Dejene, R., Chang, J., Patnaik, S., Lu, Q., Banerjee, P., Silver, J., Insinna-Kettenhofen, C., Patel, D., Lotfi, M., Malicdan, M., Hotaling, N., Maminishkis, A., Sridharan, R., Brooks, B., Miyagishima, K., Gunay-Aygun, M., Pal, R., Westlake, C., Miller, S., Sharma, R. and Bharti, K. (2018) 'Primary Cilium-Mediated Retinal Pigment Epithelium Maturation Is Disrupted in Ciliopathy Patient Cells', *Cell Rep*, 22(1), pp. 189-205.

Mazzoni, F., Safa, H. and Finnemann, S.C. (2014) 'Understanding photoreceptor outer segment phagocytosis: use and utility of RPE cells in culture', *Exp Eye Res*, 126, pp. 51-60.

Mead, B., Berry, M., Logan, A., Scott, R.A., Leadbeater, W. and Scheven, B.A. (2015) 'Stem cell treatment of degenerative eye disease', *Stem Cell Res*, 14(3), pp. 243-57.

Meissner, A., Mikkelsen, T.S., Gu, H., Wernig, M., Hanna, J., Sivachenko, A., Zhang, X., Bernstein, B.E., Nusbaum, C., Jaffe, D.B., Gnirke, A., Jaenisch, R. and Lander,

- E.S. (2008) 'Genome-scale DNA methylation maps of pluripotent and differentiated cells', *Nature*, 454(7205), pp. 766-70.
- Meregalli, M., Farini, A and Torrente, Y (2011) 'Stem Cell Therapy for Neuromuscular Diseases', in (Ed.), D.A.G. (ed.) *Stem Cells in Clinic and Research*. InTech.
- Metzker, M.L. (2010) 'Sequencing technologies - the next generation', *Nat Rev Genet*, 11(1), pp. 31-46.
- Meyer, J.S., Shearer, R.L., Capowski, E.E., Wright, L.S., Wallace, K.A., McMillan, E.L., Zhang, S.C. and Gamm, D.M. (2009) 'Modeling early retinal development with human embryonic and induced pluripotent stem cells', *Proc Natl Acad Sci U S A*, 106(39), pp. 16698-703.
- Mikkelsen, T.S., Hanna, J., Zhang, X., Ku, M., Wernig, M., Schorderet, P., Bernstein, B.E., Jaenisch, R., Lander, E.S. and Meissner, A. (2008) 'Dissecting direct reprogramming through integrative genomic analysis', *Nature*, 454(7200), pp. 49-55.
- Milam, A.H., Li, Z.Y. and Fariss, R.N. (1998) 'Histopathology of the human retina in retinitis pigmentosa', *Prog Retin Eye Res*, 17(2), pp. 175-205.
- Mills, J.O., Jalil, A. and Stanga, P.E. (2017) 'Electronic retinal implants and artificial vision: journey and present', *Eye (Lond)*, 31(10), pp. 1383-1398.
- Miyoshi, N., Ishii, H., Nagano, H., Haraguchi, N., Dewi, D.L., Kano, Y., Nishikawa, S., Tanemura, M., Mimori, K., Tanaka, F., Saito, T., Nishimura, J., Takemasa, I., Mizushima, T., Ikeda, M., Yamamoto, H., Sekimoto, M., Doki, Y. and Mori, M. (2011) 'Reprogramming of mouse and human cells to pluripotency using mature microRNAs', *Cell Stem Cell*, 8(6), pp. 633-8.
- Mizuseki, K., Sakamoto, T., Watanabe, K., Muguruma, K., Ikeya, M., Nishiyama, A., Arakawa, A., Suemori, H., Nakatsuji, N., Kawasaki, H., Murakami, F. and Sasai, Y. (2003) 'Generation of neural crest-derived peripheral neurons and floor plate cells from mouse and primate embryonic stem cells', *Proc Natl Acad Sci U S A*, 100(10), pp. 5828-33.
- Moore, A.T., Fitzke, F., Jay, M., Arden, G.B., Inglehearn, C.F., Keen, T.J., Bhattacharya, S.S. and Bird, A.C. (1993) 'Autosomal dominant retinitis pigmentosa with apparent incomplete penetrance: a clinical, electrophysiological, psychophysical, and molecular genetic study', *Br J Ophthalmol*, 77(8), pp. 473-9.
- Mordes, D., Luo, X., Kar, A., Kuo, D., Xu, L., Fushimi, K., Yu, G., Sternberg, P., Jr. and Wu, J.Y. (2006) 'Pre-mRNA splicing and retinitis pigmentosa', *Mol Vis*, 12, pp. 1259-71.
- Mordes, D., Yuan, L., Xu, L., Kawada, M., Molday, R.S. and Wu, J.Y. (2007) 'Identification of photoreceptor genes affected by PRPF31 mutations associated with autosomal dominant retinitis pigmentosa', *Neurobiol Dis*, 26(2), pp. 291-300.
- Muller, F.J., Goldmann, J., Loser, P. and Loring, J.F. (2010) 'A call to standardize teratoma assays used to define human pluripotent cell lines', *Cell Stem Cell*, 6(5), pp. 412-4.
- Muniz, A., Greene, W.A., Plamper, M.L., Choi, J.H., Johnson, A.J., Tsin, A.T. and Wang, H.C. (2014) 'Retinoid uptake, processing, and secretion in human iPS-RPE support the visual cycle', *Invest Ophthalmol Vis Sci*, 55(1), pp. 198-209.
- Murphy, D., Cieply, B., Carstens, R., Ramamurthy, V. and Stoilov, P. (2016) 'The Musashi 1 Controls the Splicing of Photoreceptor-Specific Exons in the Vertebrate Retina', *PLoS Genet*, 12(8), p. e1006256.
- Nakano, T., Ando, S., Takata, N., Kawada, M., Muguruma, K., Sekiguchi, K., Saito, K., Yonemura, S., Eiraku, M. and Sasai, Y. (2012) 'Self-formation of optic cups and storable stratified neural retina from human ESCs', *Cell Stem Cell*, 10(6), pp. 771-85.
- Nangia, V., Jonas, J.B., Khare, A. and Sinha, A. (2012) 'Prevalence of retinitis pigmentosa in India: the Central India Eye and Medical Study', *Acta Ophthalmol*, 90(8), pp. e649-50.

- Nasonkin, I.O., Merbs, S.L., Lazo, K., Oliver, V.F., Brooks, M., Patel, K., Enke, R.A., Nellissery, J., Jamrich, M., Le, Y.Z., Bharti, K., Fariss, R.N., Rachel, R.A., Zack, D.J., Rodriguez-Boulan, E.J. and Swaroop, A. (2013) 'Conditional knockdown of DNA methyltransferase 1 reveals a key role of retinal pigment epithelium integrity in photoreceptor outer segment morphogenesis', *Development*, 140(6), pp. 1330-41.
- Nathwani, B.B., Miller, C.H., Yang, T.L., Solimano, J.L. and Liao, J.C. (2014) 'Morphological differences of primary cilia between human induced pluripotent stem cells and their parental somatic cells', *Stem Cells Dev*, 23(2), pp. 115-23.
- Neidhardt, J., Glaus, E., Barthelmes, D., Zeitz, C., Fleischhauer, J. and Berger, W. (2007) 'Identification and characterization of a novel RPGR isoform in human retina', *Hum Mutat*, 28(8), pp. 797-807.
- Neidhardt, J., Glaus, E., Lorenz, B., Netzer, C., Li, Y., Schambeck, M., Wittmer, M., Feil, S., Kirschner-Schwabe, R., Rosenberg, T., Cremers, F.P., Bergen, A.A., Barthelmes, D., Baraki, H., Schmid, F., Tanner, G., Fleischhauer, J., Orth, U., Becker, C., Wegscheider, E., Nurnberg, G., Nurnberg, P., Bolz, H.J., Gal, A. and Berger, W. (2008) 'Identification of novel mutations in X-linked retinitis pigmentosa families and implications for diagnostic testing', *Mol Vis*, 14, pp. 1081-93.
- Newsome, D.A. and Kenyon, K.R. (1973) 'Collagen production in vitro by the retinal pigmented epithelium of the chick embryo', *Dev Biol*, 32(2), pp. 387-400.
- Nguyen, H.V., Li, Y. and Tsang, S.H. (2015) 'Patient-Specific iPSC-Derived RPE for Modeling of Retinal Diseases', *J Clin Med*, 4(4), pp. 567-78.
- Nguyen, M. and Arnheiter, H. (2000) 'Signaling and transcriptional regulation in early mammalian eye development: a link between FGF and MITF', *Development*, 127(16), pp. 3581-91.
- Niakan, K.K., Han, J., Pedersen, R.A., Simon, C. and Pera, R.A. (2012) 'Human pre-implantation embryo development', *Development*, 139(5), pp. 829-41.
- Nishiyama, K., Sakaguchi, H., Hu, J.G., Bok, D. and Hollyfield, J.G. (2002) 'Claudin localization in cilia of the retinal pigment epithelium', *Anat Rec*, 267(3), pp. 196-203.
- Ogata, N., Wang, L., Jo, N., Tombran-Tink, J., Takahashi, K., Mrazek, D. and Matsumura, M. (2001) 'Pigment epithelium derived factor as a neuroprotective agent against ischemic retinal injury', *Curr Eye Res*, 22(4), pp. 245-52.
- Okita, K., Nakagawa, M., Hyenjong, H., Ichisaka, T. and Yamanaka, S. (2008) 'Generation of mouse induced pluripotent stem cells without viral vectors', *Science*, 322(5903), pp. 949-53.
- Openshaw, A. (2008) 'Understanding Retinitis Pigmentosa' Michigan, U.o. Kellogg Eye Center, p. 26.
- Organisciak, D.T., Bicknell, I.R. and Darrow, R.M. (1992) 'The effects of L- and D-ascorbic acid administration on retinal tissue levels and light damage in rats', *Curr Eye Res*, 11(3), pp. 231-41.
- Osakada, F., Ikeda, H., Sasai, Y. and Takahashi, M. (2009) 'Stepwise differentiation of pluripotent stem cells into retinal cells', *Nat Protoc*, 4(6), pp. 811-24.
- Padnick-Silver, L., Kang Derwent, J.J., Giuliano, E., Narfstrom, K. and Linsenmeier, R.A. (2006) 'Retinal oxygenation and oxygen metabolism in Abyssinian cats with a hereditary retinal degeneration', *Invest Ophthalmol Vis Sci*, 47(8), pp. 3683-9.
- Pagon, R.A. (1988) 'Retinitis pigmentosa', *Surv Ophthalmol*, 33(3), pp. 137-77.
- Pan, Q., Shai, O., Lee, L.J., Frey, B.J. and Blencowe, B.J. (2008) 'Deep surveying of alternative splicing complexity in the human transcriptome by high-throughput sequencing', *Nat Genet*, 40(12), pp. 1413-5.
- Pang, J.J., Chang, B., Kumar, A., Nusinowitz, S., Noorwez, S.M., Li, J., Rani, A., Foster, T.C., Chiodo, V.A., Doyle, T., Li, H., Malhotra, R., Teusner, J.T., McDowell, J.H., Min, S.H., Li, Q., Kaushal, S. and Hauswirth, W.W. (2006) 'Gene therapy restores

vision-dependent behavior as well as retinal structure and function in a mouse model of RPE65 Leber congenital amaurosis', *Mol Ther*, 13(3), pp. 565-72.

Parfitt, D.A., Lane, A., Ramsden, C.M., Carr, A.J., Munro, P.M., Jovanovic, K., Schwarz, N., Kanuga, N., Muthiah, M.N., Hull, S., Gallo, J.M., da Cruz, L., Moore, A.T., Hardcastle, A.J., Coffey, P.J. and Cheetham, M.E. (2016) 'Identification and Correction of Mechanisms Underlying Inherited Blindness in Human iPSC-Derived Optic Cups', *Cell Stem Cell*, 18(6), pp. 769-81.

Park, J.W., Tokheim, C., Shen, S. and Xing, Y. (2013) 'Identifying differential alternative splicing events from RNA sequencing data using RNASeq-MATS', *Methods Mol Biol*, 1038, pp. 171-9.

Pawlyk, B.S., Li, T., Scimeca, M.S., Sandberg, M.A. and Berson, E.L. (2002) 'Absence of photoreceptor rescue with D-cis-diltiazem in the rd mouse', *Invest Ophthalmol Vis Sci*, 43(6), pp. 1912-5.

Pearson, R.A., Barber, A.C., Rizzi, M., Hippert, C., Xue, T., West, E.L., Duran, Y., Smith, A.J., Chuang, J.Z., Azam, S.A., Luhmann, U.F., Benucci, A., Sung, C.H., Bainbridge, J.W., Carandini, M., Yau, K.W., Sowden, J.C. and Ali, R.R. (2012) 'Restoration of vision after transplantation of photoreceptors', *Nature*, 485(7396), pp. 99-103.

Pearson, R.A., Dale, N., Llaudet, E. and Mobbs, P. (2005) 'ATP released via gap junction hemichannels from the pigment epithelium regulates neural retinal progenitor proliferation', *Neuron*, 46(5), pp. 731-44.

Pearson, R.A., Gonzalez-Cordero, A., West, E.L., Ribeiro, J.R., Aghaizu, N., Goh, D., Sampson, R.D., Georgiadis, A., Waldron, P.V., Duran, Y., Naeem, A., Kloc, M., Cristante, E., Kruczek, K., Warre-Cornish, K., Sowden, J.C., Smith, A.J. and Ali, R.R. (2016) 'Donor and host photoreceptors engage in material transfer following transplantation of post-mitotic photoreceptor precursors', *Nat Commun*, 7, p. 13029.

Penn, J.S., Li, S. and Naash, M.I. (2000) 'Ambient hypoxia reverses retinal vascular attenuation in a transgenic mouse model of autosomal dominant retinitis pigmentosa', *Invest Ophthalmol Vis Sci*, 41(12), pp. 4007-13.

Pera, M.F., Reubinoff, B. and Trounson, A. (2000) 'Human embryonic stem cells', *J Cell Sci*, 113 (Pt 1), pp. 5-10.

Polo, J.M., Anderssen, E., Walsh, R.M., Schwarz, B.A., Nefzger, C.M., Lim, S.M., Borkent, M., Apostolou, E., Alaei, S., Cloutier, J., Bar-Nur, O., Cheloufi, S., Stadtfeld, M., Figueroa, M.E., Robinton, D., Natesan, S., Melnick, A., Zhu, J., Ramaswamy, S. and Hochedlinger, K. (2012) 'A molecular roadmap of reprogramming somatic cells into iPS cells', *Cell*, 151(7), pp. 1617-32.

Puech, B., Kostrubiec, B., Hache, J.C. and Francois, P. (1991) '[Epidemiology and prevalence of hereditary retinal dystrophies in the Northern France]', *J Fr Ophtalmol*, 14(3), pp. 153-64.

Punzo, C., Kornacker, K. and Cepko, C.L. (2009) 'Stimulation of the insulin/mTOR pathway delays cone death in a mouse model of retinitis pigmentosa', *Nat Neurosci*, 12(1), pp. 44-52.

Raab, S., Klingenstein, M., Liebau, S. and Linta, L. (2014) 'A Comparative View on Human Somatic Cell Sources for iPSC Generation', *Stem Cells Int*, 2014, p. 768391.

Rachel, R.A., May-Simera, H.L., Veleri, S., Gotoh, N., Choi, B.Y., Murga-Zamalloa, C., McIntyre, J.C., Marek, J., Lopez, I., Hackett, A.N., Zhang, J., Brooks, M., den Hollander, A.I., Beales, P.L., Li, T., Jacobson, S.G., Sood, R., Martens, J.R., Liu, P., Friedman, T.B., Khanna, H., Koenekoop, R.K., Kelley, M.W. and Swaroop, A. (2012) 'Combining Cep290 and Mkks ciliopathy alleles in mice rescues sensory defects and restores ciliogenesis', *J Clin Invest*, 122(4), pp. 1233-45.

Radtke, N.D., Seiler, M.J., Aramant, R.B., Petry, H.M. and Pidwell, D.J. (2002) 'Transplantation of intact sheets of fetal neural retina with its retinal pigment epithelium in retinitis pigmentosa patients', *Am J Ophthalmol*, 133(4), pp. 544-50.

Ran, F.A., Hsu, P.D., Wright, J., Agarwala, V., Scott, D.A. and Zhang, F. (2013) 'Genome engineering using the CRISPR-Cas9 system', *Nat Protoc*, 8(11), pp. 2281-2308.

Rao, M.S. and Malik, N. (2012) 'Assessing iPSC reprogramming methods for their suitability in translational medicine', *J Cell Biochem*, 113(10), pp. 3061-8.

Rayapudi, S., Schwartz, S.G., Wang, X. and Chavis, P. (2013) 'Vitamin A and fish oils for retinitis pigmentosa', *Cochrane Database Syst Rev*, (12), p. CD008428.

Reiter, J.F., Blacque, O.E. and Leroux, M.R. (2012) 'The base of the cilium: roles for transition fibres and the transition zone in ciliary formation, maintenance and compartmentalization', *EMBO Rep*, 13(7), pp. 608-18.

RetNet 'the Retinal Information Network' Center, U.o.T.-H.H.S. Available at: <http://www.sph.uth.tmc.edu/RetNet/>.

Rinaldi, C. and Wood, M.J.A. (2018) 'Antisense oligonucleotides: the next frontier for treatment of neurological disorders', *Nat Rev Neurol*, 14(1), pp. 9-21.

Rio Frio, T., Wade, N.M., Ransijn, A., Berson, E.L., Beckmann, J.S. and Rivolta, C. (2008) 'Premature termination codons in PRPF31 cause retinitis pigmentosa via haploinsufficiency due to nonsense-mediated mRNA decay', *J Clin Invest*, 118(4), pp. 1519-31.

Rizzolo, L.J. (1999) 'Polarization of the Na⁺,K⁺-ATPase in epithelia derived from the neuroepithelium', *International Review of Cytology - a Survey of Cell Biology*, Vol 185, 185, pp. 195-235.

Roberts, W.G. and Palade, G.E. (1995) 'Increased microvascular permeability and endothelial fenestration induced by vascular endothelial growth factor', *J Cell Sci*, 108 (Pt 6), pp. 2369-79.

Robertson, J.A. (2001) 'Human embryonic stem cell research: ethical and legal issues', *Nat Rev Genet*, 2(1), pp. 74-8.

Rose, A.M., Luo, R., Radia, U.K. and Bhattacharya, S.S. (2017) 'Gene of the month: PRPF31', *J Clin Pathol*, 70(9), pp. 729-732.

Rose, A.M., Shah, A.Z., Venturini, G., Krishna, A., Chakravarti, A., Rivolta, C. and Bhattacharya, S.S. (2016) 'Transcriptional regulation of PRPF31 gene expression by MSR1 repeat elements causes incomplete penetrance in retinitis pigmentosa', *Sci Rep*, 6, p. 19450.

Rose, A.M., Shah, A.Z., Venturini, G., Rivolta, C., Rose, G.E. and Bhattacharya, S.S. (2014) 'Dominant PRPF31 mutations are hypostatic to a recessive CNOT3 polymorphism in retinitis pigmentosa: a novel phenomenon of "linked trans-acting epistasis"', *Ann Hum Genet*, 78(1), pp. 62-71.

Ryeom, S.W., Silverstein, R.L., Scotto, A. and Sparrow, J.R. (1996) 'Binding of anionic phospholipids to retinal pigment epithelium may be mediated by the scavenger receptor CD36', *J Biol Chem*, 271(34), pp. 20536-9.

Samavarchi-Tehrani, P., Golipour, A., David, L., Sung, H.K., Beyer, T.A., Datti, A., Woltjen, K., Nagy, A. and Wrana, J.L. (2010) 'Functional genomics reveals a BMP-driven mesenchymal-to-epithelial transition in the initiation of somatic cell reprogramming', *Cell Stem Cell*, 7(1), pp. 64-77.

Sasai, N. and Briscoe, J. (2012) 'Primary cilia and graded Sonic Hedgehog signaling', *Wiley Interdiscip Rev Dev Biol*, 1(5), pp. 753-72.

Sayed, N., Liu, C. and Wu, J.C. (2016) 'Translation of Human-Induced Pluripotent Stem Cells: From Clinical Trial in a Dish to Precision Medicine', *J Am Coll Cardiol*, 67(18), pp. 2161-2176.

- Scacheri, P.C. and Tesar, P.J. (2017) 'iPSC Reprogramming Is Not Just an Open and Shut Case', *Cell Stem Cell*, 21(6), pp. 711-712.
- Schaffer, A.A. (2013) 'Digenic inheritance in medical genetics', *J Med Genet*, 50(10), pp. 641-52.
- Schaffert, N., Hossbach, M., Heintzmann, R., Achsel, T. and Lührmann, R. (2004) 'RNAi knockdown of hPrp31 leads to an accumulation of U4/U6 di-snRNPs in Cajal bodies', *EMBO J*, 23(15), pp. 3000-9.
- Schneuwly, S., Klemenz, R. and Gehring, W.J. (1987) 'Redesigning the body plan of *Drosophila* by ectopic expression of the homoeotic gene *Antennapedia*', *Nature*, 325(6107), pp. 816-8.
- Scholl, H.P., Strauss, R.W., Singh, M.S., Dalkara, D., Roska, B., Picaud, S. and Sahel, J.A. (2016) 'Emerging therapies for inherited retinal degeneration', *Sci Transl Med*, 8(368), p. 368rv6.
- Schwartz, S.D., Hubschman, J.P., Heilwell, G., Franco-Cardenas, V., Pan, C.K., Ostrick, R.M., Mickunas, E., Gay, R., Klimanskaya, I. and Lanza, R. (2012) 'Embryonic stem cell trials for macular degeneration: a preliminary report', *Lancet*, 379(9817), pp. 713-20.
- Schwartz, S.D., Regillo, C.D., Lam, B.L., Elliott, D., Rosenfeld, P.J., Gregori, N.Z., Hubschman, J.P., Davis, J.L., Heilwell, G., Spirn, M., Maguire, J., Gay, R., Bateman, J., Ostrick, R.M., Morris, D., Vincent, M., Anglade, E., Del Priore, L.V. and Lanza, R. (2015) 'Human embryonic stem cell-derived retinal pigment epithelium in patients with age-related macular degeneration and Stargardt's macular dystrophy: follow-up of two open-label phase 1/2 studies', *Lancet*, 385(9967), pp. 509-16.
- Scotti, M.M. and Swanson, M.S. (2016) 'RNA mis-splicing in disease', *Nat Rev Genet*, 17(1), pp. 19-32.
- Seiler, M.J., Sagdullaev, B.T., Woch, G., Thomas, B.B. and Aramant, R.B. (2005) 'Transsynaptic virus tracing from host brain to subretinal transplants', *Eur J Neurosci*, 21(1), pp. 161-72.
- Shastry, B.S. (1994) 'Retinitis pigmentosa and related disorders: phenotypes of rhodopsin and peripherin/RDS mutations', *Am J Med Genet*, 52(4), pp. 467-74.
- Shastry, B.S. (2008) 'Evaluation of the common variants of the ABCA4 gene in families with Stargardt disease and autosomal recessive retinitis pigmentosa', *Int J Mol Med*, 21(6), pp. 715-20.
- Shay, J.W. and Wright, W.E. (2006) 'Telomerase therapeutics for cancer: challenges and new directions', *Nat Rev Drug Discov*, 5(7), pp. 577-84.
- Shintani, K., Shechtman, D.L. and Gurwood, A.S. (2009) 'Review and update: current treatment trends for patients with retinitis pigmentosa', *Optometry*, 80(7), pp. 384-401.
- Shirai, C.L., Ley, J.N., White, B.S., Kim, S., Tibbitts, J., Shao, J., Ndonwi, M., Wadugu, B., Duncavage, E.J., Okeyo-Owuor, T., Liu, T., Griffith, M., McGrath, S., Magrini, V., Fulton, R.S., Fronick, C., O'Laughlin, M., Graubert, T.A. and Walter, M.J. (2015) 'Mutant U2AF1 Expression Alters Hematopoiesis and Pre-mRNA Splicing In Vivo', *Cancer Cell*, 27(5), pp. 631-43.
- Simo, R., Carrasco, E., Garcia-Ramirez, M. and Hernandez, C. (2006) 'Angiogenic and antiangiogenic factors in proliferative diabetic retinopathy', *Curr Diabetes Rev*, 2(1), pp. 71-98.
- Singh, R.P. (2018) 'Research Developments in the Treatment of Retinal Disease: Finalists From the Inaugural Retina Research Scholar Honoree Program', *Ophthalmic Surg Lasers Imaging Retina*, 49(10), p. S2.
- Smith, A.G., Heath, J.K., Donaldson, D.D., Wong, G.G., Moreau, J., Stahl, M. and Rogers, D. (1988) 'Inhibition of pluripotential embryonic stem cell differentiation by purified polypeptides', *Nature*, 336(6200), pp. 688-90.

Smith, E.N., D'Antonio-Chronowska, A., Greenwald, W.W., Borja, V., Aguiar, L.R., Pogue, R., Matsui, H., Benaglio, P., Borooah, S., D'Antonio, M., Ayyagari, R. and Frazer, K.A. (2019) 'Human iPSC-Derived Retinal Pigment Epithelium: A Model System for Prioritizing and Functionally Characterizing Causal Variants at AMD Risk Loci', *Stem Cell Reports*, 12(6), pp. 1342-1353.

Sonoda, S., Spee, C., Barron, E., Ryan, S.J., Kannan, R. and Hinton, D.R. (2009) 'A protocol for the culture and differentiation of highly polarized human retinal pigment epithelial cells', *Nat Protoc*, 4(5), pp. 662-73.

Souied, E., Segues, B., Ghazi, I., Rozet, J.M., Chatelin, S., Gerber, S., Perrault, I., Michel-Awad, A., Briard, M.L., Plessis, G., Dufier, J.L., Munnich, A. and Kaplan, J. (1997) 'Severe manifestations in carrier females in X linked retinitis pigmentosa', *J Med Genet*, 34(10), pp. 793-7.

Spalluto, C., Wilson, D.I. and Hearn, T. (2013) 'Evidence for reciliation of RPE1 cells in late G1 phase, and ciliary localisation of cyclin B1', *FEBS Open Bio*, 3, pp. 334-40.

Spilisbury, K., Garrett, K.L., Shen, W.Y., Constable, I.J. and Rakoczy, P.E. (2000) 'Overexpression of vascular endothelial growth factor (VEGF) in the retinal pigment epithelium leads to the development of choroidal neovascularization', *Am J Pathol*, 157(1), pp. 135-44.

Spits, C., Mateizel, I., Geens, M., Mertzaniidou, A., Staessen, C., Vandeskeldel, Y., Van der Elst, J., Liebaers, I. and Sermon, K. (2008) 'Recurrent chromosomal abnormalities in human embryonic stem cells', *Nat Biotechnol*, 26(12), pp. 1361-3.

Stadtfeld, M., Maherali, N., Breault, D.T. and Hochedlinger, K. (2008a) 'Defining molecular cornerstones during fibroblast to iPS cell reprogramming in mouse', *Cell Stem Cell*, 2(3), pp. 230-40.

Stadtfeld, M., Nagaya, M., Utikal, J., Weir, G. and Hochedlinger, K. (2008b) 'Induced pluripotent stem cells generated without viral integration', *Science*, 322(5903), pp. 945-9.

Sterneckert, J.L., Reinhardt, P. and Scholer, H.R. (2014) 'Investigating human disease using stem cell models', *Nat Rev Genet*, 15(9), pp. 625-39.

Stetefeld, J. and Rugg, M.A. (2005) 'Structural and functional diversity generated by alternative mRNA splicing', *Trends Biochem Sci*, 30(9), pp. 515-21.

Stone, J.L., Barlow, W.E., Humayun, M.S., de Juan, E., Jr. and Milam, A.H. (1992) 'Morphometric analysis of macular photoreceptors and ganglion cells in retinas with retinitis pigmentosa', *Arch Ophthalmol*, 110(11), pp. 1634-9.

Strauss, O. (2009) '[The role of retinal pigment epithelium in visual functions]', *Ophthalmologe*, 106(4), pp. 299-304.

Sullivan, L.S., Bowne, S.J., Birch, D.G., Highbanks-Wheaton, D., Heckenlively, J.R., Lewis, R.A., Garcia, C.A., Ruiz, R.S., Blanton, S.H., Northrup, H., Gire, A.I., Seaman, R., Duzkale, H., Spellicy, C.J., Zhu, J., Shankar, S.P. and Daiger, S.P. (2006) 'Prevalence of disease-causing mutations in families with autosomal dominant retinitis pigmentosa: a screen of known genes in 200 families', *Invest Ophthalmol Vis Sci*, 47(7), pp. 3052-64.

Szamier, R.B. (1981) 'Ultrastructure of the preretinal membrane in retinitis pigmentosa', *Invest Ophthalmol Vis Sci*, 21(2), pp. 227-36.

Takahashi, K., Tanabe, K., Ohnuki, M., Narita, M., Ichisaka, T., Tomoda, K. and Yamanaka, S. (2007) 'Induction of pluripotent stem cells from adult human fibroblasts by defined factors', *Cell*, 131(5), pp. 861-72.

Takahashi, K. and Yamanaka, S. (2006) 'Induction of pluripotent stem cells from mouse embryonic and adult fibroblast cultures by defined factors', *Cell*, 126(4), pp. 663-76.

Takahashi, S., Kobayashi, S. and Hiratani, I. (2018) 'Epigenetic differences between naive and primed pluripotent stem cells', *Cell Mol Life Sci*, 75(7), pp. 1191-1203.

Tanackovic, G., Ransijn, A., Thibault, P., Abou Elela, S., Klinck, R., Berson, E.L., Chabot, B. and Rivolta, C. (2011) 'PRPF mutations are associated with generalized defects in spliceosome formation and pre-mRNA splicing in patients with retinitis pigmentosa', *Hum Mol Genet*, 20(11), pp. 2116-30.

Tang, Z., Zhang, Y., Wang, Y., Zhang, D., Shen, B., Luo, M. and Gu, P. (2017) 'Progress of stem/progenitor cell-based therapy for retinal degeneration', *J Transl Med*, 15(1), p. 99.

Teigelkamp, S., Achsel, T., Mundt, C., Gothel, S.F., Cronshagen, U., Lane, W.S., Marahiel, M. and Luhrmann, R. (1998) 'The 20kD protein of human [U4/U6.U5] tri-snRNPs is a novel cyclophilin that forms a complex with the U4/U6-specific 60kD and 90kD proteins', *RNA*, 4(2), pp. 127-41.

Terray, A., Fort, V., Slembrouck, A., Nanteau, C., Sahel, J.A., Reichman, S., Audo, I. and Goureau, O. (2017) 'Establishment of an induced pluripotent stem (iPS) cell line from dermal fibroblasts of an asymptomatic patient with dominant PRPF31 mutation', *Stem Cell Res*, 25, pp. 26-29.

Thomson, J.A., Itskovitz-Eldor, J., Shapiro, S.S., Waknitz, M.A., Swiergiel, J.J., Marshall, V.S. and Jones, J.M. (1998) 'Embryonic stem cell lines derived from human blastocysts', *Science*, 282(5391), pp. 1145-7.

Toops, K.A., Tan, L.X. and Lakkaraju, A. (2014) 'A detailed three-step protocol for live imaging of intracellular traffic in polarized primary porcine RPE monolayers', *Exp Eye Res*, 124, pp. 74-85.

Tucker, B.A., Mullins, R.F. and Stone, E.M. (2014) 'Stem cells for investigation and treatment of inherited retinal disease', *Hum Mol Genet*.

Tucker, B.A., Mullins, R.F., Streb, L.M., Anfinson, K., Eyestone, M.E., Kaalberg, E., Riker, M.J., Drack, A.V., Braun, T.A. and Stone, E.M. (2013) 'Patient-specific iPSC-derived photoreceptor precursor cells as a means to investigate retinitis pigmentosa', *Elife (Cambridge)*, 2, p. e00824.

Turinetto, V. and Giachino, C. (2015) 'Multiple facets of histone variant H2AX: a DNA double-strand-break marker with several biological functions', *Nucleic Acids Res*, 43(5), pp. 2489-98.

Underwood, J.G., Boutz, P.L., Dougherty, J.D., Stoilov, P. and Black, D.L. (2005) 'Homologues of the *Caenorhabditis elegans* Fox-1 protein are neuronal splicing regulators in mammals', *Mol Cell Biol*, 25(22), pp. 10005-16.

Urlaub, H., Raker, V.A., Kostka, S. and Luhrmann, R. (2001) 'Sm protein-Sm site RNA interactions within the inner ring of the spliceosomal snRNP core structure', *EMBO J*, 20(1-2), pp. 187-96.

Venturini, G., Rose, A.M., Shah, A.Z., Bhattacharya, S.S. and Rivolta, C. (2012) 'CNOT3 is a modifier of PRPF31 mutations in retinitis pigmentosa with incomplete penetrance', *PLoS Genet*, 8(11), p. e1003040.

Verbakel, S.K., van Huet, R.A.C., Boon, C.J.F., den Hollander, A.I., Collin, R.W.J., Klaver, C.C.W., Hoyng, C.B., Roepman, R. and Klevering, B.J. (2018) 'Non-syndromic retinitis pigmentosa', *Prog Retin Eye Res*, 66, pp. 157-186.

Villanueva, A., Willer, J., Bryois, J., Dermitzakis, E., Katsanis, N. and Davis, E. (2014) 'Whole exome sequencing of a dominant retinitis pigmentosa family identifies a novel deletion in PRPF31', *Invest Ophthalmol Vis Sci*.

Vithana, E.N., Abu-Safieh, L., Allen, M.J., Carey, A., Papaioannou, M., Chakarova, C., Al-Magthteh, M., Ebenezer, N.D., Willis, C., Moore, A.T., Bird, A.C., Hunt, D.M. and Bhattacharya, S.S. (2001) 'A human homolog of yeast pre-mRNA splicing gene, PRP31, underlies autosomal dominant retinitis pigmentosa on chromosome 19q13.4 (RP11)', *Mol Cell*, 8(2), pp. 375-81.

Vithana, E.N., Abu-Safieh, L., Pelosini, L., Winchester, E., Hornan, D., Bird, A.C., Hunt, D.M., Bustin, S.A. and Bhattacharya, S.S. (2003) 'Expression of PRPF31 mRNA in

patients with autosomal dominant retinitis pigmentosa: a molecular clue for incomplete penetrance?', *Invest Ophthalmol Vis Sci*, 44(10), pp. 4204-9.

Volpert, K.N., Tombran-Tink, J., Barnstable, C. and Layer, P.G. (2009) 'PEDF and GDNF are key regulators of photoreceptor development and retinal neurogenesis in reagggregates from chick embryonic retina', *J Ocul Biol Dis Infor*, 2(1), pp. 1-11.

Wahl, M.C., Will, C.L. and Luhrmann, R. (2009) 'The spliceosome: design principles of a dynamic RNP machine', *Cell*, 136(4), pp. 701-18.

Waldron, P.V., Di Marco, F., Kruczek, K., Ribeiro, J., Graca, A.B., Hippert, C., Aghaizu, N.D., Kalargyrou, A.A., Barber, A.C., Grimaldi, G., Duran, Y., Blackford, S.J.I., Kloc, M., Goh, D., Zabala Aldunate, E., Sampson, R.D., Bainbridge, J.W.B., Smith, A.J., Gonzalez-Cordero, A., Sowden, J.C., Ali, R.R. and Pearson, R.A. (2018) 'Transplanted Donor- or Stem Cell-Derived Cone Photoreceptors Can Both Integrate and Undergo Material Transfer in an Environment-Dependent Manner', *Stem Cell Reports*, 10(2), pp. 406-421.

Wang, E.T., Sandberg, R., Luo, S., Khrebtkova, I., Zhang, L., Mayr, C., Kingsmore, S.F., Schroth, G.P. and Burge, C.B. (2008) 'Alternative isoform regulation in human tissue transcriptomes', *Nature*, 456(7221), pp. 470-6.

Watanabe, K., Kamiya, D., Nishiyama, A., Katayama, T., Nozaki, S., Kawasaki, H., Watanabe, Y., Mizuseki, K. and Sasai, Y. (2005) 'Directed differentiation of telencephalic precursors from embryonic stem cells', *Nat Neurosci*, 8(3), pp. 288-96.

Weed, L.S. and Mills, J.A. (2017) 'Strategies for retinal cell generation from human pluripotent stem cells', *Stem Cell Investig*, 4, p. 65.

Weidenhammer, E.M., Ruiz-Noriega, M. and Woolford, J.L., Jr. (1997) 'Prp31p promotes the association of the U4/U6 x U5 tri-snRNP with prespliceosomes to form spliceosomes in *Saccharomyces cerevisiae*', *Mol Cell Biol*, 17(7), pp. 3580-8.

Westenskow, P.D., Moreno, S.K., Krohne, T.U., Kurihara, T., Zhu, S., Zhang, Z.N., Zhao, T., Xu, Y., Ding, S. and Friedlander, M. (2012) 'Using flow cytometry to compare the dynamics of photoreceptor outer segment phagocytosis in iPS-derived RPE cells', *Invest Ophthalmol Vis Sci*, 53(10), pp. 6282-90.

Wheway, G., Parry, D.A. and Johnson, C.A. (2014) 'The role of primary cilia in the development and disease of the retina', *Organogenesis*, 10(1), pp. 69-85.

Wheway, G., Schmidts, M., Mans, D.A., Szymanska, K., Nguyen, T.M., Racher, H., Phelps, I.G., Toedt, G., Kennedy, J., Wunderlich, K.A., Soroush, N., Abdelhamed, Z.A., Natarajan, S., Herridge, W., van Reeuwijk, J., Horn, N., Boldt, K., Parry, D.A., Letteboer, S.J., Roosing, S., Adams, M., Bell, S.M., Bond, J., Higgins, J., Morrison, E.E., Tomlinson, D.C., Slaats, G.G., van Dam, T.J., Huang, L., Kessler, K., Giessel, A., Logan, C.V., Boyle, E.A., Shendure, J., Anazi, S., Aldahmesh, M., Al Hazzaa, S., Hegele, R.A., Ober, C., Frosk, P., Mhanni, A.A., Chodirker, B.N., Chudley, A.E., Lamont, R., Bernier, F.P., Beaulieu, C.L., Gordon, P., Pon, R.T., Donahue, C., Barkovich, A.J., Wolf, L., Toomes, C., Thiel, C.T., Boycott, K.M., McKibbin, M., Inglehearn, C.F., Consortium, U.K., University of Washington Center for Mendelian, G., Stewart, F., Omran, H., Huynen, M.A., Sergouniotis, P.I., Alkuraya, F.S., Parboosingh, J.S., Innes, A.M., Willoughby, C.E., Giles, R.H., Webster, A.R., Ueffing, M., Blacque, O., Gleeson, J.G., Wolfrum, U., Beales, P.L., Gibson, T., Doherty, D., Mitchison, H.M., Roepman, R. and Johnson, C.A. (2015) 'An siRNA-based functional genomics screen for the identification of regulators of ciliogenesis and ciliopathy genes', *Nat Cell Biol*, 17(8), pp. 1074-87.

Wilkie, S.E., Vaclavik, V., Wu, H., Bujakowska, K., Chakarova, C.F., Bhattacharya, S.S., Warren, M.J. and Hunt, D.M. (2008) 'Disease mechanism for retinitis pigmentosa (RP11) caused by missense mutations in the splicing factor gene PRPF31', *Mol Vis*, 14, pp. 683-90.

- Wilmut, I., Schnieke, A.E., McWhir, J., Kind, A.J. and Campbell, K.H. (1997) 'Viable offspring derived from fetal and adult mammalian cells', *Nature*, 385(6619), pp. 810-3.
- Wong, J.C., Gao, S.Y., Lees, J.G., Best, M.B., Wang, R. and Tuch, B.E. (2010) 'Definitive endoderm derived from human embryonic stem cells highly express the integrin receptors alphaV and beta5', *Cell Adh Migr*, 4(1), pp. 39-45.
- Xu, F., Sui, R., Liang, X., Li, H., Jiang, R. and Dong, F. (2012) 'Novel PRPF31 mutations associated with Chinese autosomal dominant retinitis pigmentosa patients', *Mol Vis*, 18, pp. 3021-xxx.
- Yamanaka, S. and Blau, H.M. (2010) 'Nuclear reprogramming to a pluripotent state by three approaches', *Nature*, 465(7299), pp. 704-12.
- Yin, J., Brocher, J., Fischer, U. and Winkler, C. (2011) 'Mutant Prpf31 causes pre-mRNA splicing defects and rod photoreceptor cell degeneration in a zebrafish model for Retinitis pigmentosa', *Mol Neurodegener*, 6, p. 56.
- Yoshida, T., Ozawa, Y., Suzuki, K., Yuki, K., Ohyama, M., Akamatsu, W., Matsuzaki, Y., Shimmura, S., Mitani, K., Tsubota, K. and Okano, H. (2014) 'The use of induced pluripotent stem cells to reveal pathogenic gene mutations and explore treatments for retinitis pigmentosa', *Mol Brain*, 7, p. 45.
- Yoshihara, M., Hayashizaki, Y. and Murakawa, Y. (2017) 'Genomic Instability of iPSCs: Challenges Towards Their Clinical Applications', *Stem Cell Rev*, 13(1), pp. 7-16.
- Yu, D.Y. and Cringle, S.J. (2005) 'Retinal degeneration and local oxygen metabolism', *Exp Eye Res*, 80(6), pp. 745-51.
- Yu, G., Wang, L.G., Han, Y. and He, Q.Y. (2012) 'clusterProfiler: an R package for comparing biological themes among gene clusters', *OMICS*, 16(5), pp. 284-7.
- Yu, H.L., Chang, Z.R., Zhang, L.S., Zhang, J., Li, Z.J., Xu, J.G. and Ran, L. (2007a) '[Analysis on the status of Shigella spp antimicrobial resistance through data from the National Shigellosis Surveillance System in China, in 2005]', *Zhonghua Liu Xing Bing Xue Za Zhi*, 28(4), pp. 370-3.
- Yu, J., Hu, K., Smuga-Otto, K., Tian, S., Stewart, R., Slukvin, II and Thomson, J.A. (2009) 'Human induced pluripotent stem cells free of vector and transgene sequences', *Science*, 324(5928), pp. 797-801.
- Yu, J., Vodyanik, M.A., Smuga-Otto, K., Antosiewicz-Bourget, J., Frane, J.L., Tian, S., Nie, J., Jonsdottir, G.A., Ruotti, V., Stewart, R., Slukvin, II and Thomson, J.A. (2007b) 'Induced pluripotent stem cell lines derived from human somatic cells', *Science*, 318(5858), pp. 1917-20.
- Yuan, L., Kawada, M., Havlioglu, N., Tang, H. and Wu, J.Y. (2005) 'Mutations in PRPF31 inhibit pre-mRNA splicing of rhodopsin gene and cause apoptosis of retinal cells', *J Neurosci*, 25(3), pp. 748-57.
- Zerler, B., Moran, B., Maruyama, K., Moomaw, J., Grodzicker, T. and Ruley, H.E. (1986) 'Adenovirus E1A coding sequences that enable ras and pmt oncogenes to transform cultured primary cells', *Mol Cell Biol*, 6(3), pp. 887-99.
- Zhang, J. and Li, L. (2005) 'BMP signaling and stem cell regulation', *Dev Biol*, 284(1), pp. 1-11.
- Zhao, C., Bellur, D.L., Lu, S., Zhao, F., Grassi, M.A., Bowne, S.J., Sullivan, L.S., Daiger, S.P., Chen, L.J., Pang, C.P., Zhao, K., Staley, J.P. and Larsson, C. (2009) 'Autosomal-dominant retinitis pigmentosa caused by a mutation in SNRNP200, a gene required for unwinding of U4/U6 snRNAs', *Am J Hum Genet*, 85(5), pp. 617-27.
- Zhao, D.Y., Wintch, S.W., Ermakov, I.V., Gellermann, W. and Bernstein, P.S. (2003) 'Resonance Raman measurement of macular carotenoids in retinal, choroidal, and macular dystrophies', *Arch Ophthalmol*, 121(7), pp. 967-72.
- Zhong, X., Gutierrez, C., Xue, T., Hampton, C., Vergara, M.N., Cao, L.H., Peters, A., Park, T.S., Zambidis, E.T., Meyer, J.S., Gamm, D.M., Yau, K.W. and Canto-Soler, M.V.

(2014) 'Generation of three-dimensional retinal tissue with functional photoreceptors from human iPSCs', *Nat Commun*, 5, p. 4047.

Zhou, H., Wu, S., Joo, J.Y., Zhu, S., Han, D.W., Lin, T., Trauger, S., Bien, G., Yao, S., Zhu, Y., Siuzdak, G., Scholer, H.R., Duan, L. and Ding, S. (2009) 'Generation of induced pluripotent stem cells using recombinant proteins', *Cell Stem Cell*, 4(5), pp. 381-4.

Zhou, Z., Licklider, L.J., Gygi, S.P. and Reed, R. (2002) 'Comprehensive proteomic analysis of the human spliceosome', *Nature*, 419(6903), pp. 182-5.

Zhu, Y., Carido, M., Meinhardt, A., Kurth, T., Karl, M.O., Ader, M. and Tanaka, E.M. (2013) 'Three-dimensional neuroepithelial culture from human embryonic stem cells and its use for quantitative conversion to retinal pigment epithelium', *PLoS One*, 8(1), p. e54552.

Zrenner, E. (2013) 'Fighting blindness with microelectronics', *Sci Transl Med*, 5(210), p. 210ps16.